Universidade de Aveiro
2014

Departamento de Engenharia Mecânica
Departamento de Química
Departamento de Física
Departamento de Engenharia de Materiais e Cerâmica

SANDRA MARIA ALVES DA CRUZ

NANOCOMPÓSITOS COMO SUBSTRATOS PARA BIODETEÇÃO UTILIZANDO SERS

Universidade de Aveiro
2014

Departamento de Engenharia Mecânica
Departamento de Química
Departamento de Física
Departamento de Engenharia de Materiais e Cerêmica

SANDRA MARIA ALVES DA CRUZ

NANOCOMPOSITES AS PROBES FOR BIODETECTION BY SERS

Tese apresentada à Universidade de Aveiro para cumprimento dos requisitos necessários à obtenção do grau de Doutor em Nanociências e Nanotecnologia, realizada sob a orientação científica da Doutora Paula Alexandrina de Aguiar Pereira Marques, Equiparada a Investigadora Principal do Departamento de Engenharia Mecânica da Universidade de Aveiro e co-orientação científica da Professora Doutora Helena Isabel Seguro Nogueira, Professora Auxiliar do Departamento de Química da Universidade de Aveiro

Apoio financeiro da FCT (SFRH / BD / 68598 / 2010)

Dedico este trabalho ao Paulo e ao Pedro pelo incansável apoio.

o júri

presidente

Doutor António Manuel Melo de Sousa Pereira
Professor Catedrático do Departamento de Eletrónica, Telecomunicações e Informática da Universidade de Aveiro

Doutora Asunción Alicia de Andrés Miguel
Professora Investigadora do Instituto de Ciencia de Materiales de Madrid, Espanha

Doutor Felipe Chibante
Professor Associado da Faculdade de Engenharia da Universidade de Brunswick, Canadá

Doutor Pedro Miguel Ribeiro Viana Baptista
Professor Associado com Agregação da Faculdade de Ciências e Tecnologia da Universidade Nova de Lisboa

Doutora Maria de Fátima Guimarães Cerqueira
Professora Auxiliar da Escola de Ciências da Universidade do Minho

Doutor Tito da Silva Trindade
Professor Associado com Agregação do Departamento de Química da Universidade de Aveiro

Doutora Paula Alexandrina de Aguiar Pereira Marques
Equiparada a Investigadora Principal da Universidade de Aveiro

Doutora Helena Isabel Seguro Nogueira
Professora Auxiliar da Universidade de Aveiro

agradecimentos

Em primeiro lugar, quero agradecer à Doutora Paula Marques por todo o seu apoio incansável para eu conseguir concluir esta tese, pela sua orientação e conhecimentos científicos que me ajudaram a crescer na investigação científica, e, principalmente, pela sua amizade sincera com a qual me brindou nos bons e maus momentos.
Agradeço à Professora Helena Nogueira toda a sua orientação científica e todas as oportunidades que me proporcionou de forma a complementar a minha formação durante este doutoramento.

À Doutora Alicia de Andrés pelos estudos de Raman (e mapeamento) efectuados no seu laboratório, bem como a experiência enriquecedora que me proporcionou, em Madrid. À Prof. Nazanin Emani pelos testes de XPS dos meus materiais. À Mestre Celeste Azevedo gostaria de agradecer as análises de termogravimetria, por toda a ajuda que sempre disponibilizou para o manuseamento dos equipamentos e por toda a sua simpatia. Ao Doutor Carlos Granadeiro pela ajuda preciosa nos primeiros passos que dei na técnica de Raman e SERS.

Aos meus colegas Gil e Ricardo, pela sua ajuda incansável, e aos restantes colegas de laboratório, Nuno, Susana e Patrícia, pelo bom ambiente de trabalho e troca de conhecimentos. A todas as pessoas do departamento de Química, pela sua amizade e boa disposição, em particular, à Sónia e à Paula.

A todos os meus amigos que fui conhecendo neste longo percurso académico, em especial à Xurro, ao Tordo e à Lisa, pela sua amizade e carinho que conseguimos preservar há tantos anos...

À Fundação para a Ciência e Tecnologia pelo suporte financeiro que me possibilitou o desenvolvimento deste doutoramento.

E, por fim, mas o mais importante, agradeço a toda a minha família o apoio incondicional nestes anos que foram de muito trabalho. Ao Paulo e ao Pedro, quero agradecer todo o apoio, carinho e amor que me dão tanto alento para continuar a fazer a investigação que tanto gosto e, sobretudo, quero agradecer a compreensão da minha ausência em alguns momentos, para conseguir terminar este doutoramento. Obrigada!

palavras-chave

Óxido de grafeno, nanopartículas de ouro e prata, materiais poliméricos, nanocompósitos, difusão de Raman intensificada por superfícies, electrofiação, florestas de nanotubos de carbono.

resumo

O presente trabalho pretendeu explorar as potencialidades de nanocompósitos, baseados em nanoestruturas de carbono e nanopartículas metálicas, para a deteção de biomoléculas através da técnica de difusão de Raman intensificada por superfície (SERS, *surface-enhanced Raman scattering*).

Primeiramente foram preparados nanocompositos de álcool polivinílico com nanopartículas de prata sintetizadas através de dois métodos, ainda sem a presença de nanoestruturas de carbono. Verificou-se que estas membranas apresentaram bons resultados na identificação de ácidos nucleicos por SERS.

A síntese e caracterização do óxido de grafeno que serviu de base para a preparação dos nanocompósitos de prata e ouro foi objecto de estudo. A sua redução química com diferentes agentes redutores foi explorada, uma vez que o grau de redução deste nanomaterial pode ser um fator determinante para a aplicação pretendida (interação com biomoléculas).

A preparação de nanocompósitos de óxido de grafeno com prata e ouro foi realizada com diferentes agentes redutores. A atividade de SERS destes novos nanocompósitos foi então explorada na presença de vários analitos, em diferentes condições de aquisição dos espectros de Raman, bem como em diferentes tipos de suporte. Verificou-se que os nanocompósitos preparados com prata apresentaram a particularidade de permitirem a intensificação dos sinais de Raman das bandas D e G do grafeno. É de salientar a introdução de um novo agente redutor amigo do ambiente para síntese de compósitos de grafeno com nanopartículas metálicas: o extrato de eucalipto. Outra variável introduzida foi a preparação de nanopartículas de ouro em forma de nanoestrelas sintetizadas com hidroxilamina na presença de óxido de grafeno, tendo-se obtido assim um novo nanocompósito com potencialidades em SERS.

Com o objectivo de preparar suportes para SERS com uma topografia e porosidade adequadas à criação de locais privilegiados para a agregação de nanopartículas metálicas e para a penetração das moléculas do analito foram produzidas mantas por electrofiação. Para tal, selecionaram-se os polímeros álcool polivinílico e poliacrilonitrilo. Com esta técnica preparam-se igualmente nanocompósitos de ouro ou prata e grafeno. Estudaram-se algumas variáveis de síntese, tais como a introdução de nanopartículas e nanocompósitos *in situ*, (isto é, durante o processo de electrofiação), deposição posterior das nanopartículas e dos nanocompósitos nas fibras poliméricas (preparadas previamente) e funcionalização superficial das mantas com o objectivo de ligar os nanomateriais *a posteriori*.

Por fim, foi também explorada a potencialidade em SERS de novas estruturas compostas por florestas de nanotubos de carbono com cobertura de ouro produzidas por deposição química de vapor. Verificou-se que a detecção de bases de ADN e o próprio ADN é possível usando estes materiais.

keywords

Graphene oxide, gold and silver nanoparticles, polymeric materials, nanocomposites, surface enhanced Raman scattering, electrospinning, vertically aligned carbon nanotubes.

abstract

The present work aimed to explore the potential of new nanocomposites based on carbon nanostructures and metal nanoparticles for the detection of biomolecules through surface enhanced Raman scattering (SERS).

In a first step, polyvinyl alcohol composites were prepared incorporating silver nanoparticles by two different reduction procedures. At first without introduction of carbon nanostructures. These composites showed good results for the SERS identification of nucleic acids.

Next, the synthesis and characterization of graphene oxide was studied to be used in the preparation of silver and gold nanocomposites. The reduction of this nanomaterial with different chemical agents was explored, since its reduction degree may be a determinant factor for the application envisaged (biomolecules interaction).

The preparation of the nanocomposites with silver and gold was performed with different reducing agents. The SERS activity of these new nanocomposites was then explored in the presence of different analytes, varying the experimental conditions for Raman spectra acquisition. It was interesting to verify that the silver containing nanocomposites presented the particularity to intensify the graphene D and G bands. It is also important to highlight that a new eco-friendly reducing agent was tested for the synthesis of the graphene oxide composites, an Eucalyptus Globulus extract. Other variable introduced was the preparation of gold nanostars synthesized with hydroxylamine in the presence of graphene oxide, which allowed the preparation of a new nanocomposite with SERS potential.

Fibrous membranes were also prepared by electrospinning with the aim to prepare SERS supports with adequate topography and porosity for the formation of nanoparticles agglomerates for the creation of the so-called hot-spots and also to allow the penetration of the analyte molecules. The polymers polyvinyl alcohol and polyacrylonitrile were selected for electrospinning. Using this technique, electrospun mantles with silver and gold nanoparticles and nanocomposites were prepared. Several variables were studied, such as the introduction of the nano-fillers during the electrospinning process, later deposition of the nano-fillers on the simple electrospun polymeric fibres and surface functionalization of the simple polymeric membranes to link the nano-fillers.

At last, the potentialities of using carbon nanotubes forests, produced by chemical vapor deposition and coated with gold film by sputtering, as new SERS substrates were explored. It was found that the SERS detection of DNA bases and ADN itself is possible using these substrates.

Overall Index

List of Abbreviations

A	Adenine
AFM	Atomic force microscopy
Ag	Silver
Au	Gold
BC	Bacterial cellulose
BWF	Breit-Wigner-Fano function
C	Cytosine
DNA	Deoxyribonucleic acid
ds-DNA	Double stranded deoxyribonucleic acid
DTG	Differential termogravimetry
EF	Enhancement Factor
FTIR	Fourier transform infrared spectroscopy
FWHM	Full Width at Half Maximum
G	Guanine
GO	Graphene oxide
MGO	Metal nanoparticles-graphene oxide
NP	Nanoparticle
PVA	Poly(vinyl alcohol)
rGO	Reduced graphene oxide
SEM	Scanning electron microscopy
SERS	Surface-enhanced Raman scattering
SHsal	Tiosalicylic acid
ss-DNA	Single stranded deoxyribonucleic acid
T	Thymine
TEM	Transmission electron microscopy
TG	Termogravimetry
TGA	Termogravimetry analysis
UV-visible	Ultra violet-visible spectroscopy
XPS	X-ray Photoelectron Spectroscopy
λ	Wavelength

Figures List

Tables List

Schemes List

1. Carbon nanostructures: novel components for SERS substrates

In this chapter a general framework of the content of the thesis is shown, to provide an overview on the work developed.

The description of the main technique used in this thesis, surface-enhanced Raman scattering (SERS), is done. Also, the types and evolution of SERS substrates are described. The carbon nanostructures are also described here, with special relevance to graphene and carbon nanotubes. A brief description is made on graphene, graphene oxide and reduced graphene oxide. The properties of these carbon nanostructures that are relevant for the study developed in this thesis are also mentioned. On the other hand, the carbon nanostructures are explored in relation to surface-enhanced Raman scattering research.

The main objectives of this thesis which, in a generic way are to develop substrates based on carbon nanostructures that are active in surface-enhanced Raman scattering, are presented in the last topic.

1.1. Introduction

Specific detection of proteins characteristic of some diseases plays an important role in biochemistry and biomedical research areas. In particular, the measurement of cancer biomarkers is of major importance for early detection and high reliability prognosis of such disease. This is a great challenge for the community that is dedicated to this type of scientific research, with the development of the interface between nanoscience and medicine one of the most interesting areas of science.

Raman spectroscopy, in particular SERS (Surface-Enhanced Raman Scattering) is a new and very promising approach for specialized investigation due to its ability to identify structurally a molecule with very high sensitivity[1]. The enhancement of Raman signals has been observed up to 10^6 getting the particular case of single molecule detection. This notable enhancement provides high sensibility and offers an opportunity of development of ultra-sensitive analytical methods for chemical and biochemical detection[2]. SERS has been used as a selective and sensitive method in the detection of proteins and oligonucleotides [3].

Due to SERS recent development, it is expected that its applications are extended to the analysis of cells and tissues. The first studies have already started to be done [1,4] however, more studies are needed to assess the advantages and disadvantages of SERS related to other techniques, particularly fluorescence microscopy that uses molecular fluorophores and quantum dots. In the case of experiments *in vivo* with nanoparticles and SERS labels, the biodistribution and toxicity have been studied [5,6].

Eighty years after the discovery of the Raman effect, conventional Raman scattering has already made the transition to the clinics, for example, in the area of bacteria identification or in surgery for online monitoring by fiber optic probes. The next years will show whether SERS in targeted research as a relatively new approach will experience a similar success story[3].

Several research groups are actively working on improved designs of SERS probes with high sensitivity and reproducible signals, and the number of biomedical SERS applications is constantly increasing[3]. However, a good enhancement of the Raman

signal is required for the application to be successful being the SERS substrate the key factor[7].

Graphene is a promising material to be used as SERS substrate. Recently, graphene by itself was reported as a clear inducer of the enhancement of Raman signal intensity in adsorbed molecules[8-10]. This enhancement was attributed to charge transfer between graphene and the molecules of the analyte. Graphene and gold nanocomposites have demonstrated good results as SERS substrates[11] . The arrangement between gold nanoparticles and graphene can attribute a unique mechanism of electronic transfer or energetic between both phases which allows the observation of SERS. Also, silver nanoparticles were used in graphene-based nanocomposites to enhance Raman signals[12].

Graphene is aromatic, hydrophobic and chemical inert. It is also biocompatible and has potential bioapplications[13]. Due to exceptional charge mobility and atomic thickness graphene was been proposed as the basis to sensitive detection and chemical/biological free-label[14]. Graphene oxide (GO) is the oxidated form of graphene and this derivative can interact with nanoparticles to produce structural nanocomposites after its reduction[15]. Moreover, being a two-dimensional nanostructure with an adjustable chemical surface, functionalized graphene can produce strong interfaces with biological systems without geometric limitations[13]. Graphene has also the facility to adsorb biomolecules due to π-π stacking between its hexagonal cells and the carbon rings present in the majority of nano/biomolecules[16].

Currently, graphene has been employed in several areas that go from chemical sensors to transistors. The majority is based on the electric properties. In the last few years, researchers have become increasingly interested in developing SERS substrates based on graphene. In this work we will show the advances in this area.

1.2. Surface-enhanced Raman scattering

1.2.1. Description of SERS technique

SERS is almost 40 years old. The first SERS spectrum was recorded in 1947 by Fleischman and co-workers; and in 1977 it was shown by Jeanmaire and Van Duyne to possess what is surely the most iconic characteristic of SERS: a Raman cross-section per molecule some million-fold larger than for the same molecule in solution[17].

In these four decades, SERS phenomenon is not yet completely understood neither is predictable. The enhancement factor can be understood as a contribution of two mechanisms: (a) electromagnetic and (b) chemical. The electromagnetic mechanism occurs because the intensity of Raman scattering is directly proportional to the square of the induced dipole moment, μ_{ind}, which, in turn, is the product of the Raman polarizability, α, and the magnitude of the incident electromagnetic field, E. As a consequence of exciting the localized surface plasmon resonance (LSPR) of a nanostructured or nanoparticle metal surface, the local electromagnetic field is enhanced compared to Raman signal [18]. This mechanism is consensual in research community.

In the case of chemical mechanism, several theories are proposed: (i) metal-ligand complex formation[19], (ii) the creation of new metal to molecule or molecule to metal charge transfer resonances much like those that are common in transition metal coordination complexes[20], or (iii) the transient residence of hot electrons or electron-hole pairs out of the metal on the molecule[21]. The surface plasmon (SP) was described as a superposition of metal electron-hole pairs formed through isoenergetic transitions of magnitude equal to the frequency of SP. The hot electrons can transitorily reside on the molecule added, forming a radical anion. So, it was suggested that the molecule added can accelerate the dephasing of plasmon. Such processes occur without any doubt in adsorbed-molecule-systems but are still a great deal to chemists and physicists. Nevertheless, none of the models presented here have yet yielded a quantitative or predictive theory. So it is hard to say to what extent they contribute to the enhancement[17].

Some confusion in SERS remains between the concepts of "surface-enhancement" and "very strong Raman cross-sections" which may be endemic to the analyte adsorbed, even when it is in solution. Molecules, such as Rhodamine 6G (R6G), a known SERS probe, may have enormous Raman cross-sections and, therefore, their SERS spectra are very intense. If the molecule also fluoresces, Raman spectrum may only be recorded when such florescence is quenched, as happens when the molecule is adsorbed on a metal surface, or by using ultrafast techniques, essentially recording the Raman spectrum before the fluorescence intensity become greater, or when the system is stable enough to be able to overcome the shot noise, by using techniques that allow register the difference of intensity and an appropriate signal acquisition time. For that reason, a large Raman cross-section does not mean a large SERS enhancement[17].

The enhancement of Raman signal comes up to 10^{14} times higher than in conventional Raman scattering [22] and can detect quantities as small as single-molecule [23-25]. The two major advantages of using SERS are the high sensitivity and molecular specificity. Although SERS mechanism remains uncertain, these are the reasons why this technique has being improved and medical applications and the design of portable devices for *in vitro* diagnosis are increasingly coming realities [26-28].

1.2.2. SERS substrates

Since the first SERS spectrum was observed using a rough silver electrode, substrates have started being developed: (1) substrates without uniformity prepared by electrochemical oxidation – reduction cycles or by deposition in vacuum; (2) colloidal solutions prepared by chemical synthesis and composed by nanoparticles with a big size distribution; (3) nanoparticles with size and shape controlled by a chemical method; (4) nanostructured surfaces with size, shape and inter-particle spacing well-structured prepared by self-assembly, mold or lithography; and (5) atom-thickness materials, such as graphene and graphene oxide, with or without metal nanoparticles intercalated. Specially, in the last two to three years, SERS substrates have been more structurally controlled due to nanoscience and nanotechnology improvement.

The enhancement of the spectroscopic signal obtained can be $10^4 – 10^6$ for Ag, Au e Cu, and $10 – 10^4$ for other transition metals, such as Fe, Co, Ni, Rh, Pd and Pt by using substrates prepared by electrochemical oxidation-reduction cycles. This method is easy to use, produces stable substrates and their contamination have less chances to occur[29,30]. Colloidal suspensions of gold and silver nanoparticles started to be more used as SERS substrates after shape, size and composition of the nanoparticles could be controlled by synthetic methods. Theoretical calculations indicate an enhancement of $10^3 – 10^4$, in the case of Au, and 10^6 e 10^7, for Ag[31]. Normally, SERS signals obtained by colloidal suspensions are weak. In order to improve this result, depositing colloidal suspension of metal nanoparticles onto solid substrate is a common technique to prepare a nanoparticle monolayer to induce their coupling. Apart from being a very simple alternative it has shown very effective results. However, a nanoparticle monolayer may not have a uniform distribution and, therefore, SERS signals are not similar from equivalent substrates. Best results can be achieved by concentrating the colloidal suspension and controlling the drying time of the suspension over the solid substrate[32].

With the development of nanoscience and nanotechnology, metal nanoparticles of different sizes and shapes have been synthesized using various methods, such as chemical reduction, chemical replacement, electrochemical reduction, photochemical, thermal decomposition, and ultrasonic decomposition methods[29]. The most widely used and the simplest method is the chemical reduction, in which a metal salt is reduced to metal nanoparticles in aqueous or non-aqueous solution using reducing agents, such as sodium citrate, $NaBH_4$[33], hydrogen[34] or alcohols[34]. Normally some surfactants, such as cetyl trimethylammonium bromide (CTAB), poly(vinyl pyrrolidone) (PVP), or sodium dodecyl sulphate (SDS), are added to the solution as capping agents to prevent the aggregation or oxidation of nanoparticles. These agents have also the function of regulating the growth rate to control nanoparticles shape and size. The type of metal salt, reductant, surfactant and their relative concentration, the reaction temperature, and the solution pH influences the size, size distribution, the shape, and the aggregation state of metallic nanoparticles [26,29]. SERS substrates produced by metallic nanoparticles show some advantages: easy synthesis and low-cost; the size and shape can be controlled by reaction conditions in order to obtain the desired optical properties and maximize the enhancement signal effect;

nanoparticle aggregates can provide a higher enhancement in the specific sensitivity [35,36].

The methods to prepare highly ordered SERS substrates include the nanoparticle assembly method, the Langmuir-Blodgett (LB) method, and lithography. A chemical assembly method is used to modify the solid substrate (Si, glass, indium tin oxide (ITO), or Au film) with bifunctional molecules. One molecular moiety interacts with the solid substrate originating a compact layer and the other moiety interacts with the nanoparticle through electrostatic or chemical interaction to form a well-arranged layer of nanoparticles. Size, concentration, and surface charge of the nanoparticles, and the type do bifunctional molecules are the parameters of which depend the surface coverage and uniformity of the assembled layer. In order to prevent the aggregation of nanoparticles and to form a uniform substrate during the synthesis process, capping agents are usually added. However, the presence of the capping agent will lead to a large repulsion between nanoparticles and prevent the formation of a compact assembly layer. In the latter case, the electromagnetic interaction between nanoparticles is not highly effective and the SERS activity is low[37]. To overcome this problem, further growth of the nanoparticles by chemical or electrochemical methods has been proposed in order to reduce the interparticle spacing and increase the SERS activity[38]. The main advantage of this type of substrate, which gives an homogeneous SERS signal and has a significant surface area (up to several cm^2), is that it can be produced in a normal laboratory without complicated equipment. An alternative method is to functionalize the Au nanoparticle surface with CTAB to form a positively charged molecular bilayer which subsequently will be deposited in an ITO substrate. This type of nanoparticles will not form aggregates due to bilayer positive charge in their surface. The substrate has a very uniform SERS signal and good reproducibility and stability. One of the limitations is the CTAB signal present in SERS spectra which implies poor results when this system is applied to detect some molecules that have weak interaction with the substrate or weak Raman signal. Although this method can effectively avoid the aggregation of nanoparticles, allowing total surface of nanoparticle interacting with analyte molecules, it is still difficult to obtain a defect-free surface and to obtain a substrate with a large area.

All the problems above described can be solved using Langmuir-Blodgett technique which originally was used to prepare amphiphilic molecular films with large area on solid substrates[39]. By dissolving an amphiphilic molecule in a water-immiscible volatile solvent and dispersing the solution on the surface of the aqueous phase it forms a molecular monolayer at the interface after solvent evaporation. By changing the position of the movable barrier in the LB trough, one can change the density of the monolayer film. The film can then be deposited on the substrate by the dipping and pulling method. By dispersion of the solution of metal nanoparticles into the water phase, a layer of randomly distributed nanoparticles will be left at the interface after the evaporation of the solvent. As a result of compression of the layer through moving the barrier, an ordered layer of nanoparticles will be formed on the surface. During the compression process, the interparticle spacing will decrease, leading to strong electromagnetic coupling between nanoparticles and a significant shift of the LSPR band. The nanoparticle film can then be deposited on glass or a Si wafer by transfer to form a substrate with a surface area as large as 20 cm^2. At present, the LB technique has been successfully used to fabricate SERS films of nanorods, nanowires, and spherical, cubic, cuboctahedral, and octahedral Ag nanoparticles[40,41].

Lithography of nanospheres can also be used to produce homogeneous substrates. Aggregates of polystyrene spheres or silica with appropriate size deposited on a substrate (glass, ITO glass, silica or metallic film) form a multilayer film, where nanospheres are highly ordered and the conditions of aggregation are controlled. The formed film is used as template for vacuum deposition or electrochemical deposition to form on the template a metal film of the desired thickness[29].

As was described, a variety of methods such as chemical functionalization or lithography techniques can be used to immobilize plasmonic nanoparticles uniformly on conventional substrates such as glass, quartz and silicon substrates (which are not flexible for standard use), but the substrates need to be flexible and easily processable for the development of low cost sensors for everyday life applications. For that reason, one of the future challenges ahead of researchers is the fabrication of SERS-active devices that bring the technology from the laboratory to real-world applications[7].

Some authors have already published some works that reveal this concern. The flexible substrates can be divided into plasmonic substrates for sensing, cellulose

paper-metallic nanoparticles, polymer-metal nanofiber mats, polydimethylsiloxane (PDMS)/plastic-metallic nanoparticles, carbon nanotube-plasmonic nanoparticles and graphene-metal nanoparticles[7].

Recently, electrospinning has been presented as an interesting technique used to directly assemble gold nanorods on aligned electrospun nanofibres[42-44]. Aligned nanofibres act as micro-and nanochannels causing preferential alignment of the anisotropic Au nanorods along the fibre axis, resulting in globally anisotropic plasmonic and SERS properties. Such massive alignment of AuNRs, combined with the porous polymer fibrous mat, which provides efficient access to the analyte, showed excellent SERS effect. It is worth noting, that even with a modest density of Au nanorods on the surface of the electrospun fibres, the SERS intensity was dramatically enhanced compared to the planar counterpart. The porous nature of the nanofibrous mat enables efficient sorption and transport of the analyte molecules to the surface of the Au nanorods facilitating the observed high SERS effect.

1.3. Carbon nanostructures

1.3.1. Graphene and graphene oxide

Graphene belongs to a new class of carbon nanomaterials composed by sp^2 carbons arrange in a honeycomb structure (Figure 1.1).

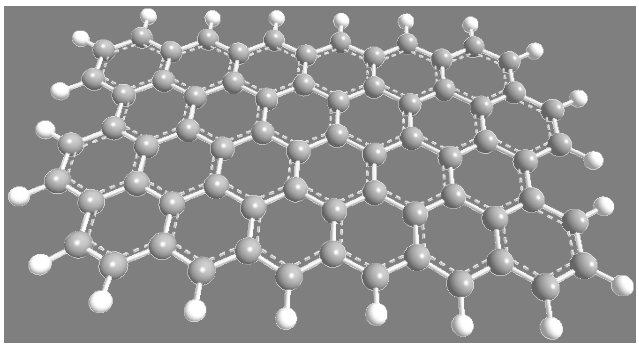

Figure 1.1 – Graphene 2D structure

Several experimentally measured properties of graphene have already surpassed those observed in other types of materials. With enhanced electrical conductivity, high

mechanical strength, high thermal conductivity, high impermeability to gases and optical transparency, graphene holds great promise as the next wonder material. Such an ideal is, however, achievable only if the large scale production of high quality graphene is attained[45].

The current state of graphene production is divided between two approaches – the bottom-up and top-down. The bottom-up approach seeks to build graphene sheets from scratch, starting with simple carbon-based molecules such as methane and ethanol. On the other hand, the top-down approach relies on the fundamental idea of extracting layers of graphene from graphite. Both methods provide graphene of contrasting quality and yield. However, in terms of high yield and low cost, the top-down approach via chemical oxidation of graphite is the most convenient method to date. Moreover, graphene obtained via such chemical treatments is important for a large portion of the graphene community that endeavours to use graphene in applications such as composites, coatings, paint/ink, transparent conductive layers, bioapplications and energy storage.

1.3.1.1. Graphene

Although "graphene" is a term widely used for a variety of carbon-based materials, the definition provided by IUPAC, in 1997 indicates that "*the term graphene should be used only when the reactions, structural relations or other properties of individual layers are discussed.*"[46]. This misunderstanding happens because when graphene oxide is reduced it restores almost the graphene structure but a certain amount of oxygen groups remain in the structure, so it is important to know the differences between all the graphene derivatives (graphene oxide and reduced graphene oxide) and graphene itself.

Graphene can be produced by two approaches: bottom-up or top-down. At the first one, graphene can growth by chemical vapour deposition (CVD), arc discharge or epitaxial growth [47-53]. At the second approach, graphene is produced by electrochemical process, sonication or micromechanical exfoliation. In fact, the latter

was the method used to isolate graphene monolayer and gave Physics Nobel Prize, in 2010, to Geim and Novoselov [54].

Graphene is a single layer of honeycomb structure of carbons with sp^2 hybridised carbon atoms arranged in a hexagonal lattice and partially filled π-orbitals above and below the plane of the sheet. However, obtaining a single layer is an extremely difficult process. In most cases, a structure with fewer layers of graphene is achieved and generally the properties refer to this group. In fact, the term "graphene" is commonly used to "monolayer", "bilayer" or "few-layer". This categorization has been made as the electronic properties of bi and few-layer (where "few" is not rigorously defined but is generally accepted as being < 10 layers) are distinct from the properties of graphite[55]. Besides the number of layers, the oxidation state is another important feature in terms of characterization. As a single layer of carbon atoms, graphene is the thinnest material known, yet it is impermeable to gases and it is stronger than steel (Young's modulus ~ 1TPa)[56]. Moreover, thermal conductivity of graphene at room temperature (up to ~ 5000 $Wm^{-1}K^{-1}$) rivals the values obtained for bundles of carbon nanotubes and is over double the next thermal conductor known, the diamond[57]. Being single layer, graphene also has an extremely high surface area with a theoretical value of 2630 m^2g^{-1} and is almost transparent, absorbing only ~ 2.3 % of white light[58]. Graphene has also shown good "foldability" recovering its electrical properties after bending and unbending[46].

1.3.1.2. Graphene oxide

Graphene oxide was discovered much earlier than graphene. In 1840s, Schafhaeutl reported the intercalation of graphite using small-molecular species, such as an acid or alkali metal, between the carbon lamellae; the exfoliation of graphite was made with sulfuric and nitric acid[59]. In 1859, Professor Brodie attempted to measure the molecular weight of the graphite. For that purpose he has used nitric acid, potassium chlorate and heat the mixture. The material was washed and re-oxidised under the same conditions up to four repetitions. The final product was termed "graphic acid" and was the first sample of graphite oxide prepared experimentally[60]. In 1898, Staudenmaier improved the oxidation method by adding potassium chlorate in small

portions and further acidifying the mixture with concentrated sulphuric acid. The final product was practically the same but more convenient since it does not require four repetitions of oxidation[61].

In 1958, Hummers and Hoffman presented a safer approach by using potassium permanganate as oxidant in a mixture of concentrated sulphuric acid and sodium nitrate[62]. The Hummers method was very well received and has been adopted by many researchers. In an effort to improve the oxidation method, Marcano in 2010 replaced *in situ* production using nitric acid with less corrosive phosphoric acid[63]. The method claimed to provide a more oxidised form of graphite oxide and highlighted a more intact graphitic basal-plane. Besides that, the possibility for large scale production of graphene oxide seems possible since the method does not involve large exothermic or release toxic gases[45].

In the last decade, graphene chemically modified has been the subject of intense study in the context of many applications such as polymer composites, energy storage and conversion, sensors, materials like "paper", field effect transistors (FET), and biomedical applications, due to the excellent electrical, optical, and mechanical properties[38].

Graphene oxide consists in stacked carbon-based sheets with many oxygen functional groups (carboxyl, hydroxyl, epoxide and carbonyl groups) which makes this compound a good candidate for the above mentioned applications. The introduction of oxygen functionality groups significantly alter van der Waals interactions between the layers and endow GO with strong hydrophilicity. The presence of these functional groups destroys the planar sp^2 carbons of graphene and converts them to sp^3 carbons by covalent bond to oxygen (Figure 1.2). Therefore the π-π electronic conjugation of graphene is destroyed in GO, resulting in a significantly decrease in electrical conductivity[64].

Notably, it has been reported that the electrical conductivity of GO can be restored close to the level of graphene by chemical reduction[64]. The electrical conductivity of reduced GO (rGO) achieves 200 – 42000 Sm^{-1} depending on the reducing conditions (reduction time, temperature, annealing time, and annealing temperature) [65-67]. The specific capacitance of rGO has been found significantly higher than that of GO.

However, the dispersibility and transparency of rGO remains poorer than those of pure GO. The reduction process removes oxygen-containing functional groups which results in a decrease of rGO dispersability in different solvents. The restoration of π-electronic conjugation and the colour change from brown to black are the main reasons for the observed decrease in transparency[64].

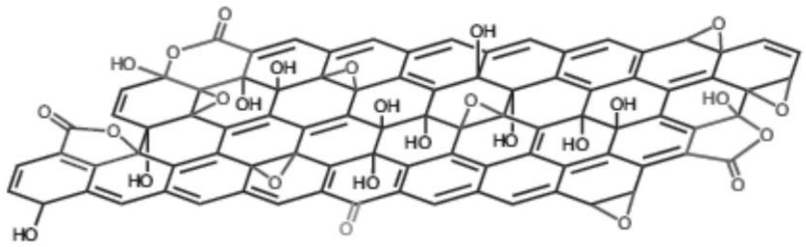

Figure 1.2 – Graphene oxide structure and the oxygen functionality groups that can be formed after the oxidation process [68,69].

1.3.1.3. Reduction of graphene oxide

The reduction of graphene oxide (rGO) can be made by chemical, thermal, electrochemical or a combination of these processes. In the chemical reduction there are several chemical compounds that can be used such as: hydrazine[70], hydroquinone[71], sodium borohydride[72], ascorbic acid[73], or poly (sodium 4-styrenesulfonate)[74]. This type of graphene oxide reduction has been efficient and is not an expensive process. The toxicity of the reducing agent is a concern due to the final applications of the reduced graphene oxide; hydrazine is one of the most toxic chemical used in the reduction of GO and ascorbic acid is labelled as eco-friendly reducer.

Thermal reduction of GO is carried out by heating the GO in various atmospheres (ultra-high vacuum, Ar, H_2, NH_3), or with different heating sources such as microwave, flash light, plasma, electric current, or heated AFM tip. In this method, oxygen functionalities are removed in the form of water, carbon dioxide, and carbon monoxide. The results show that high conductivity could be achieved when GO is

submitted to this type of treatment[75]. In comparison to chemical and thermal reduction, electrochemical reduction of GO is green and fast, and the reduced material is contaminant-free. The electrical conductivity and electrochemical stability of rGO produced by this method are higher than those of chemically or thermally obtained[64].

In addition to this three conventional reduction techniques, various other methods were used to deoxygenate GO. Cote et al. reported a chemical-free flash reduction process using a photographic camera flash to instantaneously deoxygenates GO by photothermal heating. The hydrophilicity of the flashed area was also significantly decreased than that of pure GO. In comparison to the three conventional reduction methods flash reduction is rapid, chemical-free, and energy efficient. This technique holds great promise for patterning GO films for device and composite applications[76].

The choice of reduction method is made according to the final application purpose of rGO. For example, in the case of sensors where the combination of metal nanoparticles and rGO are used, chemical reduction is the most suitable technique because this process allows the simultaneous reduction of metal nanoparticles and GO.

1.3.1.4. Graphene characterization by Raman spectroscopy

Raman spectroscopy has been widely used in electronic properties characterization of graphitic materials[77-80] . Besides being non-destructive and fast, this technique allows the characterization in terms of layers quantification and chirality of functionality groups that modifies graphene [81,82].

According to the electronic properties of graphitic materials, in Raman spectroscopy the main important bands are between 1200 and 3000 cm^{-1}. At 1350, 1580 and 2700 cm^{-1} are the bands denoted by D, G and 2D (or G'), respectively [85,86] (Figure 1.3 - A). G band is associated to E_{2g} phonon at the Brillouin zone center[87] . D band specifies the defects of graphitic material analyzed[83]. The 2D originates from a two phonon double resonance Raman process and because of that is closely related to the band structure of graphene layers [85-88].

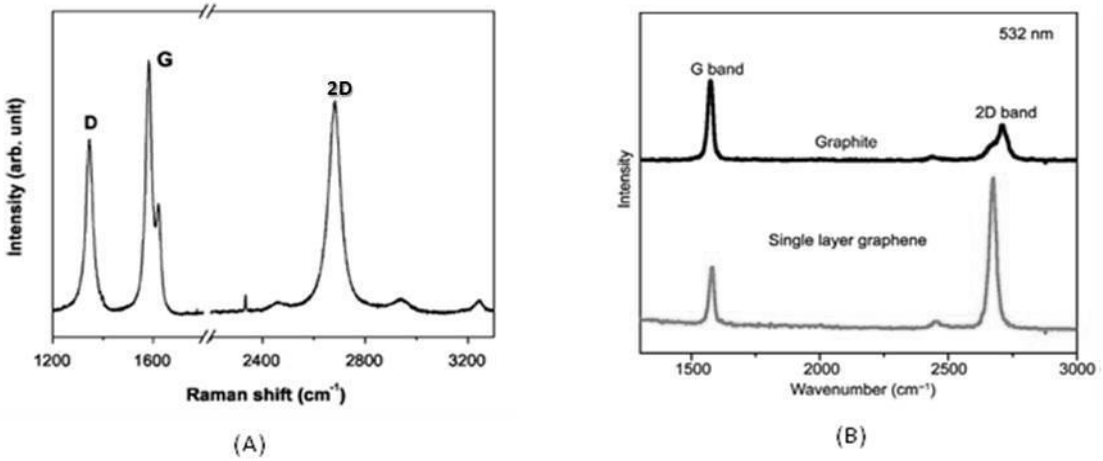

Figure 1.3 – (A) Raman spectrum of graphitic material showing the main Raman characteristic bands, D, G and 2D (orG'). The laser excitation used was 2.41 eV (514.5 nm) (Adapted from Pimenta et al., 2007)[83]. (B) Raman spectra of graphite and graphene monolayer[84].

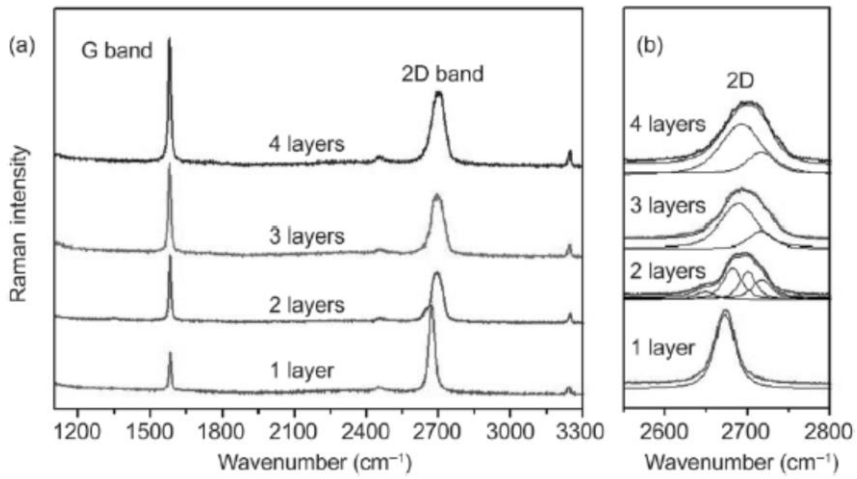

Figure 1.4 – (a) Raman spectra of graphene with 1, 2, 3, and 4 layers. (b) The enlarged 2D band regions with curve fitting. [90]

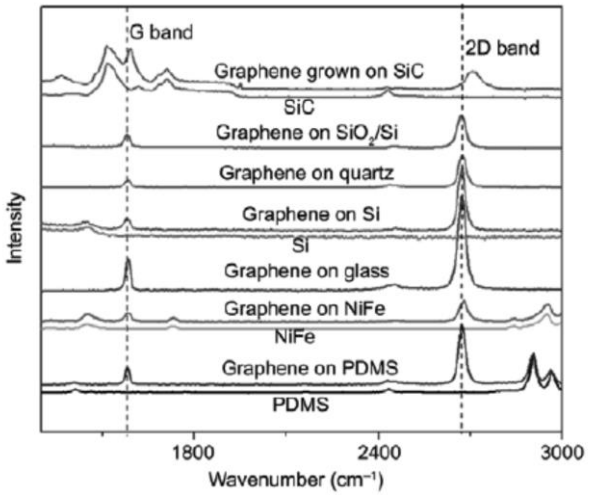

Figure 1.5 – Raman spectra of SLG on different substrates, including epitaxial monolayer graphene on SiC. [90]

A rapid and precise method to determining the number of graphene layers is needed in order to improve the graphene research and his applications. Although atomic force microscopy (AFM) measurement is the most direct way to identify the number of graphene layers, the method has a very slow throughput. Furthermore, an instrumental offset of ~0.5 nm (caused by different interactions forces) always exists, which is even larger than thickness of a graphene monolayer and data fitting is required to extract the true thickness of graphene sheets[86]. The obvious difference between Raman characteristic of graphene monolayer and graphite is 2D band (Figure 1.3 – B). For monolayer, the 2D band can be fitted with a sharp and symmetric peak while that for graphite can be fitted with two peaks. The 2D band becomes broader and blueshifted when the number of layers increases (Figure 1.4). When the Raman spectrum has a sharp and symmetric 2D band it is consensual say that we are in the presence of a graphene monolayer [89] (see Figure 1.3 – B). Unfortunately, the differences in the 2D band between two and few layers of graphene sheets are not unambiguous in the Raman spectra. Although there are differences in the 2D band, the intensity of the G band increases almost linearly as the graphene thickness increases. This can be readily understood as more carbon atoms are detected for multi-layer graphene. Therefore, the intensity of the G band can be used to determine the number of graphene layers[84].

As was already said, graphene characteristic bands in the Raman spectrum are dependent on the substrate (Figure 1.5); however, this effect is not meaningful as was shown by Ni and co-workers[84,90]. Single-layer graphene (SLG) sheet was produced on transparent (glass and quartz), flexible (PET and PDMS), conductive materials (NiFe and Si) and also in most widely used substrate SiO_2/Si; Raman spectrum of epitaxial graphene growth on SiC is also shown. The most important difference is between Raman spectra of epitaxial graphene growth on SiC and graphene deposited on all the others substrates. The first one shows a significant 2D band blueshift which can be explained by the strain effect of the substrate.

The oxidation and exfoliation processes generate changes in graphene Raman spectrum when compared to graphite (Figure 1.6). Raman spectroscopy is a widely used tool for the characterization of this type of materials because the conjugated and double carbon–carbon bonds lead to high Raman intensities. Multi-layer graphene

oxide is the one with more differences from graphite. D and G bands are slightly more intense. G band is larger, and shows a shift to higher frequencies. This shift has two reasons: the existence of areas that were not oxidised and the resonance of double bond at higher frequencies than G band of graphite, being this the main reason for the band shift[91].

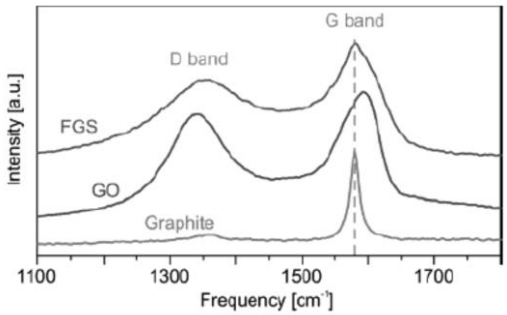

Figure 1.6 – Evolution of the Raman spectra during the oxidation and exfoliation processes for graphite, GO, and FGS (few layer graphene sheets). All the spectra correspond to an exciting laser wavelength of 514.5 nm. The position of the G band in graphite is indicated by the vertical dashed line[91].

All the studies about carbon-based materials here presented show the importance of Raman spectroscopy in structural studies useful to distinguish graphene and graphene oxide, mono- or multi-layer.

1.4. Carbon nanostructures and SERS

1.4.1. Graphene nanocomposites as SERS substrates

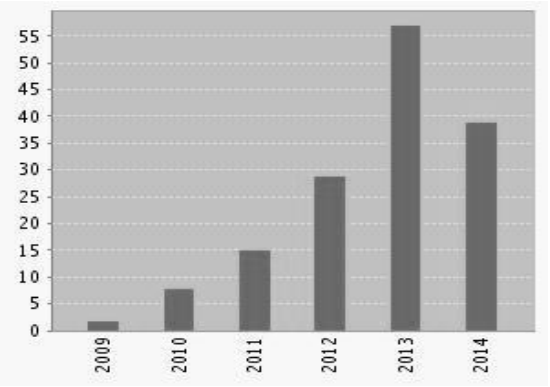

Figure 1.7 – Published Items (TITLE: *(graphene) AND* TOPIC: *(sers)*, Timespan=All years) in Each Year. Web of knowledge, 21-10-2014.

The Figure 1.7 shows the growing interest of graphene-based nanocomposites by researchers and their effort to improve this nanomaterial as an efficient SERS substrate.

In 2010, a new material was used as active-SERS substrate: graphene. Ling and co-workers[9] used graphene to detect popular molecules widely used as a Raman probe: phthalocyanine (Pc), rhodamine 6G (R6G), protoporphyin IX (PPP), and crystal violet (CV). Such molecules were deposited equally on graphene and a SiO_2/Si substrate using vacuum evaporation or solution soaking. By comparing the Raman signals of molecules on monolayer graphene and on a SiO_2/Si substrate, it can be observed that the intensities of the Raman signals on monolayer graphene are stronger than on SiO_2/Si, indicating a clear Raman enhancement effect on the surface of monolayer graphene. In the case of solution soaking, the Raman signals of the molecules are visible even though the concentration is low to 10^{-8} mol dm^{-3} or less while there is only a fluorescence background from the SiO_2/Si substrate. The intensities decrease with an increase in the number of graphene layers and the signals are not observed on graphite and highly ordered pyrolytic graphite (HOPG). The Raman enhancement factors were between 2 and 17 and were calculated by taking the signals on the SiO_2/Si substrate as references, and they were dependent on the symmetry of the molecules. This was the first report about the Raman enhancement on the surface of graphene and this work was a contribution to the SERS phenomenon explanation especially in terms of charge transfer between the analyte and the substrate.

Although the positive results with graphene as SERS substrate, the enhancement factors were not high enough for practical applications. For that reason, a combination of graphene with plasmonic nanoparticles can be foreseen for the design and fabrication of novel devices with sensing capabilities[11].

1.4.1.1. Association of metal nanoparticles with graphene nanostructures

Xu et al[12] have reported the first study using graphene and silver nanoparticles. In such report, silver-nanoparticle films using graphene oxide sheets as substrates were

prepared through the silver-mirror reaction. The enhanced Raman signal of graphene oxide sheets in the composites indicated the SERS activity of such silver particle films, and the degree of enhancement could be controlled by adjusting the density of the silver particles. Such SERS-active silver films may hold some advantages as generic SERS substrates for the study of a variety of target molecules, for example, the structural and electronic characteristics of graphene oxide sheets. Additionally, these studies also indicate the feasibility of using graphene oxide sheets as substrates for the preparation of nanoparticle films, including metal, semiconductor, and insulating particle films.

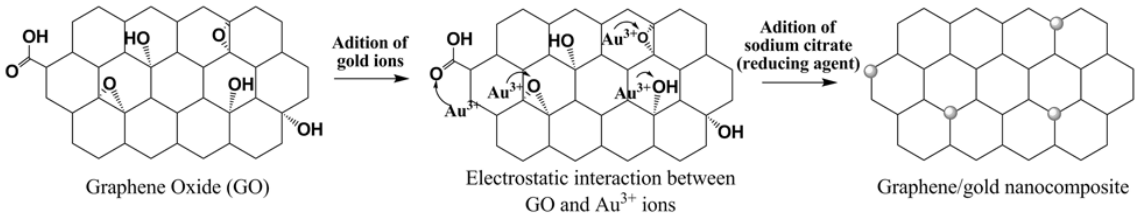

Figure 1. 8 – Scheme of nucleation and formation of gold nanoparticles on graphene oxide sheet surface[11].

The first report using graphene and gold nanoparticles as SERS substrate was published by Gonçalves et al[11]. In this work, was shown that the presence of oxygen functionalities at graphene surface provides reactive sites for the nucleation and growth of gold nanoparticles (Figure 1. 8). Gold nanoparticles are effectively grown at functionalized graphene surfaces using a simple chemical method in aqueous medium. The nucleation and growth mechanism depends on the degree of oxygen functionalization at the graphene surface sheets, no gold nanoparticles were obtained at totally reduced graphene surfaces. Additionally, these studies have shown that the graphene/gold nanocomposites act as substrates for surface enhanced Raman scattering.

After these two major contributions to developing new SERS substrates based on graphene and metallic nanoparticles, other publications have shown the potentialities

of this type of nanocomposites as sensors. Only in the last two years, about 80 papers were published on the subject.

Gold and silver nanoparticles are the metallic nanoparticles that were used in almost all the works with graphene and SERS. Also, Ga[92], Pd[93] and Cu[94] were used to decorate graphene sheets in order to enhance Raman scattering. The introduction of Ga nanoparticles on graphene sheets allows the study of charge transfer and plasmonic coupling contribution to the enhancement of Raman modes of graphene. Besides that, Ga nanoparticles on graphene/SiC show a surface plamon resonance that can be tailored from UV to the visible range[92]. CuGO nanocomposites were prepared by a reduction *in situ* using $NaBH_4$ as reducing agent. The copper nanoparticles on graphene surface produced by this method were distributed homogeneously with a controlled size[94]. The study of the introduction of Pd nanoparticles on graphene sheets surface was made in comparison to Au nanoparticles. Fu et al. have shown that Pd nanoparticles have not the plasmonic properties to enhance the Raman scattering because as SERS substrate they were considerably weaker than graphene and Au[93].

The investigation of metal nanoparticles and graphene composites has evolved to achieve greater enhancement factors. For this, the use of gold and silver nanoparticles with shapes different from spherical[95] has been greatly explored as well as the combination of these two metals in a single composite[96]. Popcorn-shaped gold nanoparticles were attached on graphene sheets and this hybrid material was used to detect HIV DNA without any labeling. Furthermore, experimental data with this novel SERS substrate show excellent reproducibility of the SERS signal[97]. Gold nano-pyramids were deposited on graphene surface to develop a biocompatible SERS platform that enables single molecule detection and provides a reproducible and uniform response. This shape of gold nanoparticles generates a high density of "hot spots" with SERS enhancement factors over 10^{10}. Gold nanoparticles were also tuned as hexagonal and triangular on graphene by thermally annealing between 600 and 800 ºC and their growth is dependent on the number of layers. The platform based on graphene and these so-called gold islands exhibit excellent SERS effect on Raman spectra of few-layer graphene with the enhancement factors up to several hundreds[98]. In Lee work[99] it is possible to see that gold nanospheres, nanorods and nanooctahedra

assembled on graphene sheets by electrostatic interactions show SERS evidence. In this study, nanorods have the highest enhancement factor of the three types of gold nanocrystals synthesized[99]. Gold-silver-graphene (Au@Ag-G) composites were prepared and are SERS-active substrates[100,101].

The nanocomposites based on graphene and metal nanoparticles are mostly produced by chemical reduction of both graphene oxide and a metal salt because the chemical reduction of graphene oxide is easier to obtain in large-scale. Moreover, the oxygen functionalities of graphene oxide allow the nucleation of metal nanoparticles and, consequently promote a good dispersion of these nanoparticles on the graphene sheet surface[11]. Some of the chemical reducing agents used are sodium citrate[11], ascorbic acid[102], tannic acid[103], N,N-dimethylformamide (DMF)[104], and etilenoglycol[93]. Gum arabic, a natural polymer, was also used to exfoliate graphene sheets and reduce silver nitrate into silver nanoparticles[105].

1.4.1.2. Different structure of SERS substrates based on graphene nanocomposites

The enhancement of Raman scattering may be promoted by a substrate containing plasmonic nanostructures, originating the SERS effect. As was mentioned in SERS sub-chapter, lithography is described as the best technique to make the substrates with this feature and to have the best results in terms of enhancement factors. However, this technique is expensive and requires specific laboratory equipment. There are studies where metal nanoparticles were deposited on a support and graphene single-layer was deposited on the top of such nanoparticles. Wang has shown a hybrid SERS-active platform consisting in a single layer of graphene covering quasi-periodic Au nano-pyramid arrays. The hexagonally arranged sharp Au tips, almost identical in size and topology, support markedly enhanced local fields and play a key role in the ultrahigh sensitive system. The tipped substrate can be fabricated in large scale with superior reproducibility[106]. Another example of using direct imprint is described in the paper of Long[107]. Polyethylene terephthalate (PET) substrates were imprinted by using porous anodic alumina (PAA) stamps with featuring periodic hexagonal cells, which were followed by evaporation of gold films.

The topography was tuned to optimize the enhancement factor by adjusting the of gold deposition time. Then a single-layer graphene covered the optimized gold nanostructures serving as the passivation layer; the final material exhibit significant SERS enhancement[107].

To overcome the disadvantages of lithography, some researchers have applied the functionalization of graphene with metal nanoparticles in order to create an active-SERS substrate with a very good dispersion of plasmonic nanostructures and aligned spacing interparticle. Chitosan (CS) was used to functionalize the surface of graphene oxide sheets. The negatively charged silver nanoparticles are disposed to form aggregates on GO/CS via electrostatic interaction, which is extremely beneficial to the SERS detection of aromatic molecules and the final composite remarkably enhance the main peaks of l-phenylalanine, in comparison with the silver nanoparticles alone, showing great potential for biomedical applications[108]. In other work, silver nanoparticles are attached to graphene functionalized with N-(trimethoxysilylpropyl) ethylenediaminetriacetic acid trisodium salt (TETA). With such a substrate, p-aminothiphenol (p-ATP) and melamine were detected with concentration as low as 2×10^{-8} and 2×10^{-7} M by SERS[109]. A globular protein, ß-lactoglobulin (BLG), was also used to decorate reduced graphene oxide sheets (RGO) and the obtained BLG-RGO composite that can be dispersed in aqueous solution with pH-sensitive solubility. Due to the adsorption of ß-Lactoglobulin on the surface of graphene sheets, the BLG-RGO composite was further used as template for Au nanoparticles assembly. These Au nanoparticles assembled on the BLG-RGO composite were shown to yield a large SERS enhancement for Rhodamine 6G[110]. Poly(diallyldimethylammonium chloride) (PDDA), a polyelectrolyte, was used to functionalize graphene oxide sheets which were decorated with silver nanoparticles. The GO/PDDA/AgNP composite was used successfully to detect folic acid with ultrahigh sensitivity. In fact, with this substrate it was possible to detect folic acid in water in a concentration of 9 nmol dm^{-3} [111].

In order to develop a specific sensor to detect 2,4,6-trinitrotoluene (TNT), the surface of silver nanoparticles were modified with p-aminothiophenol (PATP) and after that were supported on graphene sheets. This SERS substrate allows the detection of TNT with concentration as low as 10^{-11} mol dm^{-3} [112]. Other example of nanoparticle surface modification is the functionalization of gold nanoparticles with 2-mercaptopyridine.

These modified nanoparticles were then attached on graphene oxide and reduced graphene oxide sheets via π-π stacking and other molecular interactions[113].

In most of the examples mentioned the physical structure of the SERS substrate is as colloidal suspension or as deposited on some solid support, such as SiO_2/Si. Only a few attempts were made towards fabricating flexible plasmonic devices using such assembled graphene – plasmonic particle nanocomposites, despite the fact that graphene or graphene oxide can be easily processed into free- standing flexible substrates [12,114]. For example, Xu et al.[12] demonstrated the fabrication of flexible free-standing metal nanoparticle films using a graphene oxide substrate by simply drying the concentrated graphene oxide–metal nanoparticle dispersion on a glass substrate. More recently, Xu et al.[114] reported a new kind of flexible SERS substrates, the so called G-SERS (graphene-mediated SERS) tape by depositing Au nanoparticles on atomically flat graphene by vacuum thermal evaporation. In such SERS tapes, the "hot spots" that are generated in the deposited Au nanostructures by strong LSPR coupling through the single layer graphene render the graphene surface a hot surface for SERS. They also observed that the SERS signals from G-SERS were cleaner than those of pure Au nanoparticles on rigid SiO_2 substrates. Such substrates could be used for real time analysis of samples and they were even reusable by washing the substrate after the measurement. Other example was shown by Li et al. where a flexible reduced graphene oxide paper modified with silver nanoparticles was used to detect R6G with a concentration of 10^{-8} mol dm^{-3}. this type of SERS substrate is easy to process in large scale and also acts as a portable antibacterial substrate[115]. As these substrates are flexible, they could be useful for the ultrasensitive detection of any contaminants on substrates that are not flat. The field of graphene– plasmonic nanoparticle composites is relatively new and there is plenty of room for exploring the large scale fabrication of low cost flexible plasmonic sensing devices based on flexible graphene– plasmonic composite substrates[7].

1.4.1.3. Graphene-surface enhanced Raman scattering (GERS)

As was already mentioned, graphene itself show an enhancement in the Raman signal of some molecules[9], phenomenon called by some authors as Graphene Surface-enhanced Raman scattering – GERS. But it can be said that the main advantage of the use of graphene as SERS substrate is the research about chemical enhancement. There are some works which use only graphene, others use graphene and metal nanoparticles and even others compare graphene to its derivatives in terms of SERS results.

The enhancement of Raman spectral features of graphene itself was studied using metal nanoparticles. The Au nanoparticles improved spectroscopic characterization by quenching fluorescence, allowing the graphene D and G bands to be quantified, and yielding a surface enhancement [93,116,117]. Also SERS of graphene was studied using a modified Au electrode. In the latter system, both D- and G-band wavenumbers linearly depend on the potential applied. The effect was explained in terms of changes in the C-C bond length induced by electrochemical doping[118]. Other approach of graphene SERS is made with the use of silver nanoparticles. The Ag deposition on graphene induced a large enhancement in the Raman signal and caused a shift in the characteristic bands positions [119,120]. Other parameter that was also used to characterize graphene by Raman spectroscopy is the ratio of the intensities of D and G bands (ratio D/G) which increased when graphene was deposited on Ag substrate[121].

Graphene as SERS substrate by itself was firstly shown in the work of Ling et al[9]. The enhancement of Raman peaks of some dyes were compared between graphene single-layer and SiO_2 substrates and the results have showed a clear enhancement with graphene indicating the Raman enhancement effect on the surface of monolayer graphene. With this system, Raman enhancement factors were taking using Raman intensity ratios. The Raman enhancement factors were quite different for different peaks, changing from 2 to 17, and can be distinguished through three classes that correspond to the symmetry of the molecular vibrations. This enhancement was attributed to charge transfer between graphene and the molecules, which result in a chemical enhancement. After this study there were some others to improve this

concept. The enhancement factors were shown to be dependent of the reduction time of graphene oxide and SERS spectra of RhB molecules on reduced graphene oxide reproduced all important spectral fingerprints of the molecule with a negligible frequency shift[122]. Copper phtalocyanine (CuPc), a planar molecule, was used to investigate the effect of molecular orientation on the intensity of chemical enhancement using graphene as SERS substrate. In this work it was shown that the stronger the interaction, the more the Raman signal is enhanced, and the analyte-substrate interaction depend on the different molecular orientation of the analyte. Besides their contribution to understand the chemical enhancement this work has shown that the magnitude of the chemical enhancement can be used to evaluate the degree of interaction between the molecules and graphene[123]. Other contribution to chemical enhancement studies was developed by Yaghobian et al., where graphene sheets are used to enhance Raman signals of 4-mercaptobenzoic acid (4-MBA) with reproducible enhancement factors[124] . R6G was the molecule chosen to study systematically charge transfer on graphene, graphene oxide and reduced graphene oxide. Although their structural similarity, the three different substrates have shown different spectral features due to different enhancement contributions from the local chemical groups and the global π-conjugation network of the substrates. The Raman signals of R6G were increased with the number of GO layers, while shown inverse trend when graphene and reduced graphene oxide were used due to a dominant π-π stacking mechanism. The absence of electromagnetic enhancement and the rich chemical structure makes GO an excellent choice as a tunable substrate in order to study the chemical enhancement resulting from the adsorbent-substrate interaction[125].

Finally, Sil et al.[126] query the existence of SERS phenomenon using graphene. The work has shown Raman signals of different analytes adsorbed on carbonaceous materials, such as, chemically reduced graphene, graphene oxide (GO), multi-walled carbon nanotube (MWCNT), graphite and activated carbon. The analytes selected for the study were Rhodamine 6G (R6G) (in resonant conditions), Rhodamine B (RB), Nile blue (NBA), Crystal Violet (CV) and acetaminophen (paracetamol). All the analytes except paracetamol absorb and fluoresce in the visible region. Raman signals were due to resonant effect, with fluorescence suppression (in the case of fluorescent samples) owing to efficient adsorption on various carbon substrates. The enhanced

signals observed at 10^{-9} mol dm^{-3} concentrations for R6G are more due to the resonance effect rather than surface enhancement by the carbon substrates. Using this results it was shown that chemically synthesized graphene is "really" not a unique substrate for observing surface enhanced Raman signals. The results described, including the data from multiwalled carbon nanotubes, indicate that the possibility of Graphene induced surface enhanced Raman effect and the fluorescence quenching effect are open questions[126].

1.4.2. Carbon nanotubes

Carbon nanotube (CNT) is theoretically described as a cylinder fabricated of rolled up graphene sheet. It can be divided into a single or multiple walls. Nanotubes with a single wall are, commonly, denoted by single-walled carbon nanotubes (SWCNTs) and were first reported in 1993[127] while the ones with more than one wall are multi-walled carbon nanotubes (MWCNTs) and were first discovered in 1991 by Iijima[128].

These one-dimensional carbon allotropes are of high mechanical strength, rich electronic properties, high surface area, excellent chemical and thermal stability[129]. Such properties allow CNT be explored in many research fields: biomedicine (artificial implants, tissue engineering, cancer cell identification)[130,131], energy[132-134], electronic[135,136] and sensor devices[137,138]. As in graphene research, also CNT have been exploited when functionalized with metal nanoparticles. These nanocomposites can be applied in catalysis, fuel cells or chemo/biosensors[139]. The last application can be made by using electrochemical measurements or SERS identification technique[140].

In SERS, the functionalized CNT were used dispersed in solution[141], as an endoscope tip[142,143], specifically functionalized for use as an intracellular probe[144,145] or vertically aligned in a silicon support[146-148]. Vertically aligned multi-walled carbon nanotubes (VAMWCNT), or CNT forests, functionalized with gold nanoparticles showed highly sensitive SERS signals at very low target concentration down to 10 fmol dm^{-3} due to the high-density of gold nanoparticles, in a unit volume, by the densification of nanotubes[149]. Moreover, the design of 3D gold covered VAMWCNT SERS substrates on silica supports allows the patterned arrays for multiplex SERS detection[148].

Besides the advances in SERS detection using VAMWCNT arrays and the good results obtained, it still has a long way to optimize and fabricate uniform 3D SERS substrates.

1.5. Aims of the thesis

Based on the potential of SERS in the detection of biomolecules and the characteristics of carbon nanostructures, the research presented in this thesis was directed toward the development of nanostructures that can be a contribution to active SERS substrates.

The approach of getting closer the real world and the research work was one of the concerns in this project. The development of SERS substrates that could be used without restrictions and in a practical way in the chemical analysis laboratory was always present throughout the work. To this end, also the materials used in the synthesis of the nanoparticles, as well as the basis used to support graphene and nanoparticles were eco-friendly.

The general objectives of this work are:

1) Development of carbon nanocomposites based on the *in situ* synthesis of metal nanoparticles using graphene oxide. Optimize the synthesis procedure testing several reducing agents.

2) Evaluation of the performance of graphene nanocomposites in SERS, using several supports, a variety of analytes and different Raman setups.

3) Development of rigid structures that can support well distributed metal nanoparticles to enhance the Raman signal of molecular analytes. Optimize the process of polymeric membranes synthesis using the freeze-thawing technique and electrospinning. Introduce graphene nanocomposites in membranes produced by electrospinning in order to contribute for an enhancement of the detection limit of the tested analytes.

5) Optimization of the production of vertically aligned multiwall carbon nanotubes (VAMWCNT) covered with gold to achieve the best conditions to assess SERS activity for the detection of biomolecules.

1.6. Bibliography

(1) Vendrell, M.; Maiti, K. K.; Dhaliwal, K.; Chang, Y. T. Surface-enhanced Raman scattering in cancer detection and imaging. *Trends in Biotechnology* **2013**, *31*, 249-257.

(2) Alvarez-Puebla, R. A.; Liz-Marzan, L. M. SERS-Based Diagnosis and Biodetection. *Small* **2010**, *6*, 604-610.

(3) Schlucker, S. SERS Microscopy: Nanoparticle Probes and Biomedical Applications. *Chemphyschem* **2009**, *10*, 1344-1354.

(4) Liu, Z. M.; Guo, Z. Y.; Zhong, H. Q.; Qin, X. C.; Wan, M. M.; Yang, B. W. Graphene oxide based surface-enhanced Raman scattering probes for cancer cell imaging. *Physical Chemistry Chemical Physics* **2013**, *15*, 2961-2966.

(5) Keren, S.; Zavaleta, C.; Cheng, Z.; de la Zerda, A.; Gheysens, O.; Gambhir, S. S. Noninvasive molecular imaging of small living subjects using Raman spectroscopy. *Proceedings of the National Academy of Sciences of the United States of America* **2008**, *105*, 5844-5849.

(6) Qian, X. M.; Peng, X. H.; Ansari, D. O.; Yin-Goen, Q.; Chen, G. Z.; Shin, D. M.; Yang, L.; Young, A. N.; Wang, M. D.; Nie, S. M. In vivo tumor targeting and spectroscopic detection with surface-enhanced Raman nanoparticle tags. *Nature Biotechnology* **2008**, *26*, 83-90.

(7) Polavarapu, L.; Liz-Marzan, L. M. Towards low-cost flexible substrates for nanoplasmonic sensing. *Physical Chemistry Chemical Physics* **2013**, *15*, 5288-5300.

(8) Ling, X.; Moura, L. G.; Pimenta, M. A.; Zhang, J. Charge-Transfer Mechanism in Graphene-Enhanced Raman Scattering. *Journal of Physical Chemistry C* **2012**, *116*, 25112-25118.

(9) Ling, X.; Xie, L. M.; Fang, Y.; Xu, H.; Zhang, H. L.; Kong, J.; Dresselhaus, M. S.; Zhang, J.; Liu, Z. F. Can Graphene be used as a Substrate for Raman Enhancement? *Nano Letters* **2010**, *10*, 553-561.

(10) Ling, X.; Zhang, J. First-Layer Effect in Graphene-Enhanced Raman Scattering. *Small* **2010**, *6*, 2020-2025.

(11) Goncalves, G.; Marques, P. A. A. P.; Granadeiro, C. M.; Nogueira, H. I. S.; Singh, M. K.; Gracio, J. Surface Modification of Graphene Nanosheets with Gold Nanoparticles: The Role of Oxygen Moieties at Graphene Surface on Gold Nucleation and Growth. *Chemistry of Materials* **2009**, *21*, 4796-4802.

(12) Xu, C.; Wang, X. Fabrication of Flexible Metal-Nanoparticte Film Using Graphene Oxide Sheets as Substrates. *Small* **2009**, *5*, 2212-2217.

(13) Mohanty, N.; Berry, V. Graphene-based single-bacterium resolution biodevice and DNA transistor: interfacing graphene derivatives with nanoscale and microscale biocomponents. *Nano Letters* **2008**, *8*, 4469-4476.

(14) Cheng, Z.; Li, Q.; Li, Z.; Zhou, Q.; Fang, Y. Suspended graphene sensors with improved signal and reduced noise. *Nano letters* **2010**, *10*, 1864-1868.

(15) Compton, O. C.; Nguyen, S. T. Graphene Oxide, Highly Reduced Graphene Oxide, and Graphene: Versatile Building Blocks for Carbon-Based Materials. *Small* **2010**, *6*, 711-723.

(16) Song, B.; Li, D.; Qi, W. P.; Elstner, M.; Fan, C. H.; Fang, H. P. Graphene on Au(111): A Highly Conductive Material with Excellent Adsorption Properties for High-Resolution Bio/Nanodetection and Identification. *Chemphyschem* **2010**, *11*, 585-589.

(17) Moskovits, M. Persistent misconceptions regarding SERS. *Physical Chemistry Chemical Physics* **2013**, *15*, 5301-5311.

(18) Stiles, P. L.; Dieringer, J. A.; Shah, N. C.; Van Duyne, R. R. Surface-Enhanced Raman Spectroscopy. *Annual Review of Analytical Chemistry* **2008**, *1*, 601-626.

(19) Otto, A.; Billmann, J.; Eickmans, J.; Erturk, U.; Pettenkofer, C. The Adatom Model of Sers (Surface Enhanced Raman-Scattering) - the Present Status. *Surface Science* **1984**, *138*, 319-338.

(20) Adrian, F. J. Charge-Transfer Effects in Surface-Enhanced Raman-Scattering. *Journal of Chemical Physics* **1982**, *77*, 5302-5314.

(21) Michaels, A. M.; Nirmal, M.; Brus, L. E. Surface enhanced Raman spectroscopy of individual rhodamine 6G molecules on large Ag nanocrystals. *Journal of the American Chemical Society* **1999**, *121*, 9932-9939.

(22) Qian, X. M.; Nie, S. M. Single-molecule and single-nanoparticle SERS: from fundamental mechanisms to biomedical applications. *Chemical Society Reviews* **2008**, *37*, 912-920.

(23) Kneipp, K.; Wang, Y.; Kneipp, H.; Perelman, L. T.; Itzkan, I.; Dasari, R.; Feld, M. S. Single molecule detection using surface-enhanced Raman scattering (SERS). *Physical Review Letters* **1997**, *78*, 1667-1670.

(24) Dieringer, J. A.; Lettan, R. B.; Scheidt, K. A.; Van Duyne, R. P. A frequency domain existence proof of single-molecule surface-enhanced Raman Spectroscopy. *Journal of the American Chemical Society* **2007**, *129*, 16249-16256.

(25) Le Ru, E. C.; Meyer, M.; Etchegoin, P. G. Proof of single-mokeule sensitivity in surface enhanced Raman scattering (SERS) by means of a two-analyte technique. *Journal of Physical Chemistry B* **2006**, *110*, 1944-1948.

(26) Abalde-Cela, S.; Aldeanueva-Potel, P.; Mateo-Mateo, C.; Rodriguez-Lorenzo, L.; Alvarez-Puebla, R. A.; Liz-Marzan, L. M. Surface-enhanced Raman scattering biomedical applications of plasmonic colloidal particles. *Journal of the Royal Society Interface* **2010**, *7*, S435-S450.

(27) Driscoll, A. J.; Harpster, M. H.; Johnson, P. A. The development of surface-enhanced Raman scattering as a detection modality for portable in vitro diagnostics: progress and challenges. *Physical Chemistry Chemical Physics* **2013**, *15*, 20415-20433.

(28) Xie, W.; Schlücker, S. Medical applications of surface-enhanced Raman scattering. *Physical chemistry chemical physics : PCCP* **2013**, *15*, 5329-5344.

(29) Lin, X. M.; Cui, Y.; Xu, Y. H.; Ren, B.; Tian, Z. Q. Surface-enhanced Raman spectroscopy: substrate-related issues. *Anal Bioanal Chem* **2009**, *394*, 1729-1745.

(30) Ren, B.; Liu, G. K.; Lian, X. B.; Yang, Z. L.; Tian, Z. Q. Raman spectroscopy on transition metals. *Anal Bioanal Chem* **2007**, *388*, 29-45.

(31) Wang, D. S.; Chew, H.; Kerker, M. Enhanced Raman scattering at the surface (SERS) of a spherical particle. *Appl Opt* **1980**, *19*, 2256-2257.

(32) Wu, D. Y.; Li, J. F.; Ren, B.; Tian, Z. Q. Electrochemical surface-enhanced Raman spectroscopy of nanostructures. *Chem Soc Rev* **2008**, *37*, 1025-1041.

(33) Yeh, Y. C.; Creran, B.; Rotello, V. M. Gold nanoparticles: preparation, properties, and applications in bionanotechnology. *Nanoscale* **2012**, *4*, 1871-1880.

(34) Ahmadi, T. S.; Wang, Z. L.; Green, T. C.; Henglein, A.; El-Sayed, M. A. Shape-Controlled Synthesis of Colloidal Platinum Nanoparticles. *Science* **1996**, *272*, 1924-1926.

(35) Moskovits, M. The dependence of the metal--molecule vibrational frequency on the mass of the adsorbate and its relevance to the role of adatoms in surface-enhanced raman scattering. *Chemical Physics Letters* **1983**, *98*, 498-502.

(36) Diane, S. K.; Ronald, W.; Lawrence, P.; William, B. W. Surface-enhanced Raman spectroscopy of chemical vapor deposited diamond films. *Applied Physics Letters* **1990**, *56*, 1320-1322.

(37) Grabar, K. C.; Smith, P. C.; Musick, M. D.; Davis, J. A.; Walter, D. G.; Jackson, M. A.; Guthrie, A. P.; Natan, M. J. Kinetic Control of Interparticle Spacing in Au

Colloid-Based Surfaces:â€‰ Rational Nanometer-Scale Architecture. *J Am Chem Soc* **1996**, *118*, 1148-1153.

(38) Brown, K. R.; Natan, M. J. Hydroxylamine Seeding of Colloidal Au Nanoparticles in Solution and on Surfaces. *Langmuir* **1998**, *14*, 726-728.

(39) Wang, H.; Levin, C. S.; Halas, N. J. Nanosphere Arrays with Controlled Sub-10-nm Gaps as Surface-Enhanced Raman Spectroscopy Substrates. *J Am Chem Soc* **2005**, *127*, 14992-14993.

(40) Mulvihill, M.; Tao, A.; Benjauthrit, K.; Arnold, J.; Yang, P. Surface-enhanced Raman spectroscopy for trace arsenic detection in contaminated water. *Angewandte Chemie-International Edition* **2008**, *47*, 6456-6460.

(41) Tao, A. R.; Huang, J.; Yang, P. Langmuir-Blodgettry of Nanocrystals and Nanowires. *Accounts of Chemical Research* **2008**, *41*, 1662-1673.

(42) Zhang, C.-L.; Lv, K.-P.; Huang, H.-T.; Cong, H.-P.; Yu, S.-H. Co-assembly of Au nanorods with Ag nanowires within polymer nanofiber matrix for enhanced SERS property by electrospinning. *Nanoscale* **2012**, *4*, 5348-5355.

(43) Zhang, C.-L.; Lv, K.-P.; Cong, H.-P.; Yu, S.-H. Controlled Assemblies of Gold Nanorods in PVA Nanofiber Matrix as Flexible Free-Standing SERS Substrates by Electrospinning. *Small* **2012**, *8*, 648-653.

(44) Zhang, L.; Gong, X.; Bao, Y.; Zhao, Y.; Xu, M.; Jiang, C.; Fong, H. Electrospun Nanofibrous Membranes Surface-Decorated with Silver Nanoparticles as Flexible and Active/Sensitive Substrates for Surface-Enhanced Raman Scattering. *Langmuir* **2012**, *28*, 14433-14440.

(45) Chua, C. K.; Pumera, M. Chemical reduction of graphene oxide: a synthetic chemistry viewpoint. *Chemical Society Reviews* **2013**.

(46) McNaught, A. D.; Wilkinson, A.; International Union of Pure and Applied, C.: *Compendium of chemical terminology : IUPAC recommendations*; 2nd ed.; Blackwell Science: Oxford [England] ; Malden, MA, USA, 1997.

(47) Aizawa, T.; Souda, R.; Otani, S.; Ishizawa, Y. Bond softening in monolayer graphite formed on transition-metal carbide surfaces. *Physical Review B* **1990**, *42*, 11469-11478.

(48) Arnoult, W. J.; McLellan, R. B. The solubility of carbon in rhodium ruthenium, iridium and rhenium. *Scripta Metallurgica* **1972**, *6*, 1013-1018.

(49) Berger, C.; Song, Z.; Li, X.; Wu, X.; Brown, N.; Naud, C.; Mayou, D.; Li, T.; Hass, J.; Marchenkov, A. N.; Conrad, E. H.; First, P. N.; de Heer, W. A. Electronic confinement and coherence in patterned epitaxial graphene. *Science* **2006**, *312*, 1191-1196.

(50) Forbeaux, I.; Themlin, J. M.; Debever, J. M. High-temperature graphitization of the 6H-SiC face. *Surface Science* **1999**, *442*, 9-18.

(51) Fujita, T.; Kobayashi, W.; Oshima, C. Novel structures of carbon layers on a Pt(111) surface. *Surface and Interface Analysis* **2005**, *37*, 120-123.

(52) Itchkawitz, B. S.; Lyman, P. F.; Ownby, G. W.; Zehner, D. M. Monolayer graphite on TaC(111): electronic band structure. *Surface Science* **1994**, *318*, 395-402.

(53) Terai, M.; Hasegawa, N.; Okusawa, M.; Otani, S.; Oshima, C. Electronic states of monolayer micrographite on TiC(111)-faceted and TiC(410) surfaces. *Applied Surface Science* **1998**, *130-132*, 876-882.

(54) Geim, A. K. Graphene: Status and Prospects. *Science* **2009**, *324*, 1530-1534.

(55) Edwards, R. S.; Coleman, K. S. Graphene synthesis: relationship to applications. *Nanoscale* **2013**, *5*, 38-51.

(56) Lee, C.; Wei, X. D.; Kysar, J. W.; Hone, J. Measurement of the elastic properties and intrinsic strength of monolayer graphene. *Science* **2008**, *321*, 385-388.

(57) Balandin, A. A.; Ghosh, S.; Bao, W. Z.; Calizo, I.; Teweldebrhan, D.; Miao, F.; Lau, C. N. Superior thermal conductivity of single-layer graphene. *Nano Letters* **2008**, *8*, 902-907.

(58) Nair, R. R.; Blake, P.; Grigorenko, A. N.; Novoselov, K. S.; Booth, T. J.; Stauber, T.; Peres, N. M. R.; Geim, A. K. Fine structure constant defines visual transparency of graphene. *Science* **2008**, *320*, 1308-1308.

(59) Dreyer, D. R.; Ruoff, R. S.; Bielawski, C. W. From conception to realization: an historial account of graphene and some perspectives for its future. *Angewandte Chemie (International ed. in English)* **2010**, *49*, 9336-9344.

(60) Brodie, B. C. On the Atomic Weight of Graphite. *Proceedings of Royal Society of London* **1859**, *10*, 11-12.

(61) Staudenmaier, L. Verfahren zur Darstellung der Graphitsäure. *Berichte der deutschen chemischen Gesellschaft* **1898**, *31*, 1481-1487.

(62) Hummers, W. S.; Offeman, R. E. Preparation of Graphitic Oxide. *J Am Chem Soc* **1958**, *80*, 1339-1339.

(63) Marcano, D. C.; Kosynkin, D. V.; Berlin, J. M.; Sinitskii, A.; Sun, Z.; Slesarev, A.; Alemany, L. B.; Lu, W.; Tour, J. M. Improved synthesis of graphene oxide. *Acs Nano* **2010**, *4*, 4806-4814.

(64) Kuila, T.; Mishra, A. K.; Khanra, P.; Kim, N. H.; Lee, J. H. Recent advances in the efficient reduction of graphene oxide and its application as energy storage electrode materials. *Nanoscale* **2013**, *5*, 52-71.

(65) Park, O.-K.; Hahm, M. G.; Lee, S.; Joh, H.-I.; Na, S.-I.; Vajtai, R.; Lee, J. H.; Ku, B.-C.; Ajayan, P. M. In Situ Synthesis of Thermochemically Reduced Graphene Oxide Conducting Nanocomposites. *Nano Letters* **2012**, *12*, 1789-1793.

(66) Pham, V. H.; Cuong, T. V.; Hur, S. H.; Oh, E.; Kim, E. J.; Shin, E. W.; Chung, J. S. Chemical functionalization of graphene sheets by solvothermal reduction of a graphene oxide suspension in N-methyl-2-pyrrolidone. *Journal of Materials Chemistry* **2011**, *21*, 3371-3377.

(67) Ren, P.-G.; Yan, D.-X.; Chen, T.; Li, Z.-M. Temperature dependence of graphene oxide reduced by hydrazine hydrate. *Nanotechnology* **2011**, *22*, 55705-55705.

(68) Gao, W.; Alemany, L. B.; Ci, L.; Ajayan, P. M. New insights into the structure and reduction of graphite oxide. *Nat Chem* **2009**, *1*, 403-408.

(69) Loh, K. P.; Bao, Q. L.; Eda, G.; Chhowalla, M. Graphene oxide as a chemically tunable platform for optical applications. *Nature Chemistry* **2010**, *2*, 1015-1024.

(70) Stankovich, S.; Dikin, D. A.; Piner, R. D.; Kohlhaas, K. A.; Kleinhammes, A.; Jia, Y.; Wu, Y.; Nguyen, S. T.; Ruoff, R. S. Synthesis of graphene-based nanosheets via chemical reduction of exfoliated graphite oxide. *Carbon* **2007**, *45*, 1558-1565.

(71) Wang, G.; Yang, J.; Park, J.; Gou, X.; Wang, B.; Liu, H.; Yao, J. Facile Synthesis and Characterization of Graphene Nanosheets. *The Journal of Physical Chemistry C* **2008**, *112*, 8192-8195.

(72) Shin, H.-J.; Kim, K. K.; Benayad, A.; Yoon, S.-M.; Park, H. K.; Jung, I.-S.; Jin, M. H.; Jeong, H.-K.; Kim, J. M.; Choi, J.-Y.; Lee, Y. H. Efficient Reduction of Graphite Oxide by Sodium Borohydride and Its Effect on Electrical Conductance. *Advanced Functional Materials* **2009**, *19*, 1987-1992.

(73) Zhang, J.; Yang, H.; Shen, G.; Cheng, P.; Guo, S. Reduction of graphene oxide via L-ascorbic acid. *Chemical Communications* **2010**, *46*, 1112-1114.

(74) Stankovich, S.; Piner, R. D.; Chen, X.; Wu, N.; Nguyen, S. T.; Ruoff, R. S. Stable aqueous dispersions of graphitic nanoplatelets via the reduction of exfoliated graphite oxide in the presence of poly(sodium 4-styrenesulfonate). *Journal of Materials Chemistry* **2006**, *16*, 155-158.

(75) Mao, S.; Pu, H. H.; Chen, J. H. Graphene oxide and its reduction: modeling and experimental progress. *Rsc Advances* **2012**, *2*, 2643-2662.

(76) Cote, L. J.; Cruz-Silva, R.; Huang, J. Flash Reduction and Patterning of Graphite Oxide and Its Polymer Composite. *Journal of the American Chemical Society* **2009**, *131*, 11027-11032.

(77) Saito, R.; Dresselhaus, G.; Dresselhaus, M. S.: *Physical properties of carbon nanotubes*; Imperial College Press: London, 1998.

(78) Dresselhaus, M. S.: *Graphite fibers and filaments*; Springer: Berlin, 1988.

(79) Dresselhaus, M. S.; Dresselhaus, G.; Saito, R.; Jorio, A. Raman spectroscopy of carbon nanotubes. *Physics Reports* **2005**, *409*, 47-99.

(80) Jorio, A.; Saito, R.; Dresselhaus, G.; Dresselhaus, M. S.: *Raman Spectroscopy in Graphene Related Systems*; Wiley-VCH Verlag GmbH & Co. KGaA: Weinheim, Germany, 2011.

(81) Stampfer, C.; Molitor, F.; Graf, D.; Ensslin, K.; Jungen, A.; Hierold, C.; Wirtz, L. Raman imaging of doping domains in graphene on SiO[sub 2]. *Applied Physics Letters* **2007**, *91*, 241903-241907.

(82) Yu, T.; Ni, Z.; Du, C.; You, Y.; Wang, Y.; Shen, Z. Raman Mapping Investigation of Graphene on Transparent Flexible Substrate: The Strain Effect. *The Journal of Physical Chemistry C* **2008**, *112*, 12602-12605.

(83) Pimenta, M. A.; Dresselhaus, G.; Dresselhaus, M. S.; Cancado, L. G.; Jorio, A.; Saito, R. Studying disorder in graphite-based systems by Raman spectroscopy. *Physical Chemistry Chemical Physics* **2007**, *9*, 1276-1290.

(84) Ni, Z.; Wang, Y.; Yu, T.; Shen, Z. Raman spectroscopy and imaging of graphene. *Nano Research* **2008**, *1*, 273-291.

(85) Ferrari, A. C.; Meyer, J. C.; Scardaci, V.; Casiraghi, C.; Lazzeri, M.; Mauri, F.; Piscanec, S.; Jiang, D.; Novoselov, K. S.; Roth, S.; Geim, A. K. Raman Spectrum of Graphene and Graphene Layers. *Physical Review Letters* **2006**, *97*, 187401-187401.

(86) Gupta, A.; Chen, G.; Joshi, P.; Tadigadapa, S.; Eklund. Raman Scattering from High-Frequency Phonons in Supported n-Graphene Layer Films. *Nano Letters* **2006**, *6*, 2667-2673.

(87) Tan, P.; Deng, Y.; Zhao, Q. Temperature-dependent Raman spectra and anomalous Raman phenomenon of highly oriented pyrolytic graphite. *Physical Review B* **1998**, *58*, 5435-5435.

(88) Basko, D. M.; Piscanec, S.; Ferrari, A. C. Electron-electron interactions and doping dependence of the two-phonon Raman intensity in graphene. *Physical Review B* **2009**, *80*, 165413-165413.

(89) Cançado, L. G.; Reina, A.; Kong, J.; Dresselhaus, M. S. Geometrical approach for the study of G^{'} band in the Raman spectrum of monolayer graphene, bilayer graphene, and bulk graphite. *Physical Review B* **2008**, *77*, 245408-245408.

(90) Wang, Y. y.; Ni, Z. h.; Yu, T.; Shen, Z. X.; Wang, H. m.; Wu, Y. h.; Chen, W.; Shen Wee, A. T. Raman Studies of Monolayer Graphene: The Substrate Effect. *The Journal of Physical Chemistry C* **2008**, *112*, 10637-10640.

(91) Kudin, K. N.; Ozbas, B.; Schniepp, H. C.; Prud'homme, R. K.; Aksay, I. A.; Car, R. Raman Spectra of Graphite Oxide and Functionalized Graphene Sheets. *Nano Letters* **2007**, *8*, 36-41.

(92) Yi, C.; Kim, T.-H.; Jiao, W.; Yang, Y.; Lazarides, A.; Hingerl, K.; Bruno, G.; Brown, A.; Losurdo, M. Evidence of Plasmonic Coupling in Gallium Nanoparticles/Graphene/SiC. *Small* **2012**, *8*, 2721-2730.

(93) Fu, X. Q.; Bei, F. L.; Wang, X.; O'Brien, S.; Lombardi, J. R. Excitation profile of surface-enhanced Raman scattering in graphene-metal nanoparticle based derivatives. *Nanoscale* **2010**, *2*, 1461-1466.

(94) Zhang, K. Fabrication of copper nanoparticles/graphene oxide composites for surface-enhanced Raman scattering. *Applied Surface Science* **2012**, *258*, 7327-7329.

(95) Minati, L.; Benetti, F.; Chiappini, A.; Speranza, G. One-step synthesis of star-shaped gold nanoparticles. *Colloids and Surfaces a-Physicochemical and Engineering Aspects* **2014**, *441*, 623-628.

(96) Gupta, V. K.; Atar, N.; Yola, M. L.; Eryilmaz, M.; Torul, H.; Tamer, U.; Boyaci, I. H.; Ustundag, Z. A novel glucose biosensor platform based on Ag@AuNPs modified graphene oxide nanocomposite and SERS application. *Journal of Colloid and Interface Science* **2013**, *406*, 231-237.

(97) Fan, Z.; Kanchanapally, R.; Ray, P. C. Hybrid Graphene Oxide Based Ultrasensitive SERS Probe for Label-Free Biosensing. *Journal of Physical Chemistry Letters* **2013**, *4*, 3813-3818.

(98) Zhou, H.; Yu, F.; Chen, M.; Qiu, C.; Yang, H.; Wang, G.; Yu, T.; Sun, L. The transformation of a gold film on few-layer graphene to produce either hexagonal or triangular nanoparticles during annealing. *Carbon* **2013**, *52*, 379-387.

(99) Lee, Y. H.; Polavarapu, L.; Gao, N.; Yuan, P.; Xu, Q.-H. Enhanced Optical Properties of Graphene Oxide-Au Nanocrystal Composites. *Langmuir* **2012**, *28*, 321-326.

(100) Zhou, L.; Gu, H.; Wang, C.; Zhang, J.; Lv, M.; He, R. Study on the synthesis and surface enhanced Raman spectroscopy of graphene-based nanocomposites decorated with noble metal nanoparticles. *Colloids and Surfaces a-Physicochemical and Engineering Aspects* **2013**, *430*, 103-109.

(101) Zhang, L.; Jiang, C.; Zhang, Z. Graphene oxide embedded sandwich nanostructures for enhanced Raman readout and their applications in pesticide monitoring. *Nanoscale* **2013**, *5*, 3773-3779.

(102) Iliut, M.; Leordean, C.; Canpean, V.; Teodorescu, C.-M.; Astilean, S. A new green, ascorbic acid-assisted method for versatile synthesis of Au-graphene hybrids as efficient surface-enhanced Raman scattering platforms. *Journal of Materials Chemistry C* **2013**, *1*, 4094-4104.

(103) Zhang, Y.; Liu, S.; Wang, L.; Qin, X.; Tian, J.; Lu, W.; Chang, G.; Sun, X. One-pot green synthesis of Ag nanoparticles-graphene nanocomposites and their applications in SERS, H2O2, and glucose sensing. *Rsc Advances* **2012**, *2*, 538-545.

(104) Yang, Y.-K.; He, C.-E.; He, W.-J.; Yu, L.-J.; Peng, R.-G.; Xie, X.-L.; Wang, X.-B.; Mai, Y.-W. Reduction of silver nanoparticles onto graphene oxide nanosheets with N,N-dimethylformamide and SERS activities of GO/Ag composites. *Journal of Nanoparticle Research* **2011**, *13*, 5571-5581.

(105) Fan, J.; Shi, Z.; Ge, Y.; Wang, J.; Wang, Y.; Yin, J. Gum arabic assisted exfoliation and fabrication of Ag-graphene-based hybrids. *Journal of Materials Chemistry* **2012**, *22*, 13764-13772.

(106) Wang, P.; Liang, O.; Zhang, W.; Schroeder, T.; Xie, Y.-H. Ultra-Sensitive Graphene-Plasmonic Hybrid Platform for Label-Free Detection. *Advanced Materials* **2013**, *25*, 4918-4924.

(107) Long, K.; Luo, X.; Nan, H.; Du, D.; Zhao, W.; Ni, Z.; Qiu, T. Surface-enhanced Raman scattering from graphene covered gold nanocap arrays. *Journal of Applied Physics* **2013**, *114*.

(108) Wan, M.; Liu, Z.; Li, S.; Yang, B.; Zhang, W.; Qin, X.; Guo, Z. Silver Nanoaggregates on Chitosan Functionalized Graphene Oxide for High-Performance Surface-Enhanced Raman Scattering. *Applied Spectroscopy* **2013**, *67*, 761-766.

(109) Kumar, S. V.; Huang, N. M.; Lim, H. N.; Zainy, M.; Harrison, I.; Chia, C. H. Preparation of highly water dispersible functional graphene/silver nanocomposite for the detection of melamine. *Sensors and Actuators B-Chemical* **2013**, *181*, 885-893.

(110) Lu, F.; Zhang, S.; Gao, H.; Jia, H.; Zheng, L. Protein-Decorated Reduced Oxide Graphene Composite and its Application to SERS. *Acs Applied Materials & Interfaces* **2012**, *4*, 3278-3284.

(111) Ren, W.; Fang, Y.; Wang, E. A Binary Functional Substrate for Enrichment and Ultrasensitive SERS Spectroscopic Detection of Folic Acid Using Graphene Oxide/Ag Nanoparticle Hybrids. *Acs Nano* **2011**, *5*, 6425-6433.

(112) Liu, M.; Chen, W. Graphene nanosheets-supported Ag nanoparticles for ultrasensitive detection of TNT by surface-enhanced Raman spectroscopy. *Biosensors & Bioelectronics* **2013**, *46*, 68-73.

(113) Huang, J.; Zhang, L.; Chen, B.; Ji, N.; Chen, F.; Zhang, Y.; Zhang, Z. Nanocomposites of size-controlled gold nanoparticles and graphene oxide: Formation and applications in SERS and catalysis. *Nanoscale* **2010**, *2*, 2733-2738.

(114) Xu, W.; Ling, X.; Xiao, J.; Dresselhaus, M. S.; Kong, J.; Xu, H.; Liu, Z.; Zhang, J. Surface enhanced Raman spectroscopy on a flat graphene surface. *Proceedings of the National Academy of Sciences of the United States of America* **2012**, *109*, 9281-9286.

(115) Li, S.-K.; Yan, Y.-X.; Wang, J.-L.; Yu, S.-H. Bio-inspired in situ growth of monolayer silver nanoparticles on graphene oxide paper as multifunctional substrate. *Nanoscale* **2013**, *5*, 12616-12623.

(116) Qiu, C.; Zhou, H.; Cao, B.; Sun, L.; Yu, T. Raman spectroscopy of morphology-controlled deposition of Au on graphene. *Carbon* **2013**, *59*, 487-494.

(117) Schedin, F.; Lidorikis, E.; Lombardo, A.; Kravets, V. G.; Geim, A. K.; Grigorenko, A. N.; Novoselov, K. S.; Ferrari, A. C. Surface-Enhanced Raman Spectroscopy of Graphene. *Acs Nano* **2010**, *4*, 5617-5626.

(118) Matulaitiene, I.; Barkauskas, J.; Trusovas, R.; Raciukaitis, G.; Mazeikiene, R.; Eicher-Lorka, O.; Niaura, G. Potential dependence of SERS spectra of reduced graphene oxide adsorbed on self-assembled monolayer at gold electrode. *Chemical Physics Letters* **2013**, *590*, 141-145.

(119) Lee, J.; Novoselov, K. S.; Shin, H. S. Interaction between Metal and Graphene: Dependence on the Layer Number of Graphene. *Acs Nano* **2011**, *5*, 608-612.

(120) Li, L.; An, B.; Lahiri, A.; Wang, P.; Fang, Y. Doublet of D and 2D bands in graphene deposited with Ag nanoparticles by surface enhanced Raman spectroscopy. *Carbon* **2013**, *65*, 359-364.

(121) Ouyang, Y.; Chen, L. Surface-enhanced Raman scattering studies of few-layer graphene on silver substrate with 514 nm excitation. *Journal of Molecular Structure* **2011**, *992*, 48-51.

(122) Yu, X.; Cai, H.; Zhang, W.; Li, X.; Pan, N.; Luo, Y.; Wang, X.; Hou, J. G. Tuning Chemical Enhancement of SERS by Controlling the Chemical Reduction of Graphene Oxide Nanosheets. *Acs Nano* **2011**, *5*, 952-958.

(123) Ling, X.; Wu, J.; Xu, W.; Zhang, J. Probing the Effect of Molecular Orientation on the Intensity of Chemical Enhancement Using Graphene-Enhanced Raman Spectroscopy. *Small* **2012**, *8*, 1365-1372.

(124) Yaghobian, F.; Korn, T.; Schueller, C. Frequency Shift in Graphene-Enhanced Raman Signal of Molecules. *Chemphyschem* **2012**, *13*, 4271-4275.

(125) Yang, H. P.; Hu, H. L.; Ni, Z. H.; Poh, C. K.; Cong, C. X.; Lin, J. Y.; Yu, T. Comparison of surface-enhanced Raman scattering on graphene oxide, reduced graphene oxide and graphene surfaces. *Carbon* **2013**, *62*, 422-429.

(126) Sil, S.; Kuhar, N.; Acharya, S.; Umapathy, S. Is Chemically Synthesized Graphene 'Really' a Unique Substrate for SERS and Fluorescence Quenching? *Scientific Reports* **2013**, *3*.

(127) Iijima, S.; Ichihashi, T. Single-shell carbon nanotubes of 1-nm diameter. *Nature* **1993**, *363*, 603-605.

(128) Iijima, S. Helical Microtubules of Graphitic carbon. *Nature* **1991**, *354*, 56-58.

(129) Lin, Y.; Taylor, S.; Li, H. P.; Fernando, K. A. S.; Qu, L. W.; Wang, W.; Gu, L. R.; Zhou, B.; Sun, Y. P. Advances toward bioapplications of carbon nanotubes. *Journal of Materials Chemistry* **2004**, *14*, 527-541.

(130) Eatemadi, A.; Daraee, H.; Karimkhanloo, H.; Kouhi, M.; Zarghami, N.; Akbarzadeh, A.; Abasi, M.; Hanifehpour, Y.; Joo, S. W. Carbon nanotubes: properties, synthesis, purification, and medical applications. *Nanoscale Research Letters* **2014**, *9*.

(131) Goncalves, G.; Cruz, S. M. A.; Ramalho, A.; Gracio, J.; Marques, P. A. A. P. Graphene oxide versus functionalized carbon nanotubes as a reinforcing agent in a PMMA/HA bone cement. *Nanoscale* **2012**, *4*, 2937-2945.

(132) Xiong, Z.; Yun, Y. S.; Jin, H.-J. Applications of Carbon Nanotubes for Lithium Ion Battery Anodes. *Materials* **2013**, *6*, 1138-1158.

(133) Lota, G.; Fic, K.; Frackowiak, E. Carbon nanotubes and their composites in electrochemical applications. *Energy & Environmental Science* **2011**, *4*, 1592-1605.

(134) Centi, G.; Perathoner, S. Carbon Nanotubes for Sustainable Energy Applications. *Chemsuschem* **2011**, *4*, 913-925.

(135) Sgobba, V.; Guldi, D. M. Carbon nanotubes-electronic/electrochemical properties and application for nanoelectronics and photonics. *Chemical Society Reviews* **2009**, *38*, 165-184.

(136) Wu, Y.; Lin, X.; Zhang, M. Carbon Nanotubes for Thin Film Transistor: Fabrication, Properties, and Applications. *Journal of Nanomaterials* **2013**.

(137) Balasubramanian, K.; Burghard, M. Biosensors based on carbon nanotubes. *Analytical and Bioanalytical Chemistry* **2006**, *385*, 452-468.

(138) Kauffman, D. R.; Star, A. Graphene versus carbon nanotubes for chemical sensor and fuel cell applications. *Analyst* **2010**, *135*, 2790-2797.

(139) Wu, B.; Kuang, Y.; Zhang, X.; Chen, J. Noble metal nanoparticles/carbon nanotubes nanohybrids: Synthesis and applications. *Nano Today* **2011**, *6*, 75-90.

(140) Gong, H.; Peng, R.; Liu, Z. Carbon nanotubes for biomedical imaging: The recent advances. *Advanced Drug Delivery Reviews* **2013**, *65*, 1951-1963.

(141) Altun, A. O.; Youn, S. K.; Yazdani, N.; Bond, T.; Park, H. G. Metal-Dielectric-CNT Nanowires for Femtomolar Chemical Detection by Surface Enhanced Raman Spectroscopy. *Advanced Materials* **2013**, *25*, 4431-4436.

(142) Niu, J. J.; Schrlau, M. G.; Friedman, G.; Gogotsi, Y. Carbon Nanotube-Tipped Endoscope for In Situ Intracellular Surface-Enhanced Raman Spectroscopy. *Small* **2011**, *7*, 540-545.

(143) Najjar, S.; Talaga, D.; Schue, L.; Coffinier, Y.; Szunerits, S.; Boukherroub, R.; Servant, L.; Rodriguez, V.; Bonhommeau, S. Tip-Enhanced Raman Spectroscopy of Combed Double-Stranded DNA Bundles. *Journal of Physical Chemistry C* **2014**, *118*, 1174-1181.

(144) Wang, X.; Wang, C.; Cheng, L.; Lee, S.-T.; Liu, Z. Noble Metal Coated Single-Walled Carbon Nanotubes for Applications in Surface Enhanced Raman Scattering Imaging and Photothermal Therapy. *Journal of the American Chemical Society* **2012**, *134*, 7414-7422.

(145) Chen, P.; Wang, Z.; Zong, S.; Chen, H.; Zhu, D.; Zhong, Y.; Cui, Y. A wide range optical pH sensor for living cells using Au@Ag nanoparticles functionalized carbon nanotubes based on SERS signals. *Analytical and Bioanalytical Chemistry* **2014**, *406*, 6337-6346.

(146) Zhang, J.; Fan, T.; Zhang, X.; Lai, C.; Zhu, Y. Three-dimensional multi-walled carbon nanotube arrays coated by gold-sol as a surface-enhanced Raman scattering substrate. *Applied Optics* **2014**, *53*, 1159-1165.

(147) Zhang, J.; Chen, Y.; Fan, T.; Lai, C.; Zhu, Y. Vertically aligned multi-walled CNT arrays coated by gold nanoparticles for surface-enhanced Raman scattering. *Microsystem Technologies-Micro-and Nanosystems-Information Storage and Processing Systems* **2014**, *20*, 113-117.

(148) Goldberg-Oppenheimer, P.; Hutter, T.; Chen, B.; Robertson, J.; Hofmann, S.; Mahajan, S. Optimized Vertical Carbon Nanotube Forests for Multiplex Surface-Enhanced Raman Scattering Detection. *Journal of Physical Chemistry Letters* **2012**, *3*, 3486-3492.

(149) Lee, S.; Hahm, M. G.; Vajtai, R.; Hashim, D. P.; Thurakitseree, T.; Chipara, A. C.; Ajayan, P. M.; Hafner, J. H. Utilizing 3D SERS Active Volumes in Aligned Carbon Nanotube Scaffold Substrates. *Advanced Materials* **2012**, *24*, 5261-5266.

2. Ag-Poly(vinyl alcohol) polymer composites as SERS substrates for nucleic acid and DNA detection

This chapter focuses the importance of the morphology of SERS substrates to achieve the best enhancement in the Raman signals of biomolecules.

Here, a novel method to prepare composites of poly(vinyl alcohol) (PVA) with silver nanoparticles, is proposed. The silver nanoparticles are prepared using sodium citrate (Ag1) and glucose (Ag2) for silver (I) reduction. The synthesis *in situ* of silver nanoparticles in PVA (Ag1-PVA and Ag2-PVA) and subsequent crosslinking by freeze-thawing allows a good distribution of silver nanoparticles through the membranes. The drying time of hydrogels, the interaction time between the analyte and substrate, and the detection limit are parameters that are here evaluated for two different types of hydrogels of PVA and silver nanoparticles.

Both types of substrates allow the detection of nucleic acids and DNA in two conformations (double stranded and single stranded). The positive results obtained with Ag1-PVA and Ag2-PVA for nucleic acids and DNA, after four months of the preparation of hydrogels, indicate the stability of such SERS substrates.

2.1. Introduction

Detection of chemical and biological agents plays a pivotal role in medical, forensic, agricultural and environmental sciences.[1-3] Sensitive methods that allow identification of biomarkers such as proteins and nucleic acids at early state disease provide the prospect of better health and more effective therapy.[4] Technological platforms that provide sensors of high sensitivity, selectivity and stability are therefore in high demand. In particular, efforts are required for the development of efficient sensors with the ability to detect analytes in complex biological fluids like blood, urine, serum, etc.[5,6]

Since its discovery in the seventies, SERS (Surface-Enhanced Raman Scattering) has received increasing attention from researchers, not only because of its high sensitivity and the small volume of sample needed, but also due to the possible wide applicability. [7-9] Compared with normal Raman signals, SERS scattering cross-sections of molecules residing at or near the surface of roughened or nanostructured materials may be enhanced by factors up to $\sim 10^{14}$ or close to that of fluorescence. [10] This huge enhancement factor arises from the strong light-induced electric field at locations in metallic nanostructured spaces, often called "hot spots", which offer opportunities to develop ultrasensitive SERS-based biosensors. [2,11] In addition to high sensitivity, SERS features narrow Raman bands that lead to minimal background and favour multiplexing assays. Also, Raman scattering is insensitive to humidity, oxygen, and foreign species that often induce fluorescence quenching, making SERS a particularly suitable tool for applications in different environments. Consequently, SERS is recognized as one of the most promising tools for ultrasensitive chemical and biological analysis with the target of attaining the single-molecule level. [2,11,12]

For SERS, the emphasis to achieve strong enhancement is how to get a good substrate. The development and use of highly reproducible substrates is critical in the advance of SERS as a mainstream spectroscopic technique. This is particularly important in studies of large, complex molecules such as DNA or proteins, because the SERS signal in these molecules also depends significantly on molecular conformation, orientation, and binding specificity to the substrate surface. [13,14] Three major factors determine the quality of SERS substrates: the enhancement factor, the reproducibility, and the fabrication complexity.[15]

As SERS spectra of molecules adsorbed on metallic nanostructured films are much more stable and reproducible when compared with those in metal colloidal suspensions, there is much interest in the development of solid SERS substrates with large Raman enhancements and good reproductibility.[16,17] Several technologically demanding or costly approaches like electron beam lithography or focused ion beam milling are applied for fabricating SERS substrates with varieties of nanostructures; however these are too expensive for practical application.[18,19] The implementation of SERS as a widespread analytical tool requires large-scale manufacture of new substrates that, among other features, are inexpensive, easy to implement in diverse analytical contexts and of easy processing.[20]

Polyvinyl alcohol (PVA) could be considered as a good host material for metal and semiconductor nanoparticles, due to good thermo-stability and chemical resistance.[21,22] PVA hydrogels prepared by a physical method, so called freezing-thawing, are totally discharged from toxicity, have greater mechanical strength and elasticity than the gels produced by other processes, besides having a high swelling degree, and do not need a particular apparatus for its preparation.[23,24]

In the present work we describe the use of PVA as a silver nanoparticles (AgNP) supporting solid membrane. AgNP were prepared in situ, in the presence of PVA, by reaction with two environmental friendly reducing agents: sodium citrate[25] and glucose[26]. The obtained Ag-PVA composites were characterized by UV-vis spectrometry and SEM analysis and their ability to be used as active SERS substrates was tested first with rhodamine 6G (R6G). A systematic study was developed in order to optimize the drying conditions of the Ag-PVA composite and the interaction time between the analyte solution and the substrate before SERS detection. The limit of detection of the R6G with respect to each substrate was also determined.

The optimized Ag-PVA composites were then tested to detect nucleic acid bases (adenine - A, cytosine - C, guanine - and thymine G - T) and deoxyribonucleic acid (DNA) in its two conformations (single stranded - ssDNA, and double stranded - dsDNA) with distinguished sensitivity and uniformity.

2.2. Results and Discussion

2.2.1. Characterization of Ag-PVA substrates

Ag-PVA hydrogels were prepared by freeze-thawing, a simple technique that produces 3D polymeric networks able to support metallic nanoparticles.[27] Here, this methodology was applied by exposing an aqueous suspension of PVA and silver nanoparticles to repeated cycles of freezing at -20 ºC and thawing at room temperature. This process results in the formation of crystallites, due to the folding of PVA chains, that serves as physical crosslinks to render the material insoluble in water.[28] The organization of the PVA molecules is almost random and the areas filled with water molecules create a porous structure [29,30] as seen in Figure 2.1. where the porous microstructure is observed in the PVA composite after lyophylization. This simple method is done without need for specific equipment or additional chemical agents that could influence further SERS results with this substrate such as trace detection.

The Ag-PVA hydrogels were prepared using two different reducing agents for the silver ions, sodium citrate (Ag1-PVA) and glucose (Ag2-PVA). Figure 2.1). shows the SEM images of PVA, Ag1-PVA and Ag2-PVA immediately after its preparation (indicated by 0 h) and lyophilization. The SEM image of PVA alone shows a very porous and reticulated microstructure. The preparation of PVA composites with silver changes the porous structure of PVA. Ag1-PVA and Ag2-PVA composites look more compact and with a different porous organization as shown in the SEM images (Figure 2.1). The presence of silver nanoparticles is not very clear in the SEM images, in particular for Ag1-PVA it seems that the silver nanoparticles are imbibed in the PVA structure.

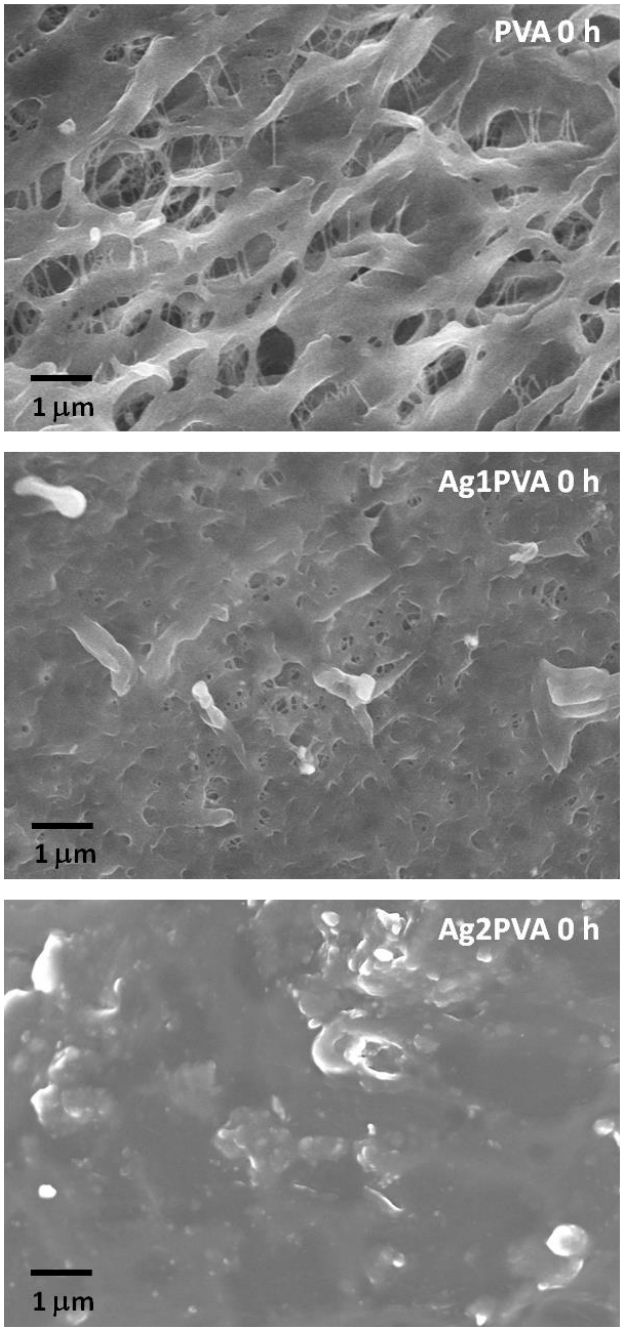

Figure 2.1 – SEM image of PVA membranes dried by lyophylization

The Ag-PVA hydrogels were dried both at room temperature (RT) (for 5, 24, 48 and 72 h after preparation, respectively) and at 105 ºC (for 3h). The aim was to analyze the influence of the presence of water inside the 3D structure of the composites and the consequent swelling degree of its PVA matrix, when using the composites as SERS substrates. After drying, the SEM images show clearly the silver nanoparticles at the

composites surface (Figure 2.2). A porous morphology is also shown for both composites, not regular in porous size or shape. The Ag1-PVA composite shows a lower amount of Ag nanoparticles than Ag2-PVA, according to the preparation methods in which it was used 3.6 and 8.9 mmol Ag^+ *per* g PVA, respectively. The Ag nanoparticles in Ag1-PVA are smaller than in Ag2-PVA, when the composites were dried at RT. Drying at 105 ºC originates the smallest Ag nanoparticles (Figure 2.2)

In these images it is shown that there are silver nanoparticles at the composites surface and possibly they are also at inner layers. Regarding the silver nanoparticles size, shape and distribution, the SEM images suggest that the Ag1-PVA composite has a lower amount of Ag nanoparticles than Ag2-PVA, being the size and shape of Ag nanoparticles in Ag1-PVA not so well defined as in Ag2-PVA, where the presence of Ag nanorods together with spherical nanoparticles is observed. Also the presence of some nanoparticle agglomerates randomly distributed is observed in both cases. Furthermore, the presence of silver nanoparticles on the surface of the membranes of PVA becomes more intense with increasing drying time and drying at 105 ° C (Figure 2.2).

Figure 2.3 shows that an increase in the drying time at RT, originates an increase in the amount of silver particles observed at the composites surface, better noticed in the SEM images shown of Ag2-PVA, which contains a larger percentage of silver. This effect is possibly due to shrinking of the PVA matrix while drying. PVA shrinking could originate a migration of the Ag particles towards the PVA surface where they tend to aggregate. The Ag particles aggregation or growth is clear from the increase in particle size when comparing the SEM image after 48 h drying with the one after 24 h drying at RT (Figure 2.3). After 72 h drying at RT, the SEM images of Ag2-PVA show two distinct regions, one with small spread Ag particles and other with much bigger aggregates, as depicted in Figure 2.3. Drying at 105 ºC originates a quicker process, with shrinking of the PVA matrix and migration of the Ag nanoparticles to the surface, but without growing and aggregation of the Ag particles (SEM images for both Ag1-PVA and Ag2-PVA in Figure 2.2, for Ag2-PVA also in Figure 2.3 for comparison purposes). The latter effect is also supported by the SERS results shown below, and will be further discussed, with the composites dried at 105 ºC being the best SERS substrates. The porous nature of the composites shown in Figure 2.2 and

Figure 2.3, makes also possible the presence of Ag particles inside the pores and at the inner surface of the material, in particular for Ag1-PVA and Ag2-PVA dried at 105ºC that show the smallest Ag particles (Figure 2.2).

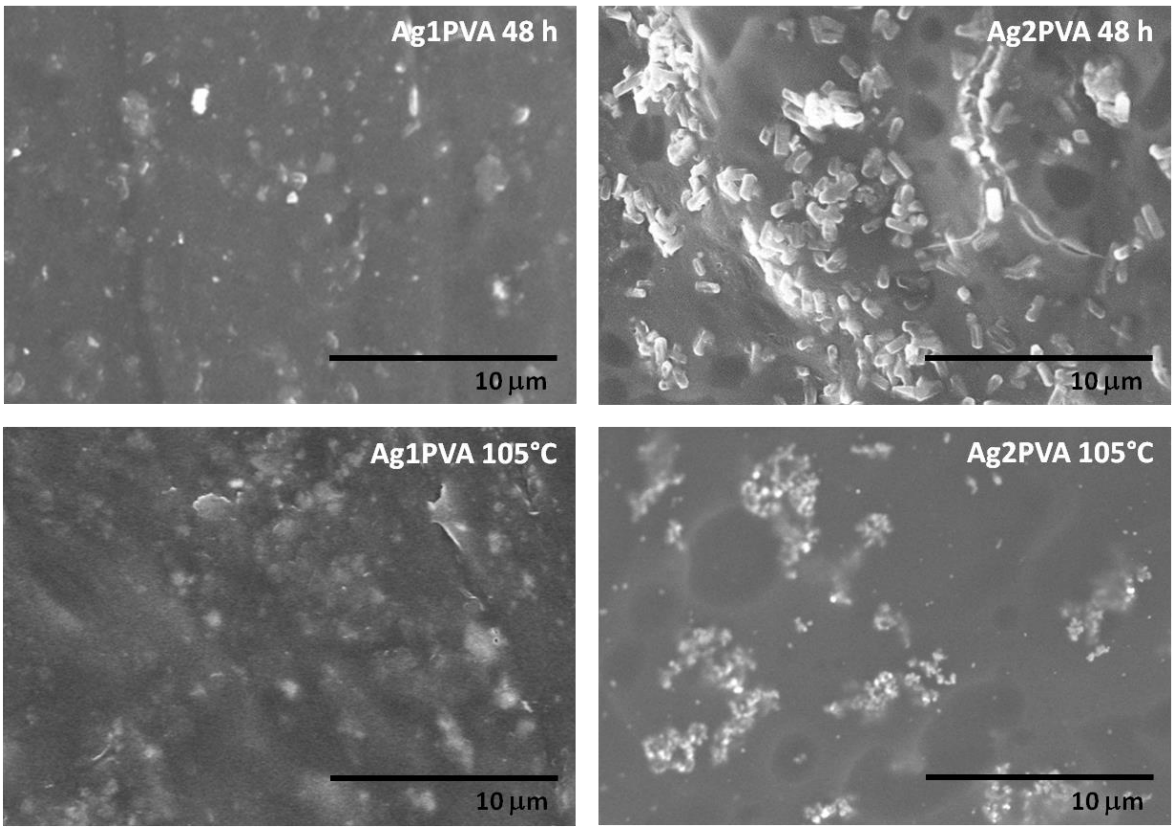

Figure 2.2 – SEM images of PVA membranes Ag1-PVA and Ag2-PVA dried in air for 48 h or dried in an oven at 105 ºC for 3 h. The samples were lyophilized immediately after reach the dried time and conditions to be observed in scanning microscope.

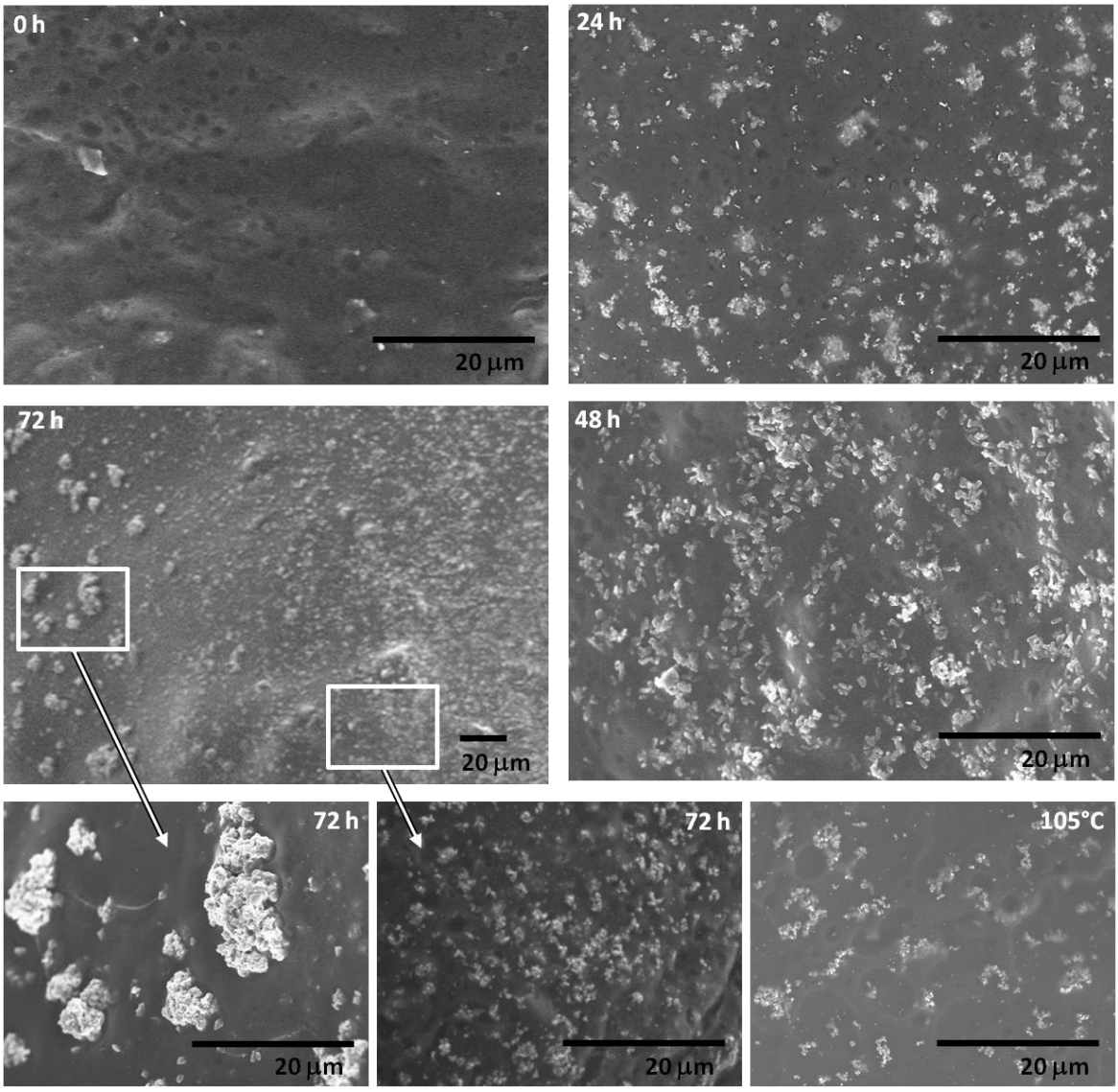

Figure 2.3 – SEM images of Ag2-PVA composite immediately after preparation (0 h), dried at RT for 24, 48 and 72 h and at 105 ºC for 3 h. The samples were lyophilized for SEM preparation.

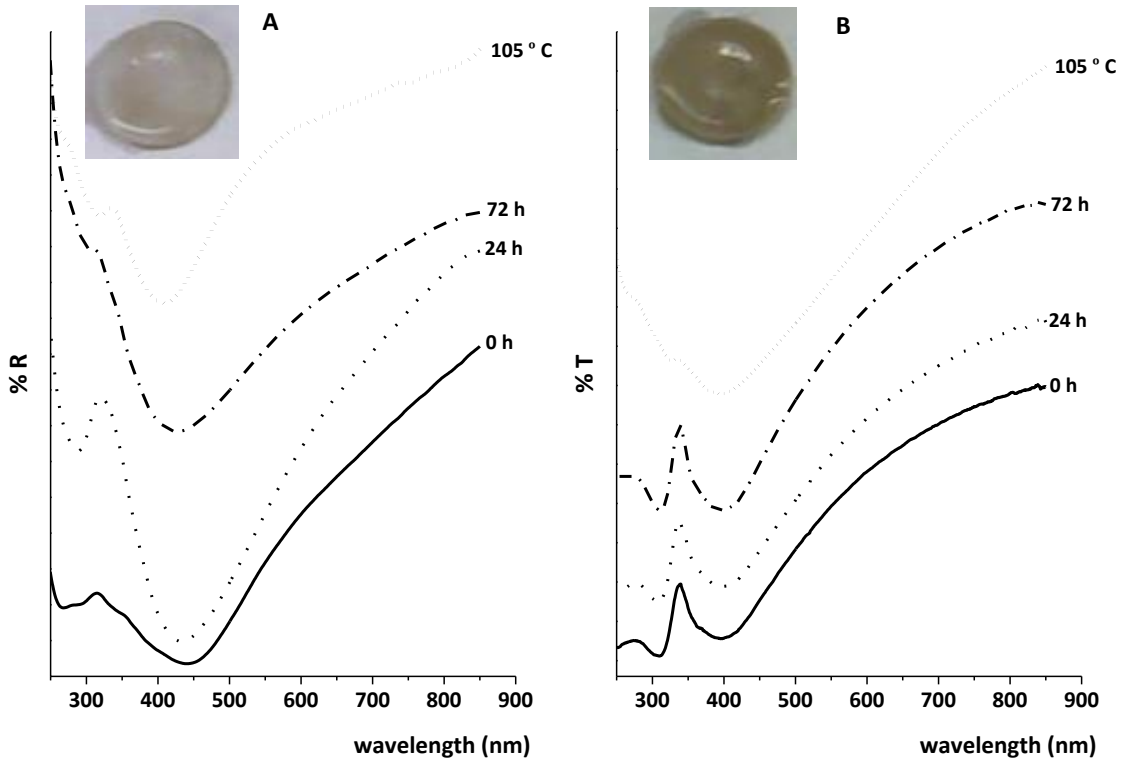

Figure 2.4 – UV-vis spectra of Ag1-PVA (left) and Ag2-PVA (right) over drying time in RT conditions (0, 24 and 72h) and dried in a oven, at 105ºC. Insets: photographs of the wet membranes before drying-

Table 2.1 – Bands position in the reflectance UV-visible spectra (λ at minimum R %) of Ag-PVA composites with different drying conditions

Drying conditions	Ag1-PVA		Ag2-PVA	
	PVA band (nm)	AgNPs band (nm)	PVA band (nm)	AgNPs band (nm)
0 h	268	441	309.5	397.5
24 h	288	434	307.5	401
72 h	302	427	312	394.5
105 ºC – 3 h	318.5	409	327	396

The reflectance spectra of the two substrates dried at different conditions, recorded in a UV-VIS spectrometer in the solid state, are plotted in Figure 2.4. In these spectra two main absorption bands are observed, the PVA band at lower wavelengths (a band at 274 nm is referred for pure PVA[27]) and the Ag nanoparticles band at higher wavelengths (around 400 nm). The minimum of reflectance of the PVA band was found to be sensitive to the drying of the matrix presenting a red shift as the polymer is becoming drier (Figure 2.4). This trend is observed for both substrates, being the values of the minimum of %R detected for higher wavelengths in the case of Ag2-PVA. This could be attributed to a lower transparency of the Ag2-PVA caused by a higher content of Ag nanoparticles as may be inferred by the colour of the wet membranes (insets in Figure 2.4) and also in agreement with SEM analysis (Figure 2.2). With respect to Ag nanoparticles peak reflection values, the results differ between Ag1-PVA and Ag2-PVA substrates. In the Ag1-PVA substrate, the minimum of reflectance values of the band attributed to Ag undergo a slight blue shift with the drying process. For the Ag2-PVA substrate, the minimum reflectance values for Ag are detected for lower wavelengths and there is not a defined variation with the drying of the substrate. The mean value of 397 nm for the minimum of reflectance is close to the reported value of 395 nm observed in pure Ag colloids and is characteristic of the plasmon resonance absorption for Ag spheres in water[31]. Though, in the SEM analysis (Figure 2.2) Ag nanorod structures were also observed. From the literature, rod-shaped silver may present two main absorption bands: longitudinal plasmon resonance at ~ 570 nm for smaller length, and a transverse plasmon mode (at ~380 nm) for higher length, and it is referred that as the length of the nanorods grew with time, the longitudinal plasmon resonance essentially disappear[32]. So, in this case the obtained spectra probably present the result of the contributions from some isolated Ag spheres together with rods contribution from the transverse plasmon mode.

2.2.2. SERS results

To register the SERS spectra, 10 μL of an aqueous solution of the analyte was added to a small portion of solid substrate (around 5x5 milimiters) and dried in air at room temperature. For comparison purposes, the Raman spectrum of a drop of the analyte in a glass slide was also recorded, after dried in air at room temperature. In the latter

case, the spectrum obtained corresponds to the Raman of the solid analyte, very distinct from the SERS spectrum, the intensity depending on the solution concentration.

2.2.2.1. Influence of substrate drying time in SERS signal

The substrates Ag1-PVA and Ag2-PVA were prepared and dried both at 105 ºC (in an oven for 3 hr) and at RT for 0, 3, 5, 7, 24, 48 and 72 hours, respectively.

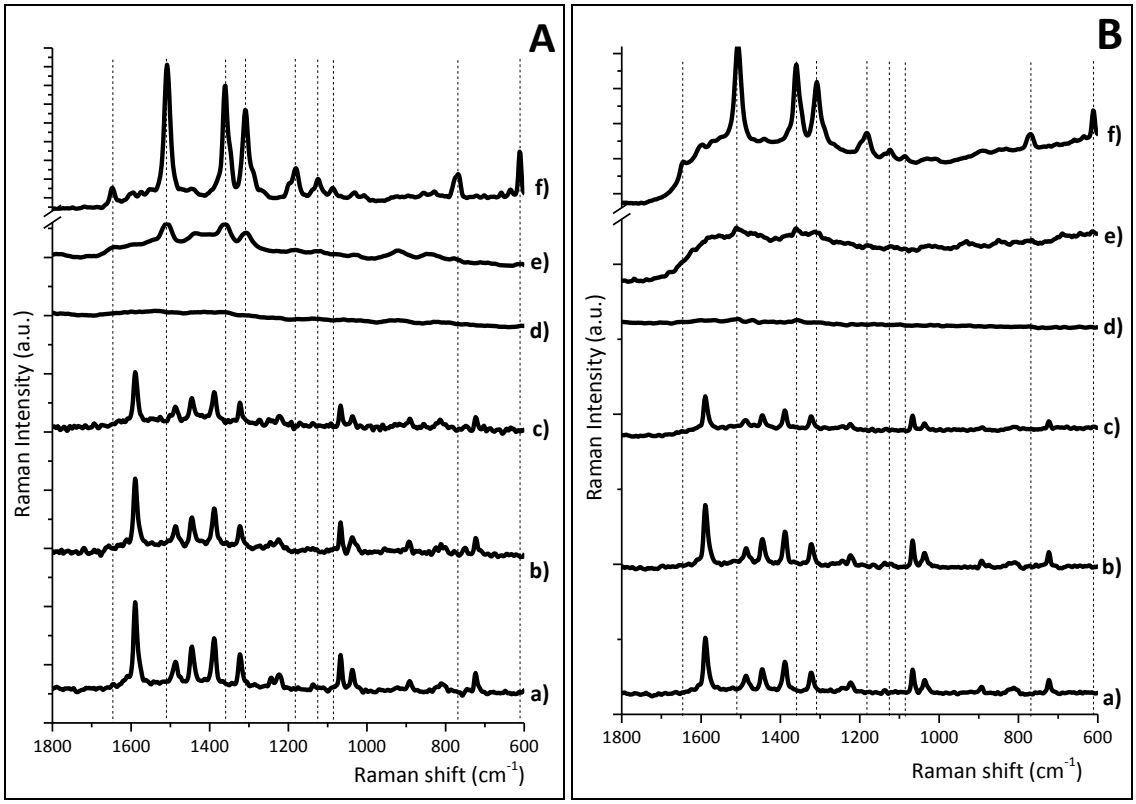

Figure 2.5 - Raman spectra of Ag1-PVA (A) and Ag2-PVA (B) substrates before drying and without addition of analyte (a); and evaluation of SERS activity for R6G in Ag1-PVA (A) and Ag2-PVA (B) when varying the drying time, (b) to (e), or after drying at 105 ºC (f). A solution of R6G 10^{-3} mol dm^{-3} was used as analyte and its characteristic bands are marked with vertical lines; drying times used were as follows (in hours): b) 0, c) 5, d) 24, e) 48, f) at 105ºC during 3h.

The substrates were tested for SERS just after the drying time was over (or after cooling down to RT, when it was heated at 105ºC), with 10 μL of a 10^{-3} mol dm^{-3} aqueous solution of R6G. The first 7 hours of drying time testing were planned to confirm if there was any influence of the substrate water content on the SERS signal of the analyte. Since during this period there was not a significant effect, longer times were used (24, 48 and 72 h) so that the amount of water within the hydrogel could further decrease (the drying process can be followed just by looking at the sample aspect that goes from a wet gel to a dried flat solid). The drying process in an oven at 105ºC was performed to assure that no water remained in the hydrogel structure of those substrates. The results show that, in fact, the drying time after preparation (or the drying temperature) influences the analyte detection by SERS (Figure 2.5).

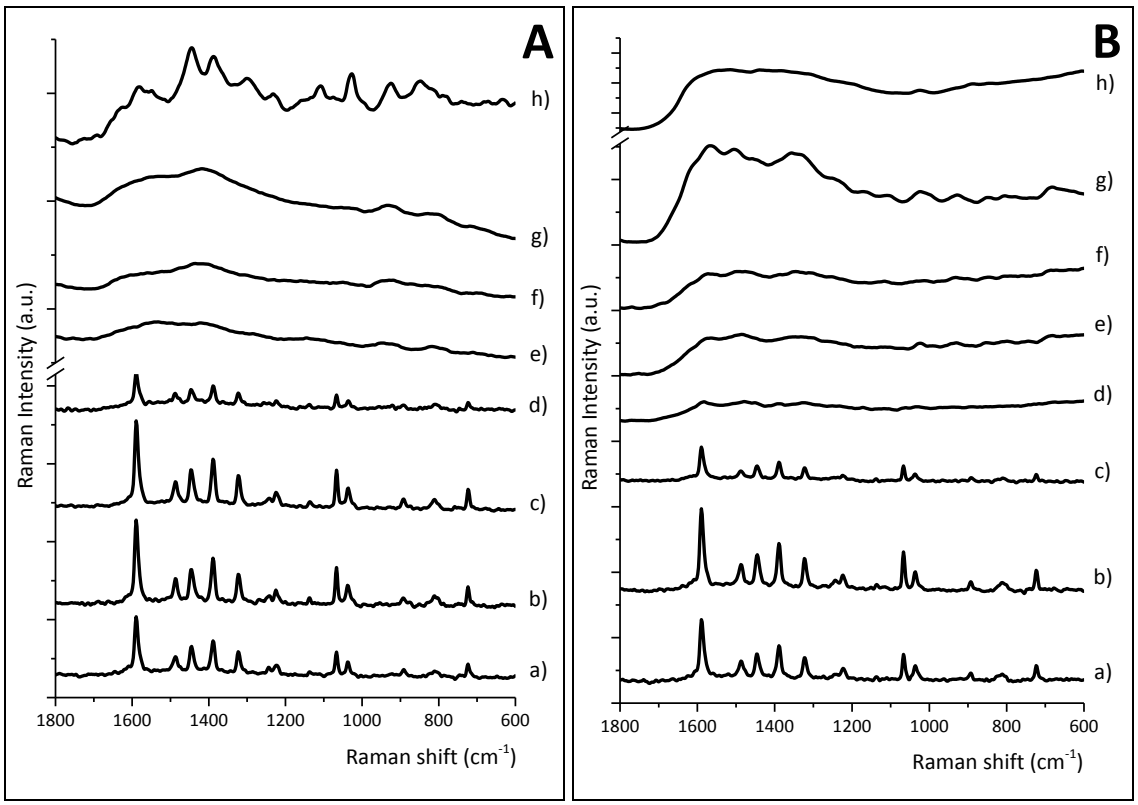

Figure 2.6 - Raman spectra of Ag1-PVA (A) and Ag2-PVA (B) for several drying times as follows (in hours): a) 0, b) 3, c) 5, d) 7, e) 24, f) 48, g) 72; and dried at 105 ºC (h).

Immediately after preparation, the Raman spectra of the hydrogels Ag1-PVA and Ag2-PVA (Figure 2.6) show a set of bands that could not be identified. The first attempt to identify these bands was running a SERS of the PVA hydrogel itself in an aqueous silver colloid, but no similarities were found with this SERS spectrum (Figure 2.7). The same pattern was observed in the Raman spectra recorded during the first seven hours of substrate drying time at room temperature. After 24 h drying no Raman signal was detected for Ag1-PVA and Ag2-PVA. Also, there was no significant Raman signal from the hydrogels dried at 105ºC (Figure 2.6).

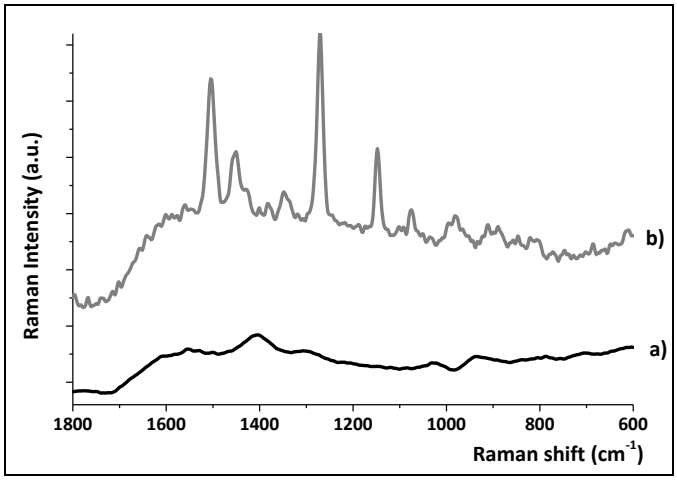

Figure 2.7 – **S**ERS spectrum of PVA in an Ag aqueous colloid (a) and Raman spectrum of only the Ag colloid for comparison purposes (b).

For the evaluation of SERS activity in Ag1-PVA and Ag2-PVA, when varying the drying time or when dried at 105 ºC, a solution of R6G 10^{-3} mol dm^{-3} was used as analyte (Figure 2.5). In the Raman spectra recorded for R6G in the several substrates obtained during the first seven hours of drying time at room temperature (Figure 2.5 b-e), the previous pattern was still observed, as obtained without addition of R6G (Figure 2.5 a and Figure 2.6). After 48 hours drying, only the characteristic SERS bands of R6G are clearly obtained both in Ag1-PVA and Ag2-PVA substrates (Figure 2.5 e). For the hydrogels dried at 105ºC, a good quality SERS spectrum was also obtained for R6G (Figure 2.5 f).

For both composites, if at the beginning of RT drying it seemed that the Ag particles were imbibed in the PVA matrix (SEM images in Figure 2.1), and could not be reached by the analyte, it seems that after 48 h there are plenty of Ag particles available that show the right aggregation state to become SERS effective (SEM images in Figure 2.2). This is shown by the SEM images and by the Raman spectra that start to show the SERS signal of R6G with a drying time of 48 h (that was not shown at 24h drying).

A completely dried substrate seems to be required to obtain the SERS spectrum of the analyte. Before drying the composites, the Ag particles seem to be imbibed in the PVA matrix and silver surface may be occupied (originating the Raman signal observed) and thus cannot be reached the adsorption of by the R6G molecules, which adsorption is blocked. The initial set of bands for the wet gel (Figure 2.6), similar in Ag1-PVA and Ag2-PVA, is possibly due to polymer or other retained in contact. SERS spectra from R6G were obtained for both Ag1-PVA and Ag2-PVA substrates after 48h drying or dried at 105ºC. The substrates used for further testing were those dried at 105ºC (assuring complete dryness) that showed the smallest silver nanoparticles and for which the best SERS signals of R6G were obtained.

2.2.2.2. Influence of interaction time between analyte and substrate in SERS signal

Since these new Ag-PVA substrates have a three-dimensional porous structure, it is important to assure that there is time for contact between the R6G analyte molecules and the metal nanoparticles inside the reticulated PVA support, before running the Raman spectra.

The following study aims to evaluate the interaction time between the analyte and the substrate that will possibly originate the best SERS signal. R6G (10 μL of aqueous R6G 10^{-3} mol dm^{-3}) was added to Ag1-PVA and Ag2-PVA substrates, respectively, that were previously dried at 105ºC. Raman spectra were collected after the following times: 0, 1, 3, 24 and 72h (Figure 2.8). R6G characteristic bands are visible in the SERS spectra immediately after addition of R6G to both Ag1-PVA and Ag2-PVA substrates. The R6G bands intensity increases for both substrates increasing the time

of interaction until 3 h. The SERS spectra obtained after 24 h are better defined. It is very interesting that after 24, or even 72 h, the SERS signal can still be observed from the R6G/Ag-PVA samples, almost without changes. When colloids are used to record SERS from distinct analytes, colloid aggregation usually occurs after 10 to 30 minutes and the SERS signal can no longer be observed.

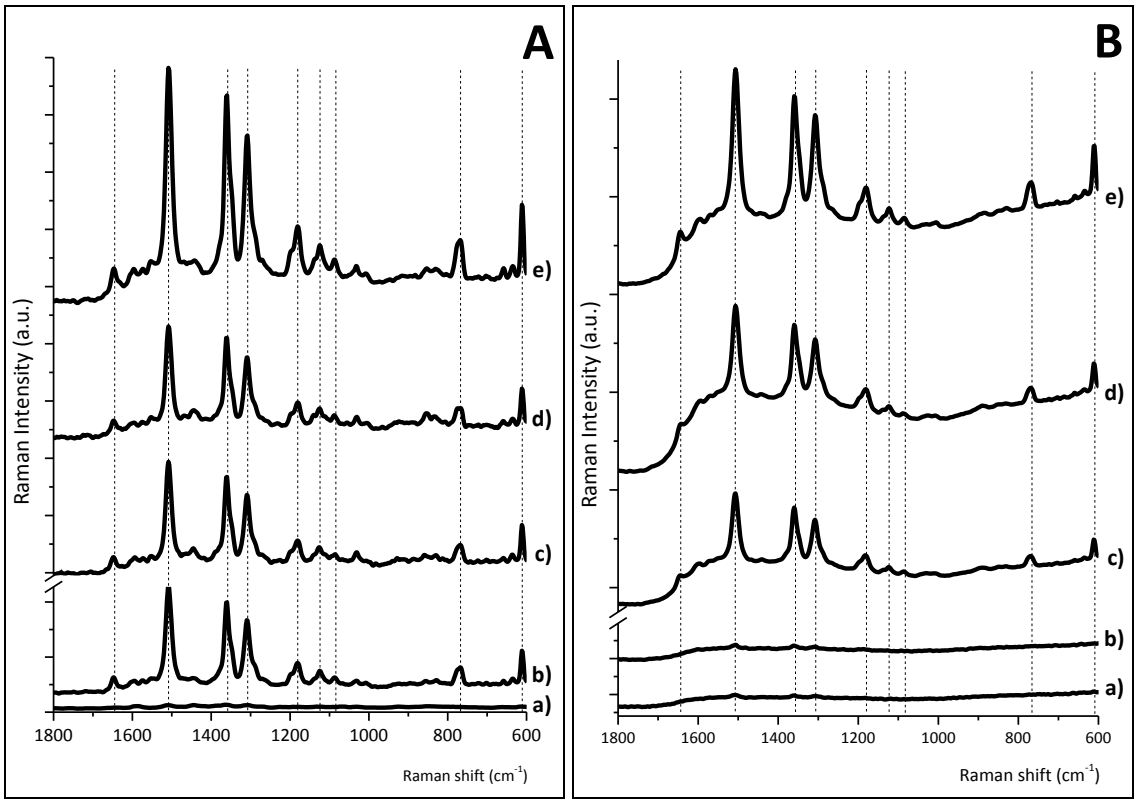

Figure 2.8 – Evaluation of SERS activity for R6G in Ag1-PVA (A) and Ag2-PVA (B) (both previously dried at 105ºC) when varying the interaction time of R6G with the substrates. A solution of R6G 10^{-3} mol dm^{-3} was used; interaction times were as follows, registered since the addition of R6G to the moment of recording the spectra (in hours): a) 0, b) 1, c) 3, d) 24, e) 72 h.

2.2.2.3. Detection limit of substrates

The determination of the detection limit of new proposed SERS substrates is always demanding. For this, and according to the previous results, it was chosen the

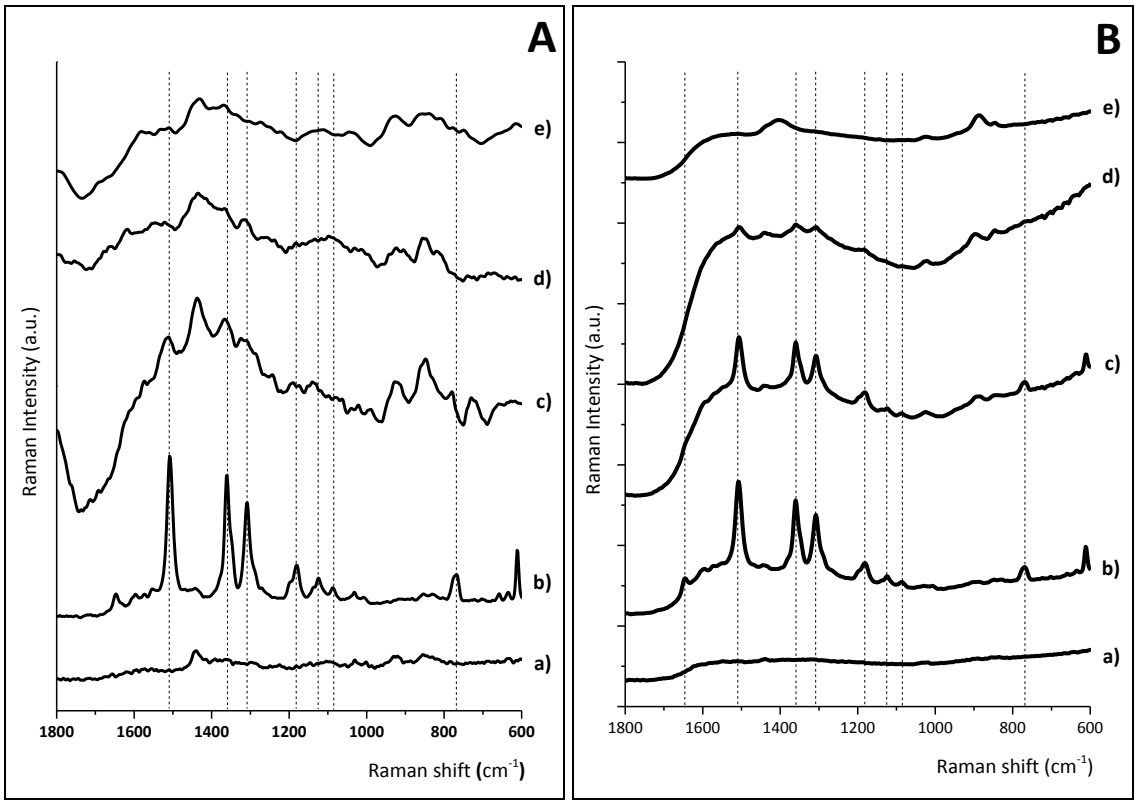

Figure 2.9 – Evaluation of SERS detection limit for R6G in Ag1-PVA (A) and Ag2-PVA (B) (both previously dried at 105ºC; interaction time analyte-substrate of 96 h in all spectra.). Raman spectra of the substrate only (a), and SERS from a R6G solution with the concentrations 10^{-3} (b), 10^{-5} (c), 10^{-6} (d) and 10^{-7} (e) moldm^{-3}, respectively, in both substrates.

substrates Ag1-PVA and Ag2-PVA dried in 105ºC and after 96 hours analyte incubation in substrates. As the previous results showed that the trend is the higher incubation time more defined spectra are, therefore it was decided to study the limit of detection of these substrates after 96 hours of interaction between the polymeric composite and R6G. The initial concentration was 10^{-3} mol dm^{-3} because was tested before in these two types of substrates with positive results. In Figure 2.9, we can see that the characteristic peaks of R6G (1650, 1450, 1300, 1190 and 600 cm^{-1}) are present in SERS spectrum for 10^{-3} mol dm^{-3} R6G aqueous solution when we used Ag1-PVA. For a concentration of 10^{-5} mol dm^{-3} of the same analyte, only 1650 and 1450 cm^{-1} bands are present in the SERS spectrum, using also Ag1-PVA. In the case of Ag2-PVA, it can be seen that the same characteristic peaks of R6G, observed for Ag1-PVA with analyte solution in concentration of 10^{-3} mol dm^{-3}, are present when we used also

R6G in 10^{-3} and 10^{-5} mol dm^{-3}. The peaks 1650, 1450, 1300 and 1190 cm^{-1} remain present in the SERS spectrum of concentration 10^{-6} mol dm^{-3} but are not present in the 10^{-7} mol dm^{-3}.

In conclusion, the SERS detection limit of R6G aqueous solutions for Ag1-PVA is 10^{-5} mol dm^{-3} and for the substrate Ag2-PVA it is 10^{-6} mol dm^{-3}. This result may is possibly be related with the higher amount of silver nanoparticles in Ag2-PVA be the substrate with more quantity of silver nanoparticles.

2.2.2.4. DNA and nucleic acids detection

The specific detection of DNA has gained importance in recent years because the number of DNA sequences of different organisms is being determined. Such sequence information can be used for the identification of the genus or species of microorganisms, diseases, or even a single individual. Fast and reliable DNA detection is not only used in research and development, it also finds increasing applications in areas like forensics, food safety control, and agriculture[33].

SERS offers several advantages for the detection of biomolecules: it is a rapid non-destrutive tool, it yields compound-specific information, and has the potential for multi-component analysis[33]. But recent advances in the research of DNA identification has been made through the use of substrates produced by using complex techniques and expensive such as nanolithography, and using DNA chain with a specific constitution of oligonucleotides[34] or a pre-treatment[35,36]. Besides, many existing DNA discrimination assays exploit the use of a synthetically attached label group that is used to detect hybridization and/or follow DNA denaturation [37-39]. This is a common problem with many DNA detection and discrimination assays, where the time, difficulty, and expense of synthetically pre-treating a target analyte greatly diminish their effectiveness. To this end, there has been a growing interest in "label-free detection", that is, the detection and discrimination of DNA without the requirement to synthetically pre-treat the DNA to be detected prior to analysis[40].

After testing a standard molecule (R6G) successfully in these new SERS substrates, in different experimental conditions and with different limit detections, DNA in the

two conformations (double stranded – dsDNA and single stranded – ssDNA) and its bases (adenine - A, cytosine - C, guanine - G and thymine - T) were applied as analyte.

This work presents two substrates which identify the DNA into its two conformations, as well as their constituent bases without any pre-treatment, fluorescent label or design of oligonucleotide chain. The DNA and their bases are used as received by provider. In addition, the substrates are produced from a simple technique without requiring specific equipment.

In general, all DNA bases were detected by both studied substrates. The identification of the analyte, in this case, depends on its structure and on the substrate used (Figure 2.10). Adenine has two peaks for the Ag2-PVA, one of them well defined, and for Ag1-PVA has only one peak. Ag1-PVA substrate is a good substrate to identify cytosine and thymine; on the other hand, with Ag2-PVA was possible identify also these bases and the guanine. The wavenumber of the main peaks relating to adenine (730 cm^{-1}), cytosine (795 cm^{-1}), and guanine (650 cm^{-1}) (Figure 2.10; Table 2.2) in observed SERS spectra are in agreement with the values found in literature[41]. Regarding thymine, in published works it is verified that this is the DNA basis with lower resolution in the SERS spectrum. Badr et al [42]conducted a study of thymine SERS spectrum on the silver nanowires surface in which used the 1064 nm laser and the obtained values of wavenumber are consisted with those found in this study, with two substrates.

SERS spectra of ssDNA (10^{-3} mol dm^{-3}) were obtained with both Ag1-PVA and Ag2-PVA substrates; for dsDNA SERS was obtained with Ag1-PVA only (Figure 2.11). As it can be seen in Figure 2.11, the substrate Ag1-PVA allows identification of the basis constituents of ssDNA: 733 (A), 970 (C), 1170 (T) and presumably 1279 cm^{-1} (G). The value assigned to guanine is in agreement with the value found in the SERS spectrum of this base from the substrate Ag2-PVA. These values are in accordance with the results obtained by Green et al[43], where analyzes the SERS spectra of oligonucleotides composed only by one of the bases (oligo A, oligo C, oligo G and oligo T). In the case of the Ag2-PVA, the two peaks observed in the spectrum of ssDNA (731, 1320 cm^{-1}) refer to adenine. Also this is the only base identified when the DNA is in a double helix conformation and using the Ag1-PVA substrate.

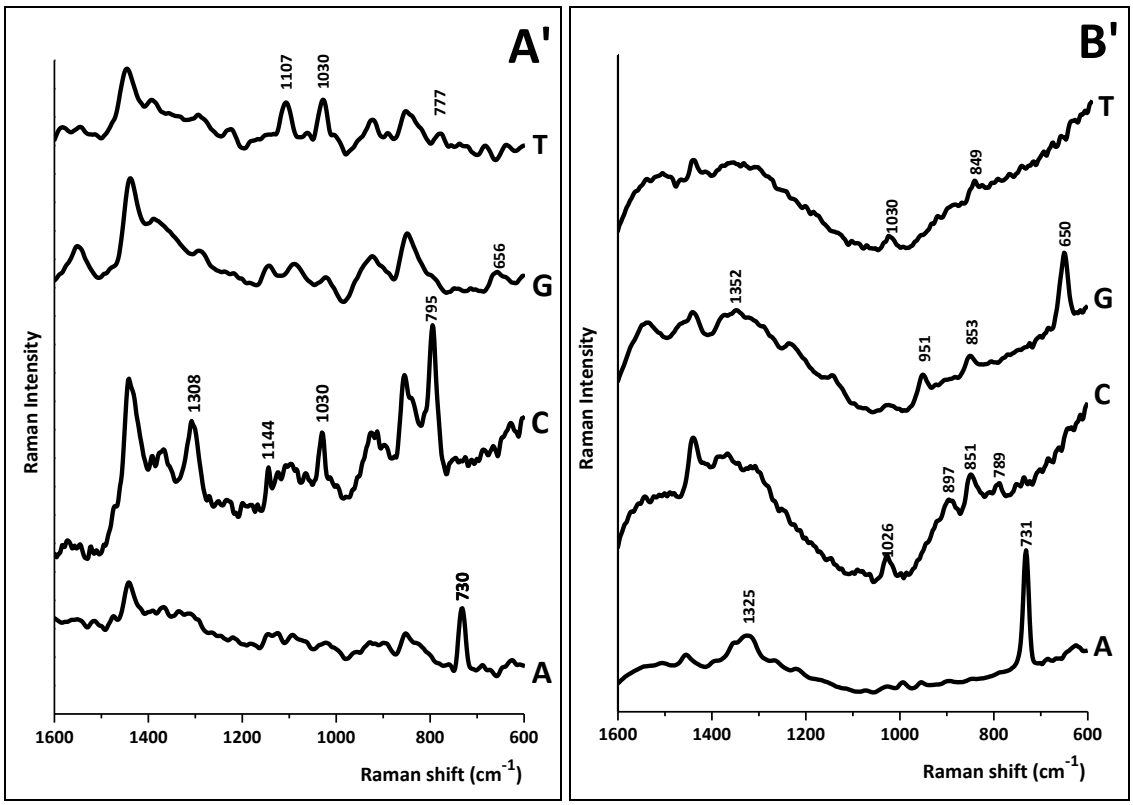

Figure 2.10 – SERS of nucleobases (10^{-3} moldm^{-3} aqueous solution) using Ag1-PVA (A') and Ag2-PVA (B') substrates (both previously dried at 105ºC; interaction time analyte-substrate of 72 h in all spectra). The characteristic bands of nucleobases are labeled in the corresponding SERS spectra: adenine (A), cytosine (C), guanine (G) and thymine (T).

The dominance of adenine modes observed in the SERS spectra is not due to the abundance of adenine base nor to its relative proximity to metal nanoparticles[13]. The 731 cm^{-1} band is assigned to a breathing mode; and the multi-component band peaking at 1320 cm^{-1} is assigned to mixed in-plane stretching motions of the six-member ring (ring skeleton vibration)[43] and indicates the denaturation of DNA[44], which is the treatment used in this experiment to produces ssDNA from double stranded DNA.

Table 2.2 – SERS characteristic bands of each DNA nucleobase and of the DNA molecule in the two conformations studied, recorded using both Ag1-PVA and Ag2-PVA composites as substrates.

Compounds	peak (cm^{-1})	
	Ag1-PVA	**Ag2-PVA**
Adenine	730	731, 1325
Cytosine	795, 1030, 1144, 1308	789, 851, 897, 1026
Guanine	656	650, 853, 951, 1352
Thymine	777, 1030, 1107	849, 1030
ssDNA	733, 970, 1150, 1279	731, 1320
dsDNA	733	

Single stranded DNA is more easily detectable than dsDNA with SERS technique due to its high surface affinity for metallic surfaces based on electrostatic interactions. So ssDNA has greater number of exposed bases, therefore an increased signal intensity is generated[34]. This is the reason why we were able to better detect ssDNA than dsDNA.

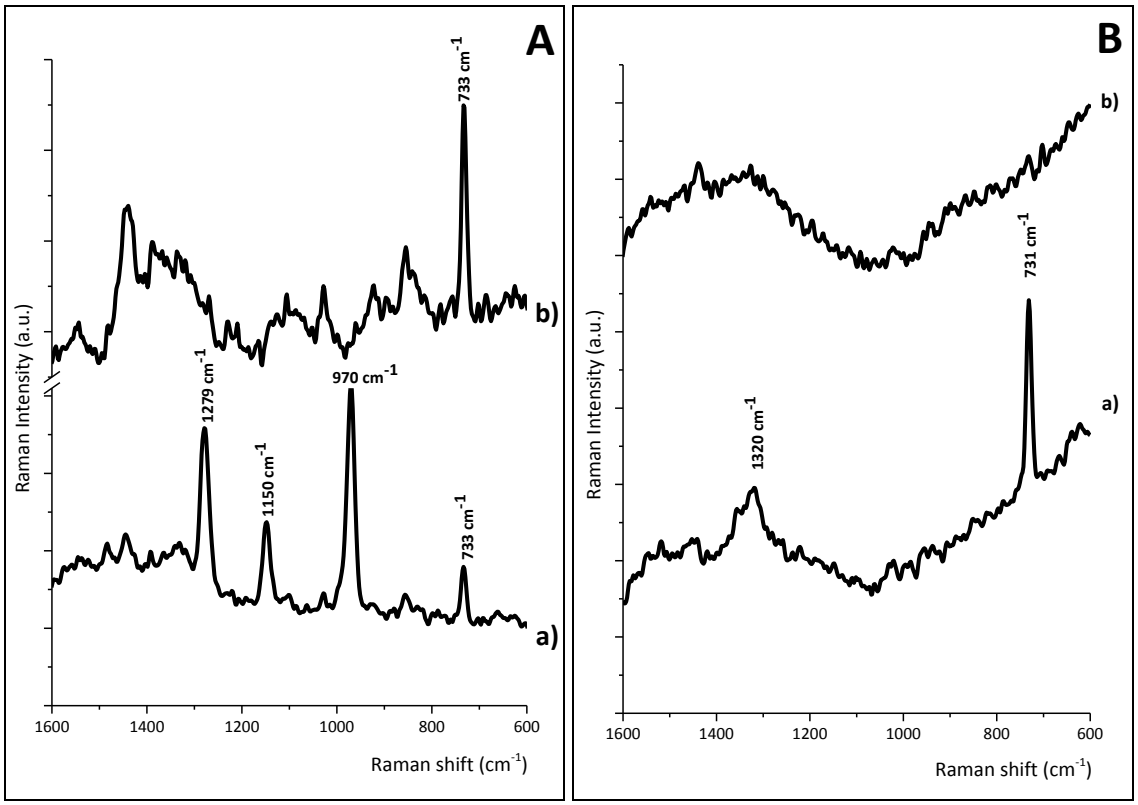

Figure 2.11 – SERS of ssDNA (a) and dsDNA (b) using Ag1-PVA (A) and Ag2-PVA (B) (substrates previously dried at 105ºC; interaction time analyte-substrate of 72 h in all spectra).

2.2.2.5. Stability of the substrates for nucleobases detection

Besides the reproducibility, the SERS substrates should be stable for a long period of time. In this work the stability of the substrates and its reproducibility were tested. The same substrates Ag1-PVA and Ag2-PVA previous described were tested four months after its preparation. The nucleic acids aqueous solutions at 1×10^{-3} moldm^{-3} and DNA (single stranded and double stranded) were the analytes chosen to perform these experiments. The analytes solutions were freshly prepared.

Generally, both SERS substrates remain its activity. All the nucleic acids (adenine, cytosine, guanine and thymine) were identified (Figure 2.12). In fact, not only the same peaks present in Figure 2.10 are present at SERS experiments performed after four months but there are some new ones. SERS spectrum of adenine shows the peak at 731 cm^{-1} detected by Ag1-PVA substrate and other two: 999 and 1323 cm^{-1}. On the other hand, in adenine SERS spectrum using Ag2-PVA is very similar to those acquired four months earlier. The detection of cytosine only have three peaks registered in this step of the work; at Ag1-PVA was not detected the peak around 1144 cm^{-1} and the peak 1026 at Ag2-PVA. The guanine has a peak at around 1000 cm^{-1} which is not present in Figure 2.10, when Ag1-PVA was used; the Ag2-PVA was not able to detect the peaks at 853 and 1352 cm^{-1}. The peak around 1300 cm^{-1} of thymine was not present in the SERS experiments performed four months earlier neither the peaks present in such SERS experiment was not present in Figure 2.12 (for Ag1-PVA). In the case of Ag2-PVA, thymine shows two peaks at 900 and 1435 cm^{-1}.

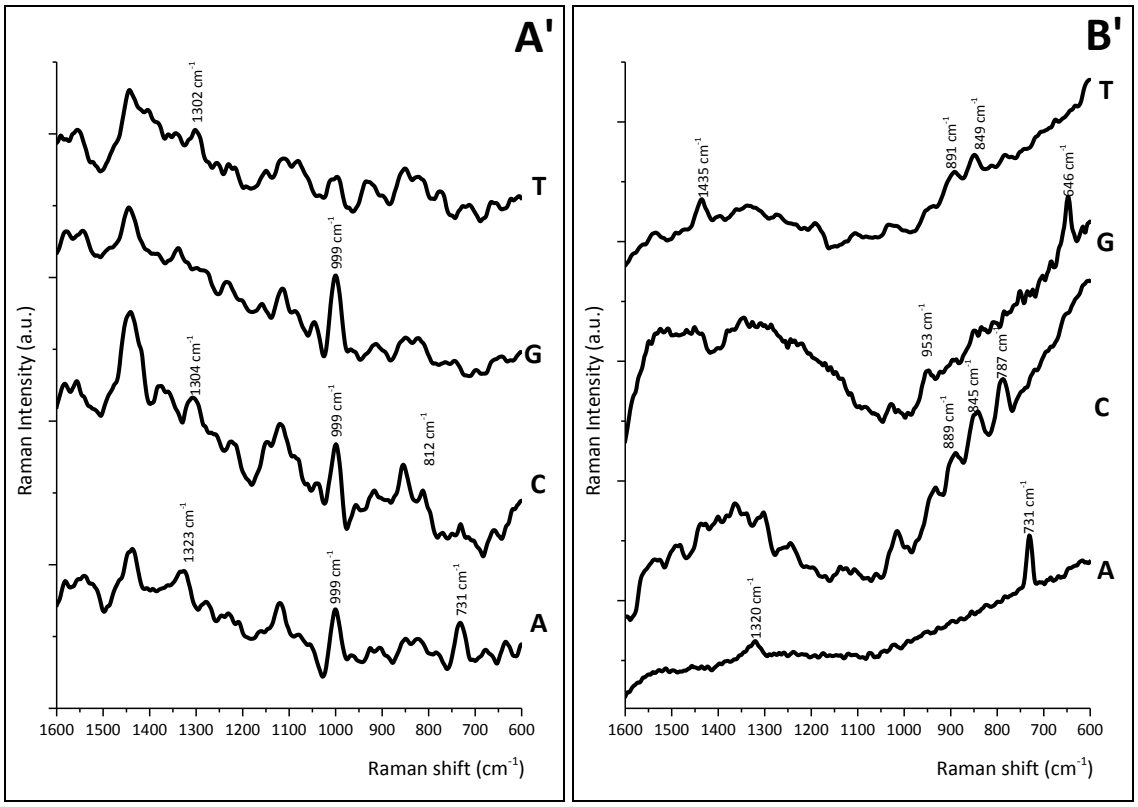

Figure 2.12 – SERS of nucleobases (10^{-3} moldm^{-3} aqueous solution) using Ag1-PVA (A') and Ag2-PVA (B') substrates (both previously dried at 105ºC; interaction time analyte-substrate of 72 h in all spectra). The characteristic bands of nucleobases are labeled in the corresponding SERS spectra: adenine (A), cytosine (C), guanine (G) and thymine (T). These experiments were performed after four months of substrates preparation.

The situation that occurred to ss and dsDNA (Figure 2.13) was similar to those nucleobases. The single stranded DNA showed the peaks 1331 and 1370 cm^{-1} besides those that were present when the substrates were used immediately after its preparation, for Ag1-PVA. In the substrate Ag2-PVA, the peaks at 806, 845, 955, 1443 and 1512 cm^{-1} are now present besides the other two that were identified at SERS spectrum four months earlier. The double stranded DNA aqueous solution was the analyte that showed more peaks besides those were showed at SERS spectra of Ag1-PVA and Ag2-PVA, immediately after its preparation.

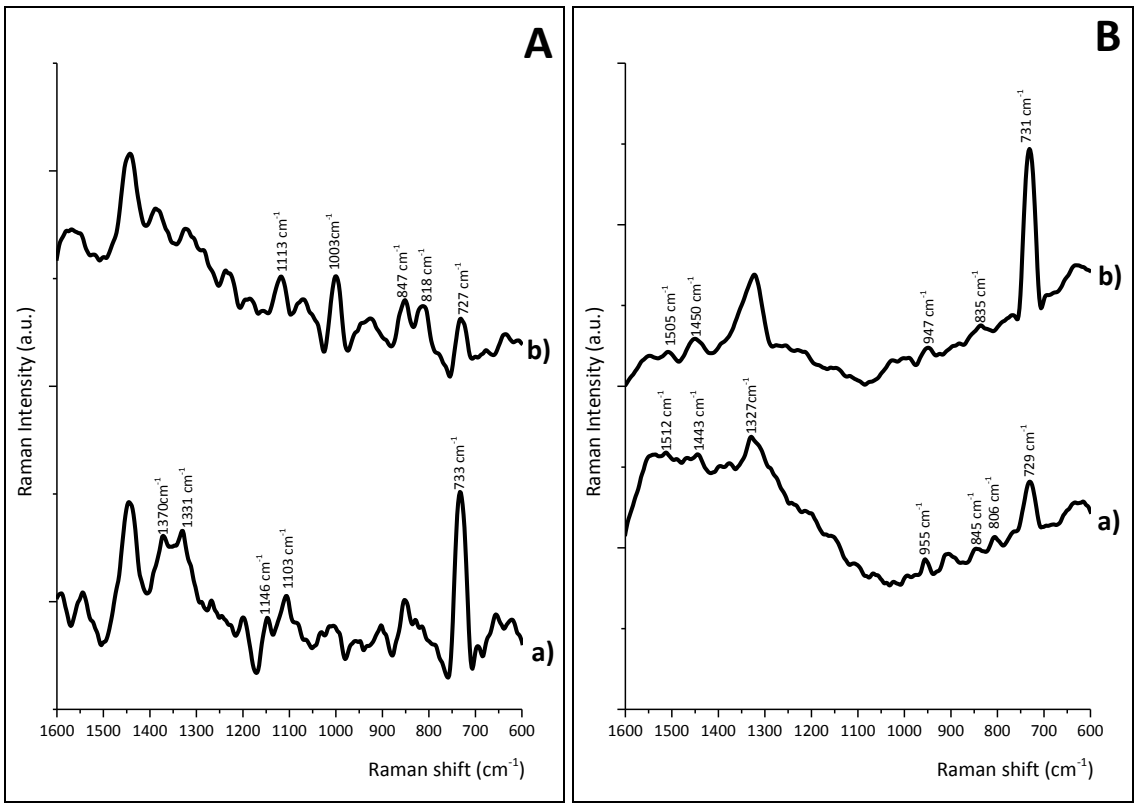

Figure 2.13 - SERS of ssDNA (a) and dsDNA (b) using Ag1-PVA (A) and Ag2-PVA (B) (substrates previously dried at 105ºC; interaction time analyte-substrate of 72 h in all spectra) after four months of substrates preparation.

2.3. Conclusions

PVA hydrogel membranes impregnated with silver nanoparticles were prepared using the freeze-thawing process. Two different reducing agents (sodium citrate and glucose) were used to prepare the Ag nanoparticles. The final materials were designated as Ag1-PVA and Ag2-PVA, respectively.

The SERS activity of these membranes was studied using rhodamine 6G as probe molecule. The parameters studied, that could affect the SERS activity were: the membrane drying time; the time of interaction between the analyte and the membrane; and detection limit of the membranes.

The best SERS results were achieved when these polymeric matrix were dried at 105 ºC for 3 hours. The SERS signals could be obtained for long time of interaction with the membranes, almost without changes. The probe molecule showed that Ag1-PVA had a limit detection of 1×10^{-5} and Ag2-PVA of 1×10^{-6} moldm^{-3} for this analyte.

These membranes were demonstrated to be good substrates to detect nucleobases and DNA in two conformations, single and double-stranded. Although the characteristic peaks of these analytes were not present in both types of Ag-PVA substrates(Ag1-PVA performed better), the adenine, cytosine, guanine and thymine were detected in each substrate. The same conclusions can be taken for the cases of ssDNA and dsDNA.

The substrates of Ag-PVA showed a good stability for long time. Moreover, the nucleic acids solutions and DNA were detected four months after preparation of the polymeric matrices.

The proposed polymeric membranes are promising potential in SERS-based detection and stable SERS substrates. Furthermore the Ag-PVA membranes are easy to handle, to prepare, are low cost and environmental eco-friendly.

2.4. Experimental Procedure

2.4.1. Preparation of Ag-PVA hydrogels

Hydrogels[45] containing 14 wt% PVA were prepared from silver nitrate solutions using two different reduction methods (method 1, sodium citrate reduction;[25] method 2, glucose reduction[26]).

Method 1: 7 g of PVA was added to an aqueous solution of $AgNO_3$ (0.5 mmol dm^{-3}, 50 mL) and the suspension formed was heated with stirring until it reached 80ºC. Then 3.76 mL of sodium citrate 0.085 M was added dropwise and the suspension was kept stirring at 80ºC during 3 hours, after which a clear solution was obtained.

Method 2: a solution of $AgNO_3$ (0.01 mol dm^{-3}, 0.0839 g in 50 mL of H_2O) was prepared. D-(+)-glucose (1.2 g) was added to the solution and sonicated for 5 minutes.

After, 1 mL of ammonia aqueous solution (25 % weight) was added, followed by 5.6 g of PVA. The final suspension was heated at 80 ºC for 3 hours, with stirring.

Freeze-thawing technique was used to promote crosslink of the polymer. The gel produced was distributed in glass containers (±1 g) and submitted to three cycles of freeze–thawing (-20ºC, +20ºC), promoting the cross-linking. After this process was complete, some of the obtained membranes were dried at 105 ºC, showing a rigid structure like a film, and the other ones were stored at +5º.

2.4.2. Preparation of analyte solutions

Aqueous solutions of adenine, cytosine, guanine, thymine, ssDNA and dsDNA 10^{-3} mol dm^{-3} were prepared. To prepare ssDNA the solution of dsDNA was heated at 90 ºC for 20 minutes and cooled in ice immediately after. Both types of DNA solutions were prepared without using any buffering agent.

2.4.3. SERS measurements

For testing both substrates in terms of interaction time and limit of detection we used R6G solution in different concentrations, and 10 μL of each solution was placed on the surface of the substrates. For SERS measurements of nucleic acids, also 10 μL of each solution was placed on the membrane and remained in interaction for 72 hours. The Raman spectra and SERS were recorded using a Bruker RFS100/S FT-Raman spectrometer (Nd:YAG laser, 1064 nm excitation).

2.5. Bibliography

(1) Agasti, S. S.; Rana, S.; Park, M.-H.; Kim, C. K.; You, C.-C.; Rotello, V. M. Nanoparticles for detection and diagnosis. *Advanced Drug Delivery Reviews* **2010**, *62*, 316-328.

(2) Song, S.; Qin, Y.; He, Y.; Huang, Q.; Fan, C.; Chen, H.-Y. Functional nanoprobes for ultrasensitive detection of biomolecules. *Chemical Society Reviews* **2010**, *39*, 4234-4243.

(3) Yan, F.; Vo-Dinh, T. Surface-enhanced Raman scattering detection of chemical and biological agents using a portable Raman integrated tunable sensor. *Sensors and Actuators B: Chemical* **2007**, *121*, 61-66.

(4) Baptista, P. V.; Doria, G.; Quaresma, P.; Cavadas, M.; Neves, C. S.; Gomes, I.; Eaton, P.; Pereira, E.; Franco, R.: Chapter 11 - Nanoparticles in Molecular Diagnostics. In *Progress in Molecular Biology and Translational Science*; Antonio, V., Ed.; Academic Press, 2011; Vol. Volume 104; pp 427-488.

(5) Kannan Balasubramanian, M. B. Biosensors based on carbon nanotubes. *Anal Bioanal Chem* **2006**, *385*, 452 – 468.

(6) Waggoner, P. S.; Craighead, H. G. Micro- and nanomechanical sensors for environmental, chemical, and biological detection. *Lab on a Chip* **2007**, *7*, 1238-1255.

(7) Fang, C.; Agarwal, A.; Buddharaju, K. D.; Khalid, N. M.; Salim, S. M.; Widjaja, E.; Garland, M. V.; Balasubramanian, N.; Kwong, D.-L. DNA detection using nanostructured SERS substrates with Rhodamine B as Raman label. *Biosensors and Bioelectronics* **2008**, *24*, 216-221.

(8) Ko, H.; Singamaneni, S.; Tsukruk, V. V. Nanostructured Surfaces and Assemblies as SERS Media. *Small (Weinheim an der Bergstrasse, Germany)* **2008**, *4*, 1576-1599.

(9) Schlücker, S.; Kiefer, W.: Chapter 9 - Selective Detection of Proteins and Nucleic Acids with Biofunctionalized SERS Labels. In *Frontiers of Molecular Spectroscopy*; Jaan, L., Ed.; Elsevier: Amsterdam, 2009; pp 267-288.

(10) He, Y.; Su, S.; Xu, T.; Zhong, Y.; Zapien, J. A.; Li, J.; Fan, C.; Lee, S.-T. Silicon nanowires-based highly-efficient SERS-active platform for ultrasensitive DNA detection. *Nano Today* **2011**, *6*, 122-130.

(11) U. S, D.; Fu, C. Y.; Soh, K. S.; Ramaswamy, B.; Kumar, A.; Olivo, M. Highly sensitive SERS detection of cancer proteins in low sample volume using hollow core photonic crystal fiber. *Biosensors and Bioelectronics* **2012**, *33*, 293-298.

(12) Zhang, B.; Wang, H.; Lu, L.; Ai, K.; Zhang, G.; Cheng, X. Large-Area Silver-Coated Silicon Nanowire Arrays for Molecular Sensing Using Surface-Enhanced Raman Spectroscopy. *Advanced Functional Materials* **2008**, *18*, 2348-2355.

(13) Barhoumi, A.; Zhang, D.; Tam, F.; Halas, N. J. Surface-Enhanced Raman Spectroscopy of DNA. *Journal of the American Chemical Society* **2008**, *130*, 5523-5529.

(14) Fabris, L.; Dante, M.; Nguyen, T.-Q.; Tok, J. B. H.; Bazan, G. C. SERS Aptatags: New Responsive Metallic Nanostructures for Heterogeneous Protein Detection by Surface Enhanced Raman Spectroscopy. *Advanced Functional Materials* **2008**, *18*, 2518-2525.

(15) Seol, M.-L.; Choi, S.-J.; Baek, D. J.; Park, T. J.; Ahn, J.-H.; Lee, S. Y.; Choi, Y.-K. A nanoforest structure for practical surface-enhanced Raman scattering substrates. *Nanotechnology* **2012**, *23*, 095301.

(16) Bi, L.; Rao, Y.; Tao, Q.; Dong, J.; Su, T.; Liu, F.; Qian, W. Fabrication of large-scale gold nanoplate films as highly active SERS substrates for label-free DNA detection. *Biosensors and Bioelectronics* **2013**, *43*, 193-199.

(17) Muniz-Miranda, M.; Pergolese, B.; Bigotto, A.; Giusti, A. Stable and efficient silver substrates for SERS spectroscopy. *Journal of Colloid and Interface Science* **2007**, *314*, 540-544.

(18) Chu, Y.; Banaee, M. G.; Crozier, K. B. Double-Resonance Plasmon Substrates for Surface-Enhanced Raman Scattering with Enhancement at Excitation and Stokes Frequencies. *ACS Nano* **2010**, *4*, 2804-2810.

(19) Romanato, F.; Pilot, R.; Massari, M.; Ongarello, T.; Pirruccio, G.; Zilio, P.; Ruffato, G.; Carli, M.; Sammito, D.; Giorgis, V.; Garoli, D.; Signorini, R.; Schiavuta, P.; Bozio, R. Design, fabrication and characterization of plasmonic gratings for SERS. *Microelectronic Engineering* **2011**, *88*, 2717-2720.

(20) Pinheiro, P. C.; Fateixa, S.; Nogueira, H. I. S.; Trindade, T. SERS study on adenine using a Ag/poly(t-butylacrylate) nanocomposite. *Spectrochimica Acta Part A: Molecular and Biomolecular Spectroscopy* **2013**, *101*, 36-39.

(21) Lin, W.-C.; Yang, M.-C. Novel Silver/Poly(vinyl alcohol) Nanocomposites for Surface-Enhanced Raman Scattering-Active Substrates. *Macromolecular Rapid Communications* **2005**, *26*, 1942-1947.

(22) Yu, D.-G.; Lin, W.-C.; Lin, C.-H.; Chang, L.-M.; Yang, M.-C. An in situ reduction method for preparing silver/poly(vinyl alcohol) nanocomposite as surface-enhanced Raman scattering (SERS)-active substrates. *Materials Chemistry and Physics* **2007**, *101*, 93-98.

(23) Hatakeyema, T.; Uno, J.; Yamada, C.; Kishi, A.; Hatakeyama, H. Gel–sol transition of poly(vinyl alcohol) hydrogels formed by freezing and thawing. *Thermochimica Acta* **2005**, *431*, 144-148.

(24) Li, J. K.; Wang, N.; Wu, X. S. Poly(vinyl alcohol) nanoparticles prepared by freezing–thawing process for protein/peptide drug delivery. *Journal of Controlled Release* **1998**, *56*, 117-126.

(25) Goncalves, G.; Marques, P. A. A. P.; Granadeiro, C. M.; Nogueira, H. I. S.; Singh, M. K.; Gracio, J. Surface Modification of Graphene Nanosheets with Gold

Nanoparticles: The Role of Oxygen Moieties at Graphene Surface on Gold Nucleation and Growth. *Chemistry of Materials* **2009**, *21*, 4796-4802.

(26) Zhao, X. S.; Ma, J. Z.; Zhang, J. T.; Xiong, Z. G.; Yong, Y. Preparation, characterization and antibacterial properties of silver-modified graphene oxide. *Journal of Materials Chemistry* **2011**, *21*, 3350-3352.

(27) Badr, Y.; Mahmoud, M. A. Enhancement of the optical properties of poly vinyl alcohol by doping with silver nanoparticles. *Journal of Applied Polymer Science* **2006**, *99*, 3608-3614.

(28) Hassan, C. M.; Ward, J. H.; Peppas, N. A. Modeling of crystal dissolution of poly(vinyl alcohol) gels produced by freezing/thawing processes. *Polymer* **2000**, *41*, 6729-6739.

(29) Bajpai, A. K.; Saini, R. Preparation and characterization of novel biocompatible cryogels of poly (vinyl alcohol) and egg-albumin and their water sorption study. *Journal of Materials Science-Materials in Medicine* **2006**, *17*, 49-61.

(30) Hassan, C.; Peppas, N. A. Structure and applications of poly(vinyl alcohol): hydrogels produced by conventional crosslinking or by freezing/thawing methods. *Advances in Polymer Science* **2000**, *153*, 37 - 65.

(31) Du, Y.; Fang, Y. Assignment of charge transfer absorption band in optical absorption spectra of the adsorbate–silver colloid system. *Spectrochimica Acta Part A: Molecular and Biomolecular Spectroscopy* **2004**, *60*, 535-539.

(32) Sun, Y.; Gates, B.; Mayers, B.; Xia, Y. Crystalline Silver Nanowires by Soft Solution Processing. *Nano Letters* **2002**, *2*, 165-168.

(33) Hering, K.; Cialla, D.; Ackermann, K.; Doerfer, T.; Moeller, R.; Schneidewind, H.; Mattheis, R.; Fritzsche, W.; Roesch, P.; Popp, J. SERS: a versatile tool in chemical and biochemical diagnostics. *Analytical and Bioanalytical Chemistry* **2008**, *390*, 113-124.

(34) Harper, M. M.; Dougan, J. A.; Shand, N. C.; Graham, D.; Faulds, K. Detection of SERS active labelled DNA based on surface affinity to silver nanoparticles. *Analyst* **2012**, *137*, 2063-2068.

(35) Miljanic, S.; Dijanosic, A.; Matosevic, I.; Piantanida, I. Intercalator-DNA interactions revealed by NIR surface-enhanced Raman spectroscopy. *Vibrational Spectroscopy* **2011**, *57*, 23-29.

(36) Graham, D.; Stevenson, R.; Thompson, D. G.; Barrett, L.; Dalton, C.; Faulds, K. Combining functionalised nanoparticles and SERS for the detection of DNA relating to disease. *Faraday Discussions* **2012**, *149*, 291-299.

(37) Harpster, M. H.; Zhang, H.; Sankara-Warrier, A. K.; Ray, B. H.; Ward, T. R.; Kollmar, J. P.; Carron, K. T.; Mecham, J. O.; Corcoran, R. C.; Wilson, W. C.;

Johnson, P. A. SERS detection of indirect viral DNA capture using colloidal gold and methylene blue as a Raman label. *Biosensors & Bioelectronics* **2009**, *25*, 674-681.

(38) van Lierop, D.; Krpetic, Z.; Guerrini, L.; Larmour, I. A.; Dougan, J. A.; Faulds, K.; Graham, D. Positively charged silver nanoparticles and their effect on surface-enhanced Raman scattering of dye-labelled oligonucleotides. *Chemical Communications* **2012**, *48*, 8192-8194.

(39) Fang, C.; Agarwal, A.; Buddharaju, K. D.; Khalid, N. M.; Salim, S. M.; Widjaja, E.; Garland, M. V.; Balasubramanian, N.; Kwong, D.-L. DNA detection using nanostructured SERS substrates with Rhodamine B as Raman label. *Biosensors & Bioelectronics* **2008**, *24*, 216-221.

(40) Johnson, R. P.; Richardson, J. A.; Brown, T.; Bartlett, P. N. A Label-Free, Electrochemical SERS-Based Assay for Detection of DNA Hybridization and Discrimination of Mutations. *Journal of the American Chemical Society* **2012**, *134*, 14099-14107.

(41) Kneipp, J.; Wittig, B.; Bohr, H.; Kneipp, K. Surface-enhanced Raman scattering: a new optical probe in molecular biophysics and biomedicine. *Theoretical Chemistry Accounts* **2010**, *125*, 319-327.

(42) Badr, Y.; Mahmoud, M. A. Effect of silver nanowires on the surface-enhanced Raman spectra (SERS) of the RNA bases. *Spectrochimica Acta Part A: Molecular and Biomolecular Spectroscopy* **2006**, *63*, 639-645.

(43) Green, M.; Liu, F.-M.; Cohen, L.; Kollensperger, P.; Cass, T. SERS platforms for high density DNA arrays. *Faraday Discussions* **2006**, *132*, 269-280.

(44) Kneipp, K.; Kneipp, H.; Itzkan, I.; Dasari, R. R.; Feld, M. S. Surface-enhanced Raman scattering and biophysics. *Journal of Physics-Condensed Matter* **2002**, *14*, R597-R624.

(45) Valente, A. J. M.; Cruz, S. M. A.; Murtinho, D. M. B.; Miguel, M. G. a.; Muniz, E. C. DNA-poly(vinyl alcohol) gel matrices: Release properties are strongly dependent on electrolytes and cationic surfactants. *Colloids and Surfaces B: Biointerfaces* **2013**, *101*, 111-117.

3. Synthesis and characterization of graphene oxide and its reduction

The synthesis of well exfoliated graphene oxide (GO) was a fundamental step for this research work. The method chosen to prepare GO was reported by Marcano, because it starts from the exfoliation of graphite flakes with chemical agents, that at the end allows to obtain large-area GO sheets with a high quantity of oxygen functional groups. These characteristics are of major importance for the synthesis the noble metal nanoparticles at the GO surface (NPs-GO).

During the preparation of the NPs-GO nanocomposites, the GO surface is reduced, because of that we considered of importance the study of the reduced GO (rGO) properties with the same chemical agents used to prepare the nanocomposites.

The characterization of the as-prepared GO showed that the nanomaterial had a good exfoliation and oxidation degree. It was found that the degree of reduction of the GO surface depend on the chemical agent used.

3.1. Introduction

The development of simple, ultrasensitive, highly selective and cost-effective biosensing platforms is essential for biological assays and clinical diagnostics. Biosensor platforms used for diagnosis purposes would benefit greatly from the development of new graphene-based nanocomposites due to the unique physical and chemical properties of graphene[1-6].

Recently, numerous graphene-based biosensing platforms have been reported to detect different biological molecules on the basis of various mechanisms being the enhancement of Raman signal one of them[7-10].

Graphene, the two-dimensional sheet of sp^2-hybridized carbon, shows excellent electrical conductivity, high transparency and flexibility. Such particular characteristics has inspired many of the envisage future applications of graphene such as sensor-devices, roll-up and wearable electronics, energy storage materials, polymer composites, and transparent electrodes[11]. Because of this plurality of applications, in the last years, the production of graphene has been a hot topic in the scientific community. Several methods have been developed such as micromechanical exfoliation of highly ordered pyrolytic graphite (HOPG)[12], chemical vapour deposition[13,14], epitaxial growth, unzipping of carbon nanotubes by chemical, electrochemical or physical methods[15-17], each of these methods presenting advantages and disadvantages.

Although, the previously referred methodologies able the production of high quality graphene sheets, most of them present the disadvantage of low production rate, high cost of the process and the need of specific apparatus which are not available in all the laboratories[18]. For these reasons, indirect methodologies to prepare graphene at a higher mass production rate, lower cost and without the need of special equipment, were explored based on the reduction of graphene oxide (GO). GO is obtained after the exfoliation of graphite powder in the presence of oxidant compounds and strong acids, following methodologies described by the Brodie[19], Staudenmaier[20], Hummer[21] or Marcano[22]. The purpose of the oxidation is to introduce oxygen-containing functional groups into the basal structure of graphene sheets. The oxygen groups are

introduced to reduce the Van der Walls force between the carbon layers within graphite, as well as to improve the stabilization of the resulting nano-sheets in water. The majority of the methods uses then ultrasonication treatment to enforce the exfoliation of GO into monolayers. GO can be then reduced to graphene using different chemical agents[23] or thermal treatments[24]. The basic strategy involve the complete exfoliation of GO into individual GO sheets followed by their in-situ reduction to produce individual graphene-like sheets.

However, as refereed before, in chapter 1, the quality of the final graphene sheets obtained from the reduction route of GO is not as high as the quality obtained from the physical methodologies, due to some defects that remain in the carbon network after the reduction process. That is the reason why these methodologies are avoided to produce graphene for applications where the conductive properties of graphene are essential[25]. Reduced GO (rGO) is not perfect graphene with lower electricity, because small amounts of functional groups remain in the basal structure and defects (holes) in the carbon network.

However, the intermediary carbon phase, GO, that presents an hydrophilic character due to the large number of oxygen-containing functional groups generated during the oxidation process is of great interest, mainly from the chemical point of view, since these groups allow the implementation of traditional chemistry methodologies to grow different organic and inorganic structures at GO surface[26,27]. This form of graphene may develop into the cheap precursor of choice to yield processable graphene in large quantities. In conclusion, the benefit of GO is its high potential to be the most versatile starting material for the preparation of functionalized graphene. It was first shown by Gonçalves et al[10], that the presence of the oxygen-groups at the surface of GO allows the nucleation and growth of the metallic nanoparticles in the carbon network. Since the GO surface has a large number of oxygen-containing functional groups[28], the distribution of the metallic nanoparticles at its surface can be successfully achieved. This approach is a possibility to prepare the so-called platforms that can be tested as SERS substrates because the electromagnetic sites (provided by the noble metal nanoparticles) are well distributed on the carbon network, which is a major requirement to obtain a good Raman signal enhancement. However, other

applications for metal nanoparticles dispersed on graphene have already shown enhanced catalytic activity as well as novel optoelectronic properties[29].

In this work, and for the reasons previously exposed, we have prepared and used GO to promote the synthesis of gold and silver nanoparticles at its surface. For this purpose we needed to select a reducing agent to promote simultaneously the reduction of the metallic ions and of the GO. There are several reducing agents referred in the literature[23], and our selection was based on the use of eco-friendly reducing agents, whenever it was possible.

Following these objectives we choose sodium citrate[30,31] and D(+)-glucose[32,33], which are the most common ones for gold and silver nanoparticles production. Additionally, we used natural sugars and phenolic compounds present in Eucalyptus globulus Labill bark aqueous extracts to prepare the nanoparticles at GO surface[34]. Furthermore, and based on a recent work published by Nergiz S.Z. et al[35] we also tried to prepare gold nanostars at GO surface using in this case, hydroxylamine, as reducing agent[36]. Hydroxylamine has a high reduction capability but weak reactivity with water and other solvents that make it an appropriate reductant for the GO reduction in aqueous suspension[36]. In resume, four different reducing agents were used to prepare the metal nanoparticles-GO nanocomposites.

In this chapter we present the results of the preparation and characterization of the GO used in this work. Initially, we present the morphologic characteristics of the as prepared GO evaluated by SEM, TEM and AFM. The evaluation of the chemical composition and structure of the same GO is then presented in the following section together with the reduced GO materials by the different chemicals, for a more clear comparison. The main idea is to evaluate the capacity of each of the selected chemicals to reduce the GO nanosheets, that is, to restore the π-network.

3.2 Results and Discussion

3.2.1. Synthesis and morphological characterization of graphene oxide

Graphene oxide with two-dimensional structure was successfully prepared via the Marcano's method[22] described in the section 3.4.1. Synthesis of graphene oxide (page 93).

Briefly, we started from graphite flakes (Figure 3.1(a)), the oxidation procedure was applied and followed by an intensive washing procedure. After a suitable ultrasonic treatment, such exfoliation can produce stable dispersions of very thin GO sheets in water. The GO product obtained exhibited the traditional brown colour (Figure 3.1(b)). It still retains a layered structure, but is much lighter in colour than graphite due to the loss of electronic conjugation brought about by the oxidation[37].

The aqueous GO solutions can be then lyophilized to obtain GO in the dry state, that is constituted by fluffy powder with a very large volume as exemplified in Figure 3.1(c).

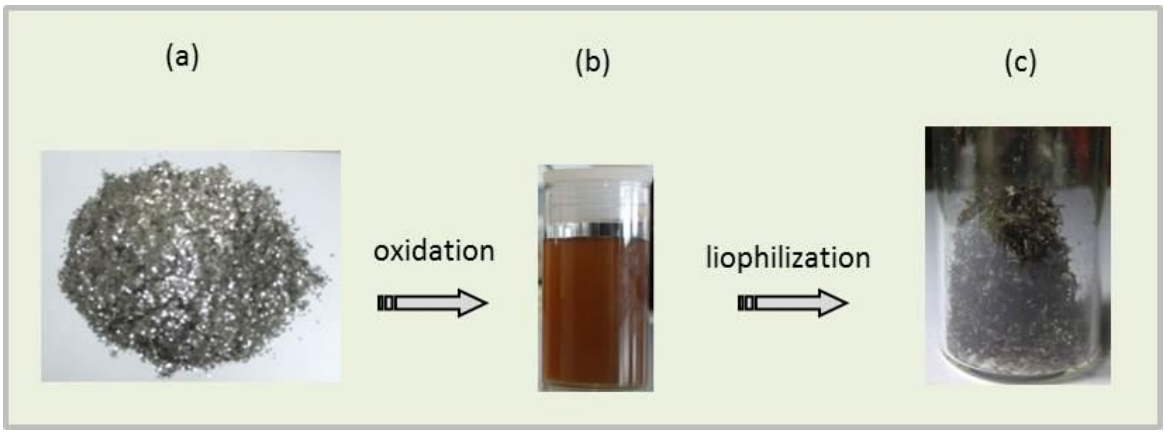

Figure 3.1 – Photographs of (a) graphite flakes, (b) GO aqueous solution and (c) dried GO by lyophilisation.

The morphology and structure of the dried GO nanosheets was investigated by SEM and TEM. Figure 3.2 presents representative SEM images of free-standing GO nanosheets with lateral sizes bigger than 3 μm, revealing a crumpled and rippled structure which can result from the drying process. The TEM images obtained are characteristics of single to few layers of graphene sheets (Figure 3.3). The presence of

corrugations (signed with the arrow in the high magnified image) results from stresses created during the transference of this nanomaterial to the TEM grids and also because of drying, as referred before.

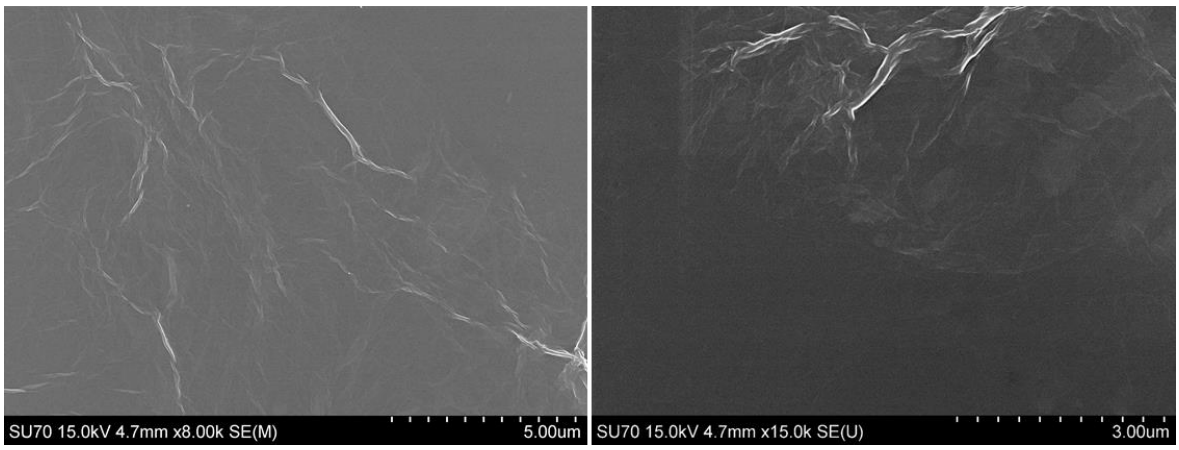

Figure 3.2 – Scanning electron micrographs of graphene oxide at lower (LEFT) and higher (RIGTH) magnifications.

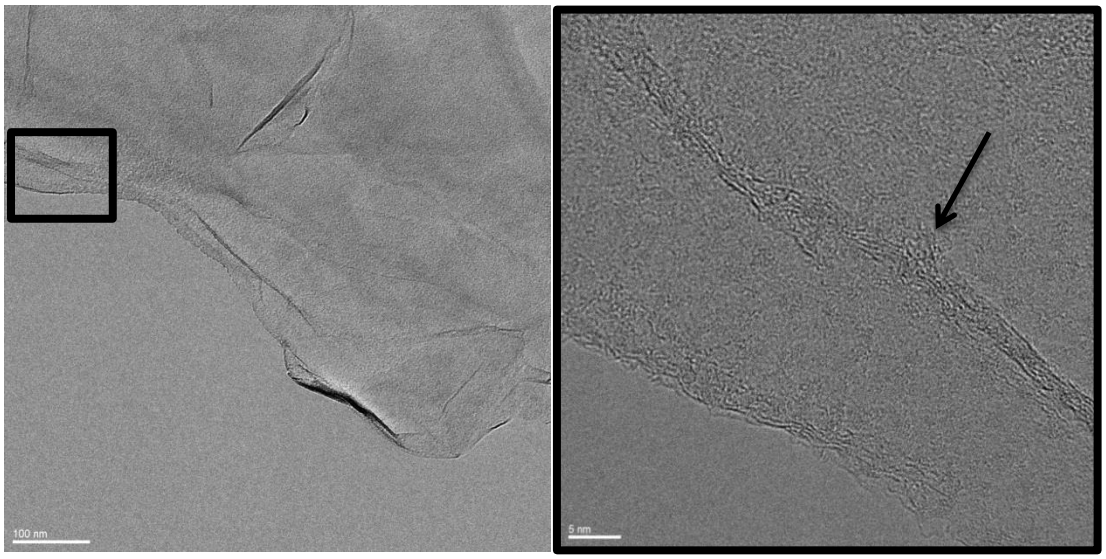

Figure 3.3 – Transmission electron micrographs of graphene oxide at lower (LEFT) and higher (RIGTH) magnifications.

AFM analysis of GO deposited on a silica substrate, revealed the presence of sheets with uniform thickness (~1.3 nm; an example is shown in Figure 3.4). These well-exfoliated samples of GO contained no sheets either thicker or thinner than the referred value, leading to a conclusion that an efficient exfoliation of GO down to few-

layers GO sheets was indeed achieved under these conditions. While a pristine graphene sheet is atomically flat with a well-known van der Waals thickness of ~0.34 nm[38], GO sheets are expected to be thicker due to the presence of covalently bound oxygen and the displacement of the sp^3-hybridized carbon atoms slightly above and below the original graphene plane.

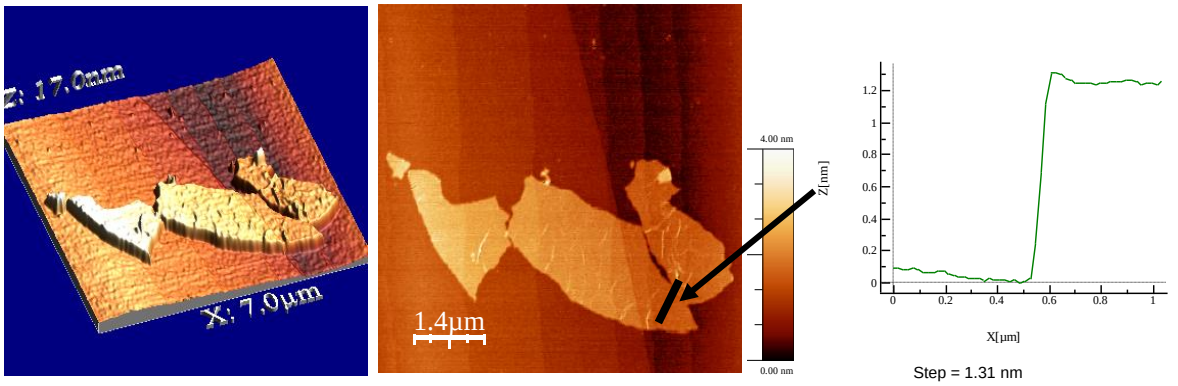

Figure 3.4– AFM analysis of GO with images of topography and deflection and its profile.

3.2.2. Chemical reduction of graphene oxide with different reducing agents and its characterization

The chemical agents used for the reduction of graphene oxide involved two chemicals traditionally used to prepare silver or gold nanoparticles. These were sodium citrate and glucose. Another two chemical were also used, a natural extract of Eucalyptus Globulus prepared by the members of the research team and hydroxylamine, a chemical with the particularity to promote the growth of gold nanostars, under particular chemical medium conditions[39].

A representation of the chemical structures of the previous referred molecules is shown in Figure 3.5.

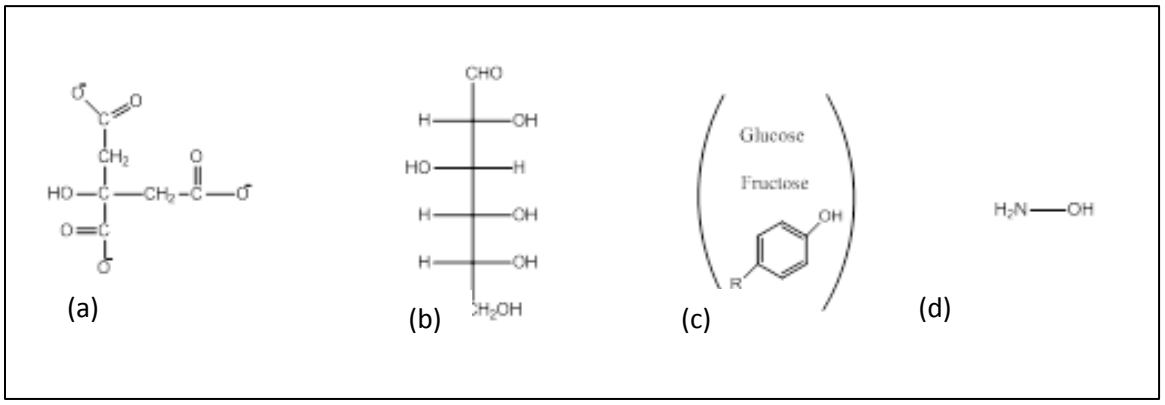

Figure 3.5 – Representation of the chemical agents used to chemically reduce the graphene oxide. (a) citrate; (b) glucose; (c) Eucalyptus Globulus extracts including a mixture of glucose, fructose and phenolic molecules; (d) hydroxylamine.

The specificity of each of the methodologies involved in the different reduction processes is described in the experimental section at the end of this chapter. Hereafter, we present the results of the structural characterization of GO in comparison with reduced GO (rGO) by the diverse methods.

3.2.2.1. UV-vis spectroscopy

The formation of stable aqueous rGO dispersions enables the reaction process to be monitored using UV-vis spectroscopy. According to the literature, GO presents two UV-vis absorption peaks centered at 230 and 300 nm, which decay gradually with the increase of reduction, eventually disappearing depending on the reduction degree[40]. Meanwhile, a new absorption peak show up around 264 nm, and red-shifted with the reduction efficiency, also the absorption in the whole spectral region may increase[41], indicating that the electronic conjugation within the reduced graphene sheets was revived upon reduction of graphene oxide[42]. It can be readily observed that the reduction causes a change in colour from yellow (GO) to black (rGO) in water.

The UV-vis spectra of GO and reduced GO with the different chemical reducing agents is represented in Figure 3.6.

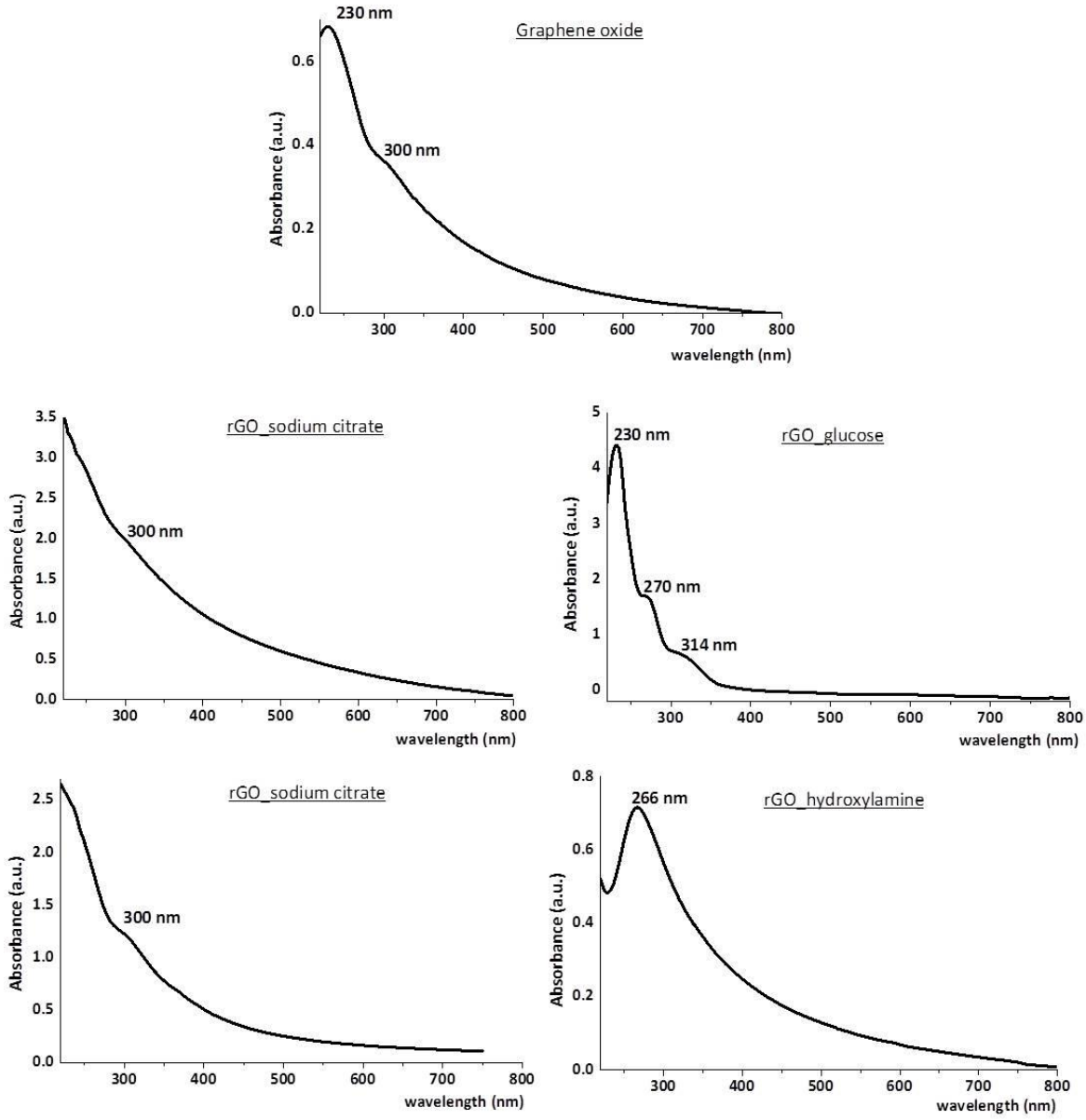

Figure 3.6 – Absorbance spectra of GO and rGO obtained with sodium citrate, glucose, hydroxylamine and eucalyptus extracts.

The UV/Vis spectrum of GO exhibits the two characteristic peaks, a maximum at 230 nm, which corresponds to π-π* transitions of aromatic C–C bonds, and a shoulder at 300 nm, which is attributed to n-π* transitions of C=O bonds[43,44]. The rGO produced by hydroxylamine, follows the disappearance of the GO peaks with the presence of a new peak at 266 nm corresponding to rGO according to literature. The observation of the curves corresponding to the GO reduction particullarly with hydroxylamine and

sodium citrate, but also with Eucalyptus extracts shows an increase of absorption in the whole spectral region providing a first hint that the GO might be reduced and the aromatic structure might be restored[40]. Finally the curve corresponding to the GO reduction by glucose seems to maintain the original GO characteristics peaks (~230 and 320 nm), together with the appearance of the rGO peak at around 270 nm. Also, in this case the absorbance of the GO peak at around 230 nm is very high, when compared with the others.

3.2.2.2. Fourier transform infrared spectroscopy

The Fourier transform infrared spectroscopy (FTIR) spectra of GO and rGO obtained with the different chemical agents are shown in Figure 3.7.

In all the spectra, we observe a strong and broad absorption peak between 3000 –3700 cm^{-1} in the high frequency area corresponding to the stretching and bending vibration of OH groups of water molecules adsorbed on the materials[45].

Based on the literature and specifically starting with GO the attribution of the peaks is as follows: the C=O stretching of COOH groups situated at edges of GO sheets are present at 1726 cm^{-1}. The absorptions due to the O–H bending vibration, epoxide groups and skeletal ring vibrations (sp^2-hybrided C=C) are observed in the range of 1500-1600 cm^{-1} [46]. The absorption at 1393 cm^{-1} may be attributed to tertiary C–OH groups. The C-O stretch from epoxy groups is responsible for a peak at 1232 cm^{-1} and finally, the alkoxy C-O stretch is visible at 1060 cm^{-1} [47,48].

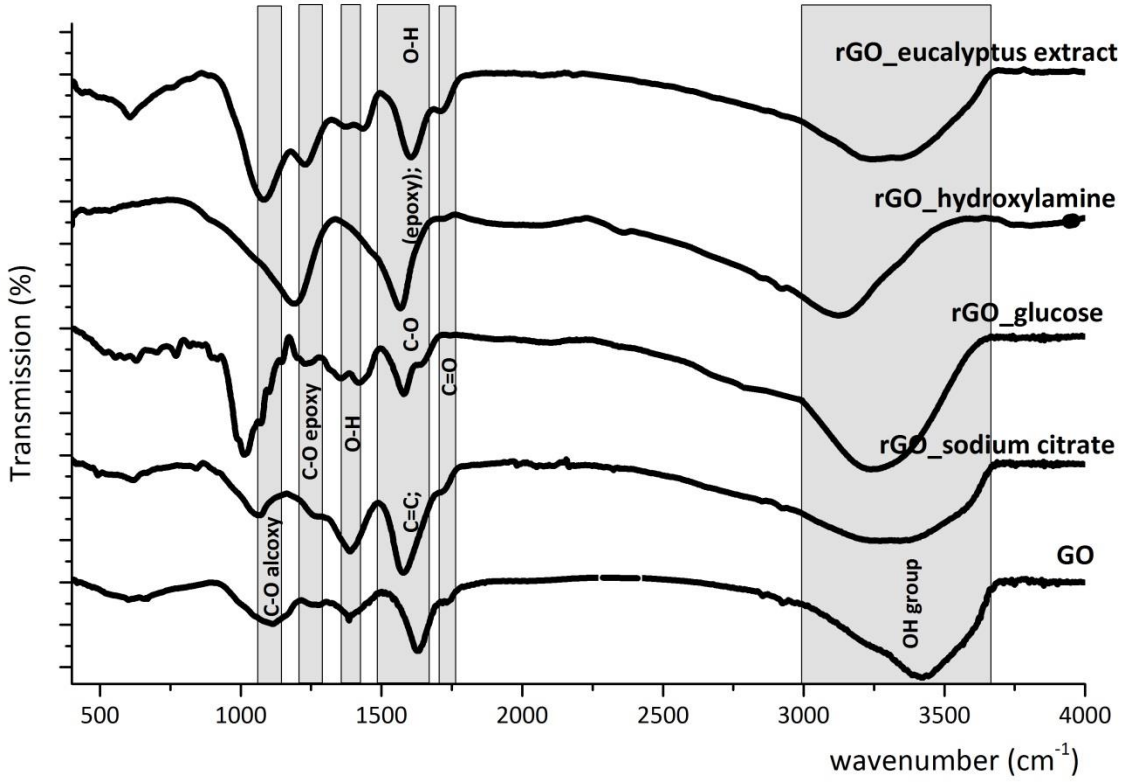

Figure 3.7 – FTIR spectra of GO and rGO reduced with the different chemical reducing agents.

With the reduction methodologies applied to GO, it was expected that the intensity of peaks associated to the oxygen functional groups would significantly diminish or even disappear, concomitantly with the restoration of the sp^2-hybrided C=C. However, as can be observed in Figure 3.7, the oxygen functional groups are still present, being difficult to conclude if there is a reduction of oxygen presence or not based on these spectra. Yet, the rGO produced from hydroxylamine treatment shows the most visible differences. A strong peak is visible at 1568 cm^{-1}, this can be attributed to C=C stretching vibration, the other broad peak centred at 1200 cm^{-1} is possibly the sum of the contributions from remaining C-O from epoxy and alcoxy groups.

The FTIR spectrum of rGO_glucose shows more peaks than those attributed to GO structure. Such presence of these peaks can be explain by the adsorption of glucose at the surface of GO.

3.2.2.3. Thermogravimetric analysis

The decomposition profiles of these samples could be understood as consequences of the different oxidation states of the carbon structures. The thermogravimetric (TG) and the corresponding differential TG (DTG) curves of the samples obtained under nitrogen atmosphere at a heating rate of 5 ^{o}C min^{-1} are shown in Figure 3.8 and Figure 3.9, respectively.

All the samples show a slight mass decrease from room temperature to 100 °C attributed to adsorbed water. In the case of GO, a significant decrease from 150 °C to 200 °C caused by pyrolysis of the oxygen-containing functional groups, generating CO, CO_2 and stream is observed. The mass of GO slowly further decreased up to 620 °C along with burning of GO by dehydration of carboxyl and epoxide groups. The temperature at which the decomposition of carbon sheets takes place is related to the integrity of the sp^2 system. Since GO has a broken sp^2 system, the thermal stability of carbon sheets is poor and GO decomposes totally at a quite low temperature with little residual graphene[49].

After the reduction treatment of GO with the different chemical agents, the removal of the thermally labile oxygen functional groups by chemical reduction results in much increased thermal stability for the reduced GO. It is expected that the system, partially or totally recovers the integrity of the sp^2 system, depending on the reduction method. This fact should lead to restoring the additional thermal stability.

Regarding the reduction with sodium citrate, there is an initial mass decrease at around 100 ^{o}C due to water adsorption. The mass loss at 300 ^{o}C corresponding to a very sharp DTG peak seems to be attributed to the loss of adsorbed citrate ions[50] at rGO surface. Small mass decrease peaks are observed that when compared with the initial GO material corresponds to a much lower presence of oxygen-containing functional groups, indicating a high reduction degree. The thermal stability of this material is much higher than GO, indicating a good level of reduction.

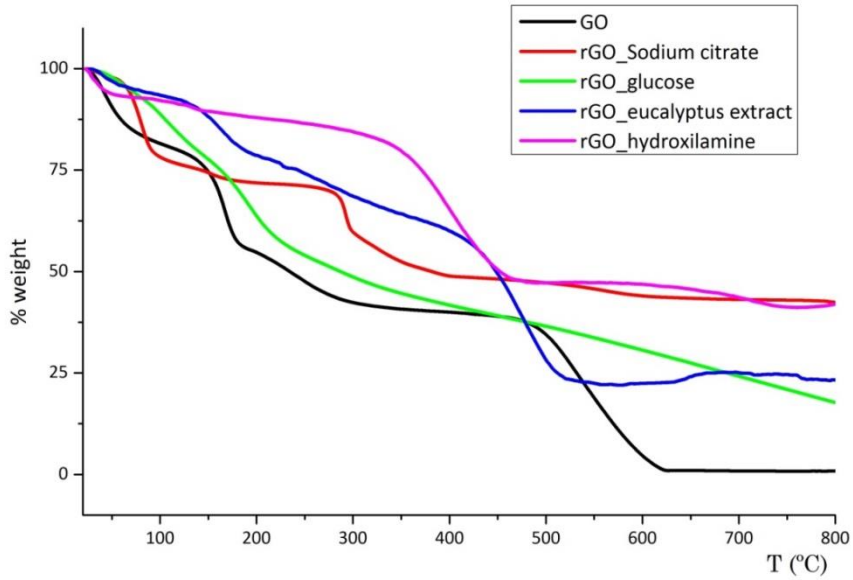

Figure 3.8 – Thermogravimetric curves of GO, and rGO reduced with sodium citrate, glucose, eucalyptus extract and hydroxylamine.

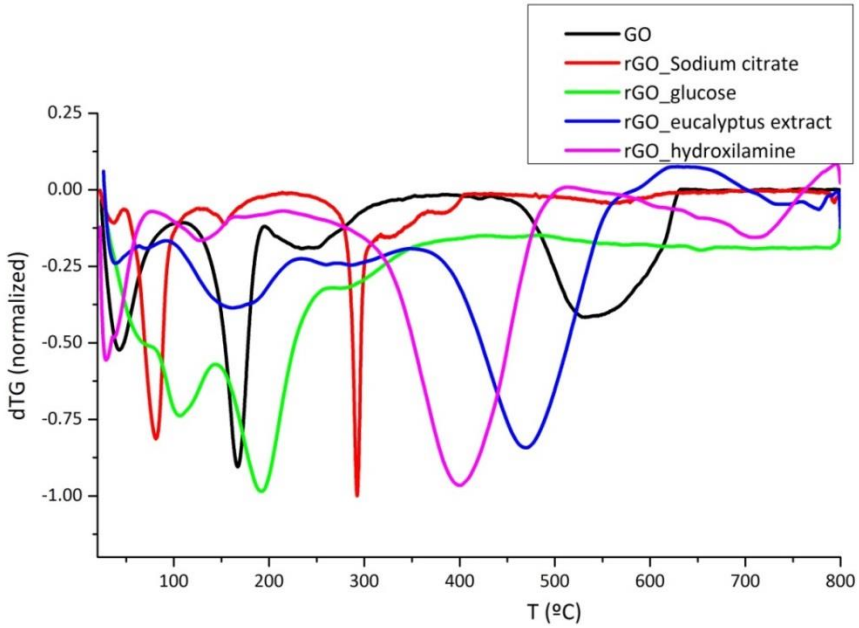

Figure 3.9 – DTG curves of GO and rGO reduced with sodium citrate, glucose, eucalyptus extract and hydroxylamine.

Concerning glucose, the TG curve shows a continuous mass loss until the maximum temperature tested (800 ºC). The initial two mass loss peaks corresponding to water and oxygen functional groups presents a displacement to higher temperatures when

compared to GO, this may indicate that some glucose molecules are adsorbed at rGO surface. This appears to be confirmed by a decomposition phase around 300 ºC which matches the temperature of thermal depolymerization of the polysaccharide[51].

The TG and DTG curves of the GO reduced by the Eucalyptus extracts follow the GO thermal behaviour with some small mass peak loss deviations. However, the total amount of labile oxygen functional groups is considerable lower in the reduced form.

The reduction with hydroxylamine shows the most thermally stable rGO, suggesting that a significant amount of the water and labile oxygen groups were removed by the hydroxylamine reduction.

3.2.2.4. X-ray Photoelectron Spectroscopy

X-ray Photoelectron Spectroscopy (XPS) analysis was conducted to elucidate the evolution of oxygen groups and confirm their degree of removal upon reduction treatment, also to determine the nature of the residual oxygen containing functional groups that remain after reduction and to clarify how the reduction treatment affects the electronic structure of GO.

The typical C 1s spectra of the samples surface under study are represented in Figures 3.10 and 3.11, also the deconvolutions of the C 1s spectra are represented in these figures. The relative concentrations of surface functional groups obtained from the deconvolution of the C1s XPS regions are summarized in the Table 3.1. The attribution of the chemical groups to the peak positions was done according to the literature[28,52,53].

The deconvolution of the C 1s XPS spectrum of the GO sample (Figure 3.10) show the presence of three different types of carbon bonds, with peaks centred at 285.0, 287.0 and 288.6 eV, corresponding to C=C/C–C, C–O/C-OH, and C=O/COOH groups, respectively[53]. From the Table 3.1, the determined ratio C/O is 0.7 which allows to verify the predominance of the carbon atoms in the oxidized state.

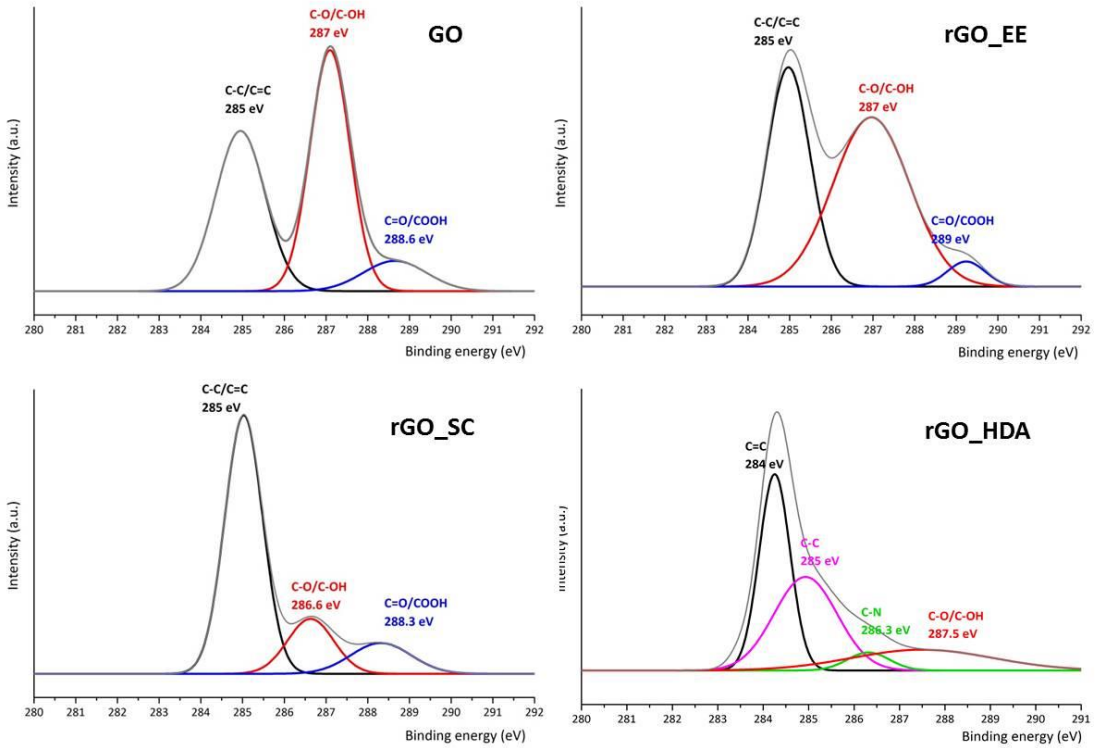

Figure 3.10 – XPS spectra and curve-fitting of C1s of GO, rGO reduced with eucalyptus extracts (rGO_EE), sodium citrate (rGO_SC) and hydroxylamine (rGO_HDA).

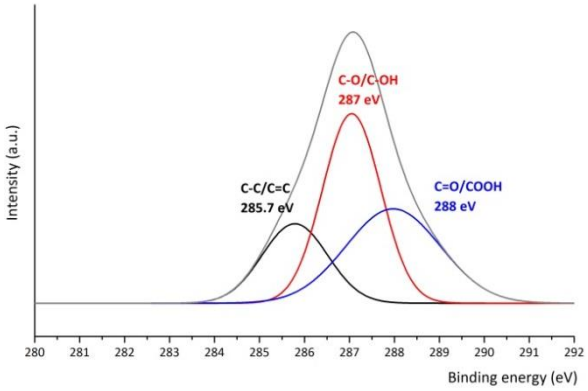

Figure 3.11 – XPS spectrum and curve-fitting of C1s of rGO_glucose as reducing agent

Table 3.1 – XPS data of GO and rGO samples obtained by using eucalyptus extract, sodium citrate and hydroxylamine.

Bond	GO		rGO_EE		rGO_SC		rGO_HDA	
	Peak BE (eV)	At. %	Peak BE (eV)	At. %	Peak BE (eV)	At. %	Peak BE (eV)	At. %
C-C/C=C	285	40.7	285	40.3	285.0	69.1	284.3 / 284.9	76.5
C-N	-	-	-	-	-	-	286.3	4.8
C-O/C-OH	287	49.4	287	55.6	286.6	17.9	287.5	18.7
C=O/COOH	288.6	9.9	289	4.0	288.3	13.1	-	-
Ratio C/O	**-**	**0.7**		**0.7**	**-**	**2.2**	**-**	**4.4**

The rGO_SC exhibits a significant decrease of the peak intensity for the C-O/C-OH (from 49.4 at% in GO to 17.9 at% in rGO_SC), an increase of the peak intensity for the C=C/C–C (from 40.7 at% in GO to 69.1 at% in rGO_SC), and an increase of the C/O ratio (0.7 to 2.2 (Table 3.1)) which is indicative of GO reduction. However, there was an increase of the C=O band at 288.3 eV (from 9.9 at% in GO to 13.1 at% in rGO_SC) which derives from sodium citrate absorption on the surface of rGO, in good agreement with TG results.

With respect to rGO_HDA, the ratio C/O of 4.4 clearly indicates the higher deoxygenation of the initial GO (Table 3.1). In the case of rGO_HDA is possible identify separately the groups C=C and C-C (Figure 3.10). An increase of the quantity of C=C and C–C (from 40.7 at% in GO to 76.5 at% in rGO_HDA) is observed together with a decrease of the oxygen groups (C-O/C-OH from 49.4 at% in GO to 18.7 at% in rGO_HDA and the disappearance of C=O/COOH in rGO_HDA). It should also be noted that a new peak emerges at 286.3 eV corresponding to the C-N bonding resultant from the functionalization of GO surface by hydroxylamine chemical treatment[53].

In the case of rGO_EE sample an increase in the intensity of the peak attributed to C-C/C=C bonds at 285 eV is observed (Figure 3.10). However the ratio C/O has the same value (0.7) as the GO sample. Moreover, rGO_EE shows an increased peak intensity for the C-O/C-OH band at 286.6 eV (from 49.4 at% in GO to 55.6 at% in rGO_EE) and a decreased intensity for the C=O band at 289 eV (from 9.9 at% in GO to 4 at% in rGO_EE). This can be explained by the possible interactions of EE molecules with GO structure. The EE are composed by several types of sugars and phenolic compounds[34], what difficult the identification of the possible interactions. In the same way, the sample rGO_glucose didn't allow obtaining credible XPS data. The curves are shown in Figure 3.11, however as can be observed, in this case there is an increase of the oxygen functional groups, what does not correspond to a reduction reaction. The explanation for this fact can be, once more, related with the interaction of glucose with GO surface.

3.2.2.5. Raman spectroscopy

The reduction of GO may be evaluated by the D/G peaks intensity ratio of the Raman spectra. The variation of the relative intensities of G band to D band in Raman spectra of GO during reduction usually reveals the change of electronic conjugation state. This change suggests an increase in the number of sp^2 domains with the reduction of GO[54].

To analyse the best performance of the reducing agents in reduction of GO, we analysed the D and G bands of the Raman spectra. For such analysis, previously was made the normalization of GO, rGO_SC, rGO_EE, rGO_G and rGO_HDA regarding the maximum of G peak. After that the fit of each band was made according to the type of curve. The function more appropriate to fit D band is the Lorentzian and to fit G band is the Breit-Wigner-Fano (BWF), since G band is an asymmetric curve caused by its resonant dispersion[55].

The ratio I_D/I_G is the most commonly used parameter to identify the reduction degree of GO, however recently another parameter was introduced which can also be helpful for this evaluation: the Full Width at Half Maximum (FWHM) of D peak[55]. The G peak has a complex origin that produces an asymmetric curve which is difficult to fit whereas D peaks fit the Lorentzian shape well. For that reason, the FWHM of (D) was chosen as new parameter to assess the reduction degree, as mentioned above.

The Raman spectra presented in this chapter were obtained using the lasers of 488 nm and 1064 nm (Figure 3.12 and Figure 3.13, respectively). The latter is not widely used to characterize graphitic materials; however this was the one most available for the present thesis work.

The Figure 3.12 show the two parameters I_D/I_G and FWHM (D) as a function of FWHM (G). The positions of the G bands are also inserted as function of two parameters chosen. The values of FWHM (G), obtained with Raman curves from the compounds analysed with Raman laser of 1064 nm, decrease as I_D/I_G increases by the following order: GO, rGO_SC, rGO, EE, rGO_G and rGO_HDA (Table 3.2). This tendency is also followed when FWHM (G) is shown as a function of FWHM (D).

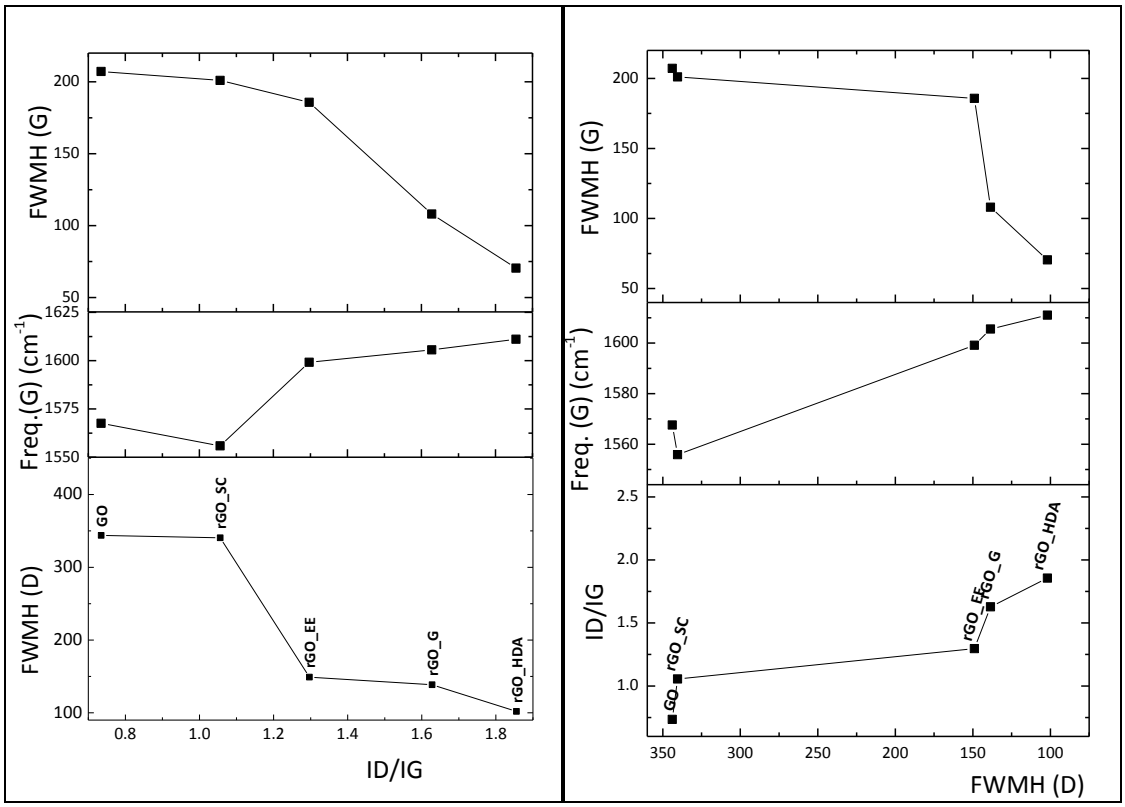

Figure 3.12 – Analysis of Raman values for GO and reduced nanocomposites using 1064 nm laser.

Table 3.2 – Raman analysis of GO and its reduced forms by Raman spectroscopy using the laser of 1064 nm. I_D and I_G are the intensities of the bands D and G, respectively; x_D and x_G are the positions of D and G peaks; FWMH (D) and FWMH (G) are the Full Width at Half Maximum of the bands D and G, respectively.

	I_D	x_D	FWMH (D)	I_G	x_G	FWMH (G)	I_D/I_G
GO	0.62	1351	343	0.85	1568	207	0.74
rGO_SC	0.79	1359	348	0.75	1556	201	1.06
rGO_EE	0.55	1304	149	0.43	1599	186	1.30
rGO_G	0.55	1291	138	0.34	1606	108	1.63
rGO_HDA	1.01	1287	101	0.54	1611	70	1.86

The Figure 3.13 shows the same parameters, obtained using the Raman laser of 488 nm, as in the Figure 3.12. In this case, by FWHM (G) in function of ID/IG, the degree of

GO reduction increases as follows: rGO_EE, rGO_SC, rGO_G and rGO_HDA. Also this series can be observed when FWHM (G) is evaluated as function of D band width. However, in the latter case, it seems that the reduction of GO are similar for rGO_EE and rGO-SC. The I_D/I_G values obtained using Raman laser of 488 nm (Table 3.3) reveal that sodium citrate is more effective than eucalyptus extracts in the reduction of GO.

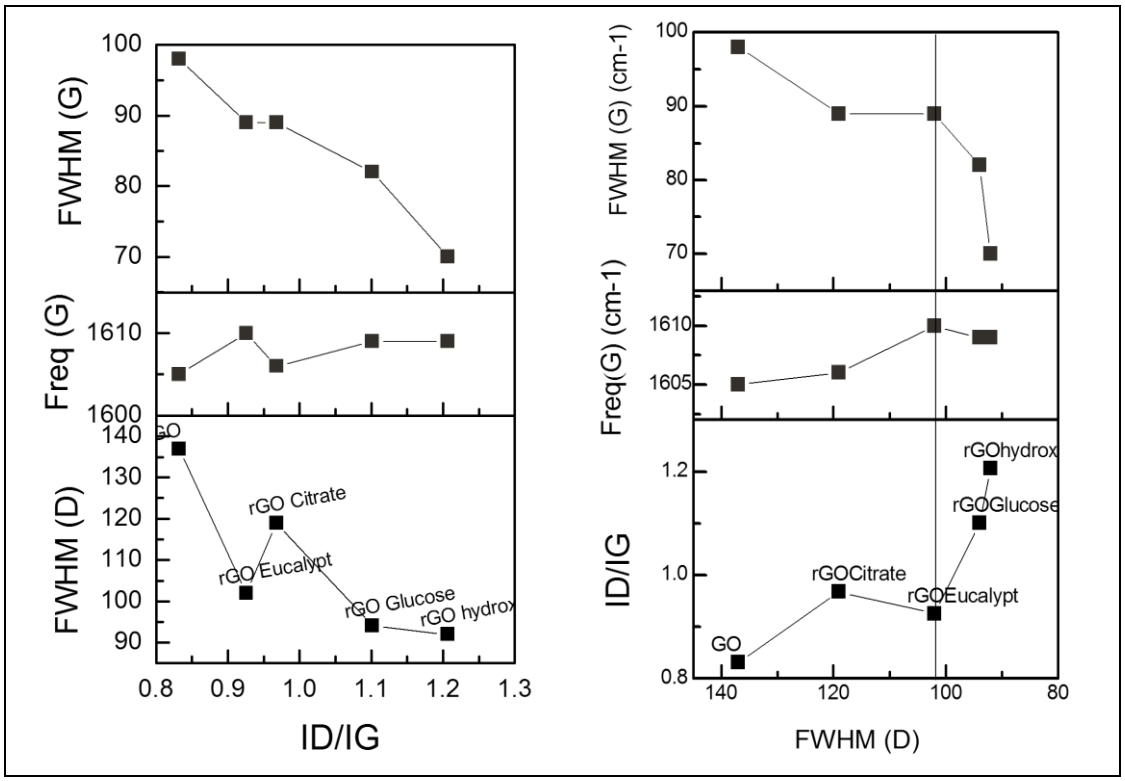

Figure 3.13– Analysis of Raman values for GO and reduced nanocomposites using 488 nm laser.

Table 3.3 – Raman analysis of GO and its reduced forms by Raman spectroscopy using the laser of 488 nm. ID and IG are the intensities of the bands D and G, respectively; xD and xG are the positions of D and G peaks; FWMH (D) and FWMH (G) are the Full Width at Half Maximum of the bands D and G, respectively.

	I_D	x_D	FWMH (D)	I_G	X_G	FWMH (G)	I_D/I_G
GO	0.79	1355	137	0.95	1605	98	0.83
rGO_SC	0.90	1350	119	0.93	1606	89	0.97
rGO_EE	0.87	1353	102	0.94	1610	89	0.93
rGO_G	0.98	1350	94	0.89	1609	82	1.10
rGO_HDA	1.11	1356	92	0.92	1609	70	1.21

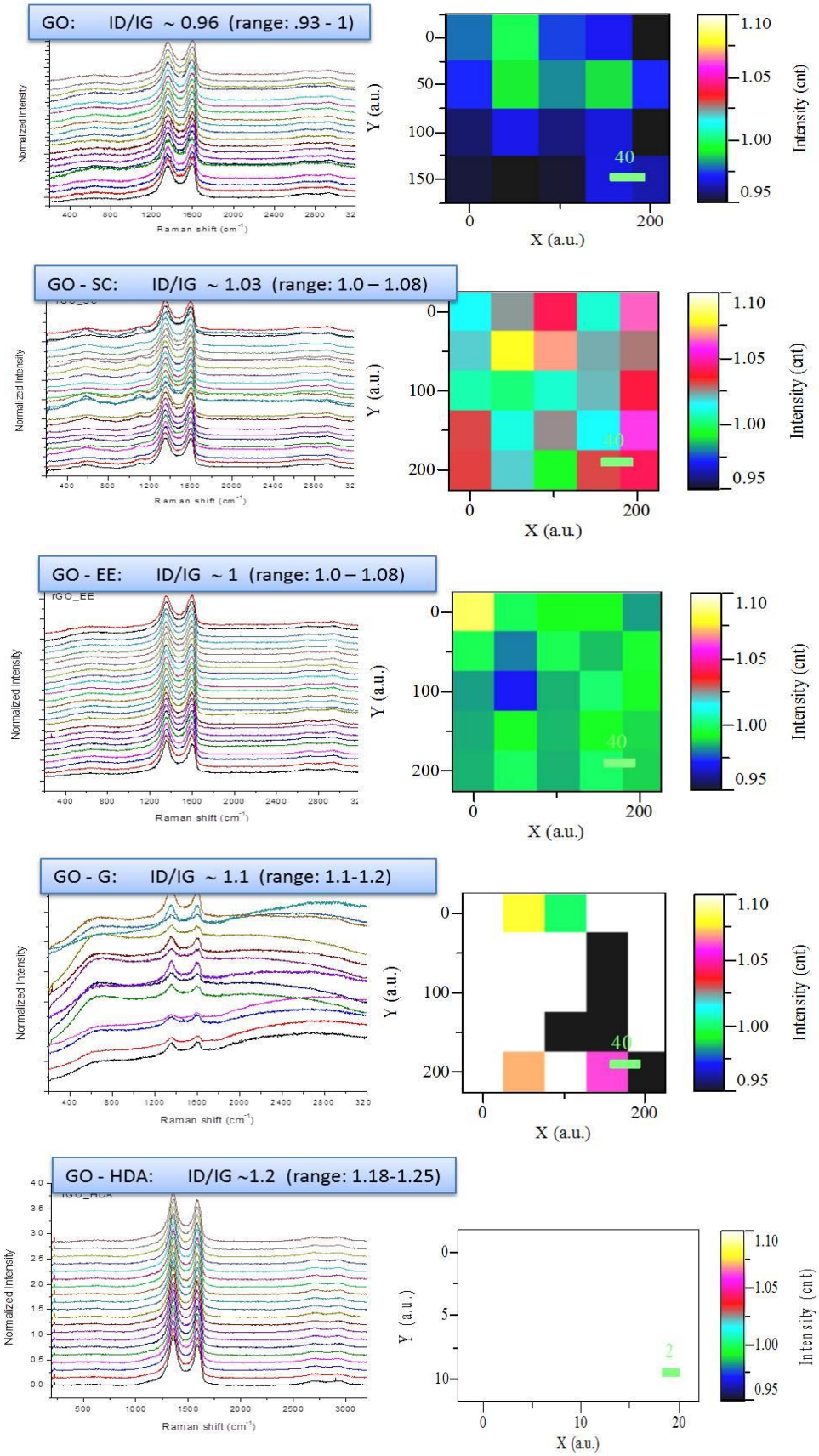

Figure 3.14 – Raman mapping of GO and reduced samples using 25 points of acquisition, laser 488 nm.

The Figure 3.14 shows the mapping (25 spectrum of each sample; the acquisition points are 40 μm from each other) and "Raman images" obtained from GO, rGO_SC, rGO_EE, rGO_G and rGO_HDA.

The homogeneity of the reduced samples can be observed by mapping images. The changes of the colour in the graphics show the changes in I_D/I_G. The image mapping of GO, rGO_EE and rGO_HDA are the most homogeneous. Besides, the mapping of rGO_SC shows a great change of colours its statistic values of I_D/I_G is similar to the results obtained after the fitting of D and G bands. In the case of rGO_G, the 25 spectra were not acquired due to the inhomogeneity of the film. However, the results obtained with the possible spectra revealed a statistic value of I_D/I_G , once again, close to the obtained with Lorentzian and BWF fitting of D and G peaks.

From the present analysis and based on these parameters, it is possible see that the higher rGO was obtained with glucose and hydroxylamine.

3.3. Conclusion

Graphene oxide was produced showing a good exfoliation (~1.3 nm of sheet thickness), a lateral size bigger than 3 μm and the oxygen-functional groups were confirmed by FTIR spectrum.

Hydroxylamine proved to be the most effective reducing agent of the set of chemical agents selected to reduce GO. This conclusion was confirmed by all characterization techniques (UV-vis, FTIR, TGA, XPS and Raman). Raman and UV-vis spectra showed that glucose seems the second more effective chemical agent to reduce GO; however this sugar was adsorbed at the surface of GO sheets as was seen in the results obtained by the techniques of FTIR, TGA and XPS.

In the case of the sodium citrate and eucalyptus extracts, the Raman analysis was not clear in what was the best to restore sp^2 C network whereas X-ray Photoelectron Spectroscopy results showed that sodium citrate was more efficient. However, the eucalyptus extracts show the same behaviour as glucose and was adsorbed at GO surface as was seen in FTIR spectra.

With the previous results it is possible to highlight the good quality of GO produced at the laboratory and conclude that the reducing agents used showed different efficiency in restoring the sp^2 carbon network of GO. Not all the oxygen functional groups were removed using these chemicals, under the experimental conditions used, and some of the chemicals were adsorbed at the final rGO material.

3.4. Experimental procedure

3.4.1. Synthesis of graphene oxide

GO was prepared by Marcano's method[22]. Briefly, 360 mL of H_2SO_4 were added to a mixture of 3 g of graphite flakes and 18 g of $KMnO_4$. 40 mL of H_3PO_4 were added to previous mixture very slowly. After 24 hours with stirring, the high viscous suspension formed was carefully added to ice. Then 10 mL of H_2O_2 were added and the suspension was heated to 50 ºC, 4 hours and after that was in sonication 1 hour. The product obtained was filtered several times and washed with deionized water. In order to obtain a GO suspension with pH 6 – 7, the filtered suspension was submitted to dialysis.

3.4.2. Reduction of graphene oxide

rGO_sodium citrate. A suspension of 0.15 mg/mL of GO (50 mL) was heated until 80 ºC, after 1.880 mL of sodium citrate (0.085 mol dm^{-3}) was added dropwise. The experimental conditions were maintained during 1 hour.

rGO_glucose. 1.2 g of D-(+)glucose was dissolved into 40 mL of a suspension of GO (0.75 mg/mL). The mixture was in sonication about 5 min. Then, 1 mL of ammonia (25%) was added and the final suspension was again in sonication, during 5 min.

rGO_eucalyptus extract. 70.75 mg of eucalyptus extract was added to a suspension of GO (0.50 mg/mL, 100 mL). The mixture was stirring for several minutes.

rGO_hydroxylamine. 2 mL of NH_2OH (100 mmol dm^{-3}) were added to a suspension of GO (0.5 mg/mL, 10 mL). The suspension was in stirring during 30 minutes and the brown yellow initial became darker. The pH was adjusted to 12 with NaOH aqueous solution (0.1 mol dm^{-3}). After that, the suspension was heated to 80 ºC, during 1 hour.

All the reduced nanocomposites were washed by centrifugation.

3.5. Bibliography

(1) Yang, K.; Li, Y.; Tan, X.; Peng, R.; Liu, Z. Behavior and Toxicity of Graphene and Its Functionalized Derivatives in Biological Systems. *Small* **2013**, *9*, 1492-1503.

(2) Feng, L.; Liu, Z. Graphene in biomedicine: opportunities and challenges. *Nanomedicine* **2011**, *6*, 317-324.

(3) Bitounis, D.; Ali-Boucetta, H.; Hong, B. H.; Min, D.-H.; Kostarelos, K. Prospects and Challenges of Graphene in Biomedical Applications. *Advanced Materials* **2013**, *25*, 2258-2268.

(4) Shen, H.; Zhang, L.; Liu, M.; Zhang, Z. Biomedical Applications of Graphene. *Theranostics* **2012**, *2*, 283-294.

(5) Zhang, Y.; Nayak, T. R.; Hong, H.; Cai, W. Graphene: a versatile nanoplatform for biomedical applications. *Nanoscale* **2012**, *4*, 3833-3842.

(6) Feng, L.; Wu, L.; Qu, X. New Horizons for Diagnostics and Therapeutic Applications of Graphene and Graphene Oxide. *Advanced Materials* **2013**, *25*, 168-186.

(7) Lu, C.-H.; Yang, H.-H.; Zhu, C.-L.; Chen, X.; Chen, G.-N. A Graphene Platform for Sensing Biomolecules. *Angewandte Chemie International Edition* **2009**, *48*, 4785-4787.

(8) He, S.; Song, B.; Li, D.; Zhu, C.; Qi, W.; Wen, Y.; Wang, L.; Song, S.; Fang, H.; Fan, C. A Graphene Nanoprobe for Rapid, Sensitive, and Multicolor Fluorescent DNA Analysis. *Advanced Functional Materials* **2010**, *20*, 453-459.

(9) Tang, L. A. L.; Wang, J.; Loh, K. P. Graphene-Based SELDI Probe with Ultrahigh Extraction and Sensitivity for DNA Oligomer. *Journal of the American Chemical Society* **2010**, *132*, 10976-10977.

(10) Goncalves, G.; Marques, P. A. A. P.; Granadeiro, C. M.; Nogueira, H. I. S.; Singh, M. K.; Gracio, J. Surface Modification of Graphene Nanosheets with Gold

Nanoparticles: The Role of Oxygen Moieties at Graphene Surface on Gold Nucleation and Growth. *Chemistry of Materials* **2009**, *21*, 4796-4802.

(11) Edwards, R. S.; Coleman, K. S. Graphene synthesis: relationship to applications. *Nanoscale* **2013**, *5*, 38-51.

(12) Novoselov, K. S.; Geim, A. K.; Morozov, S. V.; Jiang, D.; Zhang, Y.; Dubonos, S. V.; Grigorieva, I. V.; Firsov, A. A. Electric Field Effect in Atomically Thin Carbon Films. *Science* **2004**, *306*, 666-669.

(13) Merino, P.; Švec, M.; Pinardi, A. L.; Otero, G.; Martín-Gago, J. A. Strain-Driven Moiré Superstructures of Epitaxial Graphene on Transition Metal Surfaces. *ACS Nano* **2011**, *5*, 5627-5634.

(14) Campos-Delgado, J.; Romo-Herrera, J. M.; Jia, X.; Cullen, D. A.; Muramatsu, H.; Kim, Y. A.; Hayashi, T.; Ren, Z.; Smith, D. J.; Okuno, Y.; Ohba, T.; Kanoh, H.; Kaneko, K.; Endo, M.; Terrones, H.; Dresselhaus, M. S.; Terrones, M. Bulk Production of a New Form of sp2 Carbon: Crystalline Graphene Nanoribbons. *Nano Letters* **2008**, *8*, 2773-2778.

(15) Kosynkin, D. V.; Higginbotham, A. L.; Sinitskii, A.; Lomeda, J. R.; Dimiev, A.; Price, B. K.; Tour, J. M. Longitudinal unzipping of carbon nanotubes to form graphene nanoribbons. *Nature* **2009**, *458*, 872-876.

(16) Cano-Márquez, A. G.; Rodríguez-Macías, F. J.; Campos-Delgado, J.; Espinosa-González, C. G.; Tristán-López, F.; Ramírez-González, D.; Cullen, D. A.; Smith, D. J.; Terrones, M.; Vega-Cantú, Y. I. Ex-MWNTs: Graphene Sheets and Ribbons Produced by Lithium Intercalation and Exfoliation of Carbon Nanotubes. *Nano Letters* **2009**, *9*, 1527-1533.

(17) Jiao, L.; Zhang, L.; Wang, X.; Diankov, G.; Dai, H. Narrow graphene nanoribbons from carbon nanotubes. *Nature* **2009**, *458*, 877-880.

(18) Casero, E.; Alonso, C.; Vázquez, L.; Petit-Domínguez, M. D.; Parra-Alfambra, A. M.; de la Fuente, M.; Merino, P.; Álvarez-García, S.; de Andrés, A.; Pariente, F.; Lorenzo, E. Comparative Response of Biosensing Platforms Based on Synthesized Graphene Oxide and Electrochemically Reduced Graphene. *Electroanalysis* **2013**, *25*, 154-165.

(19) Brodie, B. C. On the Atomic Weight of Graphite. *Proceedings of Royal Society of London* **1859**, *10*, 11-12.

(20) Staudenmaier, L. Verfahren zur Darstellung der Graphitsäure. *Berichte der deutschen chemischen Gesellschaft* **1898**, *31*, 1481-1487.

(21) Hummers, W. S.; Offeman, R. E. Preparation of Graphitic Oxide. *J Am Chem Soc* **1958**, *80*, 1339-1339.

(22) Marcano, D. C.; Kosynkin, D. V.; Berlin, J. M.; Sinitskii, A.; Sun, Z.; Slesarev, A.; Alemany, L. B.; Lu, W.; Tour, J. M. Improved synthesis of graphene oxide. *Acs Nano* **2010**, *4*, 4806-4814.

(23) Chua, C. K.; Pumera, M. Chemical reduction of graphene oxide: a synthetic chemistry viewpoint. *Chemical Society Reviews* **2013**.

(24) Gao, X. F.; Jang, J.; Nagase, S. Hydrazine and Thermal Reduction of Graphene Oxide: Reaction Mechanisms, Product Structures, and Reaction Design. *Journal of Physical Chemistry C* **2010**, *114*, 832-842.

(25) Mu, X.; Wu, X.; Zhang, T.; Go, D. B.; Luo, T. Thermal Transport in Graphene Oxide – From Ballistic Extreme to Amorphous Limit. *Sci. Rep.* **2014**, *4*.

(26) Dreyer, D. R.; Park, S.; Bielawski, C. W.; Ruoff, R. S. The chemistry of graphene oxide. *Chem Soc Rev* **2010**, *39*, 228-240.

(27) Eigler, S.; Hirsch, A. Chemistry with Graphene and Graphene Oxide—Challenges for Synthetic Chemists. *Angewandte Chemie International Edition* **2014**, *53*, 7720-7738.

(28) Goncalves, G. A. B.; Pires, S. M. G.; Simoes, M. M. Q.; Neves, M. G. P. M. S.; Marques, P. A. A. P. Three-dimensional graphene oxide: a promising green and sustainable catalyst for oxidation reactions at room temperature. *Chemical Communications* **2014**, *50*, 7673-7676.

(29) Liu, S.; Tian, J.; Wang, L.; Li, H.; Zhang, Y.; Sun, X. Stable Aqueous Dispersion of Graphene Nanosheets: Noncovalent Functionalization by a Polymeric Reducing Agent and Their Subsequent Decoration with Ag Nanoparticles for Enzymeless Hydrogen Peroxide Detection. *Macromolecules* **2010**, *43*, 10078-10083.

(30) Zhang, Z.; Chen, H.; Xing, C.; Guo, M.; Xu, F.; Wang, X.; Gruber, H.; Zhang, B.; Tang, J. Sodium citrate: A universal reducing agent for reduction / decoration of graphene oxide with au nanoparticles. *Nano Research* **2011**, *4*, 599-611.

(31) Pristinski, D.; Tan, S. L.; Erol, M.; Du, H.; Sukhishvili, S. In situ SERS study of Rhodamine 6G adsorbed on individually immobilized Ag nanoparticles. *Journal of Raman Spectroscopy* **2006**, *37*, 762-770.

(32) Hu, Y. J.; Jin, J. A.; Wu, P.; Zhang, H.; Cai, C. X. Graphene-gold nanostructure composites fabricated by electrodeposition and their electrocatalytic activity toward the oxygen reduction and glucose oxidation. *Electrochimica Acta* **2010**, *56*, 491-500.

(33) Tang, X.-Z.; Li, X.; Cao, Z.; Yang, J.; Wang, H.; Pu, X.; Yu, Z.-Z. Synthesis of graphene decorated with silver nanoparticles by simultaneous reduction of graphene oxide and silver ions with glucose. *Carbon* **2013**, *59*, 93-99.

(34) Santos, S. A. O.; Pinto, R. J. B.; Rocha, S. M.; Marques, P. A. A. P.; Neto, C. P.; Silvestre, A. J. D.; Freire, C. S. R. Unveiling the Chemistry behind the Green Synthesis of Metal Nanoparticles. *ChemSusChem* **2014**, *7*, 2704-2711.

(35) Nergiz, S. Z.; Gandra, N.; Singamaneni, S. Self-assembled high aspect ratio gold nanostar/graphene oxide hybrid nanorolls. *Carbon* **2014**, *66*, 585-591.

(36) Zhou, X.; Zhang, J.; Wu, H.; Yang, H.; Zhang, J.; Guo, S. Reducing Graphene Oxide via Hydroxylamine: A Simple and Efficient Route to Graphene. *Journal of Physical Chemistry C* **2011**, *115*, 11957-11961.

(37) Stankovich, S.; Dikin, D. A.; Piner, R. D.; Kohlhaas, K. A.; Kleinhammes, A.; Jia, Y.; Wu, Y.; Nguyen, S. T.; Ruoff, R. S. Synthesis of graphene-based nanosheets via chemical reduction of exfoliated graphite oxide. *Carbon* **2007**, *45*, 1558-1565.

(38) Kuldeep, S.; Anil, O.; S.K., D. x.: **Polymer-Graphene Nanocomposites: Preparation, Characterization, Properties, and Applications**. In *NANOCOMPOSITES -NEW TRENDS AND DEVELOPMENTS*; Ebrahimi, F., Ed.; InTech: Croatia, 2012.

(39) Minati, L.; Benetti, F.; Chiappini, A.; Speranza, G. One-step synthesis of star-shaped gold nanoparticles. *Colloids and Surfaces a-Physicochemical and Engineering Aspects* **2014**, *441*, 623-628.

(40) Zhang, J.; Yang, H.; Shen, G.; Cheng, P.; Guo, S. Reduction of graphene oxide via L-ascorbic acid. *Chemical Communications* **2010**, *46*, 1112-1114.

(41) Zhu, C. Z.; Guo, S. J.; Fang, Y. X.; Dong, S. J. Reducing Sugar: New Functional Molecules for the Green Synthesis of Graphene Nanosheets. *Acs Nano* **2010**, *4*, 2429-2437.

(42) Li, D.; Müller, M. B.; Gilje, S.; Kaner, R. B.; Wallace, G. G.; Muller, M. B. Processable aqueous dispersions of graphene nanosheets. *Nat Nanotechnol* **2008**, *3*, 101-105.

(43) Zhang, J.; Yang, H.; Shen, G.; Cheng, P.; Zhang, J.; Guo, S. Reduction of graphene oxide vial-ascorbic acid. *Chemical Communications* **2010**, *46*, 1112-1114.

(44) Li, J.; Liu, C. Y. Ag/Graphene Heterostructures: Synthesis, Characterization and Optical Properties. *European Journal of Inorganic Chemistry* **2010**, 1244-1248.

(45) Leila, S.; A, A. A. Graphene Oxide Synthesized by using Modified Hummers Approach. *International Journal of Renewable Energy and Environmental Engineering* **2014**, *2*, 58-63.

(46) Sudesh and, N. K. a. S. D. a. C. B. a. G. D. V. Effect of graphene oxide doping on superconducting properties of bulk MgB 2. *Superconductor Science and Technology* **2013**, *26*, 095008.

(47) Nethravathi, C.; Rajamathi, M. Chemically modified graphene sheets produced by the solvothermal reduction of colloidal dispersions of graphite oxide. *Carbon* **2008**, *46*, 1994-1998.

(48) Pham, V. H.; Cuong, T. V.; Hur, S. H.; Oh, E.; Kim, E. J.; Shin, E. W.; Chung, J. S. Chemical functionalization of graphene sheets by solvothermal reduction of a

graphene oxide suspension in N-methyl-2-pyrrolidone. *Journal of Materials Chemistry* **2011**, *21*, 3371-3377.

(49) da Silva, M.; de Jesus Fraga da Costa, H.; Triboni, E.; Politi, M.; Isolani, P. Synthesis and characterization of CeO2–graphene composite. *Journal of Thermal Analysis and Calorimetry* **2012**, *107*, 257-263.

(50) Gao, J.; Wang, Y.; Hao, H. Investigations on dehydration processes of trisodium citrate hydrates. *Frontiers of Chemical Science and Engineering* **2012**, *6*, 276-281.

(51) Arrieta, A. A.; Gañán, P. F.; Márquez, S. E.; Zuluaga, R. Electrically conductive bioplastics from cassava starch. *Journal of the Brazilian Chemical Society* **2011**, *22*, 1170-1176.

(52) Bagri, A.; Mattevi, C.; Acik, M.; Chabal, Y. J.; Chhowalla, M.; Shenoy, V. B. Structural evolution during the reduction of chemically derived graphene oxide. *Nature …* **2010**, *2*, 581-587.

(53) Pei, S.; Cheng, H.-M. The reduction of graphene oxide. *Carbon* **2012**, *50*, 3210-3228.

(54) Chen, D. Z.; Li, L. D.; Guo, L. An environment-friendly preparation of reduced graphene oxide nanosheets via amino acid. *Nanotechnology* **2011**, *22*.

(55) Diez-Betriu, X.; Alvarez-Garcia, S.; Botas, C.; Alvarez, P.; Sanchez-Marcos, J.; Prieto, C.; Menendez, R.; de Andres, A. Raman spectroscopy for the study of reduction mechanisms and optimization of conductivity in graphene oxide thin films. *Journal of Materials Chemistry C* **2013**, *1*, 6905-6912.

4. AgGO and AuGO nanocomposites as SERS substrates

In this chapter, the efficiency of several types of silver-graphene (AgGO) and gold-graphene (AuGO) nanocomposites as surface-enhanced Raman scattering (SERS) substrates was investigated. After the preparation and characterization of these nanocomposites, the influence of the metal nanoparticles in the enhancement of the Raman of graphene itself was studied. Different types of supports for the SERS substrates and different analytes were studied with the SERS substrates produced.

4.1. Introduction

Recently, graphene has been shown to have a clear Raman enhancing effect, related to its unique flexible and smooth 2D honeycomb structure with a one-atom thickness[1-4]. By decorating graphene nanosheets with silver nanoparticles a significantly enhanced Raman signal of graphene was found by Xu et al.[5] Additionally, combination of these two materials can also be used to detect molecules at very low concentrations[6]. Among known strategies for generating graphene-based nanomaterials, starting from graphene oxide is the most versatile and easily scalable method. Graphene oxide has a single or few layers of carbon structured nanosheets strongly oxygenated which are able to nucleate the metal nanoparticles[5,7]. Silver and gold nanoparticles display plasmon excitation in the visible spectrum, are very easy to prepare[8-10] and their incorporation in several nanocomposites is well-known[11-13].

Combining the characteristics of graphene with those of silver or gold nanoparticles, the resultant nanomaterial can act as a SERS substrate. There are several reducing agents that have been used to synthesize graphene-based nanocomposites. Hydrazine is one of the most common and effective reducing agent for the reduction of graphene oxide but due to its toxicity and environmental protection measures, nowadays researchers are trying to replace it by eco-friendly reducing agents[14]. In this work, this was one of the concerns for the preparation of the metal nanoparticles-graphene oxide (MGO) nanocomposites and the reducing agents chosen were: sodium citrate, glucose and eucalyptus extracts. Sodium citrate have been already used in our research group to synthesize gold-graphene nanocomposites which have shown SERS activity[7]. Glucose is a well-known reducing agent used in the formation of MGO nanocomposites[15,16]. The extract of eucalyptus was also recently reported by our group as a reducing agent[17] and used to prepare MGO nanocomposites.

4.2. Results and Discussion

The nomenclature adopted to identify the MGO nanocomposites prepared with the different chemical agents was the following: MGO_sodium citrate, MGO_glucose and

MGO_eucalyptus extract (M = Ag or Au), in some cases it will be used to abbreviate MGO_SC, MGO_G and MGO_EE, respectively. In the case of gold nanocomposites hydroxylamine was also used as reducing agent[18] (AuGO_hydroxylamine or AuGO_HDA). The previous nanocomposites were evaluated for its capacity as SERS substrates in varied conditions.

4.2.1. Characterization of AgGO and AuGO nanocomposites

The AgGO and AuGO nanocomposites were synthesized according to the experimental procedure described in section 4.4. The reducing agents used were sodium citrate, glucose and eucalyptus extract (Scheme 4.1); in the case of AuGO hydroxylamine, NH_2OH, was also used.

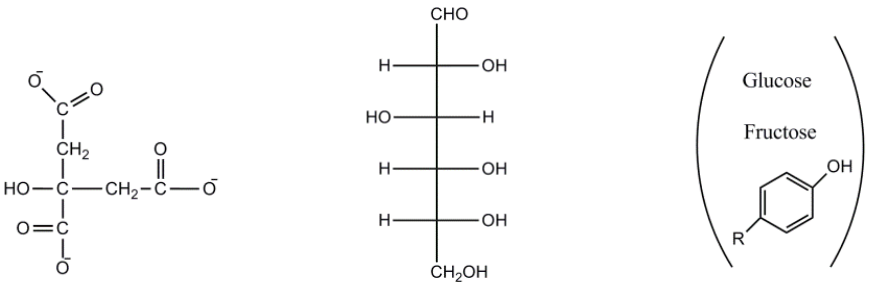

citrate glucose eucalyptus extract

Scheme 4.1 – Reducing agents used for the *in situ* synthesis of MGO nanocomposites.

The presence of oxygen-groups in the surface of GO allows the nucleation of metallic nanoparticles[7]. In the GO surface, due to the large number of oxygen-containing functional groups, the distribution of metal nanoparticles can be successfully done (Scheme 4.1). This approach is a possibility to obtain platforms that can be used as SERS substrates because the electromagnetic sites are well distributed almost "ordered", which is a requirement to obtain a good Raman signal enhancement[19]. The reduction process will affect both the metal ions, originating the metal nanoparticles,

and the graphene oxide that will be converted to reduced graphene oxide (Scheme 4.2).

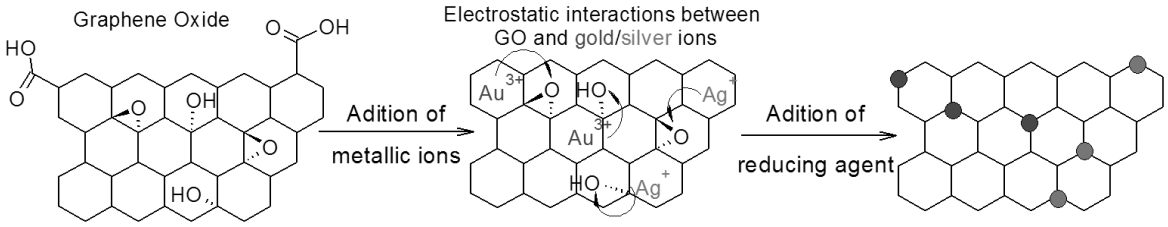

Scheme 4.2 – *In situ* synthesis of silver or gold nanoparticles in the presence of graphene oxide.

Scanning electron microscopy (SEM) and UV-vis absorption were used to characterize the as-prepared graphene-based nanocomposites (Figure 4.1 and 4.2). UV-vis spectra of the metal colloids obtained with the same reducing agents but in the absence of GO, and of GO itself were also recorded. Observing the SEM images it is possible to see the differences in the nanoparticles size depending on the reducing agent used. The reduced graphene oxide present in the metal nanocomposites continues to show transparency and the characteristic wrinkles which means that GO keeps its well exfoliated structure even after the composites preparation. In Figure 4.1, the silver nanoparticles grown in AgGO_sodium citrate and AgGO_eucalyptus extract show a very similar size, between 40 and 60 nm. This is confirmed by the UV-vis spectra of both nanocomposites and is according to previous results reported[17]. Using glucose as the reducing agent, the silver nanoparticles (AgNP) obtained are bigger than the AgNP obtained with the other two methods. The AgGO_glucose nanocomposites show AgNP with 100-200 nm of diameter. Such size differences will influence the SERS signals obtained using these composites as substrates, as will be shown later in this thesis.

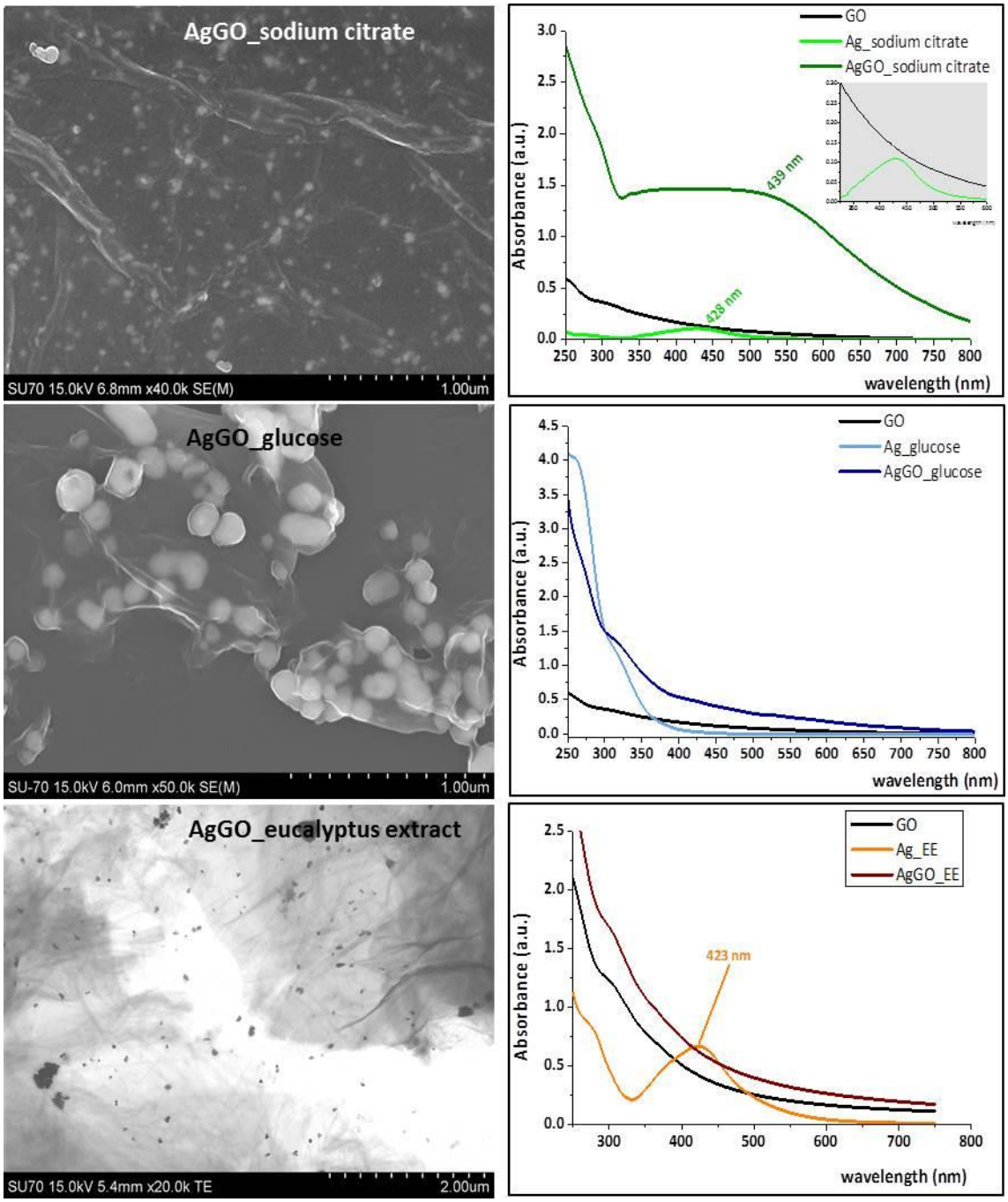

Figure 4.1 – UV-vis spectra and SEM images of AgGO nanocomposites obtained with three different reducing agents: sodium citrate, glucose and eucalyptus extract. UV-vis spectra of Ag colloids obtained with the same reducing agents but in the absence of GO, and of GO itself are also shown.

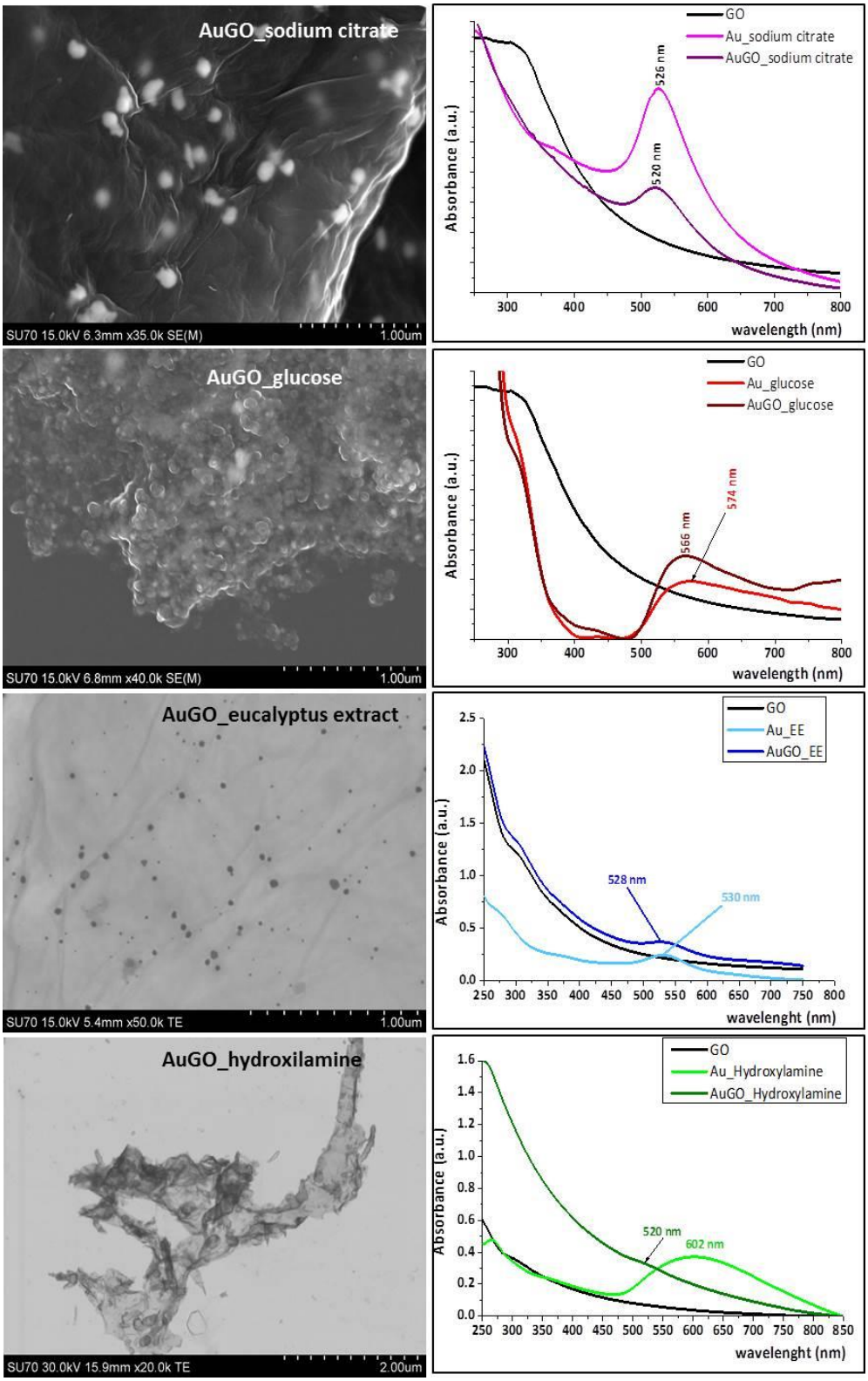

Figure 4.2 – UV-vis spectra and SEM images of AuGO nanocomposites obtained with four different reducing agents: sodium citrate, glucose, eucalyptus extract and hydroxylamine. UV-vis spectra of Au colloids obtained with the same reducing agents but in the absence of GO, and of GO itself are also shown.

In Figure 4.2, the UV-vis results indicate that when sodium citrate was used the gold nanoparticles should be quite similar in size to those produced with eucalyptus extract. However, in the SEM images, the gold nanoparticles present in the AuGO_sodium citrate nanocomposite are larger. The reduction with hydroxylamine originates gold nanoparticles with a star shape that cannot be observed in the SEM of AuGO_HDA, but is clearly shown in the SEM image of the gold colloid obtained by reduction with hydroxylamine (Figure 4.3). The λ_{max} in the UV-vis of the latter colloid is near 600 nm which is in agreement with the literature[18].

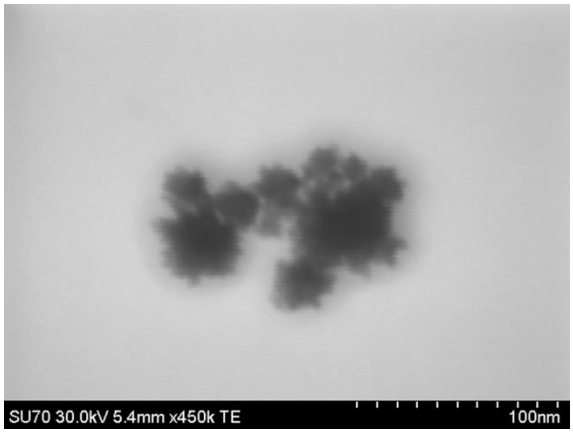

Figure 4.3 – SEM image of the star shaped nanoparticles in the gold colloid obtained by reduction with hydroxylamine.

4.2.2. SERS studies

4.2.2.1. SERS of graphene in AgGO and AuGO nanocomposites

The typical Raman bands D and G of graphene can be enhanced in the presence of metal nanoparticles. As mentioned in the introduction section of this chapter, Xu et al.[5] have demonstrated that by introducing AgNPs on reduced graphene oxide film there was an enhancement in the graphene Raman bands.

Here, we have studied the influence of growing metal nanoparticles at a GO surface, prepared by reduction with sodium citrate, glucose, eucalyptus extract and hydroxylamine, respectively, in the Raman spectra of the composites. For such analysis, the Raman laser of 488 nm was used. In Figure 4.4, each reducing agent are shown the Raman spectra of the initial GO (without reduction), rGO obtained with this agent, and the respective MGO composite.

The Raman spectrum of GO displayed the characteristic prominent D band around 1365 cm^{-1} and G band around 1595 cm^{-1} [20]. The Raman spectra of the AgGO nanocomposites showed a clear enhancement of the main typical bands of graphene, D, G and 2D, independently of the preparation method (Figure 4.4). The enhancement of the Raman bands of graphene observed in the composites is due to a SERS effect originated by the metal nanoparticles present.

The I_D/I_G ratio increases in rGO and AgGO when compared with GO, with the use of the three reducing agents (Figure 4.4). According to literature[6] this change suggested the decrease in the average size of the sp^2 domains, but more numerous in numbers upon reduction of the exfoliated GO. The exception occurs to AgGO_EE where the I_D/I_G decreases from 0.92 of GO to 0.90, which means that the reduction of oxygen groups of GO using eucalyptus extract in the presence of silver is smaller than using the other reducing agents. It is also important to refer that, in the three cases studied, the I_D/I_G ratio slightly decreases from the rGO to AgGO nanocomposites, this could be probably related with the presence of the AgNPs that disrupt the sp^2 domains.

It is referred that the Raman signals of graphene enhanced by silver nanoparticles, mainly arise from the SERS EM effect [4]. However, the enhancement of the Raman signals of the three AgGO nanocomposites varied significantly, which can be seen by the results obtained from I_D (AgGO)/I_D (GO) and I_G (AgGO)/I_G (GO) (Figure 4.6).

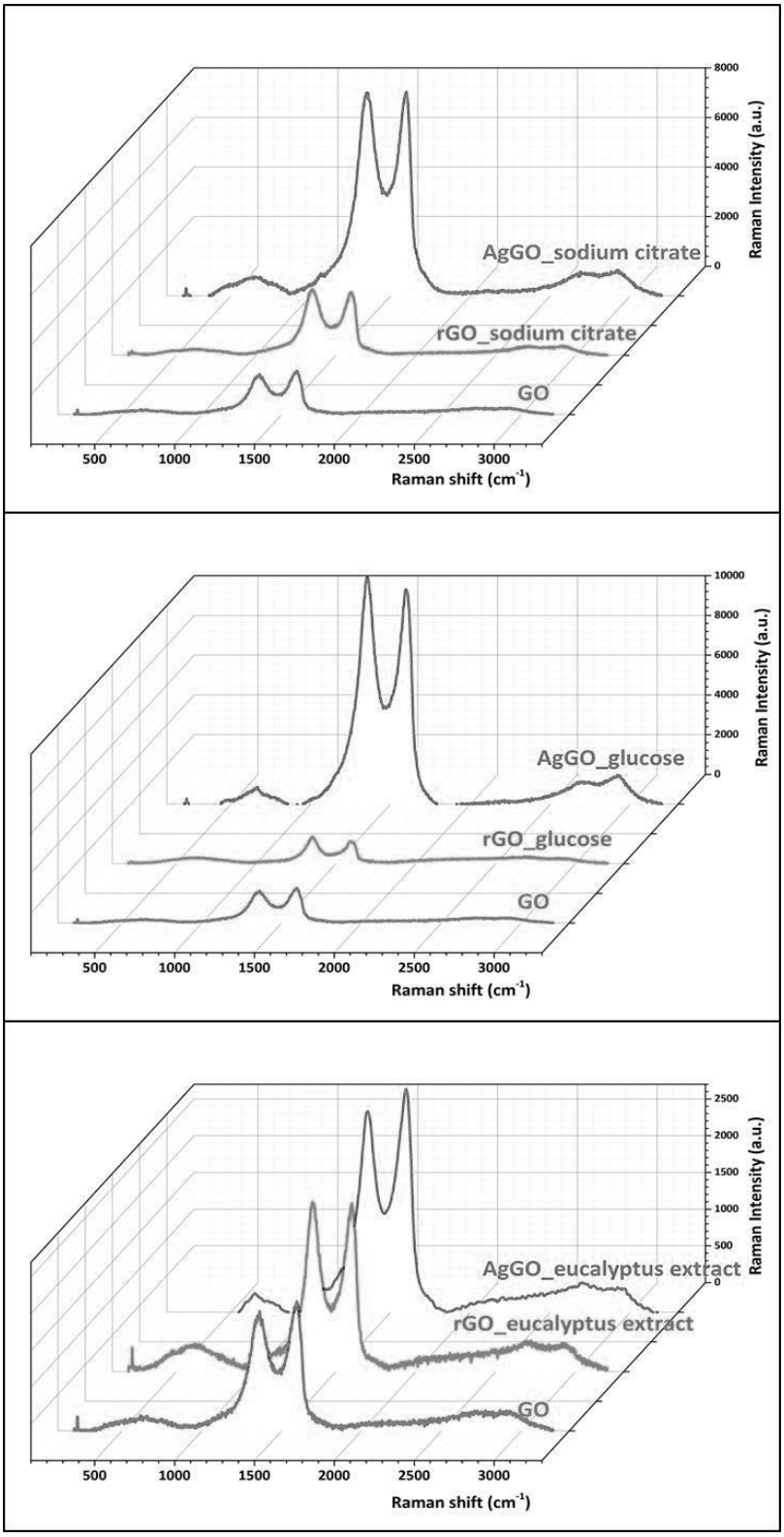

Figure 4.4 – Typical Raman bands of GO and rGO and AgGO nanocomposites prepared by using sodium citrate, glucose and eucalyptus extracts.

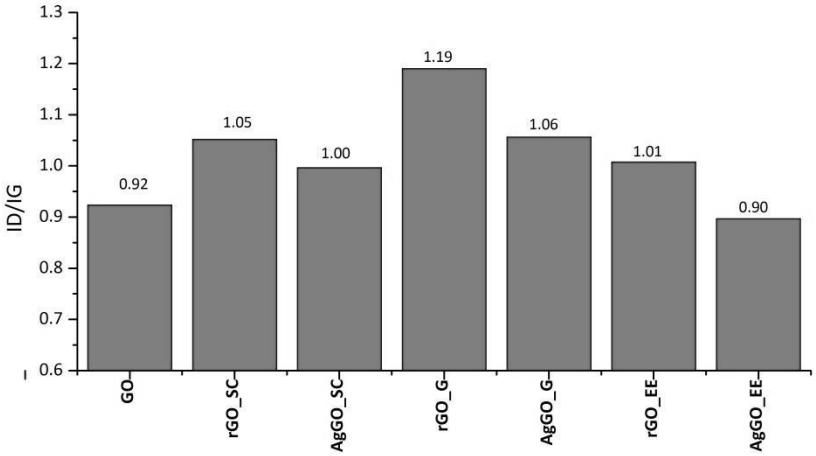

Figure 4.5 – Ratio I_D/I_G of GO and rGO and AgGO nanocomposites prepared by using sodium citrate, glucose and eucalyptus extracts.

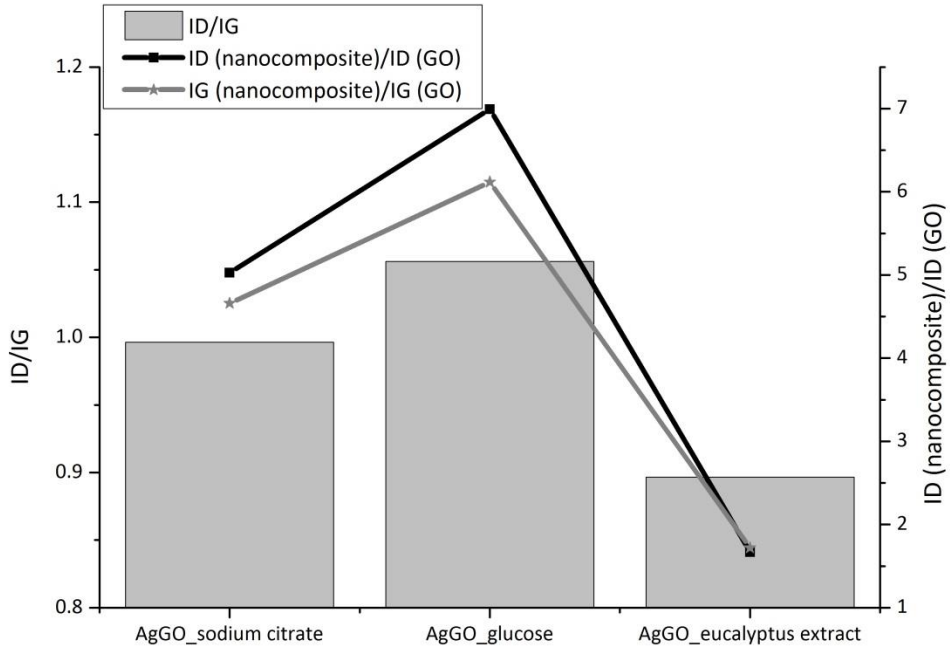

Figure 4.6 – Comparison between the rations I_D/I_G of each AgGO nanocomposite and I_D (reduced sample)/I_D (GO). Also the comparison was made related with I_G (reduced sample)/I_G (GO).

In the case of AuGO nanocomposites (Figure 4.7), only the nanoparticles of gold synthesized with hydroxylamine increase the intensity of D and G bands of the graphene matrix.

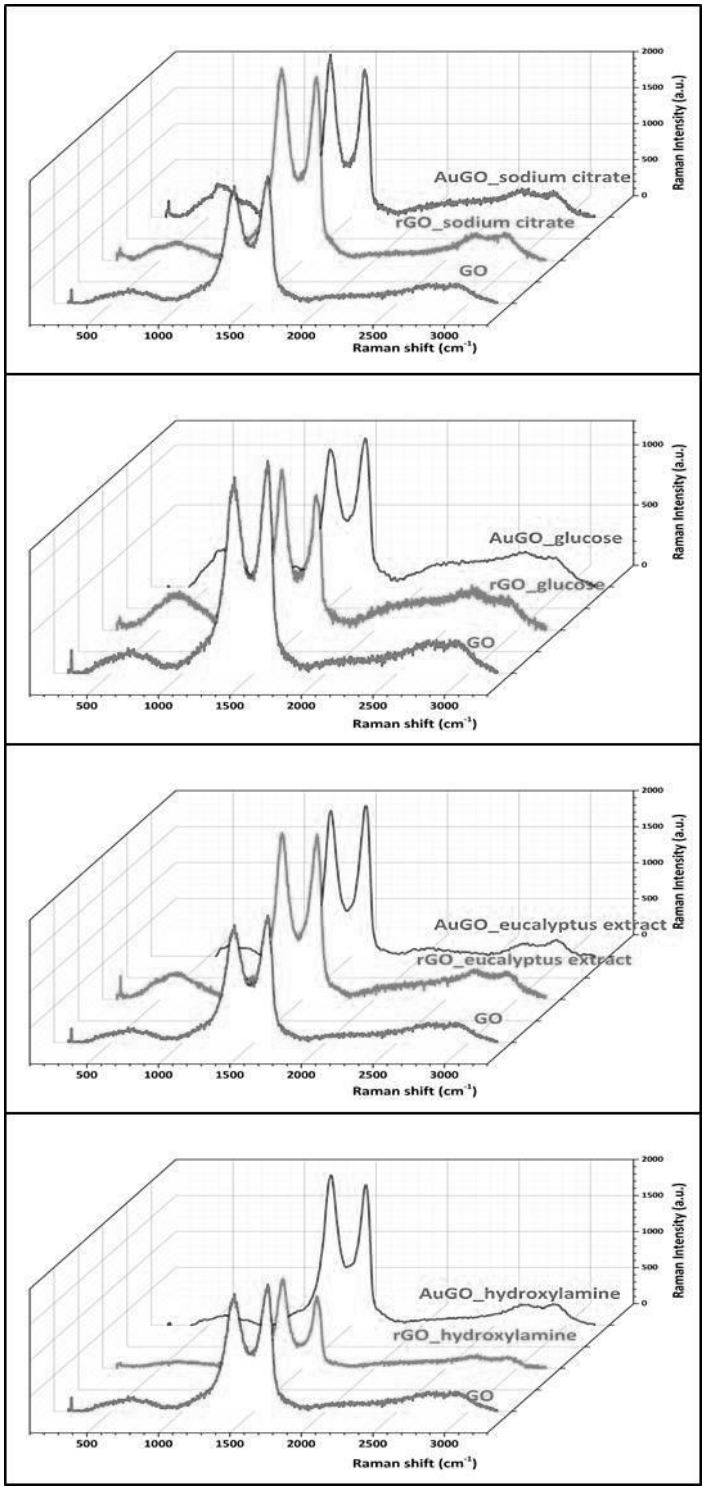

Figure 4.7 – Raman typical bands of GO and rGO and AuGO nanocomposites prepared by using sodium citrate, glucose, eucalyptus extracts and hydroxylamine.

Likewise the I_D/I_G increases in reduced GO, also the I_D/I_G in the presence of gold nanoparticles increases with the use of the four reducing agents (Figure 4.8). This change suggested the decrease in the average size of the sp^2 domains, but more numerous upon reduction of the GO[6]. The reduction of hydroxylamine is noticeable with I_D/I_G of 2.9.

It is well-known that the Raman signals of graphene can be enhanced by gold nanoparticles, which mainly arise from the SERS EM effect. However, in this case, the intensification of Raman signals were not noticeable (Figure 4.9). In the case of AuGO_glucose, the ratios I_D (nanocomposite)/ I_D (GO) and I_G (nanocomposite)/ I_G (GO) show a decrease of Raman intensities of D and G bands. All the other composites have a slightly enhancement of such bands.

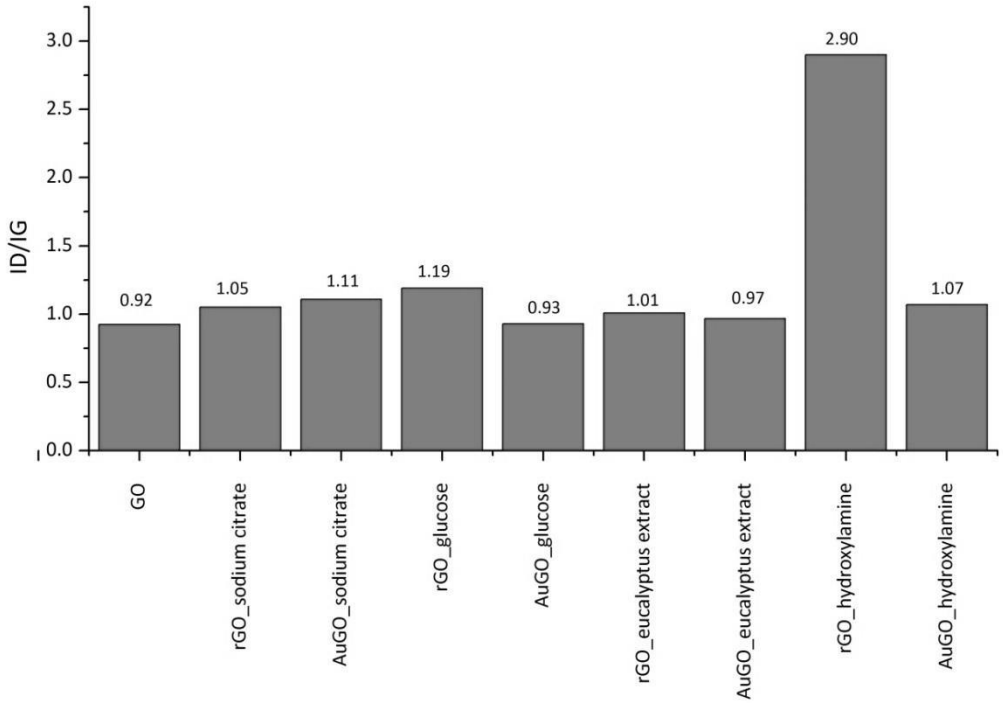

Figure 4.8 – Ratio I_D/I_G of GO and rGO and AuGO nanocomposites prepared by using sodium citrate, glucose, eucalyptus extracts and hydroxylamine.

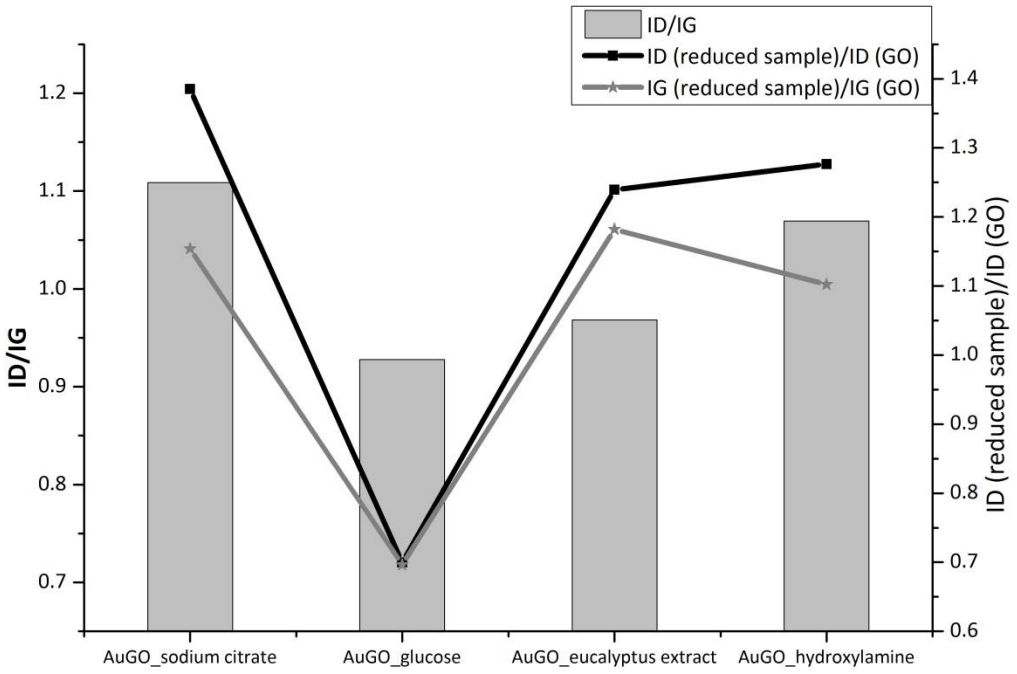

Figure 4.9 – Comparison between the rations I_D/I_G of each AuGO nanocomposite and I_D (reduced sample)/I_D (GO). Also the comparison was made related with I_G (reduced sample)/I_G (GO).

4.2.2.2. SERS substrates with AgGO and AuGO nanocomposites

Although the AgGO and AuGO nanocomposites, with the potential SERS activity, were characterized in suspension (as produced), the fabrication of SERS active substrates with easy to handle properties at low cost was one objective. One way to achieve this purpose is to support these suspensions by spreading in an adequate and easily to handle material. To support the nanocomposites suspensions we chose materials that were already available in the laboratory (filter paper and glass slides) or that were easy to produce (PVA membranes). These supports present different roughness which is one of the materials characteristics that can influence the SERS activity itself.

The MGO_sodium citrate and MGO_glucose (M = Ag and Au) were the selected nanocomposites and the laser used was the 1064 nm. For this study, thiosalicylic acid (SHsal) was the analyte chosen to test the SERS activity. The silver and gold

nanocomposites were tested in suspension or deposited in glass slides, filter paper and in PVA membranes (Figures 4.11 to 4.14).

To test the homogeneity of the substrate the AgGO nanocomposite was chosen, a SERS mapping of 25 regions of AgGO_sodium citrate with SHsal 1×10^{-3} mol dm^{-3} deposited on a glass slide was made. This type of mapping was recorded using a laser of 488 nm. Observing the spectra in Figure 4.10 it is possible to see the homogeneity of the SERS activity in the several points of the substrate area tested.

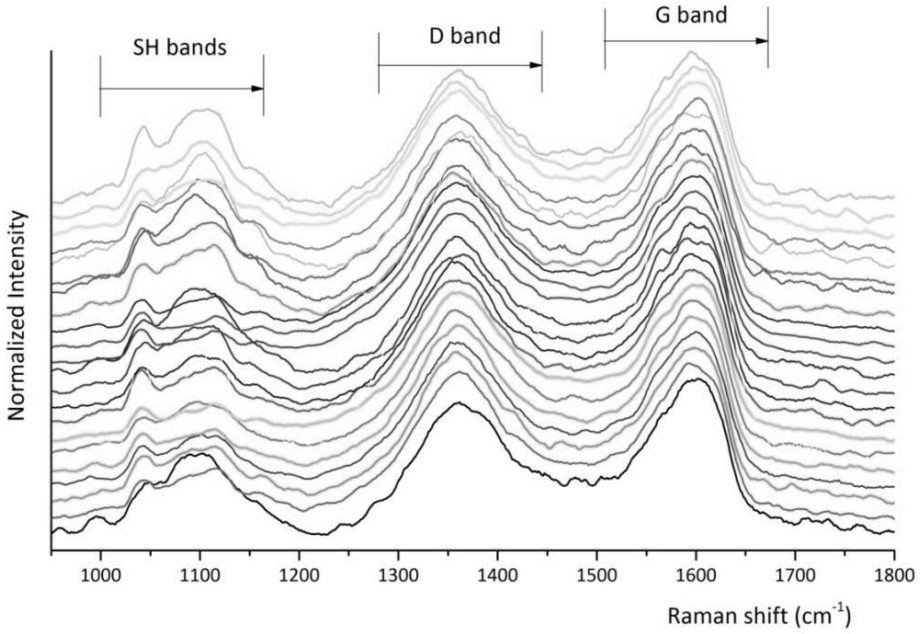

Figure 4.10 – Raman spectra from 25 spots of a glass slide in which it was deposited SHsal in AgGO_sodium citrate.

In the following Figures 4.11 to 4.14 the spectra on the left correspond to substrates reduced with sodium citrate, and the spectra on the right correspond to substrates reduced with glucose (as stated on the top). The study includes the SERS substrates used as suspension and deposited in the supports chose, namely glass slides, filter paper and PVA membranes.

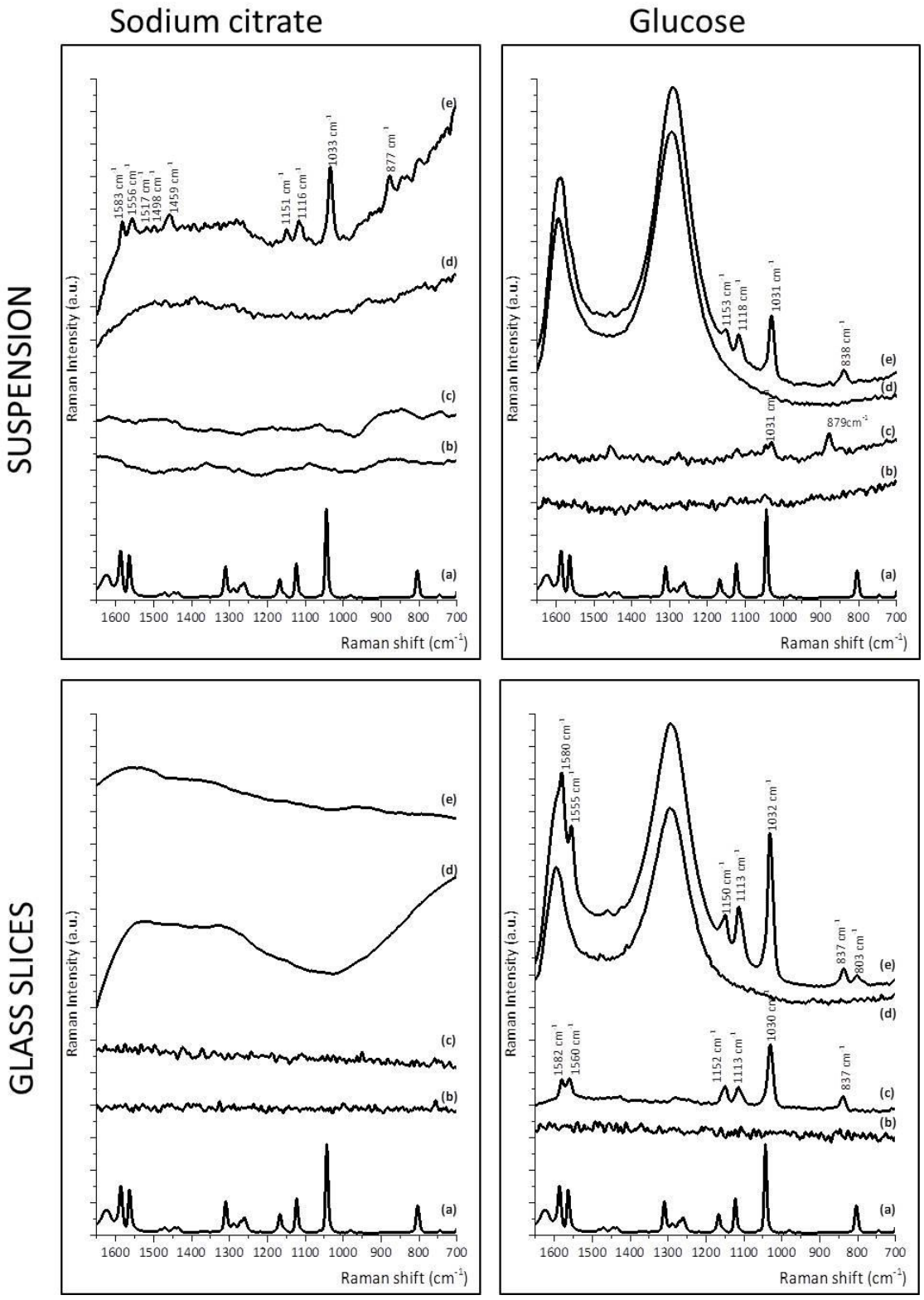

Figure 4.11 – SERS spectra of SHsal 10^{-3} mold m^{-3} in: AgGO_sodium citrate and AgGO_glucose both in suspension and glass slides (e). SERS spectra of SHsal 10^{-3} mol dm^{-3} in: Ag_sodium citrate and Ag_glucose both in suspension and glass slides (c). Raman spectra of solid SHsal (a) and of the substrates Ag_sodium citrate and Ag_glucose (b) and AgGO_sodium citrate and AgGO_glucose (d).

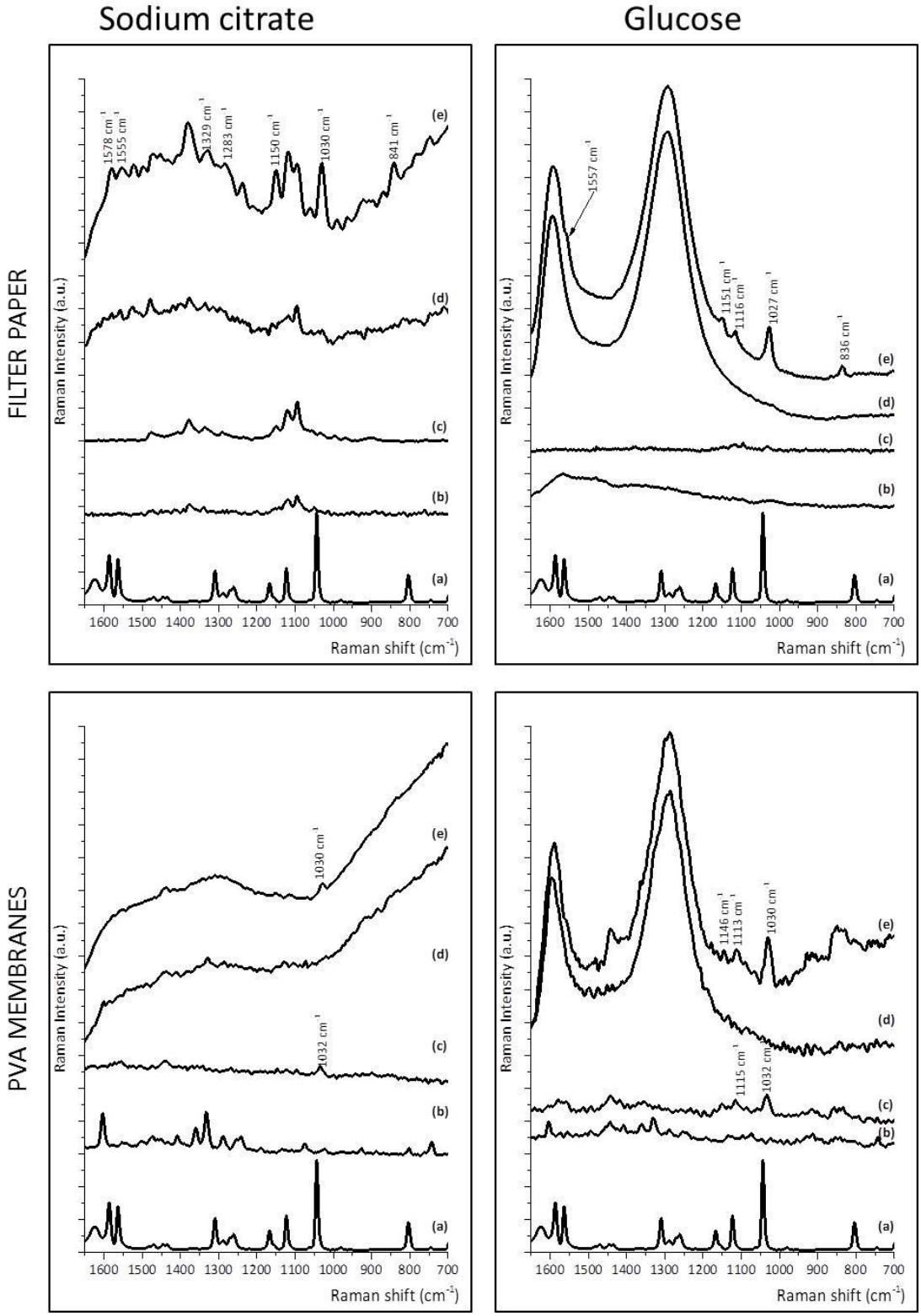

Figure 4.12 – SERS spectra of SHsal 10^{-3} mold m^{-3} in: AgGO_sodium citrate and AgGO_glucose both in filter paper and PVA membranes (e). SERS spectra of SHsal 10^{-3} mold m^{-3} in: Ag_sodium citrate and Ag_glucose both in filter paper and PVA membranes (c). Raman spectra of solid SHsal (a) and of the substrates Ag_sodium citrate and Ag_glucose (b) and AgGO _sodium citrate and AgGO_glucose (d).

Figure 4.11 and Figure 4.12 show a comparative study of the AgGO nanocomposites and Ag colloids (obtained under the same reduction conditions), as SERS substrates in the detection of SHsal. A clear SERS spectrum of SHsal was obtained in the substrates of AgGO_sodium citrate both in suspension and supported in filter paper. In the case of AgGO_glucose, the composite originated the SERS bands of SHsal in all conditions (suspension and supported in glass slides, filter paper and PVA membranes). Ag_glucose deposited in glass slides was the only substrate of silver nanoparticles only, without graphene, to originate the SERS of SHsal. The experiments with the nanocomposite AgGO_glucose also show the SERS bands of graphene, together with the bands of SHsal when the analyte was added. AgGO_glucose deposited on glass slides was the support that showed the best performance for the detection of SHsal molecules with more intense bands than in the other supports.

Figure 4.13 and Figure 4.14 show a comparative study of the AuGO nanocomposites and Au colloids (obtained under the same reduction conditions), as SERS substrates in the detection of SHsal. A clear SERS spectrum of SHsal was obtained in the substrates of AuGO_sodium citrate both in suspension and supported in glass slides and in filter paper. In the case of AuGO_glucose, the composite originated the SERS bands of SHsal in suspension and supported in PVA membranes. Au_glucose deposited in PVA membranes was the only substrate of gold nanoparticles only, without graphene, to originate the SERS of SHsal. The experiments with the nanocomposite AuGO_glucose also show the SERS bands of graphene, together with the bands of SHsal when the analyte was detected. AuGO_glucose deposited on PVA membranes was the support that showed the best performance for the detection of SHsal molecules.

Similar studies with the nanocomposites MGO_eucalyptus extract (M = Ag or Au) and AuGO_hydroxylamine, did not show a SERS signal for SHsal.

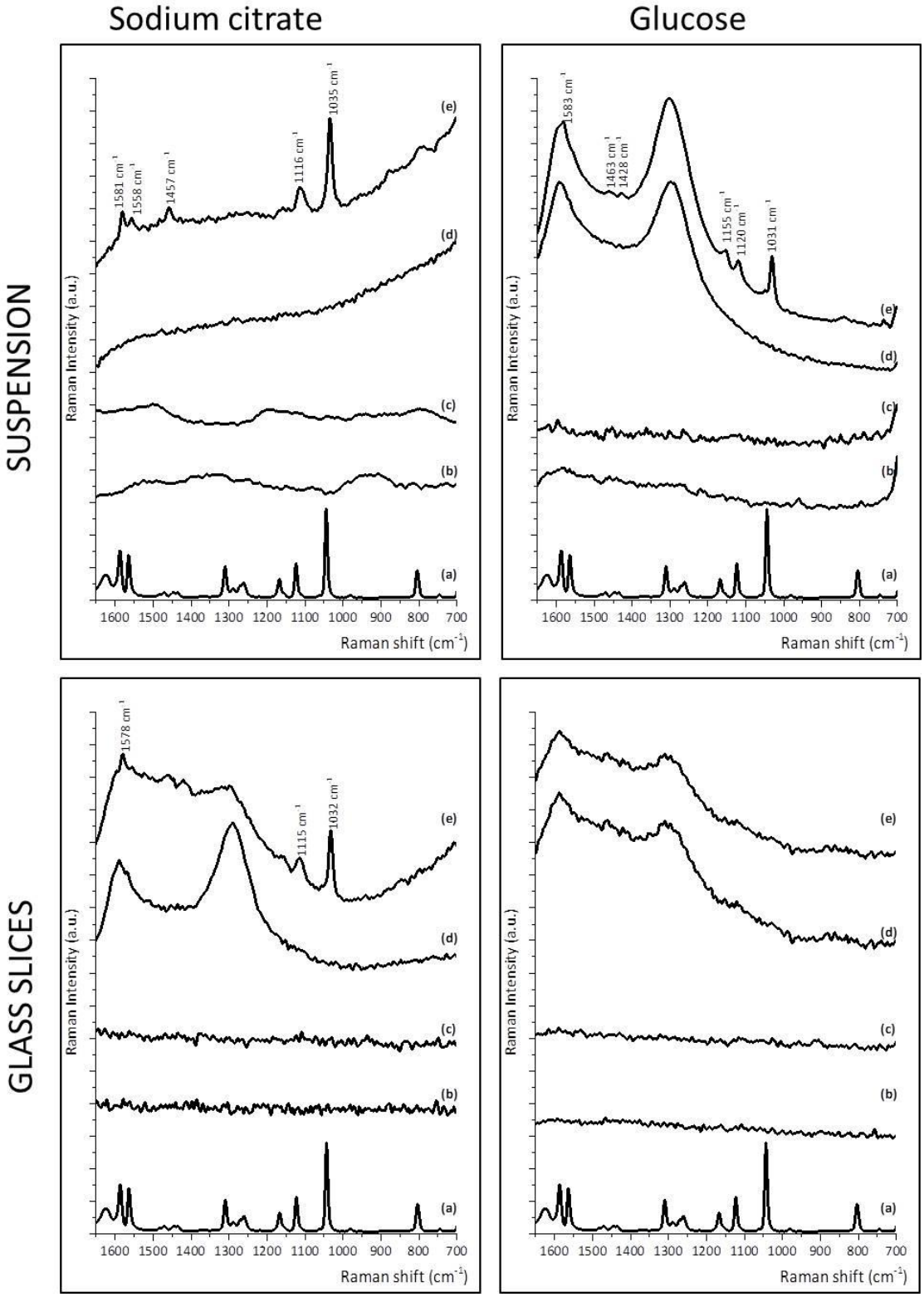

Figure 4.13 – SERS spectra of SHsal 10^{-3} mold m^{-3} in: AuGO_sodium citrate and AuGO_glucose both in suspension and glass slides (e). SERS spectra of SHsal 10^{-3} mold m^{-3} in: Au_sodium citrate and Au_glucose both in suspension and glass slides (c). Raman spectra of solid SHsal (a) and of the substrates Au_sodium citrate and Au_glucose (b) and AuGO_sodium citrate and AuGO_glucose (d).

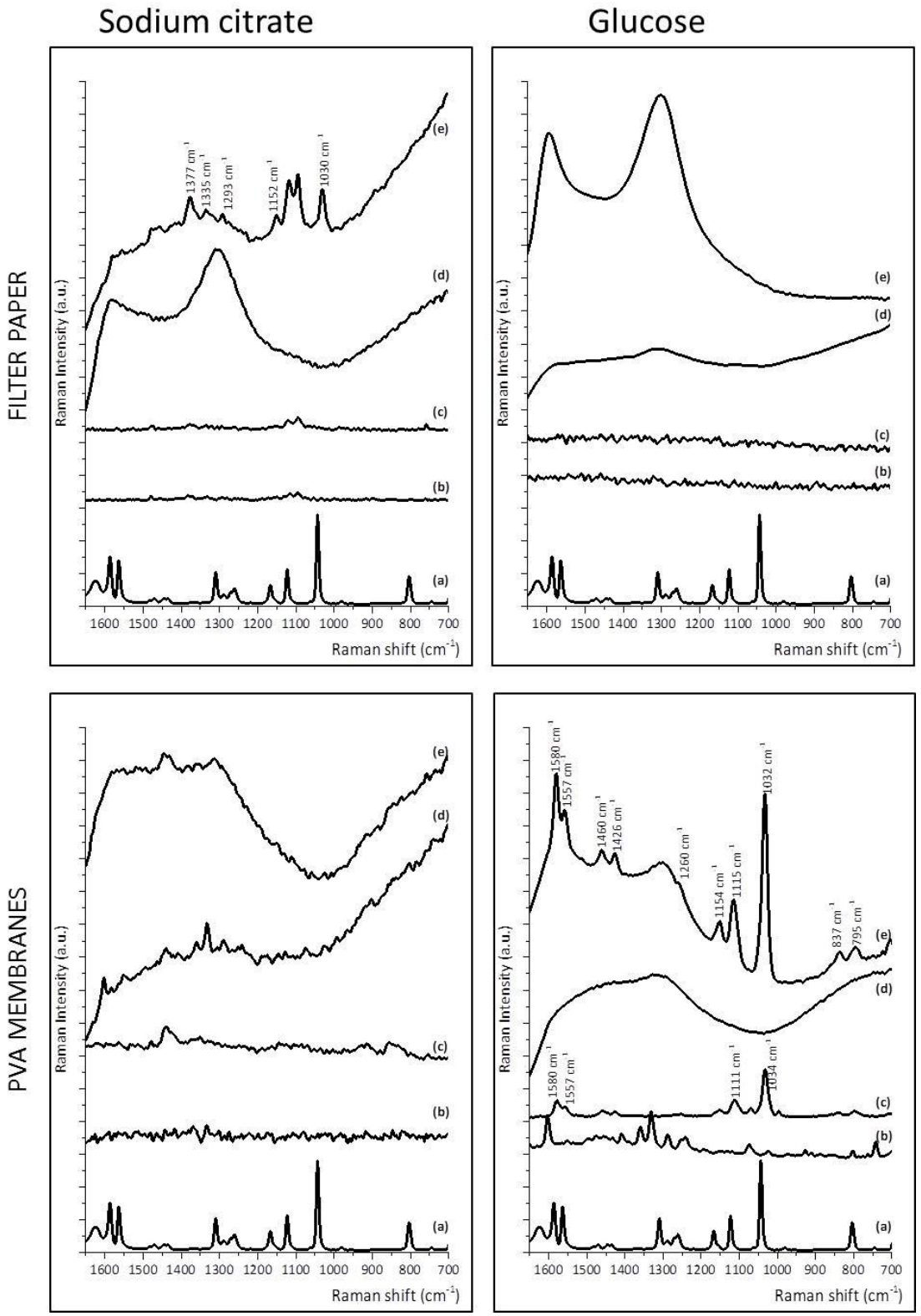

Figure 4.14 – SERS spectra of SHsal 10^{-3} mold m^{-3} in: AuGO_sodium citrate and AuGO_glucose both in filter paper and PVA membranes (e). SERS spectra of SHsal 10^{-3} mold m^{-3} in: Au_sodium citrate and Au_glucose both in filter paper and PVA membranes (c). Raman spectra of solid SHsal (a) and of the substrates Au_sodium citrate and Au_glucose (b) and AuGO _sodium citrate and AuGO_glucose (d).

4.3. Conclusion

The environmental eco-friendly reducing agents, sodium citrate, glucose and eucalyptus extract, can be used to prepare nanocomposites of graphene and silver or gold nanoparticles. Glucose was the reducing agent that originated the biggest nanoparticles (around 100 nm) in the case of silver.

Using the laser of 1064 nm and for detection of SHsal ethanolic solution, both AgGO and AuGO nanocomposites were active as SERS substrates. The best substrates for SERS, with SHsal as analyte, were AgGO_glucose deposited on glass slides and AuGO_glucose deposited on PVA membranes; with better performance than the correspondent nanometal substrates without graphene.

4.4. Experimental procedure

4.4.1. Preparation of active SERS substrates

4.4.1.1. AgGO and AuGO nanocomposites

4.4.1.1.1. Sodium citrate

The reduction of metallic complexes was made by sodium citrate[7]. 7.5 mg of GO was added to a 5 mg of $AgNO_3$ ($HAuCl_4$) dissolved in 50 mL of deionized water ($6x10^{-4}$ mol dm^{-3} of $AgNO_3$ and $2.4x10^{-4}$ mol dm^{-3} of $HAuCl_4$). The mixture was with stirring during 30 min to promote the interaction of silver (gold) ions with graphene oxide surface. After that, the suspension was heated until 80 ºC, after which 3.760 mL of sodium citrate (85 mmol dm-3) was added dropwise. The experimental conditions were maintained during 1 hour. After cooling to room temperature, the suspension was washed by centrifugation.

4.4.1.1.2. Glucose

The synthesis of nanocomposites was based on method used by Zhao et al[16]. 1.2 g of D-(+)glucose was dissolved into 30 ml of a suspension of GO (1.5 mg/mL) under sonication during 5 min. 1 mL of ammonia (25%) was added to 10 mL of $AgNO_3$ (0.050 mol dm^{-3}, 0.0839 g, v = 10 mL). Both phases were mixed and kept in sonication during 5 minutes. After 24h, the suspension showed a grey precipitate, confirming the formation of AgGO_glucose nanocomposite. The same procedure was made using 10 mL of 0.050 mol dm^{-3} $HAuCl_4$ (0.1970 g).

4.4.1.1.3. Eucalyptus extracts

The synthesis of AgGO_eucalyptus extract was made dissolving 0.0068 g of $AgNO_3$ in 40 mL ($1x10^{-3}$ mol dm^{-3}) of GO 0.5 mg/mL[17]. In the case of AuGO_eucalyptus extract 0.0157 g of $HAuCl_4$ in 40 mL ($1x10^{-3}$ mol dm^{-3}) of GO 0.5 mg/mL. The mixture was in stirring during 10 minutes and after that the eucalyptus extracts (0.0283 g) were added. The stirring was kept for about 5 minutes to ensure the complete dissolution of reducing agent. The silver nanoparticles were formed after 24 hours[17].

4.4.1.1.4. Hydroxylamine

An aqueous solution 100 mM (2 mL) of NH2OH was prepared and the pH was adjusted to 12.0 – 12.5 with a 0.1M NaOH solution in stirring[18]. 200 μL of a 10 mM solution of HAuCl4 in water and 255 μL of 4mg/mL GO suspension (final concentration of GO was 0.51 mg/mL) were, simultaneously, introduced into the vial under vigorous stirring. The color of the solution changed to dark blue/black. The nanoparticles were purified by centrifugation to remove the NaOH from the suspension. The AuNS were stored in water at room temperature.

4.4.1.2. PVA membranes

14 g of PVA (Mw 89,000 – 98,000; 99% hydrolysed) was dissolved in 100 mL of water during 4 hours, at 80 ºC with vigorous stirring. Approximately, 1 g of this solution was placed in a glass container and was crosslink by three cycles of freeze-thawing (+20 ºC, -20 ºC)4 [21]. After complete this process, the final membranes were dried by lyophilisation.

4.4.2. SERS measurements

The Raman spectra and SERS were recorded using a Bruker RFS100/S FT-Raman spectrometer (Nd:YAG laser, 1064 nm excitation). Micro-Raman experiments were performed at room temperature using the 488 nm line of an Ar+ laser with an incident power in the 1–8 mW range. The light was focused and collected with an Olympus microscope (100_ objective) and a "super-notchplus" filter from Kaiser was used to eliminate elastic light. The scattered light was analyzed with a Jobin Yvon HR-460 monochromator coupled to a liquid nitrogen cooled CCD.

Suspension. 500 μL of each substrate was mixed with 20 μL of thiosalicylic acid ethanolic solution 0.1 M. The final suspension was analysed as prepared by placing 200 μL in NMR tube.

Glass slices and filter paper. SERS measurement was made by placing 20 μL of the suspension previous prepared on a glass slice/filter paper and allowing drying at room temperature.

PVA membranes. The PVA membranes were dipped on 500 μL graphene-nanocomposites suspensions during 24 hours. After that, they were removed from suspensions and let dry at room temperature. Thiosalicylic acid was dropped (10 μL) on the top of PVA membranes and 30 minutes after that SERS effect was assessed.

4.5. Bibliography

(1) Ling, X.; Xie, L. M.; Fang, Y.; Xu, H.; Zhang, H. L.; Kong, J.; Dresselhaus, M. S.; Zhang, J.; Liu, Z. F. Can Graphene be used as a Substrate for Raman Enhancement? *Nano Letters* **2010**, *10*, 553-561.

(2) Sun, S.; Wu, P. Competitive surface-enhanced Raman scattering effects in noble metal nanoparticle-decorated graphene sheets. *Physical Chemistry Chemical Physics* **2011**, *13*, 21116-21120.

(3) Yang, H. P.; Hu, H. L.; Ni, Z. H.; Poh, C. K.; Cong, C. X.; Lin, J. Y.; Yu, T. Comparison of surface-enhanced Raman scattering on graphene oxide, reduced graphene oxide and graphene surfaces. *Carbon* **2013**, *62*, 422-429.

(4) Sun, S. T.; Wu, P. Y. Competitive surface-enhanced Raman scattering effects in noble metal nanoparticle-decorated graphene sheets. *Physical Chemistry Chemical Physics* **2011**, *13*, 21116-21120.

(5) Xu, C.; Wang, X. Fabrication of Flexible Metal-Nanoparticte Film Using Graphene Oxide Sheets as Substrates. *Small* **2009**, *5*, 2212-2217.

(6) Zhou, Y.; Cheng, X.; Du, D.; Yang, J.; Zhao, N.; Ma, S.; Zhong, T.; Lin, Y. Graphene-silver nanohybrids for ultrasensitive surface enhanced Raman spectroscopy: size dependence of silver nanoparticles. *Journal of Materials Chemistry C* **2014**, *2*, 6850-6858.

(7) Goncalves, G.; Marques, P. A. A. P.; Granadeiro, C. M.; Nogueira, H. I. S.; Singh, M. K.; Gracio, J. Surface Modification of Graphene Nanosheets with Gold Nanoparticles: The Role of Oxygen Moieties at Graphene Surface on Gold Nucleation and Growth. *Chemistry of Materials* **2009**, *21*, 4796-4802.

(8) Evanoff, D. D.; Chumanov, G. Synthesis and optical properties of silver nanoparticles and arrays. *Chemphyschem* **2005**, *6*, 1221-1231.

(9) Kretschmer, F.; Muehlig, S.; Hoeppener, S.; Winter, A.; Hager, M. D.; Rockstuhl, C.; Pertsch, T.; Schubert, U. S. Survey of Plasmonic Nanoparticles: From Synthesis to Application. *Particle & Particle Systems Characterization* **2014**, *31*, 721-744.

(10) Li, N.; Zhao, P.; Astruc, D. Anisotropic Gold Nanoparticles: Synthesis, Properties, Applications, and Toxicity. *Angewandte Chemie-International Edition* **2014**, *53*, 1756-1789.

(11) Huang, J.; Zong, C.; Shen, H.; Cao, Y.; Ren, B.; Zhang, Z. Tracking the intracellular drug release from graphene oxide using surface-enhanced Raman spectroscopy. *Nanoscale* **2013**, *5*, 10591-10598.

(12) Zhou, L.; Gu, H.; Wang, C.; Zhang, J.; Lv, M.; He, R. Study on the synthesis and surface enhanced Raman spectroscopy of graphene-based nanocomposites decorated with noble metal nanoparticles. *Colloids and Surfaces a-Physicochemical and Engineering Aspects* **2013**, *430*, 103-109.

(13) Lee, J.; Shim, S.; Kim, B.; Shin, H. S. Surface-Enhanced Raman Scattering of Single- and Few-Layer Graphene by the Deposition of Gold Nanoparticles. *Chemistry-a European Journal* **2011**, *17*, 2381-2387.

(14) Li, N.; Cao, M.; Hu, C. Review on the latest design of graphene-based inorganic materials. *Nanoscale* **2012**, *4*, 6205-6218.

(15) Tang, X.-Z.; Li, X.; Cao, Z.; Yang, J.; Wang, H.; Pu, X.; Yu, Z.-Z. Synthesis of graphene decorated with silver nanoparticles by simultaneous reduction of graphene oxide and silver ions with glucose. *Carbon* **2013**, *59*, 93-99.

(16) Zhao, X. S.; Ma, J. Z.; Zhang, J. T.; Xiong, Z. G.; Yong, Y. Preparation, characterization and antibacterial properties of silver-modified graphene oxide. *Journal of Materials Chemistry* **2011**, *21*, 3350-3352.

(17) Santos, S. A. O.; Pinto, R. J. B.; Rocha, S. M.; Marques, P. A. A. P.; Neto, C. P.; Silvestre, A. J. D.; Freire, C. S. R. Unveiling the Chemistry behind the Green Synthesis of Metal Nanoparticles. *ChemSusChem* **2014**, *7*, 2704-2711.

(18) Minati, L.; Benetti, F.; Chiappini, A.; Speranza, G. One-step synthesis of star-shaped gold nanoparticles. *Colloids and Surfaces a-Physicochemical and Engineering Aspects* **2014**, *441*, 623-628.

(19) Lin, X. M.; Cui, Y.; Xu, Y. H.; Ren, B.; Tian, Z. Q. Surface-enhanced Raman spectroscopy: substrate-related issues. *Anal Bioanal Chem* **2009**, *394*, 1729-1745.

(20) Stankovich, S.; Dikin, D. A.; Piner, R. D.; Kohlhaas, K. A.; Kleinhammes, A.; Jia, Y.; Wu, Y.; Nguyen, S. T.; Ruoff, R. S. Synthesis of graphene-based nanosheets via chemical reduction of exfoliated graphite oxide. *Carbon* **2007**, *45*, 1558-1565.

(21) Valente, A. J. M.; Cruz, S. M. A.; Morán, M. C.; Murtinho, D. B.; Muniz, E. C.; Miguel, M. G. Release of DNA from cryogel PVA-DNA membranes. *eXPRESS Polymer Letters* **2010**, *4*, 480-487.

5. Electrospun fibrous membranes decorated with noble nanoparticles

Fibres of Poly(vinyl alcohol) (PVA) and polyacrylonitrile (PAN) were prepared by electrospinning with *in situ* or *ex situ* inclusion of noble nanoparticles or noble NPs/graphene nanocomposite. To the PVA microfibers, the freeze-thawing method was applied and the SERS activity was tested with and without the application of this treatment. The PAN fibres were imbibed with noble NPs/graphene nanocomposites. In this case, the fibrous mantles were used without and with functionalization with hydroxylamine.

5.1. Introduction

Different types of SERS substrates have been developed involving either pure or supported nanostructured metals, mostly gold and silver. A fundamental limitation of these planar metal SERS-active surfaces is that analyte molecules must rely on slow diffusion from the bulk solution to the surface to facilitate molecule-metal interactions, an essential prerequisite for SERS detection. Thus long detection times are required to achieve reasonable sensitivities for planar SERS sensors, which is unfavourable for online real-time analysis. At the same time, the effective surface area of planar nanoparticle-presenting substrates is limited. A simpler and widely employed approach to SERS detection is to directly mix metal colloids with target analytes[1]. The metal nanoparticle aggregates containing many "hot spots" in solution can present a large total surface area, thus facilitating effective interactions with analytes and generation of strong Raman scattering emission. In comparison to SERS sensing using nanostructured metal films, which are inherently planar detectors, this approach allows direct probing of analytes within a defined volume of solution, thereby providing higher sensitivity. However, metal colloid aggregates are inherently unstable and tend to precipitate from solution, resulting in loss of SERS signals. The addition of surfactants or hydrophilic polymers can stabilize the colloids, but these reagents are known to interfere with the SERS signals of target analytes[2,3]. It would thus be advantageous to develop a SERS detection element capable of providing high sensitivity through the use of volumetric detection together with the excellent stability of planar nanostructured surfaces, while simultaneously offering enhanced analyte-metal interactions for rapid online detection.

Interestingly, natural nanofibrillar structures such as bacterial cellulose (BC) with silver nanoparticles can act as active SERS substrates[4]. Bacterial cellulose was used as a template to grow Ag nanoparticles. Due to the distinctive three-dimensional (3D) nanofibrillar structure of BC, the resulting nanocomposites were made up of interconnected nanofilaments with discrete Ag nanoparticles at their surfaces originating active SERS substrates. The high interfacial area provided by Ag-BC cellulosic matrix for the deposition of Ag nanoparticles where organic ligands can adsorb, lead to strong Raman enhancement. The importance of substrate three-

dimensionality for SERS was highlighted by several researchers [3,5,6]. In contrast to conventional planar SERS detectors, 3D structures combines convective flow and short diffusion length scales to significantly reduce the time required for analyte molecules to reach the SERS-active surfaces. Furthermore, when compared to colloidal solutions, the 3D nanostructures concentrate the metal and present a very high surface area, resulting in much greater interaction between analyte molecules and SERS-active sites. However, most of the methodologies used to prepare these substrates such as sputtering, physical vapour deposition or electron beam lithography are extremely difficult to find in conventional laboratories. To further facilitate and broaden the SERS application, it is important to explore facile, cost effective, scalable, and reproducible approaches for the preparation of nanostructured SERS substrates with controlled morphologies and structures of nanoparticle aggregations to achieve ultrahigh SERS activities/sensitivities.

Electrospinning is a remarkably robust and versatile approach to synthesize large-scale 3D networked nanofibre membranes with extremely high surface area-to-volume ratios, uniformity and mechanical resilience which could be used as nanostructure-frameworks to assemble hierarchical nanostructures for 3D SERS substrates[7]. The nanomaterials-processing technique of electrospinning provides a versatile approach for the convenient fabrication of fibres with diameters typically ranging from tens to hundreds of nanometers.

Noble metal nanoparticles embedded electrospun nanofibres have been studied widely due to their applications in catalysis, antimicrobial, microelectronics, etc[8]. The SERS application of these types of structures has also raised the interested of several researchers[9-13].

The preparation of SERS substrates containing noble metal nanoparticles involves two main routes: The noble metal NPs can be embedded in the electrospun nanofibers or assembled onto the outer surfaces of the electrospun nanofibres. In the former case, the analyte molecules are required to permeate into the nanofibres to access the SERS-active noble metal NPs encapsulated inside the polymer nanofibres, which may be not applicable to some target analytes. In the second possibility, the assembled nanoparticles are more available to directly interact with the analyte.

For example, Xiaofei Li et al.[11] prepared electrospun PVA nanofibres embedded with Au–Ag alloy NPs. The NPs were obtained by co-reduction of $AgNO_3$ and $HAuCl_4$, with sodium citrate as a reducing agent in the presence of dilute PVA aqueous solution. Then, the substrates of PVA/Au–Ag nanofibers were successfully prepared by electrospinning. Different SERS signals of PVA/Au–Ag nanofibre could be observed with different analyte molecules (4-mercaptobenzoic acid (4-MBA), pyridine, and thiophenol) molecules. Interestingly, the electrospun PVA/Au–Ag nanofibre substrate showed the better SERS sensitivity in comparison with the drop-cast film. Minhua Cao et al[12] also prepared PVA nanofibres with high concentration of Au NPs on the fibres and high sensitivity in the surface enhanced Raman scattering was obtained. The high concentration of Au NPs was prepared in 10 wt% PVA solution by one step synthesis. The distance between adjacent Au NPs became closer with the increasing the amount of NPs. SERS spectra showed a significant Raman signal enhancement of 4-MBA molecules, which were absorbed on the surface of PVA/Au nanofibres, even under a relatively low concentration (10^{-6} mol dm^{-3}). The nanofibres also showed the better SERS performance in comparison to the cast-films.

The assembling of SERS-active noble metal NPs onto the outer surfaces of the electrospun nanofibres was also tested for several authors. For example, Ag nanoparticles were decorated on polyacrylonitrile[14] or poly(methyl methacrylate) nanofibre frameworks[15] via wet-chemistry routes, and Au nanorods were assembled on poly(2-vinyl pyridine) nanofibre-frameworks by a drop-cast method[16] or immobilized onto polycaprolactone nanofibre-frameworks via polyelectrolyte decoration. In these cases, the assembled NPs on the outer surface of the electrospun nanofibres are the key building blocks to achieve SERS-activity, which facilitate analyte molecules to be trapped directly onto the “hot-spots”.

From the above, it is clear that when considering the development of highly active solid substrates for SERS, the surface geometry, that is the micro- and nano-topography of the substrates, is an important parameter to consider. In this chapter we present the work developed with the aim to obtain efficient and free standing SERS substrate materials prepared by electrospinning. Electrospun nanofibrous membranes can combine the flexible and portable properties of the polymeric membrane mats and the plasmonic activity of noble NPs with and without graphene.

Since poly(vinyl alcohol) (PVA) was used to produce membranes with silver nanoparticles as SERS substrates (Chapter 2) and this polymer is also widely used to produce electrospun fibres, we studied the preparation of such type of fibres with Ag NPs and AgGO nanocomposites.

We also tested the assembling of previously prepared NPs and NPs/GO nanocomposites on polyacrylonitrile (PAN) electrospun mantles used as a physical support for the suspensions.

5.1. Results and Discussion

Many parameters can affect the electrospinning process, including (a) the solution properties such as polymer molecular weight, viscosity, conductivity, elasticity, and surface tension; (b) process parameters such as electric potential, flow rate, distance between needle tip and collector, needle inner diameter; and (c) ambient parameters like temperature, humidity, and air velocity in the electrospinning chamber. For example, the polymer solution for electrospinning should have a concentration high enough to maintain polymer entanglement, but not too high to inhibit deformation caused by the electric field. Improper distance between needle and collector may result in a rough and beaded mat with the porosity also severely decreased. The applied voltage can produce ionized solution and generate elongation and splitting, which would form a uniform fibre structure at a proper level. Whereas, boosting the voltage to an extreme high value would result in an unstable electrospinning. In a word, electrospinning parameters are quite essential which deserve serious attention.

The polymeric structures of the two polymers used to prepare the electrospun membranes, PVA and PAN, are represented in Figure 5.1.

Figure 5.1 – Chemical structure of polymers used to produce electrospun fibres: a) poly(viny alcohol) and b) polyacrylonitrile.

We used three different approaches to prepare the electrospun mats for SERS measurements. These different approaches were selected sequentially as a consequence of the successive results obtained during the experimental work.

-In the first case, we prepared PVA suspensions with the addition of Ag colloid (Ag-PVA) or AgGO suspension (AgGO-PVA). In both cases, glucose was used as the reducing agent of silver. These suspensions were directly electrospun after the adjustment of the electrospinning parameters;

-In the second case, we choose PAN because we found that it was easier to process the fibres from this polymer than from PVA. First, we prepared simple PAN fibres and after, the NPs or the nanocomposites were assembled by dipping the PAN mantle inside the suspensions aiming to promote a physical adsorption of the NPs and the nanocomposites on the electrospun membrane. The materials produced by this method were denoted by NP_sodium citrate_PAN, NP_glucose_PAN, NPGO_sodium citrate_PAN and NP_glucose_PAN, according to the reducing agent used;

-Finally, we treated the as-spun PAN fibres with hydroxylamine (HAD) aiming to promote the surface functionalization through amidoxime (-C(NH_2)=N-OH) groups, following a method described by Lifeng Zhang[14]. The amidoxime group is a coordinating/chelating group with high affinity to metal ions, then allowing the nucleation of metal nanoparticles. The introduction of graphene in this system was also performed as described in the experimental methodology. The prepared materials were denoted by nanocomposites-HDA-PAN.

5.1.1. Ag-PVA electrospun membranes

The 14% (w/w) PVA mantle produced by electrospinning presented an inhomogeneous size distribution of the fibres without beads (Figure 5.2 (left)). In the presence of Ag NPs, the fibres presented similar morphology to the ones without Ag NPs but with beads formation (Figure 5.2 (right)). From SEM observation, only a few Ag NPs prepared by the method described by Zhao et al.[17] are visualized. It's not straightforward to say if these Ag NPs are at the surface, or impregnated in the fibres. However, most of the Ag NPs should be inside the fibres, the UV-vis spectroscopy indicates its presence by the localized plasmon resonance surface, typical for silver at 436 nm (Figure 5.5).

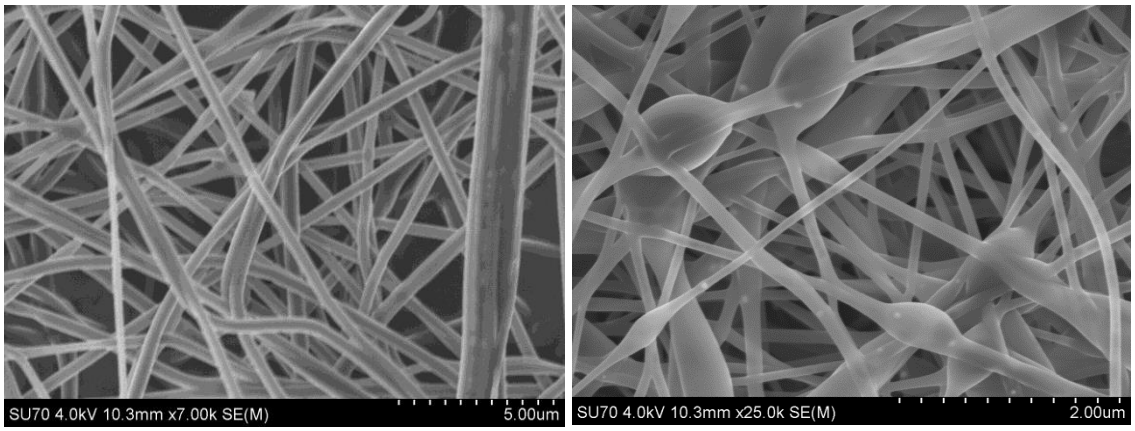

Figure 5.2 – Scanning electron micrographs of 14% (w/w) PVA (LEFT) and of Ag-PVA (RIGHT)

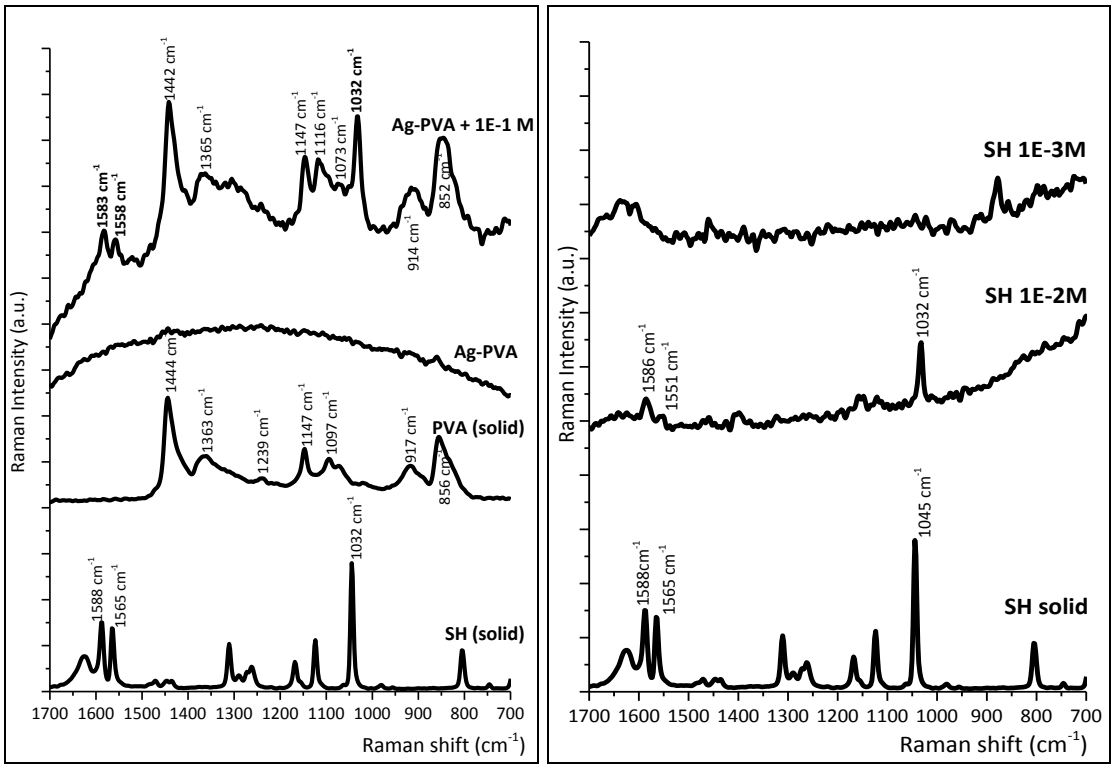

Figure 5.3 – LEFT: Raman spectra of (a) SH solid, (b) PVA solid, c) PVA electrospun mantle and d) SERS spectrum of SHsal 10^{-1} mol dm^{-3} using Ag-PVA mantle. RIGHT: Raman spectrum of SHsal 10^{-2} and 10^{-3} mol dm^{-3} aqueous solution.

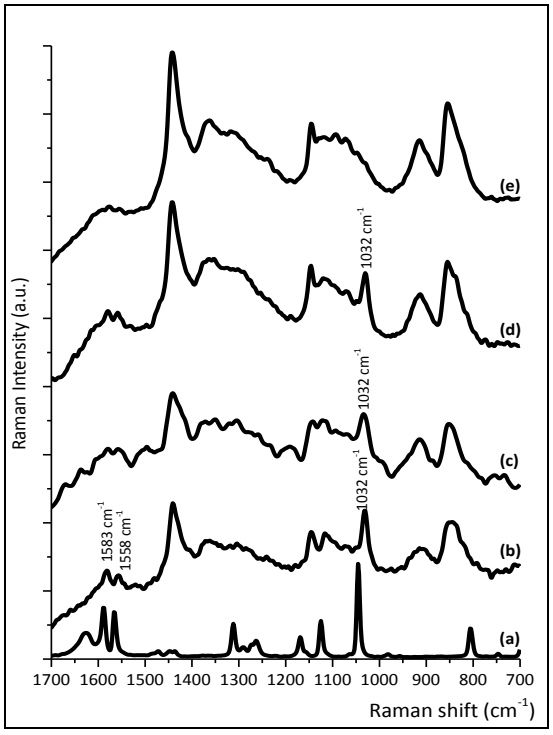

Figure 5.4 – Detection of SHsal in Ag-PVA with SERS technique. SHsal solid (a) was inserted as reference. SHsal solution was deposited on the Ag-PVA membranes at (b) 10^{-1} mol dm^{-3}, (c) 10^{-2} mol dm^{-3}, (d) 10^{-3} mol dm^{-3}, (e) 10^{-4} mol dm^{-3} concentrations.

The SERS activity/sensitivity of Ag-PVA nanofibrous membranes was studied with thiosalicylic acid (SHsal) as the probe molecule. In a first approach, the Ag-PVA membrane was tested as SERS substrate using SHsal ethanolic solution at a concentration of 10^{-1} mol dm^{-3}. In Figure 5.3 (LEFT) it is possible to observe that when the SHsal solution was deposited on Ag-PVA membrane (red line) Raman signals from SHsal (at 1583, 1558 and 1032 cm^{-1}) are present. All the other peaks are from PVA polymer. Since the Ag-PVA substrate showed no characteristic Raman peaks from PVA (grey line), it is possible say that the peaks signed at red curve (except 1583, 1558 and 1032 cm^{-1}) are the confirmation of SERS effect with respect to PVA. However, the peaks attributed to SHsal are not SERS effect but are Raman peaks. To confirm this statement, the same quantity of SHsal solutions 10^{-2} and 10^{-3} mol dm^{-3}, which was used in the Ag-PVA membranes, was deposited on a glass slice and let it dry. After dried, the Raman spectra of such solutions were made and are shown in Figure 5.3 (RIGHT). The solution of SHsal at concentration of 10^{-2} mol dm^{-3} showed Raman peaks which means that the peaks attributed to SHsal (10^{-1} mol dm^{-3}) when such solution was deposited on Ag-PVA cannot be described as SERS effect but as Raman signals.

These results showed that Ag-PVA can act as SERS substrate for PVA. However was important verify the sensitivity of this material to the analyte solution. In Figure 5.4 are the Raman spectra of SHsal in several concentrations (10^{-1} to 10^{-4} mol dm^{-3}) deposited on Ag-PVA. It is possible observe that Ag-PVA has the capability of detect SHsal solution at 10^{-3} mol dm^{-3} by SERS technique.

Figure 5.5 shows the λ_{max} of the Ag-PVA with SHsal in several concentrations. The change in the local dielectric due to molecule absorption was measured by a shift in the localized surface plasmon resonance (LSPR) λ_{max}[18]. When the SHsal was deposited on the Ag-PVA nanofibrous membranes, the λ_{max} shifted depending on the concentration of SHsal ethanolic solution. Although more studies are needed to accurate the tendency of Ag-PVA λ_{max} shifts according the concentration of Raman probe molecule it can be said that the results showed in Figure 5.5 confirm the results of SERS spectrum in terms of limit detection of SHsal in Ag-PVA nanofibrous membranes.

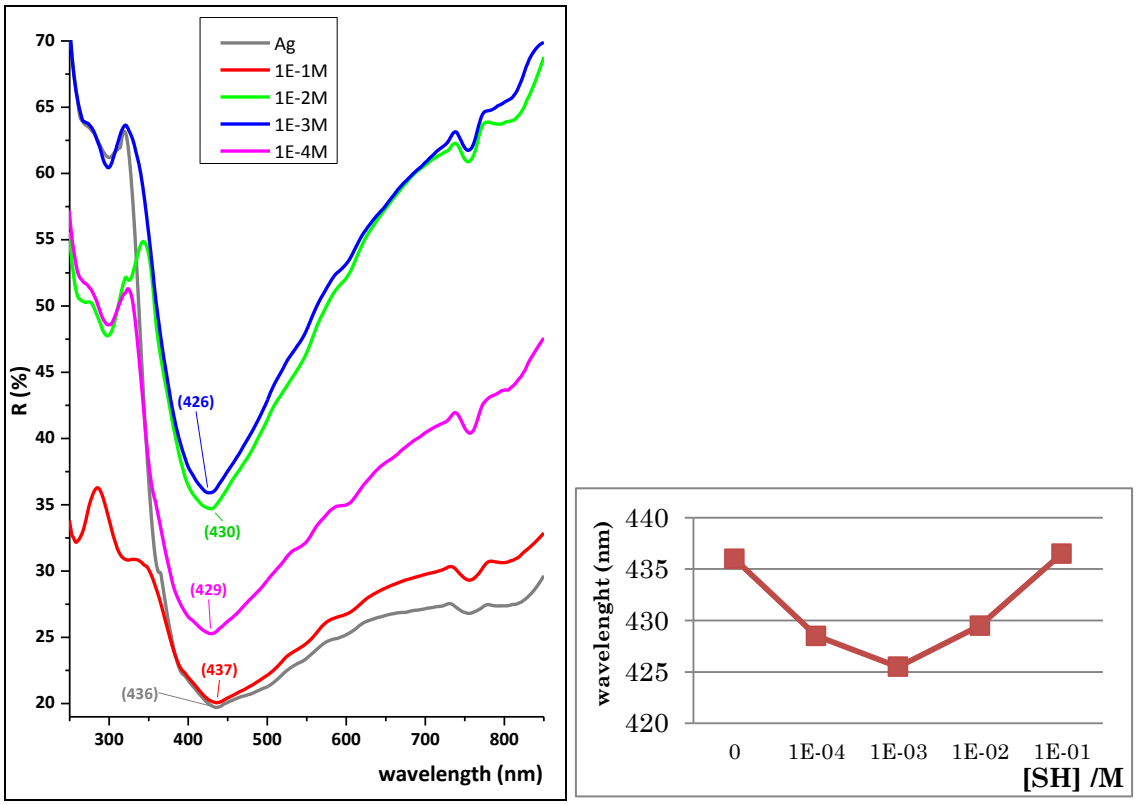

Figure 5.5 –Reflectance spectra of the same samples that were tested in SERS experiments (LEFT). The position of the reflectance minimum as function of SHsal concentration added on Ag-PVA is showed in graphic at the image (RIGHT).

The capability of sensing SHsal at the 10^{-3} mol dm^{-3} concentration and the enhancement of PVA Raman peaks made the Ag-PVA nanofibrous membrane a substrate active in SERS analysis.

5.1.2. AgGO-PVA electrospun membranes

There is increasing number of studies with focus on exploring the SERS efficiencies of composites of metal nanoparticles and graphene given the superior SERS capabilities of both metal nanoparticles and graphene based materials. SERS signals arising from graphene/metal hybrid structures are also shown to be higher compared to the

individual components[19]. For instance, SERS signals of probe molecules such as rhodamine 6G and methylene blue are shown to be further enhanced several-fold when compared against those of pure metal nanoparticles, with detection limits reaching nanomolar (nM) levels[20].

To try to enhance the limit detection of the previously prepared Ag-PVA fibre mantles, we prepared AgGO suspension using glucose as the reducing agent based on the method described by Zhao et al.[17]. These AgGO nanocomposites were then introduced in the PVA solution before electrospinning.

Although PVA has good mechanical properties in the dry state, its applications can be limited by its hydrophilicity[21]. During the experimental work we started to face this limitation and because of that we decided to introduce the crosslink procedure to these fibres. Linear polymer can be joined by other chains at points along their lengths to make cross-linked structures for the improvement of mechanical properties and anti-water solubility[21]. PVA hydrogels can be cross-linked through the use of bifunctional agents such as glutaraldehyde, by using electron beam or γ-radiation, or by a 'freezing-thawing' process. The later process avoids toxicity issues; furthermore, these physically cross-linked materials also exhibit higher mechanical strength and elasticity than PVA gels cross-linked by other methods[22]. Due to mentioned reasons, AgGO-PVA (about 0.06 AgGO/PVA (w/w)) was exposed to freeze-thawing crosslinking and the effects of this process in SERS measurements were considered.

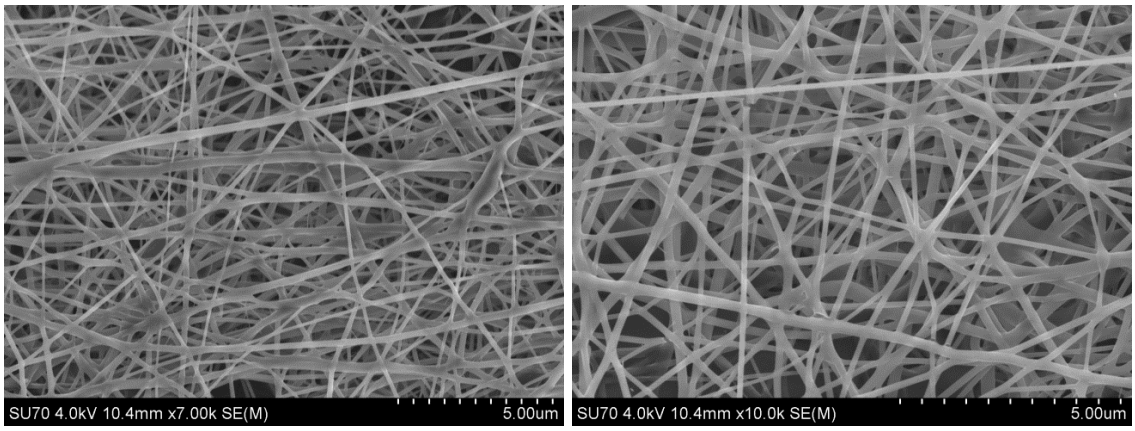

Figure 5.6 – SEM images of AgGO-PVA (about 0.06 AgGO/PVA (w/w)) without crosslinking effect (LEFT) and after freeze-thawing process (RIGHT).

From the SEM observation, the entanglement of the AgGO-PVA nanofibrous membranes with and without crosslinking is identical. However, after cross-linking the fibres seems to show a small increment in the average size diameter (Figure 5.6, Left).

Although, the presence of AgGO in the PVA mantles is not clear from the SEM observation, the Raman spectroscopy shows the presence of GO. The ratio I_D/I_G has the same value for both types of mantles, which was expected since the crosslinking process should not change the reduction degree of AgGO present in the PVA fibres (Figure 5.7).

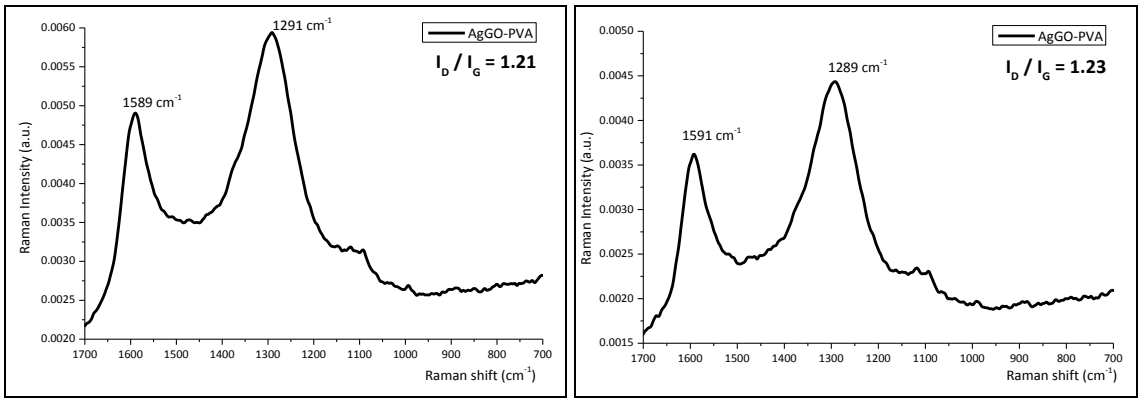

Figure 5.7 – Raman analysis of AgGO-PVA without (left) and with crosslinking (right).

The same SERS experiments previously described for the Ag-PVA membranes (section 6.2.1) were also performed with AgGO-PVA membranes with and without crosslinking (Figure 5.8).

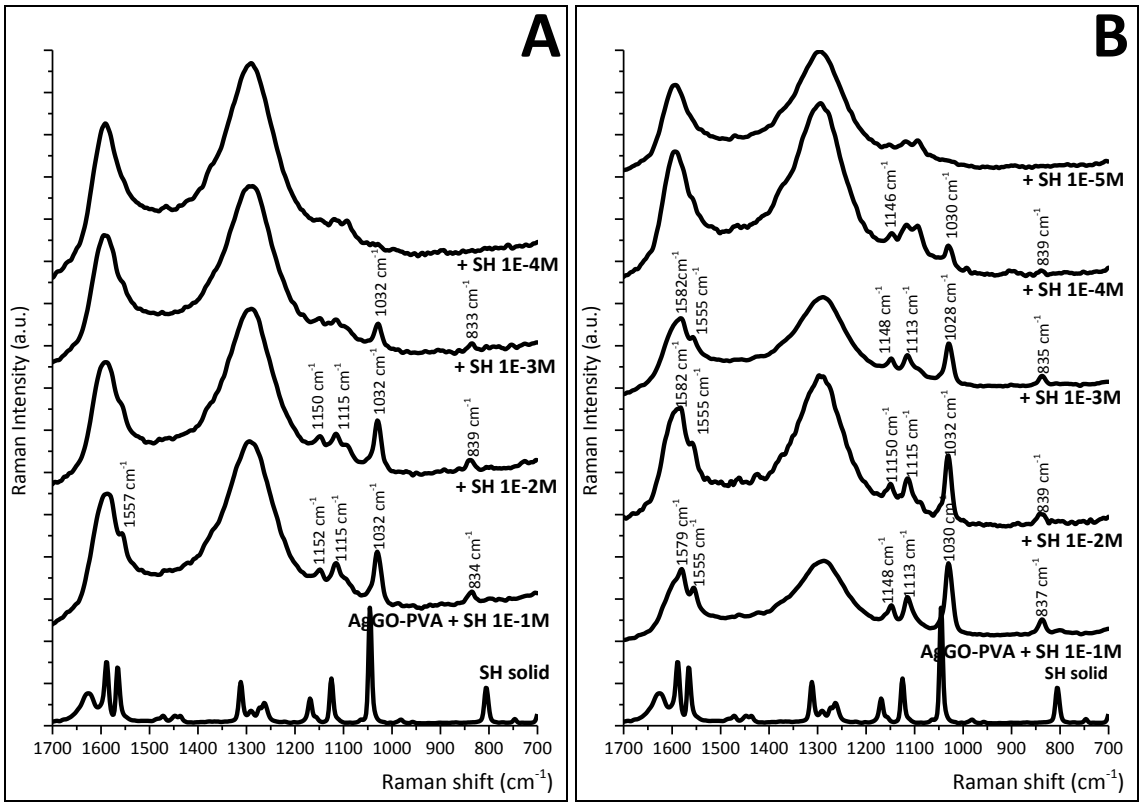

Figure 5.8 – SHsal detection by SERS spectra using AgGO-PVA without crosslinking (A) and after with crosslinking (B). (a) SHsal solid was inserted as reference. SHsal was tested at (b) 10^{-1} mol dm^{-3}, (c) 10^{-2} mol dm^{-3}, (d) 10^{-3} mol dm^{-3}, (e) 10^{-4} mol dm^{-3}, and (f) 10^{-5} mol dm^{-3} concentrations. In the case of AgGO-PVA without crosslinking the concentration of 10^{-5} mol dm^{-3} was not tested since 10^{-4} mol dm^{-3} SHsal solution was not identified with this membrane.

The typical peak of SHsal around 1030 cm^{-1} was identified by AgGO-PVA without crosslinking at concentrations of 10^{-3} mol dm^{-3}. This limit of detection is the same as found with Ag-PVA nanofibrous membranes without GO. However, in this case it is possible to identify others SHsal Raman peaks at around 840, 1115 and 1150 cm^{-1}. These SHsal peaks were not previously detected in the absence of GO.

The detection limit of the SHsal at the freeze-thawed AgGO-PVA membranes surface increased until 10^{-4} mol dm^{-3}, which seems to indicate that the crosslinking process improved the analyte detection by SERS. Moreover, besides the Raman peak of SHsal around 1030 cm^{-1}, other two, at approximately 840 and 1150 cm^{-1}, were identified also at the limit concentration detected.

The reflectance spectra were made for the same samples tested in SERS experiments for AgGO-PVA with and without crosslinking, in the same way as to Ag-PVA samples (Figure 5.9). The λ_{max} showed for the AgGO-PVA without crosslinking is at 348 nm whereas for the AgGO-PVA with crosslinking is at 359 nm which means that the agglomeration of the silver nanoparticles is different. In the case of the Ag-PVA with crosslinking shows that the cycles of freeze-thawing can be responsible for silver aggregates, since the LSPR λ_{max} of Ag nanoparticles is redshifted. We should also remind that in the present case, the Ag NPs are localized at the graphene surface and nor freely dispersed in the polymer fibres.

Contrary to the results obtained to Ag-PVA, the LSPR λ_{max} of Ag nanoparticles present in AgGO composites did not show a direct relationship with the SHsal concentration deposited on the AgGO-PVA mantles (Figure 5. 10). One possible reason for this behaviour is that the presence of graphene sheets can also influence the LSPR of the silver nanoparticles.

From the previous results and with respect to the detection limit of the testing molecule used, it seems that the crosslinking process can help to increase the potential use of these types of membranes as SERS substrates. A tentative explanation for this observation may be related with a rearrangement between the fibres, characteristic of the cross-linking procedure, that simultaneously promote the re-arrangement of the nano-fillers that may became closer and promote more SERS active sites.

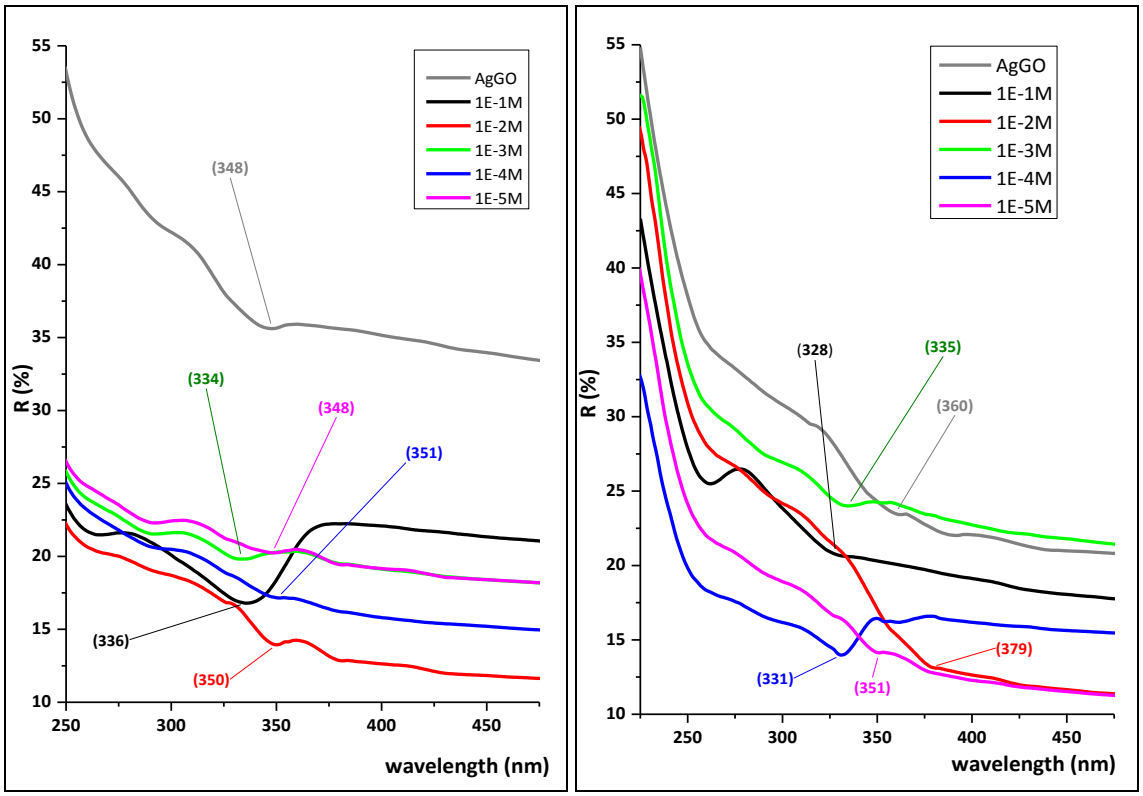

Figure 5.9 – Reflectance spectra of the same samples that were tested in SERS experiments. AgGO-PVA without (LEFT) and with crosslinking (RIGHT)

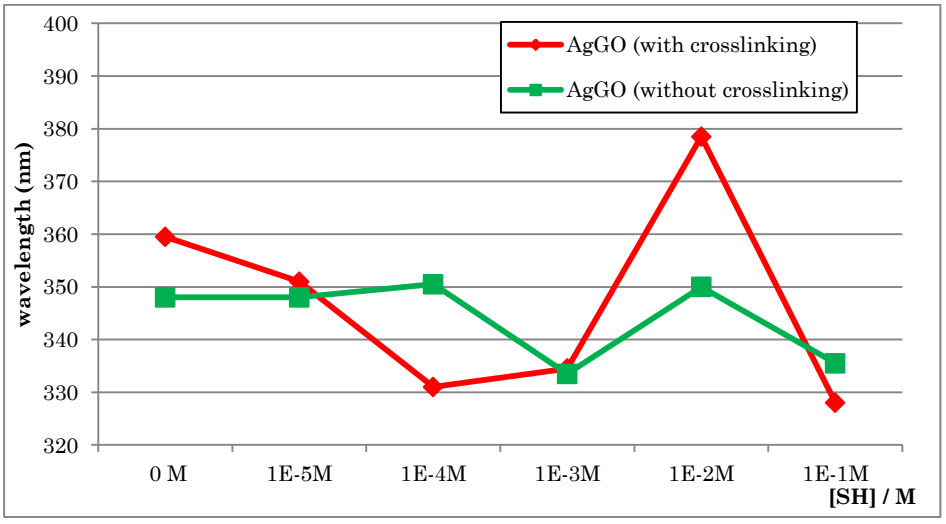

Figure 5. 10 – Analysis of reflectance minimum from the AgGO-PVA (with and without crosslinking) interacting with thiosalicylic acid at 0, 10^{-1}, 10^{-2}, 10^{-3}, 10^{-4} and 10^{-5} mol dm^{-3} concentrations.

5.1.3. Polyacrylonitrile (PAN) mantles imbibed on colloidal suspensions

The polyacrylonitrile (PAN) is widely used to form fibres by electrospinning. PAN is not soluble in water what can constitute an advantage over PVA if the final electrospun mantles are conceived as a substrate to detect analytes in aqueous solution.

According to literature, metal nanoparticles attached to electrospun fibres can adsorb analytes directly on their surfaces, leading to larger SERS sensitivity. Such type of SERS substrates can be prepared by attaching metal nanoparticles onto electrospun fibres via methods such as drop-casting, electroplating, sputter-coating, chemical reduction, and electroless plating [16,23-27]. These fibrous substrates possess interesting properties such as thermal diffusivity, conductivity, electrocatalytic activity, and SERS sensitivity. For instance, Singameni et al. [16] described a high SERS sensitivity obtained from a substrate composed by oriented Au nanorods on electrospun nanofibres prepared using the drop-cast method.

5.1.3.1. Non functionalized PAN electrospun mantles

In this work, PAN 14% (w/w) electrospun mantle was produced according to the parameters described in 5.3.2.2 section. The resultant fibre PAN mats present several beads randomly dispersed through the fibres, as can be observed in the SEM images (Figure 5.11). Although it could be possible to continue optimizing the electrospinning parameters in order to minimize the beads presence, this was not considered of utmost importance for the present work, since these defects could somehow help the support of the NPs and NPsGO nanostructures.

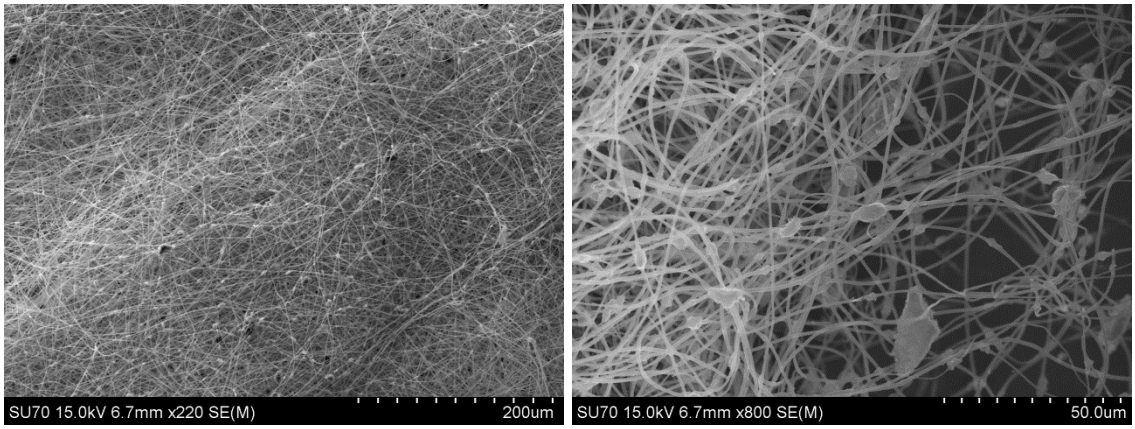

Figure 5.11 – SEM images of electrospun PAN mantle.

These fibre mantles were then used as a sorbent to support silver and gold NPs from colloidal suspensions, prepared by reduction using sodium citrate and glucose reducing agents. The same procedure was used with suspensions containing AgGO and AuGO nanocomposites in suspension prepared also using both reducing agents referred before.

The characterization of these materials by SEM and UV-vis spectroscopy is summarized in Figure 5.12.

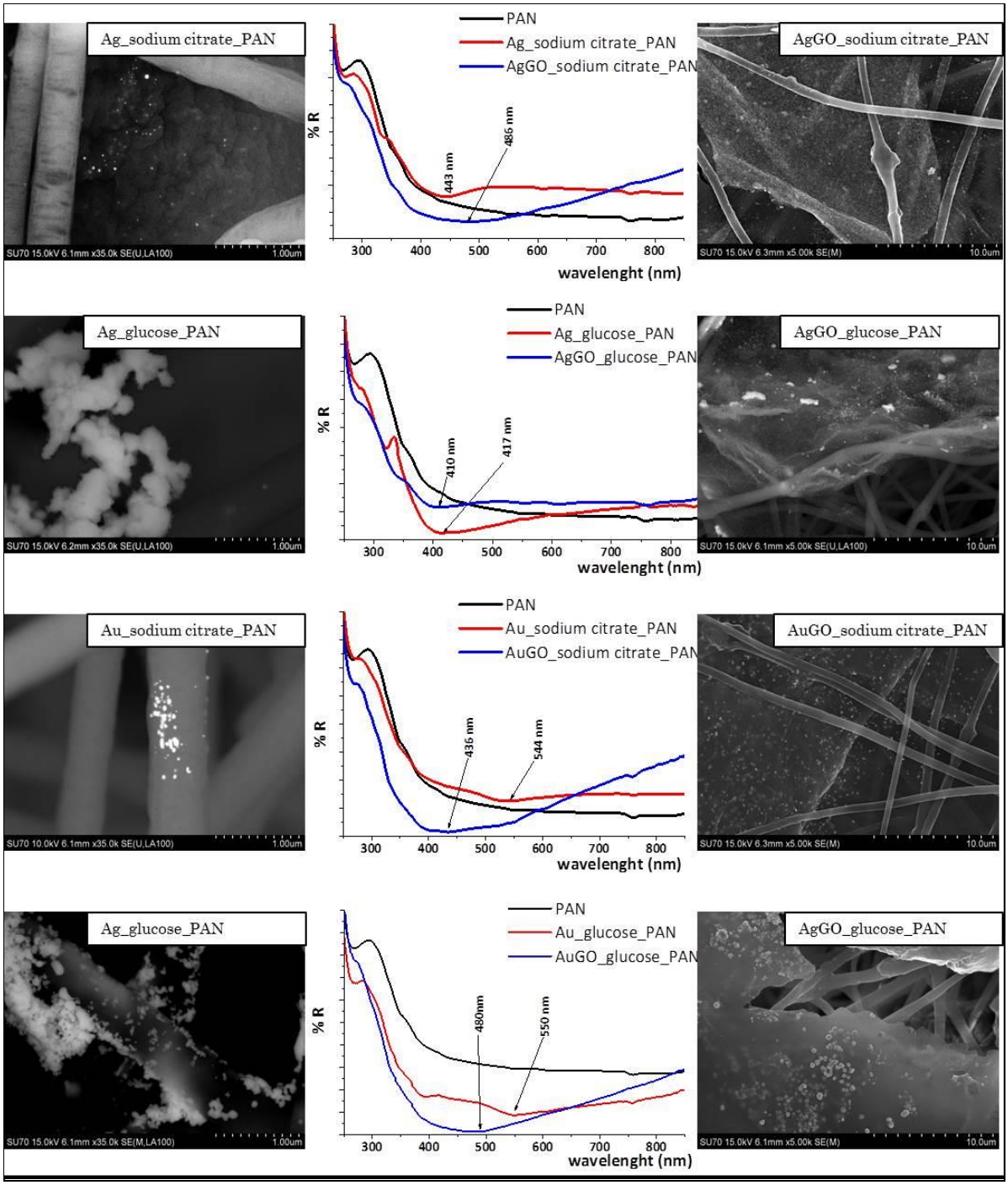

Figure 5.12 – SEM images of graphene-based nanocomposites with silver and gold nanoparticles: AgGO_sodium citrate, AuGO_sodium citrate, AgGO_glucose, AuGO_glucose, and corresponding colloidal suspensions impregnated onto PAN membranes. The transmittance spectra of all materials were also inserted.

First of all, from these characterization results (Figure 5.12), it is possible to see that the nanomaterials were really entrapped in the PAN electropun network, particularly in the case of the NPsGO nanocomposites. This latter statement can be understood due to size constrains.

The SEM images (Figure 5.12) show that the glucose produces metal nanoparticles bigger than those produced with sodium citrate. The λ_{max} absorbance of Ag_sodium citrate_PAN was not according the SEM images; the λ_{max} absorbance in 430 nm indicates bigger nanoparticle than in Ag_glucose_PAN (417 nm). The maximum absorbance peak positions of Au_sodium citrate_PAN (544 nm) and Au_glucose_PAN (550 nm) are according to SEM images.

The distribution of silver and gold nanoparticles is uniform at the graphene oxide surface and these nanocomposites are really entrapped in the electrospun fibres. The metal nanoparticles prepared via glucose show some aggregates on the PAN fibres whereas the nanoparticles in Ag_sodium citrate_PAN and Au_sodium citrate_PAN are well distributed but difficult to identify by SEM due to their small size.

All the produced PAN mantles were tested for SERS activity (Figure 5.13). Similarly to the previous PVA membranes, SHsal ethanolic solution at10^{-3} mol dm^{-3} concentration was the Raman probe deposited on PAN membranes.

Although the intensity was very weak, the typical Raman peak of SHsal, around 1030 cm^{-1}, was present in AgGO_sodium citrate_PAN, AgGO_glucose_PAN and AuGO_glucose_PAN.

In the case of Au_glucose_PAN it was possible to identify four peaks of SHsal: 998, 1070 and 1563 cm^{-1} with very weak intensity and at 1027 cm^{-1} with medium intensity.

For Ag_glucose_PAN, seven peaks of SHsal were identified, one very strong (1029 cm^{-1}), three medium (1112, 1155 and 1558 cm^{-1}) and three very weak (838, 1457 and 1579 cm^{-1}).

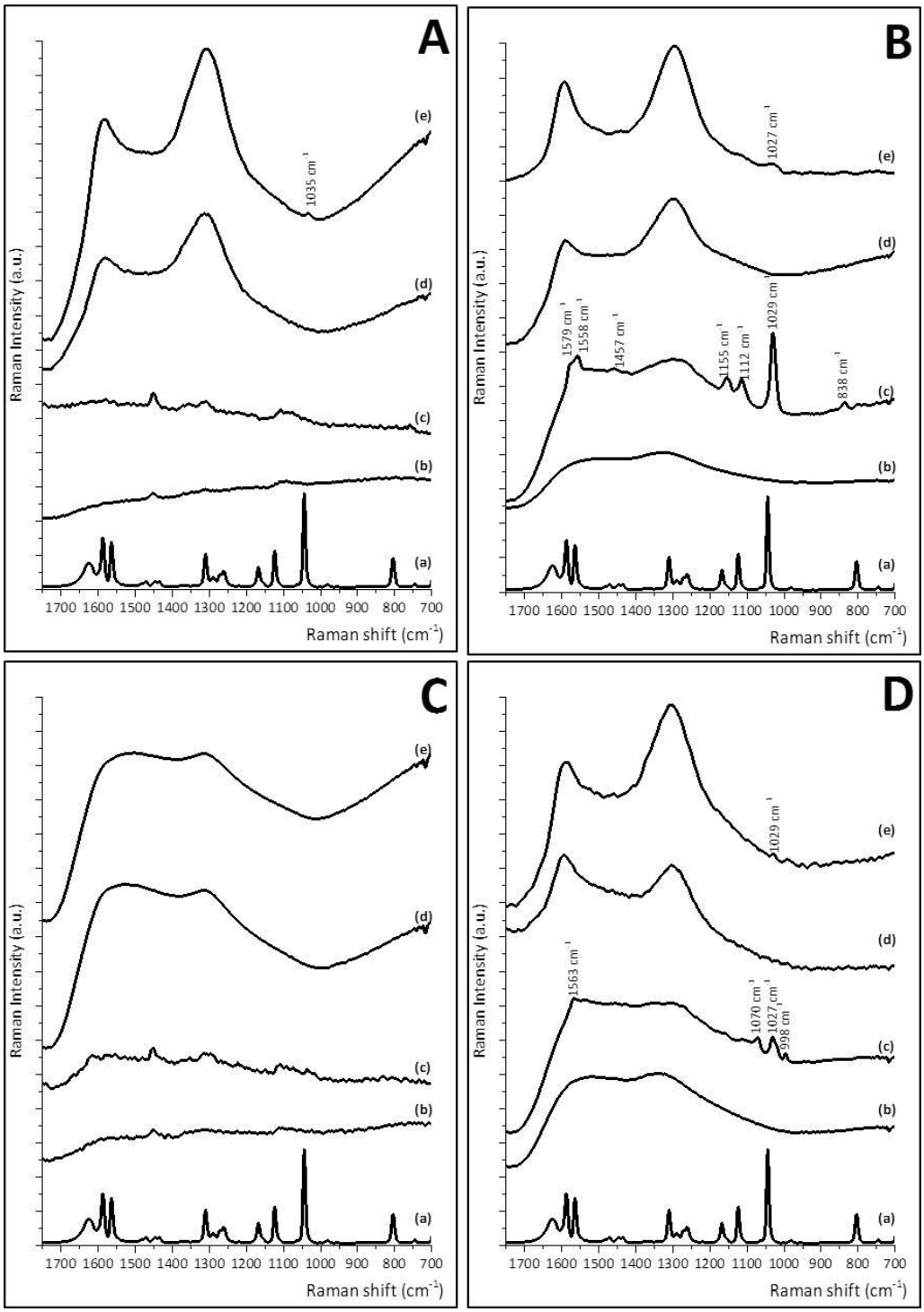

Figure 5.13 – **A**- (a) SHsal, (b) Ag_sodium citrate_PAN, (c) Ag_sodium citrate_PAN+SHsal, (d) AgGO_sodium citrate_PAN, (e) AgGO_sodium citrate_PAN+SHsal. **B**- (a) SH, (b) Ag_glucose_PAN, (c) Ag_glucose_PAN+SHsal, (d) AgGO_glucose_PAN, (e) AgGO_glucose_PAN+SHsal. **C** - (a) SHsal, (b) Au_sodium citrate_PAN, (c) Au_sodium citrate_PAN+SHsal, (d) AuGO_sodium citrate_PAN, (e) AuGO_sodium citrate_PAN+SHsal. **D** - (a) SH, (b) Au_glucose_PAN, (c) Au_glucose_PAN+SHsal, (d) AuGO_glucose_PAN, (e) AuGO_glucose_PAN+SHsal.

The present approach to prepare PAN mantles followed by its immersion on suspensions, in general, produces materials that can act as SERS substrates. The homogeneity and the good distribution of the nanoparticles and graphene oxide sheets at the top of PAN mantles can be exploited to other applications besides SERS, such as catalysis[28,29].

5.1.3.2. Functionalized PAN electrospun mantles

Another approach to link the metal NPS to the electrospun PAN fibres was adapted from a methodology described by Zhang et al[14]. These authors prepared flexible and active SERS substrates by electroless plating of Ag NPs on the surface of electrospun nanofibers via a seed-mediated growth process. First they functionalized PAN microfibers using hydroxylamine (HDA), followed by seeding with palladium NPs to promote the Ag NPs growth. Here, this methodology was adapted to functionalize the electrospun PAN-based membranes before the interaction with Ag NPs and AgGO nanocomposites (please see section 6.4.3.2.2). The methodology followed to prepare these materials is schematized in Figure 5. 14.

The surface modification and activation of the fibres produced by electrospinning can significantly influence the deposition of Ag NPs on the microfibers. The surface of PAN microfibers was modified through amidoxime (-C(NH_2)=N-OH) surface functionalization. Amidoximation of PAN microfibers resulted in the formation of −C(NH_2)=N−OH groups on the fibre surfaces, leading to a considerable increase of hydrophilicity for the microfibrous membranes[14].

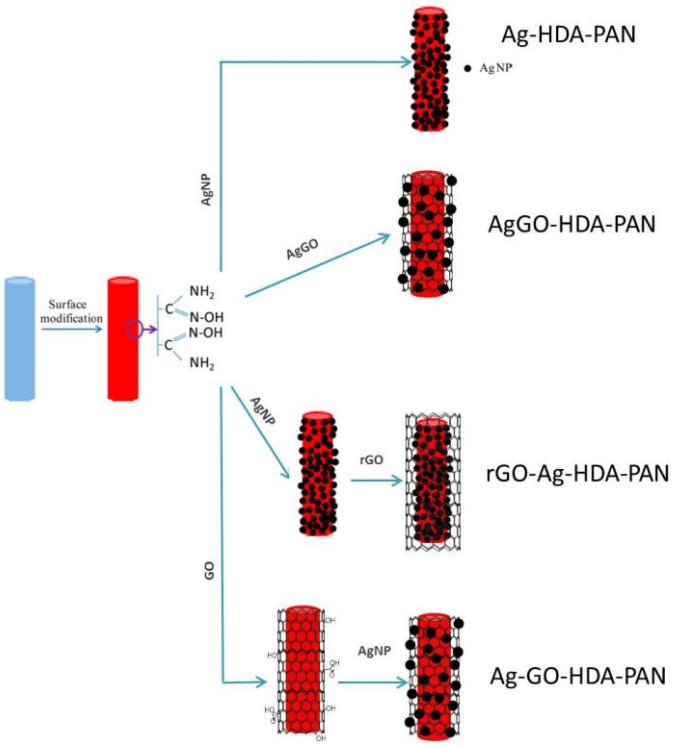

Figure 5. 14 – Preparation scheme of four different types of materials produced with PAN functionalized: Ag-HDA-PAN, AgGO-HDA-PAN, rGO-Ag-HDA-PAN and Ag-GO-HDA-PAN.

As schematized in Figure 5.14, four different routes to prepare new materials were followed. A common initial preparation of the fibres was done: the activation of the PAN fibre surfaces with hydroxylamine (HAD). The amidoxime functionalized PAN fibres were then i) immersed on AgNPs colloidal suspension overnight (Ag-HAD-PAN); ii) immersed on AgGO suspension overnight (AgGO-HAD-PAN); iii) on AgNPs colloidal suspension overnight dried and after immersed on a GO suspension previously reduced with HAD (rGO) for 24 hr, (rGO-Ag-HAD-PAN); iv) immersed in GO suspensions with different concentrations during 24 hr, followed by Ag NPs attachment as referred in the previous point.

The presence of Ag NPs in the substrate Ag-HDA-PAN was confirmed by SEM (Figure 5.15) and also qualitative EDS analysis confirmed the silver presence (not shown). The UV-vis absorbance shows a maximum at approximately 370 nm, which is a well-known peak position that indicates the presence of silver nanoparticles[30].

The SEM image of AgGO-HDA-PAN indicates the coating of the functionalized PAN fibres with the AgGO sheets, showing a good dispersion through the fibres (Figure 5.15).

The substrate rGO-Ag-HDA-PAN, clearly show the presence of rGO covering the fibres with the Ag NPs on the top (Figure 5.15). In the Ag-GO-HDA-PAN, the presence of GO sheets is also clearly observed in SEM image; however it seems that the GO sheets were mainly wrapped around the PAN fibres (Figure 5.15).

All the previous materials prepared were tested with Rodhamine 6G (R6G) for their SERS activity. The aqueous solution of Raman probe was drop-cast onto the surface of the substrates.

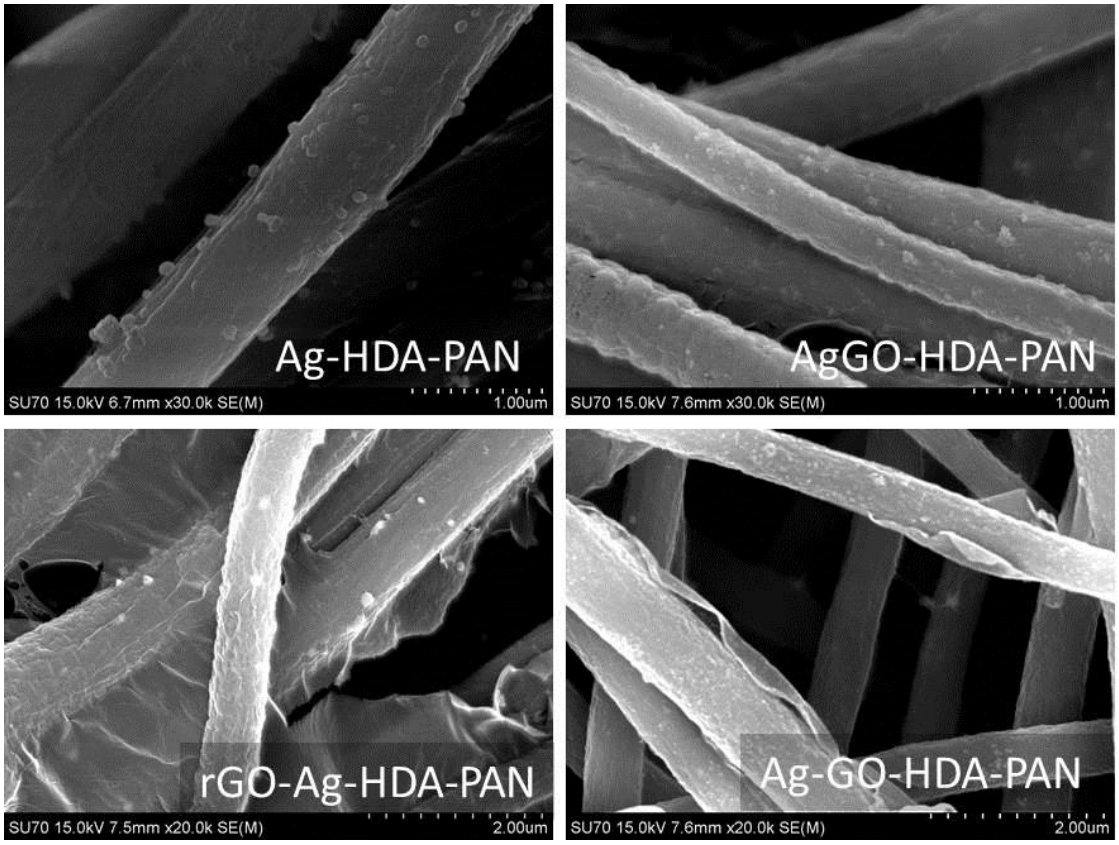

Figure 5.15 – SEM images from the samples Ag-HDA-PAN, AgGO-HDA-PAN, rGO-Ag-HDA-PAN, and Ag-GO-HDA-PAN.

The substrate Ag-HDA-PAN showed a very good SERS spectrum for R6G at 10^{-3} mol dm^{-3} concentration, being possible to identify the peaks localized at 775, 1183, 1306, 1360, 1449, 1505, 1597, and 1643 cm^{-1} (Figure 5.16). Almost the same peaks were identified at 10^{-5} mol dm^{-3}. Surprisingly, at the concentration of R6G 10^{-6} mol dm^{-3} any peak was observed.

The absorbance spectra of all these samples were acquired (Figure 5.17). The shift of LSPR λ_{max} as function of R6G concentration shows that the shift of λ_{max} starts to stabilize between 10^{-4} and 10^{-5} mol dm^{-3}. Such result is according to SERS results in terms of limit detection of this substrate.

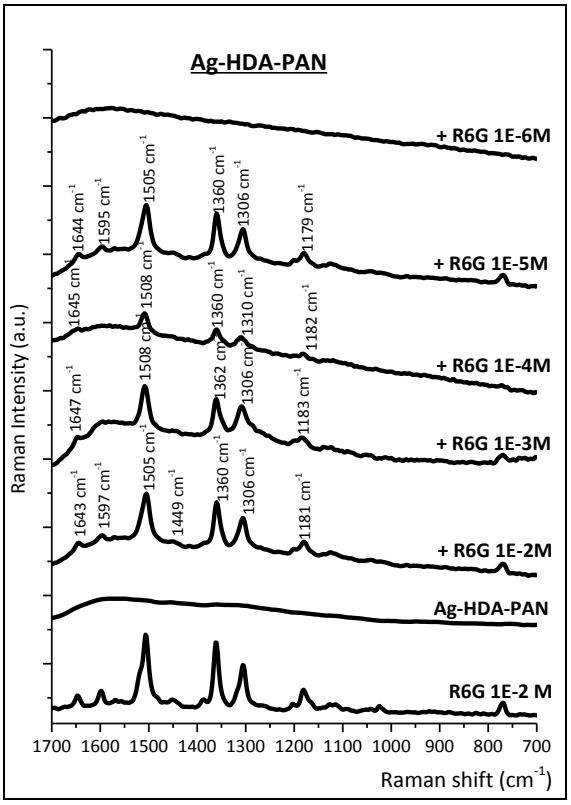

Figure 5.16 – Limit of detection of R6G in Ag-HDA-PAN substrate. The Raman spectra of R6G at 10^{-2} mol dm^{-3} concentration was also inserted for comparison.

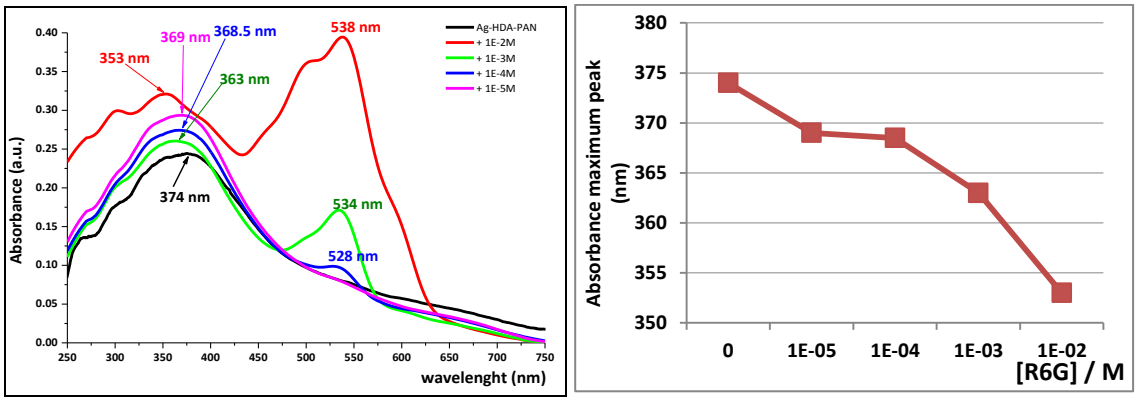

Figure 5.17 – Absorbance spectra of Ag-HDA-PAN samples with R6G at 0, 10^{-2}, 10^{-3}, 10^{-4} and 10^{-5} mol dm^{-3} concentration deposited on the mantles (LEFT). The shift of the peak LSPR position of silver nanoparticles was analysed as a function of R6G concentration (RIGHT).

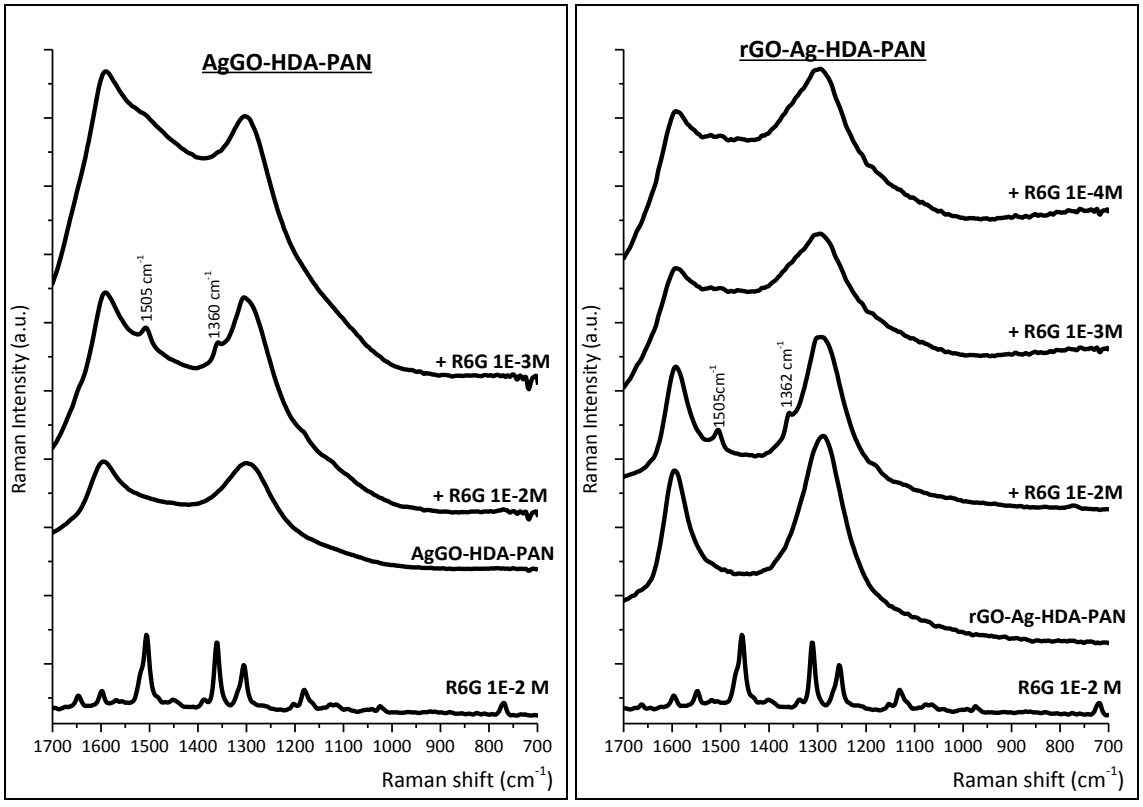

Figure 5.18 – Raman spectra of R6G using AgGO-HDA-PAN and rGO-Ag-HDA-PAN.

In the case of AgGO-HDA-PAN and Ag-rGO-HDA-PAN (Figure 5.18), the R6G molecule was only identified at 10^{-2} mol dm^{-3} in both substrates, which means that the peaks at 1360 and 1505 cm^{-1} are Raman intensities because the R6G at this concentration, deposited onto a glass slice, show the same peaks. In rGO-Ag-HDA-PAN with R6G at 10^{-3} mol dm^{-3}, there was a formation of a plateau between 1350 and 1500 cm^{-1} which rises doubt if this effect indicates SERS activity. So the 10^{-4} mol dm^{-3} concentration was tested and confirmed that only reliable R6G peaks occurs at 10^{-2} mol dm^{-3}. These results indicate that these two substrates did not act as SERS substrates.

The quantity of GO in AgGO-HAD-PAN was 0.18 mg/mL, which means a proportion of 1:1 to Ag:GO. So, for the preparation of Ag-GO-HDA-PAN the quantity of GO chosen to be added was 0.18 mg/mL. The SERS spectrum of 10^{-3} mol dm^{-3} R6G indicates the presence of its most intense peak at 1505 cm^{-1} (Figure 5.19). However the intensity of the peak is very weak and because of that we decided to decrease the ratio between Ag:GO. New materials were prepared with 0.09 mg/mL and 0.06 mg/mL of GO repeating the experimental procedure. The SERS spectra of R6G with these new materials (Figure 5.20) show that the Ag-0.09GO-HDA-PAN was the more efficient one for R6G detection. The specimen with 0.09 mg/mL of GO shows the peaks of R6G localized at 775, 1181, 1308, 1360, 1509 and 1645 cm^{-1} at 10^{-3} mol dm^{-3}, and at 1509 cm^{-1} at 10^{-4} mol dm^{-3}, although with very weak intensity.

The presence of D and G bands at 1290 and 1580 cm^{-1} was shown in all SERS spectra of all the substrates based on PAN fibres. Its intensities can supress the identification of the probe molecule; on the other hand, when the SERS peaks show an intensity enough to overlap the D and G bands, it is possible say that we are in the presence of a good SERS substrate. This is what happens with Ag-0.09GO-HDA-PAN flexible microfibrous substrate.

The work present here shows significant suggestions to tune a material that can combine the EM and CM in order to obtain a substrate that can be selective and sensitive to several biomolecules.

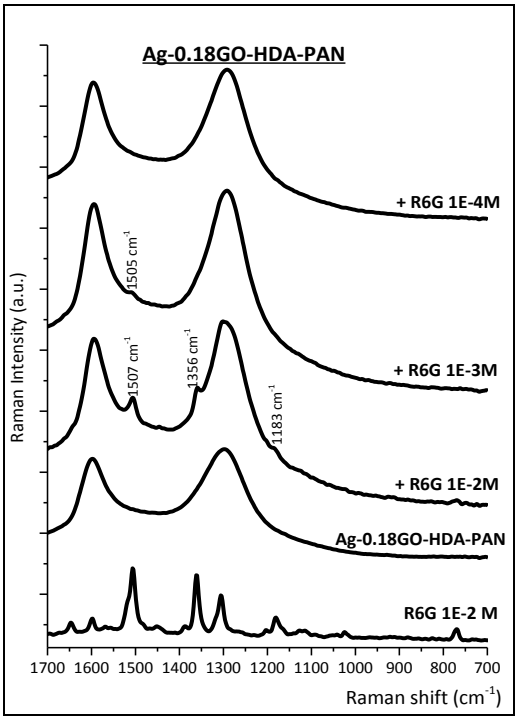

Figure 5.19 – SERS spectra of R6G at several concentrations in Ag-0.18GO-HDA-PAN.

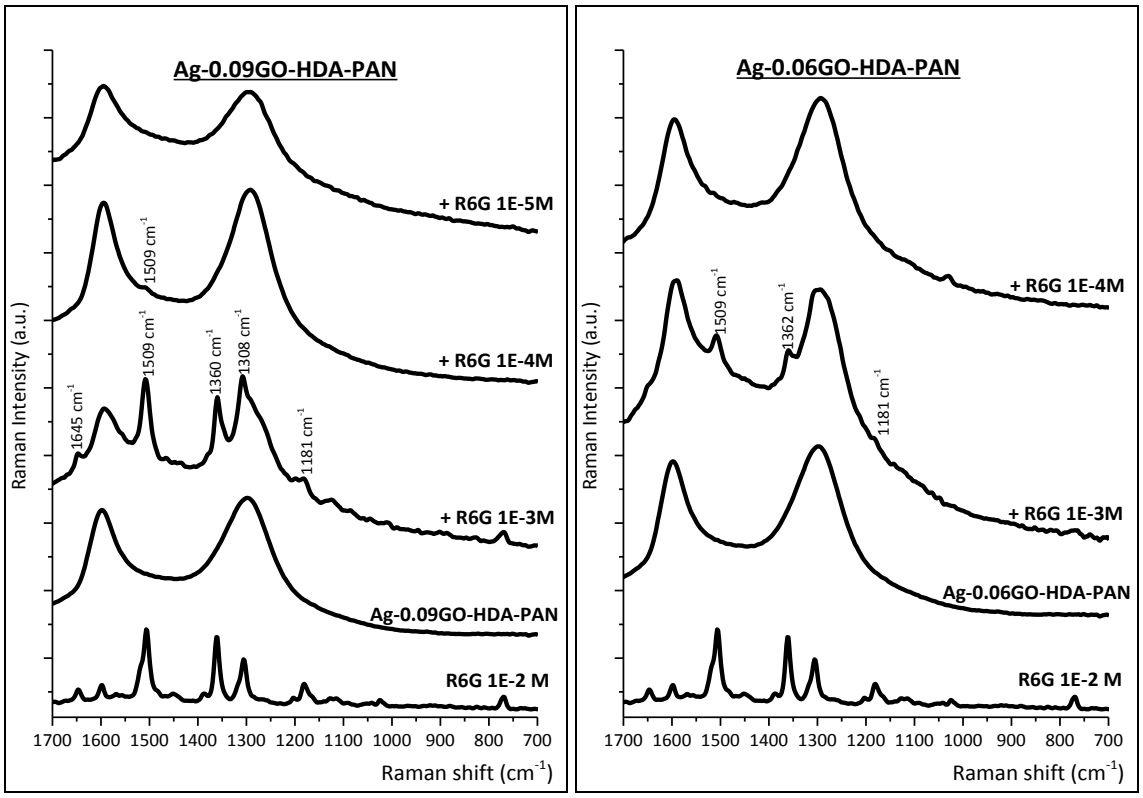

Figure 5.20 – SERS spectra of R6G in several concentrations using Ag-0.09GO-HDA-PAN and Ag-0.06GO-HDA-PAN.

5.2. Conclusion

In the present work the potentialities of several types of materials based on the polymeric electrospun fibres for SERS detection were shown. The PVA and PAN were the polymers chosen.

The materials based on PVA, where the synthesis method is based on the inclusion of silver nanoparticles and graphene oxide into the fibres, the best results where achieve for the membrane with AgGO after the occurrence of the cross-linking process. SHsal was detected at 10^{-4} mol dm^{-3}. For the PVA membranes the cross-linking seems to be crucial for the enhancement of the Raman intensities of the probe molecule. This could be related with the morphology of the substrates which may interfere with the SERS active sites.

The substrates AgGO_sodium citrate, AgGO_glucose_PAN and AuGO_glucose_PAN acts as SERS substrates. In the first one, the presence of graphene oxide potentiates the enhancement of Raman peaks, since in the correspondent substrate without graphene there was no Raman peak of SHsal. In the other two substrates, the Ag_glucose_PAN and Au_glucose_PAN shows better enhancement of Raman intensities than the correspondent substrates with GO. So it can be said that with glucose as reducing agent, the presence of GO is not favourable to SERS substrate, in substrates prepared by drop-casting.

The PAN activated substrates were tested for SERS experiments tuning the structure composition of the substrate. The best enhancement of Raman intensities was obtained for Ag-0.09GO-HDA-PAN substrate, however, the substrate which has only silver nanoparticles act as SERS substrates with a sensitivity to 10^{-5} mol dm^{-3} of R6G, with a very high resolution of SERS peaks. In fact, this is the best result in the set of materials produced based on fibres and showed in this work.

All the results shown here contribute to the discussion of the preparation of flexible and manageable substrates to SERS applications.

5.3. Experimental procedure

5.3.1. Synthesis of colloidal suspensions and composites-based on graphene

Graphene oxide was prepared by Marcano's method[31].

GO-based nanocomposites were prepared by two different methods. The first one was denoted by "metal_sodium citrate". The reduction of metal complexes was made based on a previous method described by our work group[32]. 7.5 mg of GO was added to a 50 mL of 0.24 mmol dm^{-3} $HAuCl_4.3H_2O$ aqueous solution. The mixture was stirred during 30 min to promote the interaction of gold ions with GO surface. After that, the suspension was heated until 80 ºC, after which 1.880 mL of sodium citrate (85 mmol dm^{-3}) was added dropwise. The experimental conditions were maintained during 1 hour. The final product was "AuGO_sodium citrate". The same experiment was made using silver nitrate (AgGO_sodium citrate).

In the second method, denoted by "metal_glucose", the reducing agent used was glucose. The synthesis of nanocomposites was based on method used by Zhao et al[17], using $HAuCl_4.3H_2O$. 1.2 g of D-(+)glucose was dissolved into 30 mL of a suspension of GO (1.5 mg/mL) under sonication during 5 min. 1 mL of ammonia (25%) was added to 10 mL of $HAuCl_4.3H_2O$ (50 mmol dm^{-3}). Both phases were mixed and kept in sonication during 5 minutes. The final product was "AuGO_glucose". The same experimental procedure was followed to prepare silver and GO nanocomposites ("AgGO_glucose").

The experimental procedure described were repeated using only the metal complexes, without GO (Au_sodium citrate, Ag_sodium citrate, Au_glucose, Ag_glucose). Both type of suspensions, with and without GO, were used as prepared.

5.3.2. Preparation of electrospun nanofibrous membranes

5.3.2.1. PVA

5.3.2.1.1. Ag-PVA and AgGO-PVA

700 mg of PVA was added to 5 mL of Ag_glucose performing a 14% PVA concentration (approximately). The mixture was heated at 80 ºC, during 3 hours with slow stirring. The solution was loaded into 5 mL syringe which had a properly tube attached at the open end, and such tube had a stainless steel needle at the opposite end. The needle was connected to the emitting electrode of high-voltage supply capable of generating DC voltages in the range of 0-50 kV. An aluminium foil (64 cm of length and 10 cm of width) was used as the collection screen which was connected to the ground electrode of the power supply (400 rpm) with the distance between the screen and the needle tip of 8 – 10 cm. The electrospinning was carried out at 19 ºC – 22 ºC, and relative humidity 22 % - 23%. In order to obtain continuous and homogeneous nanofibres, the voltage applied was 23 kV, in a rate of 0.1mL/h. The final mantle was dried in air before being detached from the aluminium foil. The same procedure was made using AgGO_glucose suspension.

5.3.2.2. PAN

1.4 g of PAN was dissolved in 10 mL of DMF, with stirring during approximately 18 h. The use of electrospinning apparatus was the same as describe in previous section. Here, the experimental conditions were the following: 2000 rpm of the collector at 12 cm of the needle, the voltage applied was 20 kV, in a rate of 1.2 mL/h. The procedure was followed at 19 ºC – 22 ºC, and relative humidity 62 % - 50%.

5.3.2.2.1. PAN imbibed on colloidal suspensions

Squares (7 cm x 7 cm, approximately) of PAN mantle were cut and placed upon a filter paper inside a Buckner funnel. 5 mL of each suspension of metal nanoparticles (Au_sodium citrate, Ag_sodium citrate, Au_glucose, Ag_glucose) and graphene nanocomposites (AuGO_sodium citrate, AgGO_sodium citrate, AuGO_glucose, AgGO_glucose) were filtered on PAN squares. As the filter papers showed the colouring of the suspensions, all the PAN squares and the correspondent filter papers were dried in air.

5.3.2.2.2. Functionalization of PAN membranes

Ag-HDA-PAN

Prior to the growth of Ag NPs, as-electrospun PAN fibrous membranes were first treated in 1 mol dm^{-3} NH_2OH aqueous solution at 70 °C for 5 min; some −C≡N groups on the surface of nanofibres reacted with NH_2OH, leading to the formation of $-C(NH_2)=N-OH$ groups. After the treatment, the obtained amidoxime surface-functionalized PAN (HDA-PAN) fibrous membranes were thoroughly rinsed in distilled water and dried before the growth of Ag NPs.

The AgNPs colloidal suspension was prepared by Lee and Meisel method. 90 mg of $AgNO_3$ was dissolved in 500 mL (0.18 mg/mL) of ultra-pure H_2O and brought to boiling. A solution of 1% sodium citrate (10 mL) was dropwise added. The solution was kept on boiling during 1 hour. The Ag sol was yellow-greenish at the final of synthesis.

Finally, HAD-PAN was immersed in 30 mL of Ag colloidal suspension overnight. The Ag-HAD-PAN was washed with distilled water and let dried in air.

rGO-Ag-HDA-PAN

Reduced graphene oxide (rGO) was previous prepared using hydroxylamine as the following description: hydroxylamine (final concentration of 100 mmol dm^{-3}) was added to 50 mL of 0.5 mg/mL GO with vigorous stirring. The pH of mixture was kept

at 12 and heated in an oil bath at 85 ºC; meanwhile the colour of the mixture changed from yellowish brown to homogeneous black indicating the reduction took place. The Ag-HAD-PAN was impregnated with rGO (0.18 mg/mL) during ~24h. The fibrous membrane was thoroughly rinsed with distilled water and dried in air before characterization and SERS evaluation.

Ag-GO-HDA-PAN

In this case, GO was used as the bridge between HAD-PAN and silver NPs. HAD-PAN was immersed in GO suspensions with different concentrations, 0.18, 0.09 and 0.06 mg/mL, during 24 h. After the interaction with Ag colloidal suspension, the mantle Ag-GO-HAD-PAN was tested in SERS. The substrates were referred as Ag-0.18GO-HDA-PAN, Ag-0.09GO-HDA-PAN and Ag-0.06GO-HDA-PAN.

AgGO-HDA-PAN

Previously, a suspension composed by GO and Ag NPs was synthesized based on Lee and Meisel method. 18 mg of silver nitrate was added to 100 mL of GO 0.18 mg/mL suspension. The mixture heated until boiling. After 10 minutes of reflux, 2 mL of sodium citrate 20 mg/mL was added dropwise. The boiling was kept during about 60 min and the suspension changed the yellow brownish colour to black. In this synthesis, the characteristic changing colour of Ag colloid was not present due to simultaneous reduction of GO. After that, the same functionalization described to Ag-HAD-PAN was followed but in this case using the AgGO previous described in this section and at the final AgGO-HAD-PAN was produced.

5.3.3. SERS experiments

A piece of PVA and PAN composites was cut (approximately 5 × 10 mm) and 4 μL of SHsal in several concentrations were deposited on their surface. In the case of functionalized PAN mantles, 4 μL of R6G in different concentrations was deposited on the PAN pieces and let dried. Raman spectra were acquired using Bruker RFS100/S FT-Raman spectrometer (Nd:YAG laser, 1064 nm excitation). All the experiments

were acquired with 500 scans but the voltage used was dependent of the material used (50 – 300 mW).

5.4. Bibliography

(1) Abalde-Cela, S.; Aldeanueva-Potel, P.; Mateo-Mateo, C.; Rodriguez-Lorenzo, L.; Alvarez-Puebla, R. A.; Liz-Marzan, L. M. Surface-enhanced Raman scattering biomedical applications of plasmonic colloidal particles. *Journal of the Royal Society Interface* **2010**, *7*, S435-S450.

(2) Alvarez-Puebla, R. A.; Liz-Marzan, L. M. Traps and cages for universal SERS detection. *Chemical Society Reviews* **2012**, *41*, 43-51.

(3) Liu, J.; White, I.; DeVoe, D. L. Nanoparticle-functionalized porous polymer monolith detection elements for surface-enhanced Raman scattering. *Anal Chem* **2011**, *83*, 2119-2124.

(4) Marques, P. A. A. P.; Nogueira, H. I. S.; Pinto, R. J. B.; Neto, C. P.; Trindade, T. Silver-bacterial cellulosic sponges as active SERS substrates. *Journal of Raman Spectroscopy* **2008**, *39*, 439-443.

(5) Tang, H.; Meng, G.; Huang, Q.; Zhang, Z.; Huang, Z.; Zhu, C. Arrays of Cone-Shaped ZnO Nanorods Decorated with Ag Nanoparticles as 3D Surface-Enhanced Raman Scattering Substrates for Rapid Detection of Trace Polychlorinated Biphenyls. *Advanced Functional Materials* **2012**, *22*, 218-224.

(6) Fan, Y.; Cheng, H.; Zhou, C.; Xie, X.; Liu, Y.; Dai, L.; Zhang, J.; Qu, L. Honeycomb architecture of carbon quantum dots: a new efficient substrate to support gold for stronger SERS. *Nanoscale* **2012**, *4*, 1776-1781.

(7) Qian, Y.; Meng, G.; Huang, Q.; Zhu, C.; Huang, Z.; Sun, K.; Chen, B. Flexible membranes of Ag-nanosheet grafted polyamide-nanofibers as effective 3D SERS substrates. *Nanoscale* **2014**, *6*, 4781-4788.

(8) Dong, G.; Xiao, X.; Liu, X.; Qian, B.; Liao, Y.; Wang, C.; Chen, D.; Qiu, J. Functional Ag porous films prepared by electrospinning. *Applied Surface Science* **2009**, *255*, 7623-7626.

(9) Amarjargal, A.; Tijing, L. D.; Shon, H. K.; Park, C.-H.; Kim, C. S. Facile in situ growth of highly monodispersed Ag nanoparticles on electrospun PU nanofiber membranes: Flexible and high efficiency substrates for surface enhanced Raman scattering. *Applied Surface Science* **2014**, *308*, 396-401.

(10) Yang, H.; Huang, C. Z. Polymethacrylic acid-facilitated nanofiber matrix loading Ag nanoparticles for SERS measurements. *Rsc Advances* **2014**, *4*, 38783-38790.

(11) Li, X.; Cao, M.; Zhang, H.; Zhou, L.; Cheng, S.; Yao, J.-L.; Fan, L.-J. Surface-enhanced Raman scattering-active substrates of electrospun polyvinyl alcohol/gold-silver nanofibers. *Journal of Colloid and Interface Science* **2012**, *382*, 28-35.

(12) Cao, M.; Cheng, S.; Zhou, X.; Tao, Z.; Yao, J.; Fan, L.-J. Preparation and surface-enhanced Raman performance of electrospun poly(vinyl alcohol)/high-concentration-gold nanofibers. *Journal of Polymer Research* **2012**, *19*.

(13) He, D.; Hu, B.; Yao, Q.-F.; Wang, K.; Yu, S.-H. Large-Scale Synthesis of Flexible Free-Standing SERS Substrates with High Sensitivity: Electrospun PVA Nanofibers Embedded with Controlled Alignment of Silver Nanoparticles. *Acs Nano* **2009**, *3*, 3993-4002.

(14) Zhang, L.; Gong, X.; Bao, Y.; Zhao, Y.; Xu, M.; Jiang, C.; Fong, H. Electrospun Nanofibrous Membranes Surface-Decorated with Silver Nanoparticles as Flexible and Active/Sensitive Substrates for Surface-Enhanced Raman Scattering. *Langmuir* **2012**, *28*, 14433-14440.

(15) Bao, Y.; Lai, C.; Zhu, Z.; Fong, H.; Jiang, C. SERS-active silver nanoparticles on electrospun nanofibers facilitated via oxygen plasma etching. *Rsc Advances* **2013**, *3*, 8998-9004.

(16) Lee, C. H.; Tian, L.; Abbas, A.; Kattumenu, R.; Singamaneni, S. Directed assembly of gold nanorods using aligned electrospun polymer nanofibers for highly efficient SERS substrates. *Nanotechnology* **2011**, *22*.

(17) Zhao, X. S.; Ma, J. Z.; Zhang, J. T.; Xiong, Z. G.; Yong, Y. Preparation, characterization and antibacterial properties of silver-modified graphene oxide. *Journal of Materials Chemistry* **2011**, *21*, 3350-3352.

(18) Dmitriev, A.; Bingham, J.; Hall, W. P.; Van Duyne, R.: Exploring the Unique Characteristics of LSPR Biosensing. In *Nanoplasmonic Sensors*; Integrated Analytical Systems; Springer New York, 2012; pp 29-58.

(19) Kim, Y.-K.; Han, S. W.; Min, D.-H. Graphene Oxide Sheath on Ag Nanoparticle/Graphene Hybrid Films as an Antioxidative Coating and Enhancer of Surface-Enhanced Raman Scattering. *Acs Applied Materials & Interfaces* **2012**, *4*, 6545-6551.

(20) Zhang, Z.; Xu, F.; Yang, W.; Guo, M.; Wang, X.; Zhanga, B.; Tang, J. A facile one-pot method to high-quality Ag-graphene composite nanosheets for efficient surface-enhanced Raman scattering. *Chemical Communications* **2011**, *47*, 6440-6442.

(21) Ding, B.; Kim, H. Y.; Lee, S. C.; Shao, C. L.; Lee, D. R.; Park, S. J.; Kwag, G. B.; Choi, K. J. Preparation and characterization of a nanoscale poly(vinyl alcohol) fiber aggregate produced by an electrospinning method. *Journal of Polymer Science Part B-Polymer Physics* **2002**, *40*, 1261-1268.

(22) Valente, A. J. M.; Cruz, S. M. A.; Morán, M. C.; Murtinho, D. B.; Muniz, E. C.; Miguel, M. G. Release of DNA from cryogel PVA-DNA membranes. *eXPRESS Polymer Letters* **2010**, *4*, 480-487.

(23) He, H.; Cai, W.; Lin, Y.; Dai, Z. Silver Porous Nanotube Built Three-Dimensional Films with Structural Tunability Based on the Nanofiber Template-Plasma Etching Strategy. *Langmuir* **2011**, *27*, 1551-1555.

(24) Carlberg, B.; Ye, L.-L.; Liu, J. Surface-Confined Synthesis of Silver Nanoparticle Composite Coating on Electrospun Polyimide Nanofibers. *Small* **2011**, *7*, 3057-3066.

(25) Jia, W.; Wang, Y.; Basu, J.; Strout, T.; Carter, C. B.; Gokirmak, A.; Lei, Y. Nanoengineered Transparent, Free-Standing, Conductive Nanofibrous Membranes. *Journal of Physical Chemistry C* **2009**, *113*, 19525-19530.

(26) Sinha-Ray, S.; Zhang, Y.; Yarin, A. L. Thorny Devil Nanotextured Fibers: The Way to Cooling Rates on the Order of 1 kW/cm(2). *Langmuir* **2011**, *27*, 215-226.

(27) Ochanda, F.; Jones, W. E., Jr. Fabrication and thermal analysis of submicron silver tubes prepared from electrospun fiber templates. *Langmuir* **2007**, *23*, 795-801.

(28) Goncalves, G. A. B.; Pires, S. M. G.; Simoes, M. M. Q.; Neves, M. G. P. M. S.; Marques, P. A. A. P. Three-dimensional graphene oxide: a promising green and sustainable catalyst for oxidation reactions at room temperature. *Chemical Communications* **2014**, *50*, 7673-7676.

(29) Jiang, D.-H.; Yang, C.-H.; Tseng, C.-M.; Lee, S.-L.; Chang, J.-K. Metal/graphene nanocomposites synthesized with the aid of supercritical fluid for promoting hydrogen release from complex hydrides. *Nanoscale* **2014**, *6*, 12565-12572.

(30) Vasylyev, S.; Damm, C.; Segets, D.; Hanisch, M.; Taccardi, N.; Wasserscheid, P.; Peukert, W. Synthesis of silver nanoparticles in melts of amphiphilic polyesters. *Nanotechnology* **2013**, *24*, 115604.

(31) Marcano, D. C.; Kosynkin, D. V.; Berlin, J. M.; Sinitskii, A.; Sun, Z.; Slesarev, A.; Alemany, L. B.; Lu, W.; Tour, J. M. Improved synthesis of graphene oxide. *Acs Nano* **2010**, *4*, 4806-4814.

(32) Goncalves, G.; Marques, P. A. A. P.; Granadeiro, C. M.; Nogueira, H. I. S.; Singh, M. K.; Gracio, J. Surface Modification of Graphene Nanosheets with Gold Nanoparticles: The Role of Oxygen Moieties at Graphene Surface on Gold Nucleation and Growth. *Chemistry of Materials* **2009**, *21*, 4796-4802.

6. Gold covered vertically aligned multi-walled carbon nanotube arrays as highly sensitive SERS substrates

In this chapter, the forests of vertically aligned multi-walled carbon nanotubes covered by gold (VAMWCNT_Au) were used as surface-enhanced Raman scattering (SERS) substrates. The detection limit for nucleobases was investigated as well as the detection of DNA.

6.1. Introduction

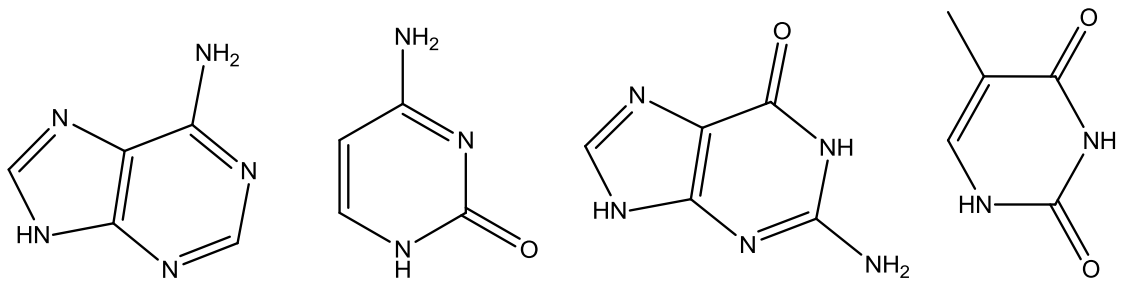

Adenine Cytosine Guanine

Thymine

Scheme 6.1 – Nucleobases used as SERS analytes.

Surface-enhanced Raman scattering (SERS) is an analytical tool for chemical and biological sensing due its capacity of Raman signal amplification by factors up to 10-14 orders of magnitude, providing ultra-high sensitivity reaching single-molecule detection[1]. The enhancement factor is due to electromagnetic[2] and chemical mechanisms[3]. The latter can be explained when the charge transfer-assisted complex formation occurs between the molecule and the surface. The electromagnetic mechanism is associated to a local electromagnetic field enhanced by excited surface plasmons on a metal surface. In order to increase the selectivity and the limit of detection, researchers have improved SERS substrates tuning size and shape of the 1D metal nanostructures which are, normally, the basis of such platforms. Also the deposition of the metal nanoparticles was made in flexible supports (cellulose-paper, polymer mats[4]), in silicon wafers or glass, using several techniques such as lithography. Recently, 3D nanostructures (nanowires, nanorods, ordered Au particle arrays, nanoporous silicon, nanotube arrays, and cavity nano antenna arrays with dense plasmonic nanodots) have been proposed as SERS substrates.

Carbon nanotubes (CNT) have been the subject of extensive research because of their excellent electrical, thermal and mechanical properties. The application of CNT in

SERS substrates is a research topic with increasing interest that has been addressed in several ways: vertically aligned in a silicon support[5-7], used as an endoscope tip[8,9] or specifically functionalized for use as an intracellular probe[10]. Vertically aligned multi-walled carbon nanotube (VAMWCNT) arrays functionalized with gold nanoparticles generate hot-spots after the deposition of analyte solution. These hot-spots are the key for a better Raman signal magnification.

In this work, we show the potential of the vertically aligned multi-walled carbon nanotubes covered with gold nanoparticles to detect the four nucleobases (adenine, cytosine, guanine, and thymine) and the deoxyribonucleic acid molecules. SERS results obtained for such molecules are stable during, at least, 24 hours, and the enhancement factors are between 10^3 and 10^5.

6.2. Results and discussion

6.2.1. Characterization of VAMWCNT-Au

The SEM images in Figure 6.1 shows a uniformity of the structures with vertical aligned multi-walled carbon nanotubes covered by gold (VAMWCNT_Au).

The Raman characteristic bands of VAMWCNT_Au and their relative intensity in two different points of the material indicates its homogeneity. The I_D/I_G ratio in both locations was about 1.3. (Figure 6.2).

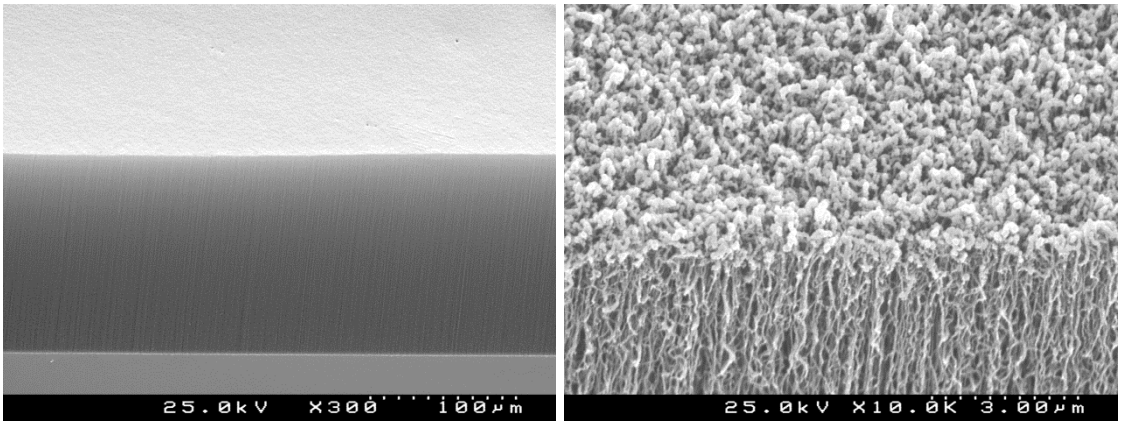

Figure 6.1 – SEM images of VAMWCNT-Au arrays.

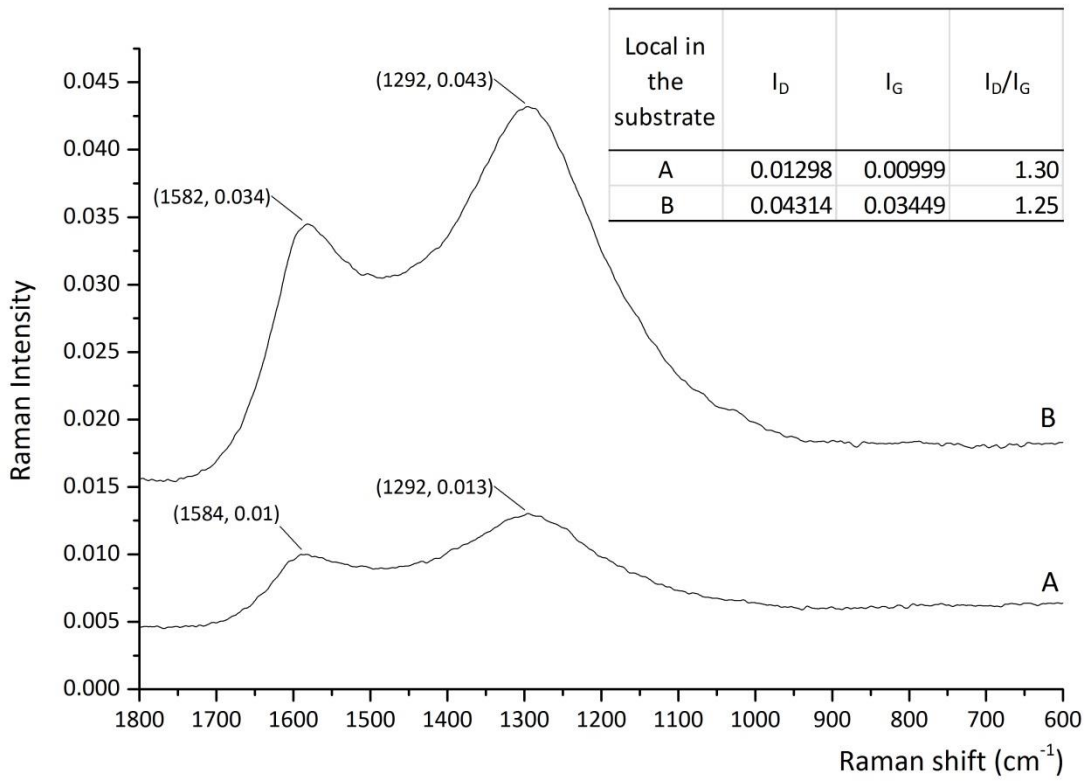

Figure 6.2 – Raman spectra of two different spots in the same VAMWCNT-Au substrate (A, B). Both Raman spectra show a ratio I_D/I_G ~1.3.

SERS results are dependent on composition, size, and interparticle spacing of plasmonic nanoparticles[11] which, are the active components of SERS substrates. In this study the substrates were formed by VAMWCNT and gold nanoparticles, it was important to verify what was the concentration of AuNP that produced the best SERS results. For this study we chosen thiosalicylic acid (SHsal, 0.1M) which is a well-known SERS probe. 4μL of an ethanolic solution of SHsal was deposited on the surface of VAMWCNT_Au substrates with different gold deposition time (5, 15 and 30 minutes). All the spectra were acquired at the same conditions: 350 mW and 50 scans. The most intense peak of SHsal solution (~1030 cm^{-1}) appears in all substrates but the spectrum which shows more SHsal bands and more intense was correspondent to VAMWCNT with 30 min of gold deposition (Figure 6.3). So, this type of substrate was the one used in the SERS studies of nucleic acids and DNA molecule.

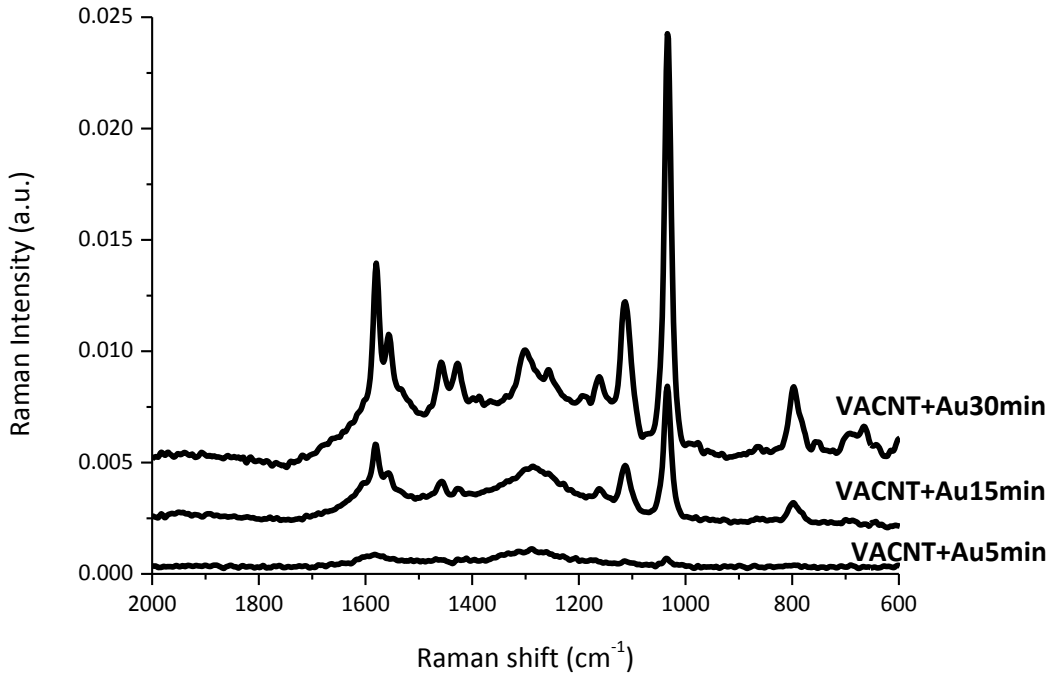

Figure 6.3 – SERS spectra of thiosalicylic acid 0.1 mol dm^{-3} using VAMWCNT_Au with 5, 15 and 30 minute of gold deposition.

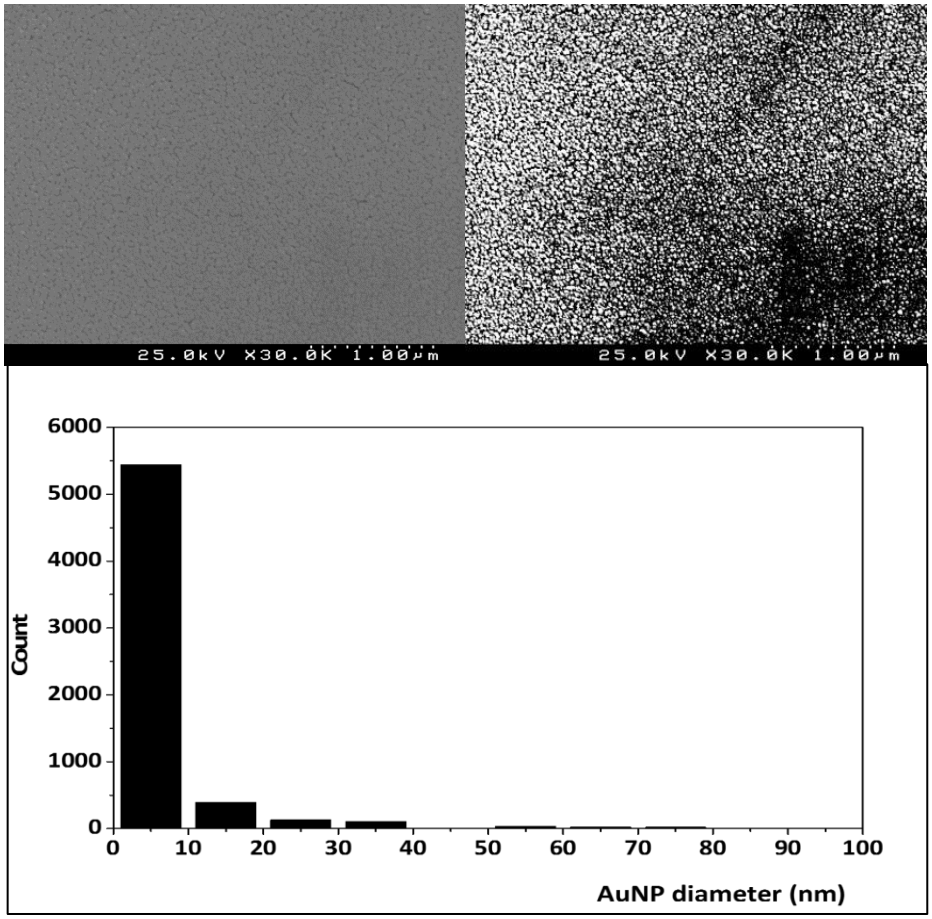

Figure 6.4 – SEM images and statistic study of gold nanoparticles diameter on Si surface

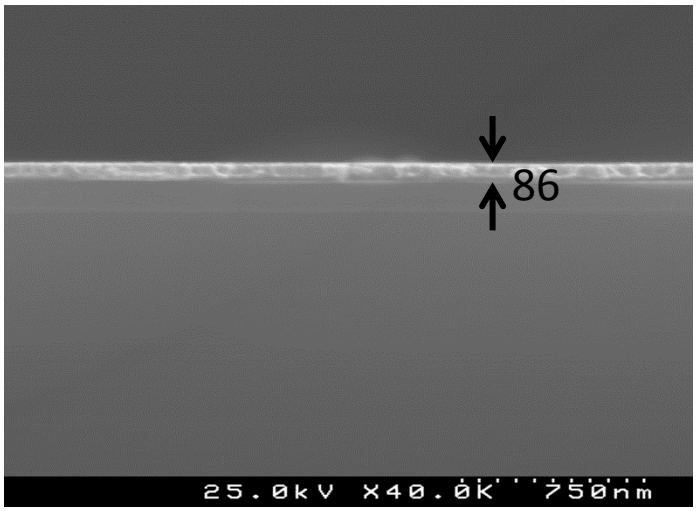

Figure 6.5 – Cross-section of gold nanoparticle deposition on Si

The same deposition time of gold nanoparticles was made into a Si surface in order to compare, not only SERS substrates efficiency but also the thickness of gold nanolayers. The nanoparticles of gold were deposited during 30 min on Si and have about 5 nm of diameter (Figure 6.4). This calculation was made using the Image J software. The 30 min of gold deposition produced a layer of gold with 86 nm (Figure 6.5). This statistic value was also calculated by using Image J.

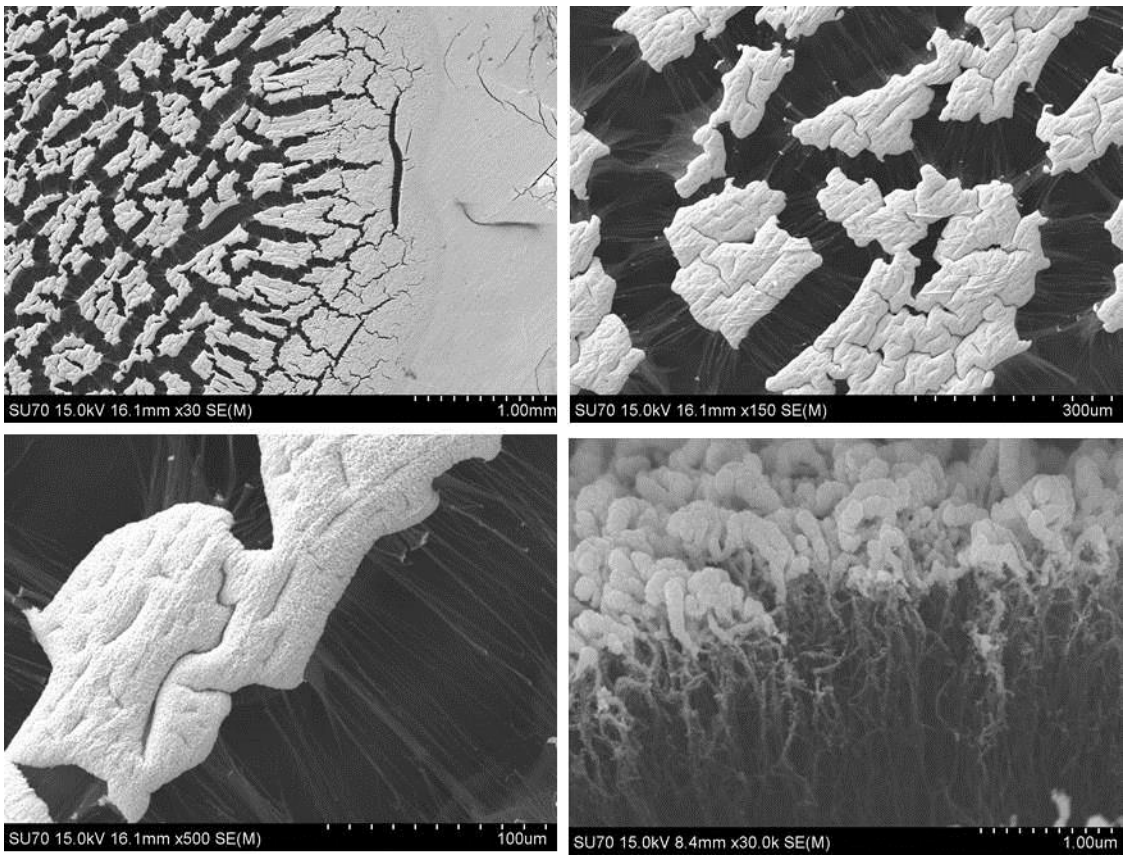

Figure 6.6 – SEM images of VAMWCNT-Au substrates after the deposition of 4 μL of aqueous thiosalicylic acid 0.1 moldm^{-3}.

After the application of nucleic acid solutions on VAMWCNT_Au, the top view of the substrates was changed from a flat-like surface to small gold islands (SEM images in Figure 6.6). This feature changes was the key-point to the enhancement of Raman intensity observed that will be observed with these substrates in all tested analytes.

This phenomenon was in agreement with the results obtained in the studies of Boisen et al on silicon nanopillars covered by silver[12] or gold[13].

6.2.2. SERS studies

VAMWCNT_Au substrates were tested with the four nucleobases and DNA solutions (Figure 6.7). Adenine was detected in a concentration of 10^{-5} mol dm^{-3} as lower limit. Also cytosine has shown some peaks at the same concentration. Guanine and thymine were detected at 10^{-4}M. All the spectra acquired for all bases of DNA were repeated 24h after the first acquisition and all have shown good reproducibility. For such reason, SERS results did not show dependence on interaction time between analyte and plasmonic surface with this type of substrates. For comparison, all the experiments were performed using gold substrates on Si (Figure 6.8). The adenine and cytosine were detected at the concentration of 10^{-5} $moldm^{-3}$ whereas guanine and thymine was detected only at concentrations of 10^{-4} mol dm^{-3}. This means that for all tested species, the limit of detection obtained was the same as with VAMWCNT_Au. But the identification of the analyte was more complete with the substrates that contain carbon nanotubes; the number of characteristic bands is smaller in the case of using Au_substrates. Moreover, the better quality of the spectra acquired from carbon structures covered with gold is evident. In this work, no spectrum was submitted into a mathematical treatment in order to improve the signal/noise ratio. The same procedure was made in the experiments where gold deposited on Si substrates was used. The signal/noise ratio was very low in the latter case being some analyte bands confused with noise. In fact, only the bands at 737, 795 and 666 cm^{-1} for adenine, cytosine and guanine, respectively, are well defined. All the other bands that were identified are poorly defined.

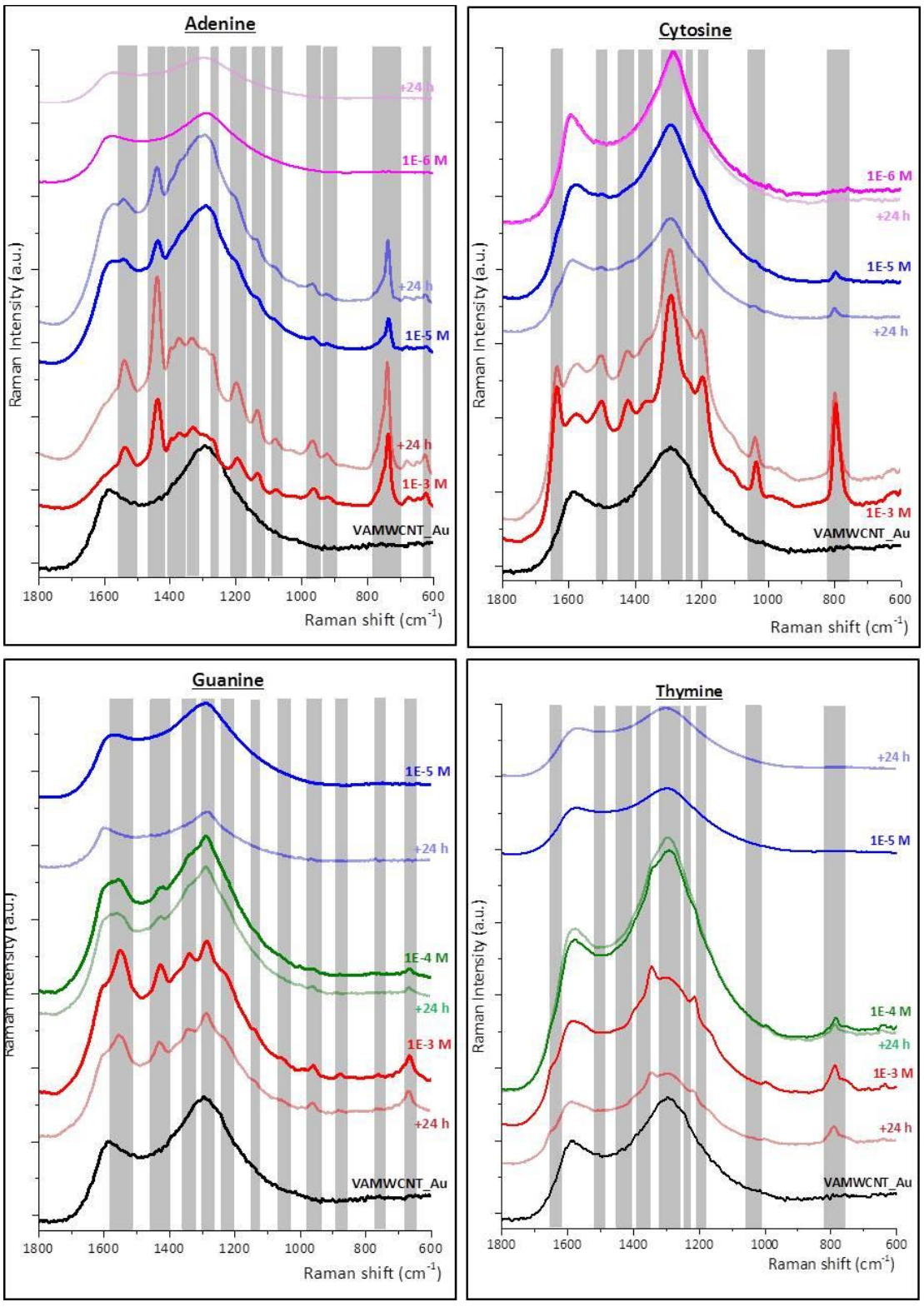

Figure 6.7 – Detection limit of nucleobases in VAMWCNT_Au substrate: adenine, cytosine, guanine and thymine. For all nucleobases concentration, the specta were assessed 24 h after its deposition on the Au substrate.

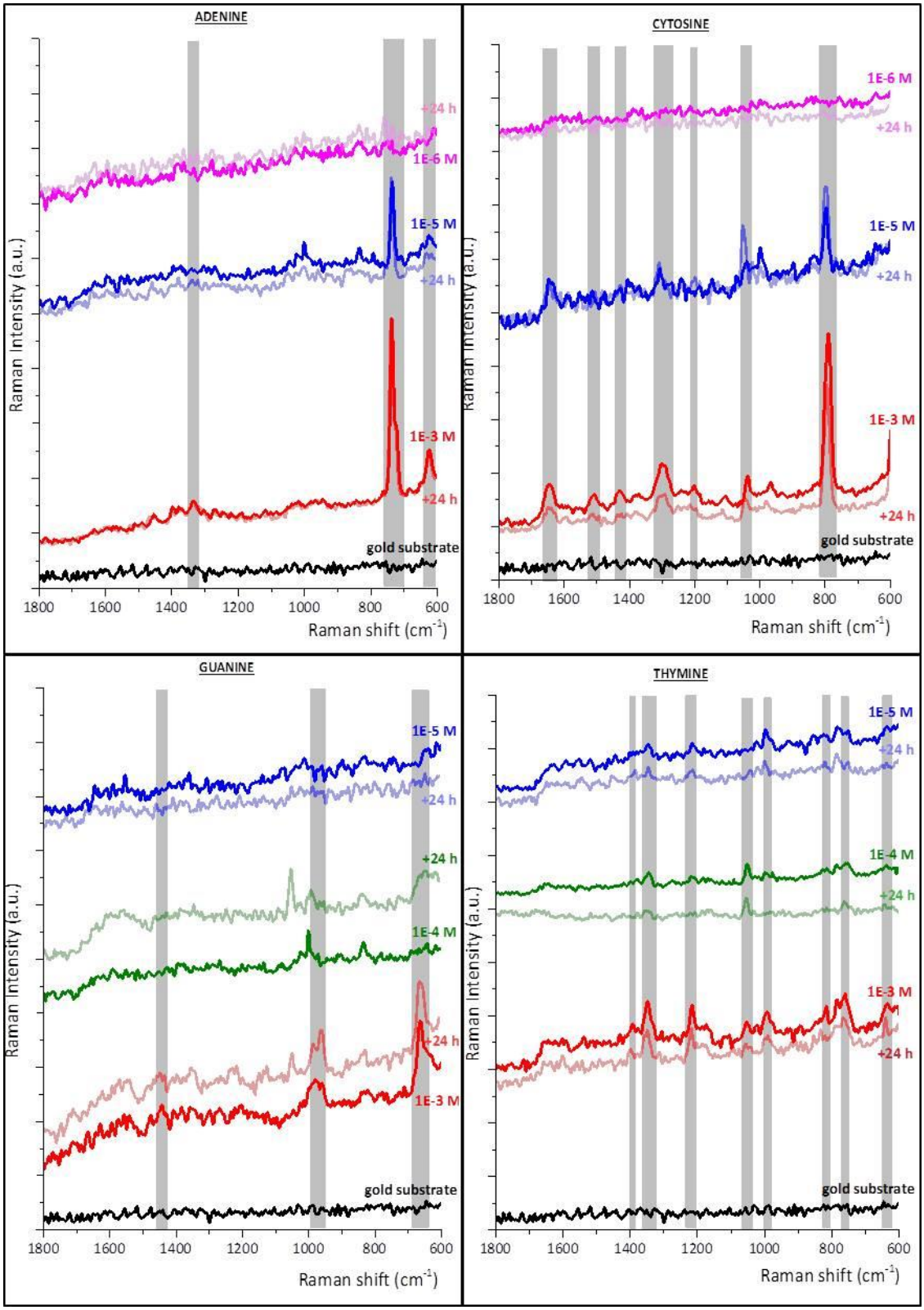

Figure 6.8 – Detection limit of nucleobases in Au substrate: adenine, cytosine, guanine and thymine. For all nucleobases concentration the spectra were assessed 24 h after its deposition on the Au substrate.

The contribution of each band of each analyte can be observed in Figure 6. 9. The SERS spectra of the 10^{-3} $moldm^{-3}$ of each analyte were deconvoluted in order to analyse the contribution in terms of the analyte bands and CNT bands. With the exception of cytosine, in all SERS spectra the CNT bands (D and G) have the major contribution in terms of absolute intensity of the signal. The deconvolution was made by fitting the peaks with the Lorentz function using Origin 9.0 software.

VAMWCNT_Au substrates provided a vibrational analysis very complete for the molecules studied. The proposal of the assignment bands are in the Table 6.1. to Table 6. 4. The deconcolution made by Origin software was not able to show the contribution of all the peaks for thymine. The peaks localized at 1649 and 1394 cm^{-1} of thymine were assigned as “very weak” which means that its intensity were very weak and, probably, this was the reason why identification was not possible by deconvolution.

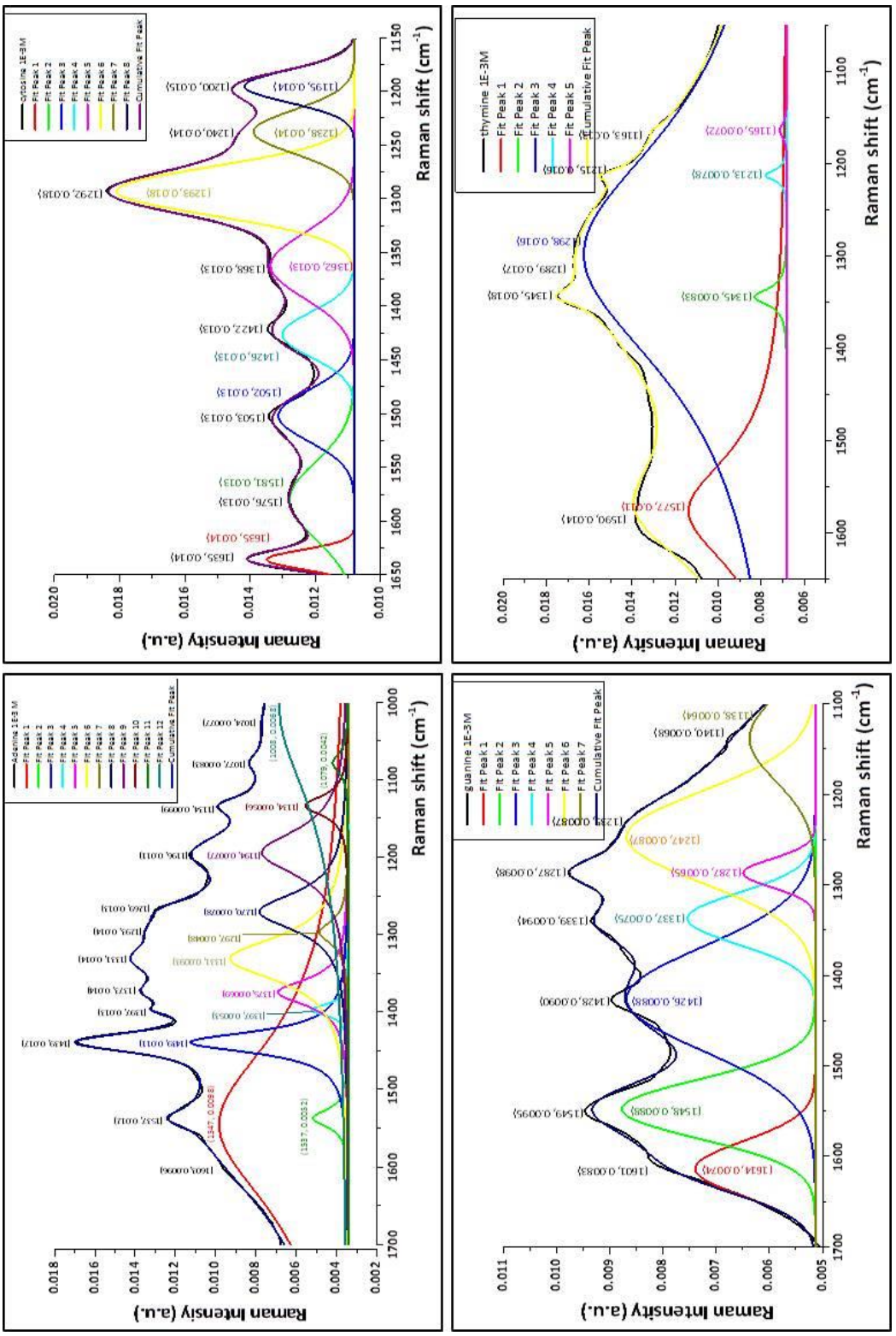

Figure 6. 9 – Deconvolution of adenine (top left), cytosine (top right), guanine (down left) and thymine (down right) 1x10^{-3} M SERS spectra obtained by adsorption on VAMWCNT_Au substrate to identify the contribution of carbon nanostructure bands in the Raman spectra.

Table 6. 1– Observed characteristic bands in the SERS and Raman spectra of adenine. To the assignment of the SERS bands, the solid Raman spectrum of adenine was used for comparison, and in order to calculate the enhancement factor, the Raman spectrum of a solution of 0.067M adenine was used.

Band positions / cm^{-1}		Assignment	Raman Intensity (a.u.)		Line shift compared with RS	EF	
SERS	RS		SERS	RS (solid)		VAMWCNT_Au	Au
1603.0	-	G band	0.0096	-	-	-	-
1541.3^{s}	-	Ring[11], stretching N-C, bending N-H[12]	0.01229	-	-	1.7E+05	-
1439.0^{vs}	1481.5	C-Me[13]	0.0169	0.04422	-42.5	7.8E+05	-
1396.6^{vw}	1417.9	C-Me[13]; stretching C-N, C-C, bending C-H[12]	0.01317	0.0129	-21.3	1.7E+05	-
1373.5^{w}	1371.6	NH-C=O[13]; bending C-H, N-H, stretching C-N[12]	0.01369	0.02252	1.9	9.4E+04	-
1331.1^{w}	1331.1	bending C-H, N-H, stretching C-N[12]	0.01423	0.0809	0.0	3.8E+04	2.3E+00
1296.0	-	D band	0.01352	-	-	-	-
1269.4^{vw}	1246.2	Ring+CH[13]; bending C-H, N-H, stretching N-C[12]	0.01304	0.02119	23.2	9.6E+04	-
1198.0^{m}	1161.4	-CH+CN[13]; bending CH, N-H, stretching C-N[12]	0.0113	0.000656	36.6	2.1E+05	-
1134.4^{w}	1124.7	stretching C-N, bending N-H, C-H[12]	0.00989	0.03191	9.7	-*	-
1078.5^{w}	-		0.00836	-	-	-*	-
1024.5^{vw}	1022.5	NH_2[12]	0.00774	0.01201	2.0	-*	-
962.7^{m}	939.6	Deformation in five-membered ring[12]	0.00845	0.03272	23.1	1.3E+05	-
920.3^{vw}	897.2	Ring deformation, stretching C-N[12]	0.00763	0.01366	23.1	4.0E+04	-
737.1^{vs}	721.7	ring, NH_2 bend[14]; ring breath whole molecule (distorted)[12]	0.0136	0.1229	15.4	2.4E+05	1.6E+01
623.3^{w}	615.6	deformation in six-membered ring[12]	0.008	0.00754	7.7	1.6E+05	1.5E+01

vs = very strong, s = strong, m = medium, w = weak, vw = very weak
*This characteristic peaks of adenine were not present at Raman spectra of adenine 0.067 M aqueous solution used to calculate the enhancement factor.

Table 6. 2 – Observed characteristic bands in the SERS and Raman spectra of cytosine. To the assignment of the SERS bands, the solid Raman spectrum of cytosine was used for comparison, and in order to calculate the enhancement factor, the Raman spectrum of a solution of 0.067M cytosine was used.

Band positions / cm^{-1}		Assignment	Raman Intensity (a.u.)		Line shift compared with RS	EF	
SERS	RS		SERS	RS (solid)		VAMWCNT_Au	Au
1635.8[s]	1651.2	Stretching O=C-N-[13]	0.01409	0.0118	-15.4	4.8E+05	7.2E+00
1576.0	1583.0	G Band	-	-	-	-	-
1502.7[m]	1531.6	Stretching -N-C-N-C[13]	0.01343	0.00881	-28.9	1.2E+05	4.3+00
1421.7[w]	1460.3		0.01346	0.00579	-38.6	2.0E+05	7.1+00
1367.7[vw]	1360.0	Stretching C-N+C=C[13]	0.01343	0.00884	7.7	1.8E+04	-
1292.5[vs]	1273.2	D band, Stretching N-C=C[13]	0.01840	0.03966	19.3	6.8E+05	1.1E+01
1240.4[vw]	1246.2	-	0.01437	0.02133	-5.8	5.5E+03	
1200.0[m]	-	Bending (C-H, C-N)[13]	0.01455	-	-	2.1E+05	3.1+00
1105.4[vw]	1107.4	Stretching (N-Ring, C-H)[13]	0.01008	0.00998	-2.0	-*	-
1036.0[s]	970.0	Rocking NH_2, bending C-H[13]	0.01058	0.00982	66.0	2.4E+05	1.1E+01
795.0[vs]	791.1	Ring breathing[13]	0.01323	0.06514	3.9	2.1E+05	1.4E+01

Table 6. 3 – Observed characteristic bands in the SERS and Raman spectra of guanine. To the assignment of the SERS bands, the solid Raman spectrum of guanine it was used for comparison, and in order to calculate the enhancement factor, the Raman spectrum of a solution of 0.067M guanine was used.

Band positions / cm^{-1}		Assignment	Raman Intensity (a.u.)		Line shift compared	EF	
SERS	RS		SERS	RS (solid)	with RS	VAMWCNT_Au	Au
1601.0	1580.0	G Band	-	-	-	-	-
1549.0^{vs}	1550.0	Stretching N-C—C-N+C-N, scissoring NH, bending NH[15]	0.00946	0.04595	-1.0	2.7E+05	3.2E+00
1427.5^{s}	1388.9	Bending N-H, C-H, stretching –NH-C(NH_2)=, =N-C=C, -N=CH-NH-[16]	0.00896	0.04503	38.6	1.2E+05	4.4E+00
1338.8^{w}	1358.1	Stretching -C=N-, -C-N-[13]; Bending N-H, stretching =C-N-[15]	0.00935	0.02721	-19.3	5.4E+04	-
1286.7^{m}	1263.6	D band, stretching -C=N-C-, N-C[13]; Stretching =C-N=, -NH-CO-C=CN-NH-,-H_2NC=N-, bending =CH-, rocking NH_2[15]	0.00977	0.04718	23.1	8.4E+04	-
1236.6^{vw}	1232.8	Bending C-H, stretching C=N[13]; Bending =CH-, stretching =C-N=CH-[15]	0.00874	0.06026	3.8	-	-
1140.2^{vw}	1153.7	Stretching -C=N, N-ring-C-N=[13]; Rocking NH2 , stretching –CO-NH-[15]	0.00680	0.00687	-13.5	2.2E+04	-
1055.3^{vw}	1045.7	Stretching –NH-C(NH_2)=N-[15]	0.00582	0.00573	9.6	-	-
960.8^{w}	935.7	Stretching –N-ring, N=C[13]; ring deformation[15]	0.00558	0.00521	25.1	-	-
879.8^{vw}	847.0	Stretching =N-C, bending -N-C=N-[13]	0.00527	0.01298	32.8	-	-
762.2^{vw}	710.1	Bending C=O, C-H[17]	0.00526	0.00533	52.1	-	-
665.8^{m}	648.4	Breathing six-membered ring (wagging –N=CH-NH-[13])[15]	0.00589	0.00540	17.4	4.0E+04	4.7E+00

Table 6. 4 – Observed characteristic bands in the SERS and Raman spectra of thymine. To the assignment of the SERS bands, the solid Raman spectrum of thymine was used for comparison, and in order to calculate the enhancement factor, the Raman spectrum of a solution of 0.067M thymine was used.

Band positions / cm^{-1}		Assignment	Raman Intensity (a.u.)		Line shift compared with	EF	
SERS	RS		SERS	RS (solid)	RS	VAMWCNT_Au	Au
1649.3^{vw}	1670.5	Stretching C=O[13, 18, 19]	0.01078	0.0646	-21.2	7.0E+04	1.3E+00
1585.6	1583.0	G band	-	-	-	-	-
1394.8^{vw}	1408.2	-	0.01466	0.0093	-13.4	2.1E+04	2.0E+00
1344.6^{s}	1367.7	Bending N-H[19], stretching C=O[13]; bending CH_3[18, 19]	0.01748	0.0683	-23.1	2.4E+05	5.4E+00
1292.5	1290.0	D band	-	-	-	-	-
1215.4^{m}	1213.4	Stretching Ring, C-CH_3[13, 18, 19]	0.01546	0.00539	2	4.9E+04	-
1163.3^{vw}	1155.6	Bending =C-H, stretching C-NH-[13, 19], bending CH_3[18]	0.01299	0.00675	7.7	1.7E+05	6.0E+00
997.5^{w}	982.0	Rocking C-CH_3[13], stretch ring[18, 19]	0.00977	0.01461	15.5	1.7E+05	2.2E+00
787.3^{s}	804.6	Stretching NH-ring[13], deformation ring[18, 19]	0.01088	0.01451	-17.3	2.3E+04	3.7E+00
758.3^{vw}	739.0	Ring breathing[13, 18, 19]	0.00993	0.03208	19.3	9.5E+04	2.8E+00
636.8^{w}	615.6	Bending –NH-CO-[13], deformation of ring[18]	0.00962	0.02356	21.2	4.5E+04	2.2E+00

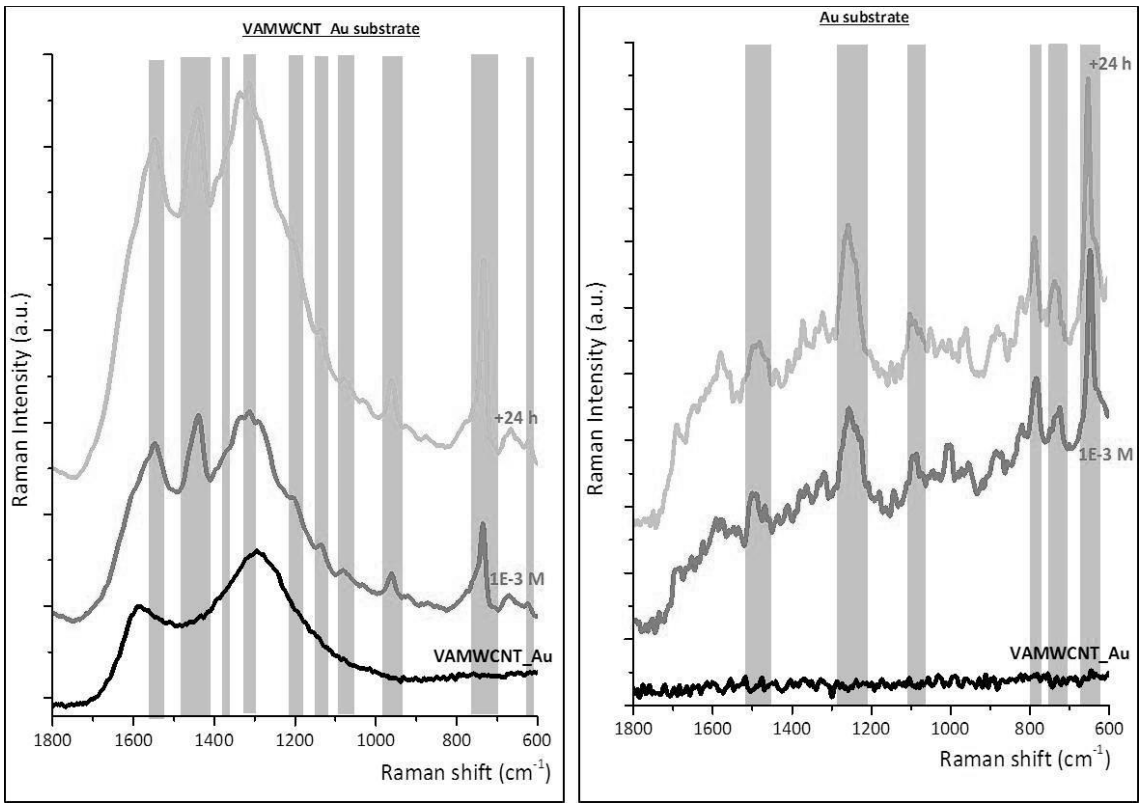

Figure 6.10 – Detection of dsDNA (b) 10^{-3} M, (c) 10^{-3} M after 24h of interaction in (a) MWCNT_Au (left) and Au (right) substrates.

Double-stranded DNA was also used as Raman reporter in VAMWCNT_Au substrates (Figure 6.10). The signal/noise ratio showed by such spectrum was also good as with the other tested molecules. Once again, in the case of gold substrates the presence of noise affected the analysis of SERS signals. Table 6.5 shows the vibrations corresponding to the SERS bands obtained for DNA with the substrates studied in this work.

Table 6.5 – Observed characteristic bands in the SERS and Raman spectra of DNA. To the assignment of the SERS bands, the solid Raman spectrum of DNA was used for comparison.

Band positions / cm^{-1}		Assignment
SERS	RS	
1600.1		G band
1549.0	1557.0	Ring[14], Stretching N-C[15 16 17], scissoring NH, bending NH[15,17] A, C, G
1439.1	1408.2	C-Me[16], Bending N-H, C-H, stretching –NH-C(NH_2)=, =N-C=C, -N=CH-NH-[18] A, C, G
1367.7	1369.6	NH-C=O[16]; bending C-H, N-H, stretching C-N[15 16] (A) A, C
1313.7	1323.4	Stretching C-N[15], =C-N=,-H_2NC=N-[17], C=O, N-C=C[16], rocking NH_2[17], bending =CH-[17], N-H[19], CH_3[19,20] A, C, T
1286.7		D band
1199.9	1244.3	Bending (N-H) [15] (C-H, C-N)[16], Stretching C-N[15], Ring, C-CH_3[16,19,20] A, C, T
1136.3	1090	stretching C-N[16 15], bending N-H, C-H[15], Rocking NH2 , stretching –CO-NH-[17] A, G
1076.5	1014.8	Rocking NH_2, bending C-H[16] A, C
957.0	1011.0	Stretching –N-ring, N=C[16]; ring deformation[15,17] A, G
735.2	724.0	Ring breathing[15,16,19,20] A, C, T
625.3	614.0	deformation in ring[15 20], Bending –NH-CO-[16] A, T

In the same way as in chapter 6 of this thesis, the shift of localized surface plasmon resonance (LSPR) of gold nanoparticles interacting with the analyte was evaluated. Figure 6.11 shows UV-vis spectra, in reflectance mode, of VAMWCNT after the deposition of 4 μL of each nucleobases solution with all tested concentrations. The

LSPR of gold nanoparticles showed a position displacement depending on the tested concentration. Cytosine, guanine and thymine have caused a major red-shift at the lowest concentration detected by SERS measurements, i.e., 10^{-5} moldm^{-3} in the case of cytosine, and 10^{-4} moldm^{-3} for the other two nucleic acids. Adenine showed a different trend, the SPR showed a red-shift with the concentration solutions decreasing (Figure 6.11 and Table 6.6). In fact, by the graphics showed in Figure 6.12, where the LSPR positions are represented as function of the nucleobase concentration, it is possible to see that LSPR positions of VAMWCNT with adenine and cytosine becomes to start stabilizing at 10^{-5} moldm^{-3} and with thymine at 10^{-4} moldm^{-3}. These results are in agreement with the detection limit found with SERS results.

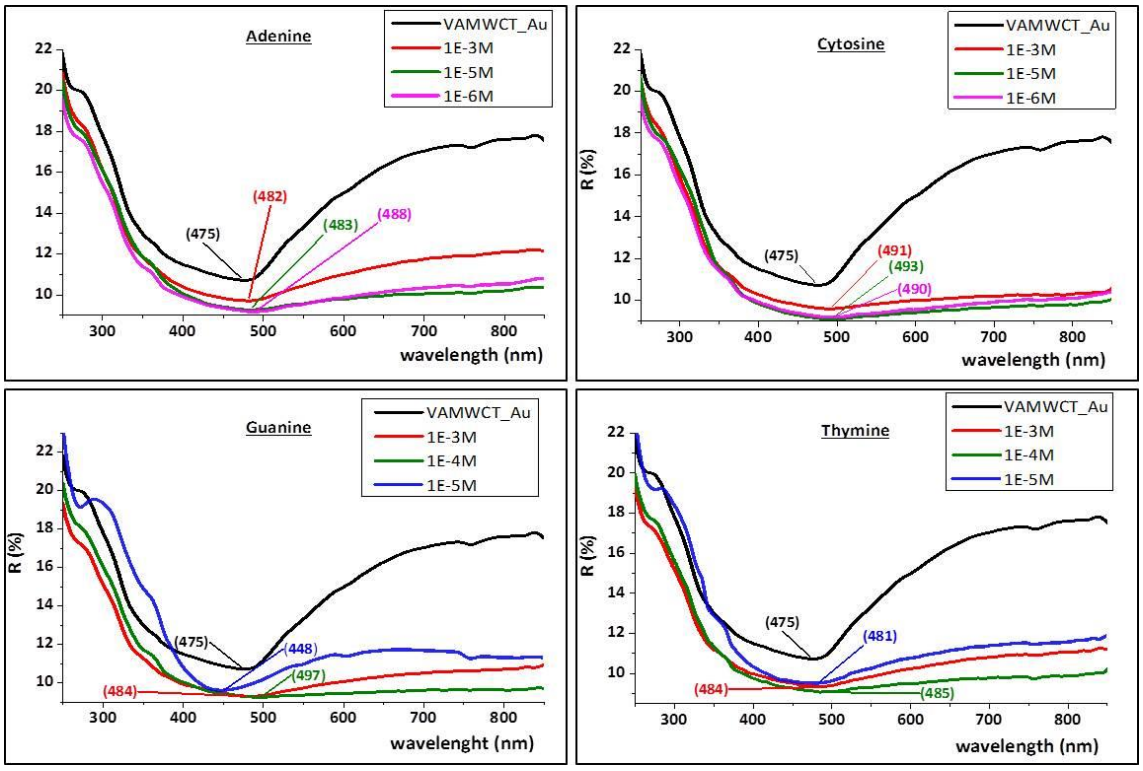

Figure 6.11 – UV-vis reflectance spectra of VAMCNT_Au substrates and of the same substrates with addition of nucleic acids in the same concentrations used in SERS analysis.

Table 6.6 – Au LSPR peaks positions of VAMWCNT_Au substrates with nucleic acid solutions in different concentrations

		0 M	1E-3M	1E-4M	1E-5M	1E-6M
Au LSPR	adenine	475.0	481.5	-	483.0	487.5
	cytosine	475.0	490.5	-	493.0	490.0
	guanine	475.0	483.5	496.5	448.0	-
	thymine	475.0	484.0	485.0	480.5	-

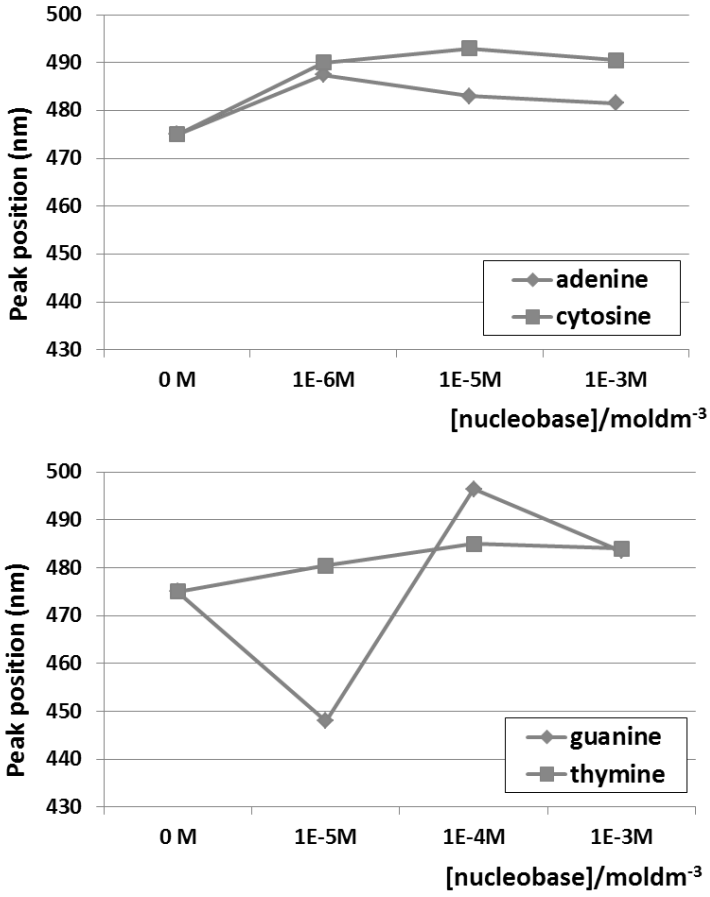

Figure 6.12 – The influence of the concentration of nucleobases solutions in Au SPR peaks position of the VAMWCNT_Au substrates.

6.2.3. SERS Enhancement Factor calculation

The magnitude of SERS enhancement can be estimated calculating the enhancement factor (EF). Although this parameter is maintained only as a comparative factor, it is an important tool to assess the efficiency of the substrates. We have estimated the EF considering that the analyte molecules were adsorbed on the gold surface of VAMWCNT-Au substrates, in an estimated depth of 290 μm, as measured from the SERS images.

The EF can be calculated using the following equation[21]:

$$EF = \frac{I_{SERS}/N_{Surf}}{I_{RS}/N_{vol}} \quad (1)$$

Where I_{SERS} and I_{RS} are SERS and Raman signals intensities, N_{Surf} is the number of analyte molecules adsorbed in the scattering volume of SERS spectra and N_{vol} is the average number of molecules present at the scattering volume of Raman spectra.

An analyte aqueous solution 0.067 M was used to measure the Raman intensity for EF calculations. The scattering volume is the volume of analyte excited by the laser. Considering a laser spot diameter of 350 μm and the 5mm thickness of the glass tube used for the aqueous sample, the scattering volume for Raman was $4.81X10^{-7}$ dm^3, and N_{vol} is $3.22X10^{-8}$ mol.

N_{Surf} is calculated by $\mu_{SERS} \times V_{SERS}$, where μ_{SERS} is the density of the analyte in SERS substrate and V_{SERS} is the scattering volume of SERS. When the drop of aqueous analyte solution ($4X10^{-6}$ dm^3, $1x10^{-3}$ M) was deposited on the substrate, the drop spread through it creating a volume in a cylinder shape with a diameter of 4 mm and 290 μm height. V_{SERS} was calculated using the laser spot diameter (350 μm) and the estimated value of its depth inside the substrate (37.150 μm). So, N_{Surf} was $3.92X10^{-12}$ and the final equation was

$$EF = \frac{I_{SERS}/N_{Surf}}{I_{RS}/N_{vol}} = \frac{I_{SERS} \times N_{vol}}{I_{RS} \times N_{Surf}} \Leftrightarrow EF = \frac{I_{SERS}}{I_{RS}} \times 8217 \quad (2)$$

The EF was also calculated for flat gold-Si substrates. In this case, its height was estimated at 86 nm. The diameter of the spreading solution analyte at its surface was considered the same as in the VAMWCNT-Au substrates (4mm), and EF equation was

$$EF = \frac{I_{SERS}/N_{Surf}}{I_{RS}/N_{vol}} = \frac{I_{SERS}\times N_{vol}}{I_{RS}\times N_{Surf}} \Leftrightarrow EF = \frac{I_{SERS}}{I_{RS}} \times 1053 \qquad (3)$$

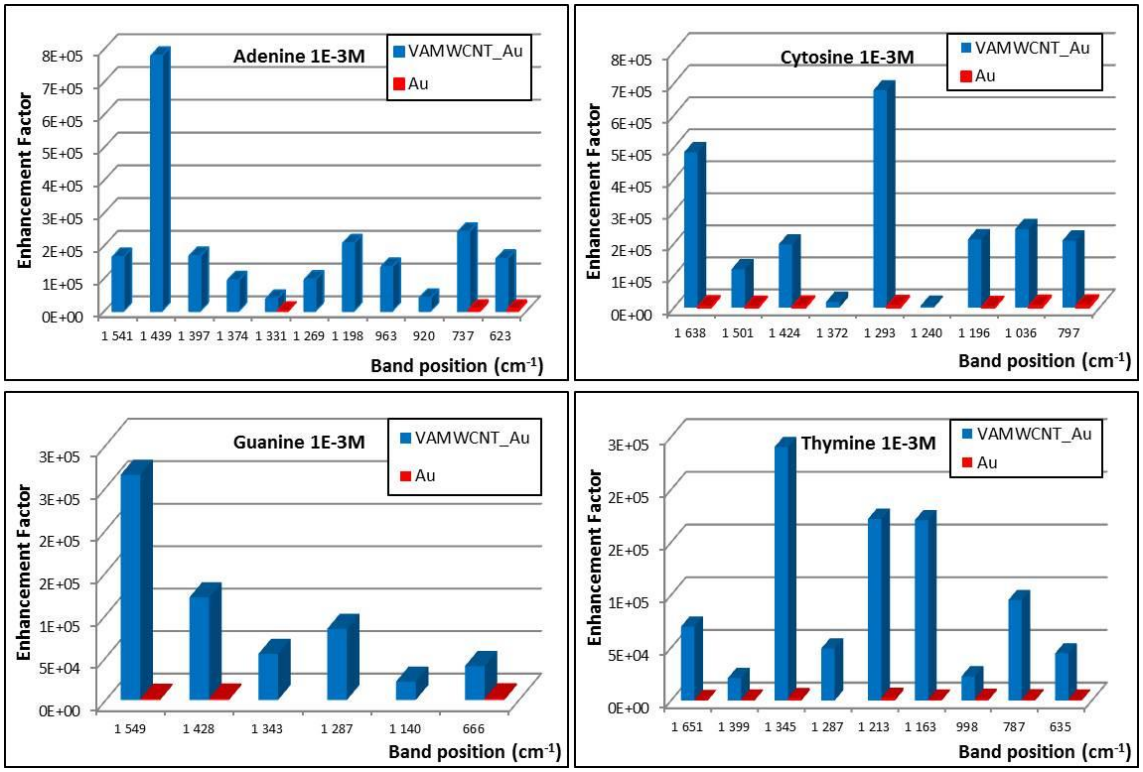

Figure 6.13 – Comparison of the EF calculated for the several bands characteristic of adenine, cytosine, guanine and thymine present in SERS spectra obtained using VAMWCNT-Au and Si-Au substrates to detect 4 µL of adenine 10^{-3} mol dm^{-3}.

The enhancement factor was calculated for all the bands identified which had correspondence to the Raman spectra of the concentrated aqueous solutions of the analytes (Figure 6.13). The carbon nanostructures based-substrates provided EF between $1x10^4$ and $8x10^5$ for the four nucleic acid molecules. In the case of Au_Si substrates the EF maximum obtained was 10 which confirms the efficiency of the VAMWCNT_Au.

The explanation of such EF provide from the leaning effect of the VAMWCNT_Au substrate[12]. When a droplet of an aqueous solution was deposited onto the substrate, and letting evaporate, surface tension caused the vertical aligned carbon nanotubes to lean towards their nearest neighbours, thus creating self-assembled hot spots. Analyte molecules adsorbed at the tips of the carbon nanotube were, then, located exactly in the hot spots as the nanotubes leaned together. This self-assembling mechanism creates a large number of electromagnetic hot spots inside the laser excitation area, as was shown in other published works using carbon nanotubes[22] or silicon nanopillars[12,13].

6.3. Conclusions

New substrates of vertically aligned multi-walled carbon nanotubes covered by gold nanoparticles (VAMWCNT_Au) were prepared in order to evaluate its development in SERS detection.

VAMWCNT_Au showed good performance in the detection of adenine and cytosine with concentrations as low as 10^{-5} moldm^{-3}. Guanine and thymine were detected using the same type of SERS substrates with lowest concentrations of 10^{-4} moldm^{-3}. Also the DNA molecule was detected.

The well-defined Raman peaks of nucleic acids, enhanced by the presence of VAMWCNT_Au, is a novelty in biomolecules detected by SERS. This good definition allows the estimation of the analyte peaks and substrate peaks contribution.

6.4. Experimental Procedure

6.4.1. Preparation of VAMWCNT_Au and Au substrates

CNT forest growth was carried out in a hot-wall thermal CVD reactor using a C2H2 (purityP 99.6%, 300 ppm of H2O, Praxair)–H2 (purityP99,999%, 62 ppm of H2O,

Praxair)–Ar (purity P99,9999%, 60.5 ppm of H2O, Praxair) gas mixture at atmospheric pressure. The reactor consists of a 5 cm inner diameter quartz tube housed inside a furnace, equipped with mass flows, electrovalves and a PC control station for automatic operation.

In a typical growth run, the substrates were placed in a quartz boat and loaded into the cold zone of the reactor, with the furnace already heated at the temperature of set-point. The reactor tube was then pumped down to 3 Pa and subsequently filled up with Ar to reach the atmospheric pressure. Afterwards, the quartz boat was pushed to the centre of the hot zone using a stainless steel arm, allowing a fast heating. Then, a two stepped annealing process was initialised. Firstly, in an inert flow of Ar (1000 sccm), followed by a treatment in a reductive flow of Ar/H2 (v/v) = 0.4 (700 sccm). Subsequently, the Ar and H2 flows were adjusted and the C2H2 was added for the CNTs synthesis. After the growth step, the C2H2 and H2 flows were cut off and the quartz tube was flushed with Ar flow to remove the reactive gases. Finally, the quartz boat was pulled to the cold zone for a fast cooling down to room temperature in around 2min. The furnace and the empty quartz boat were then purged with O2 in the hot zone during 10 min to burn out the carbon residuals, becoming the system, after that, ready for a new growth run[23].

The gold nanoparticles were deposited on the top of VAMWCNT and Si, using the sputtering equipment, under vacuum, for 30 min. The final substrates obtained were VAMWCNT_Au and Si_Au.

6.4.2. SERS measurements

The nucleobases solutions were prepared immediately before SERS experiments. 4 µL of each analyte solution were deposited on the top of SERS substrates and dried during 30 minutes before the spectrum acquisition. After 24h, all the spectra were again acquired in order to check if the interaction time between the analyte and substrate has some influence on the sensibility of substrate.

All the spectra were acquired with 500 scans, using a FT-Raman Bruker RFS -100/s spectrometer, 1064 nm laser with power 350 mW.

6.5. Bibliography

(1) Kneipp, J.; Kneipp, H.; Kneipp, K. SERS--a single-molecule and nanoscale tool for bioanalytics. *Chem Soc Rev* **2008**, *37*, 1052-1060.

(2) Stiles, P. L.; Dieringer, J. A.; Shah, N. C.; Van Duyne, R. R. Surface-Enhanced Raman Spectroscopy. *Annual Review of Analytical Chemistry* **2008**, *1*, 601-626.

(3) Lombardi, J. R.; Birke, R. L.; Lu, T. H.; Xu, J. Charge-transfer theory of surface enhanced Raman-spectroscopy - Herzberg-Teller contributions. *Journal of Chemical Physics* **1986**, *84*, 4174-4180.

(4) Polavarapu, L.; Liz-Marzán, L. M. Towards low-cost flexible substrates for nanoplasmonic sensing. *Physical chemistry chemical physics : PCCP* **2013**, *15*, 5288-5300.

(5) Zhang, J.; Fan, T.; Zhang, X.; Lai, C.; Zhu, Y. Three-dimensional multi-walled carbon nanotube arrays coated by gold-sol as a surface-enhanced Raman scattering substrate. *Applied Optics* **2014**, *53*, 1159-1165.

(6) Goldberg-Oppenheimer, P.; Hutter, T.; Chen, B.; Robertson, J.; Hofmann, S.; Mahajan, S. Optimized Vertical Carbon Nanotube Forests for Multiplex Surface-Enhanced Raman Scattering Detection. *Journal of Physical Chemistry Letters* **2012**, *3*, 3486-3492.

(7) Zhang, J.; Chen, Y.; Fan, T.; Lai, C.; Zhu, Y. Vertically aligned multi-walled CNT arrays coated by gold nanoparticles for surface-enhanced Raman scattering. *Microsystem Technologies-Micro-and Nanosystems-Information Storage and Processing Systems* **2014**, *20*, 113-117.

(8) Niu, J. J.; Schrlau, M. G.; Friedman, G.; Gogotsi, Y. Carbon Nanotube-Tipped Endoscope for In Situ Intracellular Surface-Enhanced Raman Spectroscopy. *Small* **2011**, *7*, 540-545.

(9) Najjar, S.; Talaga, D.; Schue, L.; Coffinier, Y.; Szunerits, S.; Boukherroub, R.; Servant, L.; Rodriguez, V.; Bonhommeau, S. Tip-Enhanced Raman Spectroscopy of Combed Double-Stranded DNA Bundles. *Journal of Physical Chemistry C* **2014**, *118*, 1174-1181.

(10) Wang, X.; Wang, C.; Cheng, L.; Lee, S.-T.; Liu, Z. Noble Metal Coated Single-Walled Carbon Nanotubes for Applications in Surface Enhanced Raman Scattering

Imaging and Photothermal Therapy. *Journal of the American Chemical Society* **2012**, *134*, 7414-7422.

(11) Lin, X. M.; Cui, Y.; Xu, Y. H.; Ren, B.; Tian, Z. Q. Surface-enhanced Raman spectroscopy: substrate-related issues. *Anal Bioanal Chem* **2009**, *394*, 1729-1745.

(12) Schmidt, M. S.; Hubner, J.; Boisen, A. Large Area Fabrication of Leaning Silicon Nanopillars for Surface Enhanced Raman Spectroscopy. *Advanced Materials* **2012**, *24*, OP11-OP18.

(13) Yang, J.; Palla, M.; Bosco, F. G.; Rindzevicius, T.; Alstrom, T. S.; Schmidt, M. S.; Boisen, A.; Ju, J.; Lin, Q. Surface-Enhanced Raman Spectroscopy Based Quantitative Bioassay on Aptamer-Functionalized Nanopillars Using Large-Area Raman Mapping. *Acs Nano* **2013**, *7*, 5350-5359.

(14) Xiao, Y. J.; Chen, Y. F.; Gao, X. X. Comparative study of the surface enhanced near infrared Raman spectra of adenine and NAD(+) on a gold electrode. *Spectrochimica Acta Part a-Molecular and Biomolecular Spectroscopy* **1999**, *55*, 1209-1218.

(15) Giese, B.; McNaughton, D. Surface-enhanced Raman spectroscopic and density functional theory study of adenine adsorption to silver surfaces. *Journal of Physical Chemistry B* **2002**, *106*, 101-112.

(16) Otto, C.; Vandentweel, T. J. J.; Demul, F. F. M.; Greve, J. Surface-enhanced Raman-spectroscopy of DNA bases. *Journal of Raman Spectroscopy* **1986**, *17*, 289-298.

(17) Giese, B.; McNaughton, D. Density functional theoretical (DFT) and surface-enhanced Raman spectroscopic study of guanine and its alkylated derivatives - Part 2: Surface-enhanced Raman scattering on silver surfaces. *Physical Chemistry Chemical Physics* **2002**, *4*, 5171-5182.

(18) Giese, B.; McNaughton, D. Interaction of anticancer drug cisplatin with guanine: Density functional theory and surface-enhanced Raman spectroscopy study. *Biopolymers* **2003**, *72*, 472-489.

(19) Shang, Z.-G.; Ting, D. N.; Wong, Y. T.; Tan, Y. C.; Ying, B.; Mo, Y.-J. A study of DFT and surface enhanced Raman scattering in silver colloids for thymine. *Journal of Molecular Structure* **2007**, *826*, 64-67.

(20) Aroca, R.; Bujalski, R. Surface enhanced vibrational spectra of thymine. *Vibrational Spectroscopy* **1999**, *19*, 11-21.

(21) Le Ru, E. C.; Blackie, E.; Meyer, M.; Etchegoin, P. G. Surface enhanced Raman scattering enhancement factors: a comprehensive study. *Journal of Physical Chemistry C* **2007**, *111*, 13794-13803.

(22) Dawson, P.; Duenas, J. A.; Boyle, M. G.; Doherty, M. D.; Bell, S. E. J.; Kern, A. M.; Martin, O. J. F.; Teh, A. S.; Teo, K. B. K.; Milne, W. I. Combined Antenna and

Localized Plasmon Resonance in Raman Scattering from Random Arrays of Silver-Coated, Vertically Aligned Multiwalled Carbon Nanotubes. *Nano Letters* **2011**, *11*, 365-371.

(23) Mata, D.; Silva, R. M.; Fernandes, A. J. S.; Oliveira, F. J.; Costa, P. M. F. J.; Silva, R. F. Upscaling potential of the CVD stacking growth method to produce dimensionally-controlled and catalyst-free multi-walled carbon nanotubes. *Carbon* **2012**, *50*, 3585-3606.

7. Final remarks

In this chapter a reflection is made about the experimental work realized and the results obtained. Considerations are made about the positive results obtained together with some weaknesses that were also identified, towards the future preparation of easily manageable active SERS substrates for the detection of biomolecules.

The study was set out to explore the preparation of active SERS nanocomposites comprising metal nanoparticles associated to carbon nanostructures. The study was also directed to support these nanocomposites on a physical support (membrane or film) easy to handle, inexpensive and reproducible. The reason to explore the preparation of these nanocomposites and study their SERS activity is to contribute for the development of new substrates for the specific detection of biomolecules.

In a first step, polyvinyl alcohol (PVA) composites were prepared incorporating silver nanoparticles initially without introduction of carbon nanostructures. Several experimental parameters were considered to obtain the best SERS analysis. The dried samples at 105 ºC showed the best SERS results. These membranes were stable for long periods of time (more than 4 months) and showed the ability to identify nucleic acids by SERS.

Next, the synthesis and characterization of graphene oxide (GO) was implemented to be used in the preparation of silver and gold nanocomposites. Well exfoliated GO nano-sheets (single or few layers) were produced at the laboratory. The reduction of this nanomaterial with different chemical agents was explored, since its reduction degree may be a determinant factor for the application envisaged (biomolecules interaction). The chemical reducing agents were selected based on a low toxicity criteria and were glucose, sodium citrate, eucalyptus globulus extracts and hydroxylamine. These reducing agents showed different efficiency to restore the sp^2 carbon network of graphene. Also, not all the oxygen functional groups were completely removed using these chemicals, under the experimental conditions used. Additionally, from the characterization results it was possible to conclude that some molecules from the reducing agent were adsorbed at the final rGO material (even after washing procedure) what could interfere with the SERS activity determination.

The preparation of the graphene nanocomposites with silver and gold was performed with the different reducing agents previously referred. The SERS activity of these new nanocomposites was then explored in the presence of thiosalicylic acid, varying the experimental conditions for Raman spectra acquisition. It was interesting to

verify that both the silver and the gold containing nanocomposites presented the particularity to intensify the graphene D and G bands.

Fibrous membranes were also prepared by electrospinning with the aim to prepare SERS supports with different topography and porosity able to promote the creation of particular nanoparticles distribution for the establishment of the so-called hot-spots. The polymers polyvinyl alcohol and polyacrylonitrile were selected for electrospinning. Using this technique, electrospun mantles with silver and gold nanoparticles and the corresponding graphene nanocomposites were prepared. Several variables were studied, such as the introduction of the nano-fillers during the electrospinning process, posterior deposition of the nano-fillers on the simple electrospun polymeric fibres and surface functionalization of the simple polymeric membranes to later link the nano-fillers. The results obtained showed that this is a promising methodology to prepare SERS active substrates, although much more optimization work is needed, there is still plenty of room for improvements of this methodology.

At last, the potentialities of using carbon nanotubes forests, produced by chemical vapour deposition and coated with gold film by sputtering, as new SERS substrates were explored. It was found that these nanostructures were suitable for SERS detection of DNA bases and DNA itself, representing an interesting route to be optimized and explored in future work. It is important to highlight the good definition of the Raman spectra achieved with this type of substrates for these biomolecules.

Summarizing, in this work a great variety of materials was prepared. Several substrates confirmed a good potential for SERS detection of the analytes tested. However, as was verified in this thesis, there are a huge number of variables that may interfere with the outcome of a good SERS activity and consequently the detection of vestigial concentration of the probe molecules. For example, the probe molecules used in this study may not be the most adequate for the specific substrates prepared in this work, there are a plenty of other possible analytes to evaluate. Future work could include, for example, the selection of a restricted number of the most promising substrates and the study of this selection with different type of analytes.

Using metal-graphene nanocomposites as SERS substrates instead of the metal alone was shown to give better results in some specific conditions, but there is a plethora of variables involved. Further efforts should be devoted to the design and synthesis of noble metal-graphene nanocomposites to further improved SERS performance. It remains a grand challenge for creating a general substrate that can detect diverse target analytes. Taking advantages of the high affinity of graphene oxide toward aromatic molecules and the SERS property of nanostructured metals, these composites exhibit great potential for diverse aromatic molecules sensing.

Future work must include, after a systematic study of the previously referred parameters, the surface modification of the most promising substrates to fine-tune their SERS activity and make them specific to identify certain biomolecules. In this way, a contribution to the development of manageable SERS sensors for the selective detection of biomolecules in targeted research could be achieved.

Annex

MATERIALS:

R6G was purchase to Aldrich. Cytosine, thymine, adenine, guanine, deoxyribonucleic acid (low molecular weight from salmon sperm) and PVA (MW 89,000-98,000, 99+% hydrolyzed) were supplied by Sigma.

Graphite flakes, H_2O_2, H_2SO_4, H_3PO_4 and $KMnO_4$ were purchase from Sigma Aldrich.

PVA (Mw 89,000-98,000, 99+% hydrolysed) was purchase by Sigma Aldrich, AgNO3 (99.9999%) was purchase by Aldrich Chem. Co. The polyacrylonitrile (PAN) average Mw 150,000, N,N-dimethylformamide (DMF), ammonium hydroxide (NH_4OH), tetrachloroauric (III) acid ($HAuCl_4.3H_2O$), D(+)-glucose, sodium citrate tribasic dihydrate ($HOC(COONa)(CH_2COONa)_2 \cdot 2H_2O$), silver nitrate ($AgNO_3$, 99.9999% trace metals basis), palladium(II) chloride, ≥99.9%, tin(II) chloride, hydroxylamine solution, 50 wt. % in H_2O, thiosalicylic acid (SHsal) and rhodamine 6G were purchase from the Sigma-Aldrich Chemical Co. and used without further purification.

The filter paper used as support of PAN mantle was Filtrak (392), 7 cm of diameter and 100 g/cm2.

CHARACTERIZATION TECHNIQUES:

Scanning electron microscopy (SEM) images were obtained using a FEG-SEM Hitachi S4100 microscope operating at 25 kV.

The optical spectra were recorded using a Jasco V-560 UV-vis spectrophotometer; the samples were recorded in the absorbance and reflectance mode.

Transmission electron microscopy (TEM) was performed using a Hitachi H-9000 operating at 300 kV. The samples for TEM were prepared by depositing an aliquot of the graphene suspension onto a carbon-coated copper grid and then letting the solvent evaporate.

The FTIR spectra of different samples of graphene were recorded from KBr pellets (Aldrich, 99%, FT-IR grade) with a Mattson 7000 FT-IR spectrometer with resolution 8 and 256 interferograms.

A Digital Instruments MultiMode scanning probe microscope (SPM) with a Nanoscope IIIA controller in tapping mode was used for the AFM measurements.

For thermogravimetric measurements a TGA - Shimadzu, TGA-50, was used with a nitrogen flow rate of 20 mL/min and a temperature rate of 5 ºC/min, between 20 and 800 ºC.

The Raman spectra and SERS were recorded using a Bruker RFS100/S FT-Raman spectrometer (Nd:YAG laser, 1064 nm excitation).

Micro-Raman experiments were performed at room temperature using the 488 nm line of an Ar+ laser with an incident power in the 1–8 mW range. The light was focused and collected with an Olympus microscope (100X objective) and a "super-notchplus" filter from Kaiser was used to eliminate elastic light. The scattered light was analyzed with a Jobin Yvon HR-460 monochromator coupled to a liquid nitrogen cooled CCD.